PHOTOCHEMICAL CONVERSIONS USING SYNTHETIC PORPHYRINS AS PHOTOCATALYSTS

THESIS

Submitted to the

GOA UNIVERSITY

For the degree of

DOCTOR OF PHILOSOPHY
IN CHEMISTRY

By

Shrinivas Dinkarrao Gokakakar

Department of Chemistry
Goa University

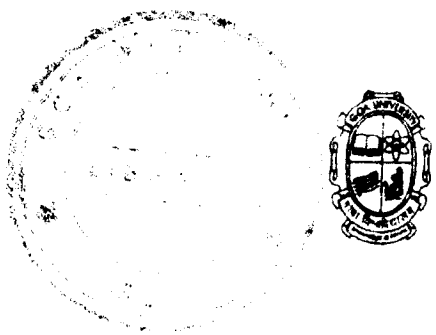

April 2008

DECLARATION

I, Shri S. D. Gokakakar, hereby declare that this thesis entitled "Photochemial conversions using synthetic metalloporphyrins as photocatalysts" for the degree of doctor of philosophy in Chemistry is the outcome of my own study undertaken under the guidance of Dr. A. V. Salker, Department of Chemistry, Goa University. It has not previously formed the basis for the award of any degree, diploma or certificate of this or any other University. I have duly acknowledged all the sources used by me in the preparation of this thesis.

Place: Taleigao-plateau

Date: 28.04.2008

S. D. Gokakakar

(Candidate)

EXAMINED BY

22/10/08

22.10.08

CERTIFICATE

This is to certify that the thesis entitled "Photochemial conversions using synthetic metalloporphyrins as photocatalysts" submitted by the candidate Shri. S. D. Gokakakar, for the award of the degree of Doctor of Philosophy in Chemistry is based on the literature survey / laboratory experiments carried out by him during the period of study under my guidance. I further state that the research work presented in the thesis has been carried out independently by him and due acknowledgement has been made whenever outside facilities has been availed of.

Place: Taleigao- plateau

Date: 28.04.08

Dr. A. V. Salker,

Research Guide,

Department of Chemistry

Goa University.

Acknowledgement

I am really indebted to Dr. Arun V. Salker for being a constant source of knowledge, guidance and cooperation during this research work.

I express my sincere thanks to Dr. J. B. Fernandes, Head and Dr. K. S. Rane, former Head, Department of Chemistry for extending access to all facilities required from time to time.

I am extremely grateful to the University Grants commission (UGC) for sanctioning me a study leave for two years under Faculty Improvement Programme (F. I. P.) during tenth plan.

I express my sincere appreciation for Shri Ravi S. Naik, President of P. E. S. Society, Dr. A. S. Dinge, Principal, management members and other staff members of P. E. S. S. R. N. S. College of Arts and Science, who have encouraged me for the successful completion of this research work.

I would like to thank Dr. B. R. Srinivasan, Dr. S. G. Tilve, Dr. V. M. S. Verenkar and Dr. V. S. Nadakarni, from the Department of Chemistry, Goa University, for their kindly suggestions and help required from time to time. It is also my pleasure to thank non-teaching staff members of the Department of Chemistry Goa University.

My special thanks are to Dr. M. N. Kulkarni, Dr. A. V. Deshpande, Dr. S. H. Bhosale Dr. B. L. Malik and Dr. R. G. Shetkar for their varied help as and when required.

It is my privilege to express my sincere thanks to Dr. Gundurao, IIT Mumbai, Dr. Rajmohan, NCL, Pune, Dr. Parameshvaran, NIO, Goa, Shri P. K. Ajikumar, IGCAR, Kalpakkam, Tamil Nadu, Sophisticated Analytical Instrument Facility (SAIF), IIT, Mumbai, and M. J. Laboratory, Mumbai for providing instrumental facilities and subsequent relevant discussions.

I am thankful to all research fellows who have helped me directly and indirectly with special emphasis to Shri Ratan G. Mahalsekar, Shri Satish J. Naik, Shri R. S. Narendra Babu, Shri Ashish R. Naik and Shri Mahesh Majik.

I am also thankful to Dr. Konnur, Shri Vikrant Malavankar and other staff members of the library, Goa University for their outstanding help in procuring the variety of papers from different universities in India.

I am profusely thankful to my father, and my Guru, P. P. S. S. Kawade for being the pioneers behind the entire research work. I express a sense of deep appreciation for my wife Mrs. Sampada, daughter Miss Yogini and son Mast Hrishikesh for managing the whole situation efficiently in my absence at home. I express my humble gratitude towards my all family members for their ceaseless co-operation during the course of this research work.

Lastly, the author is solely responsible for any possible errors and shortcomings in this thesis despite the best efforts, to make it immaculate.

Place: Taleigao-plateau

Date: 28.04.2008

(S. D. Gokakakar)

Contents

CHAPTER 1

Introduction

Many industrial and textile processes are releasing large quantities of dyes and pigment wastes in the environment. The demand for azo dyes by the various industries, contribute to the extent of 60-70%. During the course of production and application about 10-15% of the dyes are lost in the environment as coloured effluent wastes[1]. Thus the natural quality of water is degraded and a threat is posed to the environment due to water pollution problems. As far as current legislation regarding waste water is concerned, the majority of the countries undertake the treatment by physical, chemical and biological methods before it is released into environment [2, 3, 4]. The physical methods involve reverse osmosis, flocculation, membrane filtration and adsorption on activated charcoal[5, 6, 7]. Chemical methods involve chlorination, ozonation[8] and degradation with mineralization. Bio-treatment of dyes is less popular because of resistance to aerobic degradation and time consuming. It is also frequently seen that some of the azo-dyes are degraded anaerobically to give aromatic amines which are carcinogenic and further they are degraded aerobically [9, 10]. In azo-dyes the destruction of chromophoric structure is important for the removal of colour. The sulphonic acid groups present in the structure are playing a role of weak auxochrome and increase the solubility of dye in water. Conventional biological treatments are also used to treat the water but due to hazardous effects of reactive dyes on microbial population the efficiency of process is reduced [11]. Under the present scenario of water pollution control, there is a need for clean, non-toxic and fresh water for the welfare of the society. In this connection oxidative degradation processes seem to be promising [12, 13, 14, 15].

There are scanty reports of heterogeneous photocatalysis by organic semiconductor materials and it may be a progressive technology in future in dealing with global pollution problems [16, 17, 18]. In this context, synthetic porphyrins may be of vital importance [19] due to following reasons:

i) They are structurally related to important biologically important compounds (heme, chlorophyll, vitamin B_{12}, cytochrome etc.)

ii) They are powerful chelating agents.

iii) They absorb radiation energy at certain wavelengths, including the visible spectral range, and may act as radiation sensitizers or protecting agents against radiation.

iv) A sulphonated derivative of meso-tetraphenylporphyrin was recently reported to be more selective and found to be very useful in clinical science.

Further, research conducted for several years has proved the versatility of porphyrins in various areas of life. These extraordinarily important compounds can act as catalysts in many chemical reactions; they also play the role of pigments and dyes, semiconductors and photoconductors, analytical reagents and in photodynamic therapy (PDT). In near future they may be used in molecular switches, as active elements of biosensors, elements of selective electrodes, non-linear optical materials, parts of electrochromic displays [20] or special equipment involving solar and conventional energy, also in the synthesis of new types of chemical structures, molecular wires or porphyrin complexes with fullerenes [21].

Among the three parent synthetic porphyrins[22], viz. porphin, tetraazaporphyrin and meso-tetraphenylporphyrin (TPP), it was felt worthwhile to focus on TPP, due to its symmetry in structural aspects and ease in synthesis under normal

experimental conditions. Thus attractive features of TPP have compelled to use it in a wide variety of model studies [23, 24, 25]. When desired metals are substituted in the hole of N_4^{-2} moiety of porphinato ligand, then corresponding compounds are called metalloporphyrins (MTPP). Metalloporphyrins are essentially involved in various fundamental biological processes, such as electron transport, catalysis of redox reactions, storage and transport of oxygen, and photosynthetic energy conversions[26]. This remarkable diversity of functions is achieved by suitable modifications of their basic electronic structure. Especially the electrons located on the central metal atom and its axial ligands play an important role in controlling the catalytic properties of metalloporphyrins [27]. In general, due to a strong perturbation of π system on the porphyrin ring, the occurrence of irregular optical spectra[28] indicates the presence of additional valence orbitals in the porphyrin frontier orbital. The electrons of the central substituent are frequently involved in low-energy excited states of irregular MTPP. This feature makes them promising candidates for photocatalysts, particularly when a redox active metal is coordinated. From the view point of potential applications in photocatalysis and solar energy conversion, light-sensitive coordination compounds of TPP are of particular interest, since they are able to participate in photochemical multielectron transfer reactions[29,30]. Various free-base and metalloporphyrins were synthesized by standard methods[31-35] and in some cases syntheses were based on newly devised methods.

In the present investigations the photocatalytic degradation of azo-dyes such as Amido Black 10B, Methyl Orange and Ponceau S were carried out in aqueous

medium at pH 6, 7 and 10 with the help of solar radiations. Similarly, Rhodamine B, a xanthene type dye was photodegraded in acetone medium. For the degradation of the dyes, the above synthesized porphyrins were used as photocatalys.

The present investigation includes:

1. Synthesis of porphyrins

A) Synthesis of non-aqueous porphyrins

i) Synthesis of free-base TPP

ii) Synthesis of metalloporphyrins (MTPP) such as

a) Cobalt tetraphenylporphyrin (CoTPP) b) Nickel tetraphenylporphyrin (NiTPP)

c) Copper tetraphenyl porphyrin (CuTPP) d) Zinc tetraphenyl porphyrin (ZnTPP)

d) Silver tetraphenyl porphyrin (AgTPP)

e) Tetraphenyl porphinatomanganese(III)chloride (MnTPPCl)

f) μ-Oxo-bis[tetraphenylporphinatomanganese(III) [O-$(MnTPP)_2$]

g) Tetraphenylporphinatoiron(III)chloride (FeTPPCl)

h) μ-Oxo-bis[tetraphenylporphinatoiron(III)] [O-$(FeTPP)_2$]

i) Tetraphenylporphinatotin(IV)chloride ($SnTPPCl_2$)

B) Synthesis of aqueous or water soluble porphyrins

i) Synthesis of free-base tetra sodium meso-tetra(p-sulphophenyl)porphyrin ($TPPS_4$)

ii) Synthesis of metalloporphyrins ($MTPPS_4$)

a) $CoTPPS_4$ b) $NiTPPS_4$ c) $CuTPPS_4$ d) $ZnTPPS_4$ e) $AgTPPS_4$

f) $MnTPPS_4Cl$ g) $FeTPPS_4Cl$ h) [O-$(FeTPPS_4Cl)_2$] i) $SnTPPS_4Cl_2$.

CHAPTER 2

Review of literature

In recent past, the attention has been focused on the use of porphyrin materials as model structures for explaining the general behaviour of the organic solid state, and more particularly on their technological possibilities in various types of devices, electrodes and solid catalysts for dealing with pollution problems or energy generating processes[36,37,38]. The structures, reactivity, and biological functions of metalloporphyrins continue to be the subjects of considerable investigations. Knowledge of interactions between the metal, the porphyrin ring, and associated molecules is of vital importance in an understanding of biological function of metalloporphyrins. Recent crystallographic studies on the structures of metalloporphyrins in the solid phase have shown that there can be considerable geometric flexibility in the conformation of the porphyrin ring and location of the metal atom[39,40,41,42]. This type of information promises to be of great value in disclosing the mechanisms of porphyrin catalysis.

2.1 Synthetic Porphyrins

In synthetic porphyrins, in general, three types of porphyrins are used by inorganic chemists as models for various reactions. viz. octaethyl porphyrin (OEP), meso-tetraphenyl porphyrin (TPP) and meso-tetra(p-tolyl) porphyrin(TTP). Tetraphenyl porphyrin (TPP) is most widely used by porphyrin chemists because of its easy synthesis than OEP. The phenyl groups in the structure favour crystallization of the TPP. In the case of p-substituted phenyl

groups, the shapes of the o- and m-phenyl ^{1}Hnmr signals assist in the assignment of the coordination type[43,44]. Furthermore, the tetraphenyl moiety has a greater π-acceptor capacity than the octaethyl porphyrin. In the present work, we have focused our attention towards TPP, $TPPS_4$ and their corresponding metalloporphyrins with di-, tri-, and tetravalent metal ions as photocatalysts. Therefore, it is necessary to know their salient features with respect to synthesis, structural features, properties and applications.

2.2 Synthesis of porphyrins

The synthesis of water insoluble free-base TPP is carried out by many research workers. Paul Rothemund[45] generalized the synthesis by condensing more than twenty five aliphatic, aromatic and heterocyclic aldehydes with pyrrole in the sealed tubes at 140 °C to 150 °C. The above synthesis was further modified to condensation of benzaldehyde and pyrrole in pyridine solution, in a sealed tube at 220 °C for forty eight hours[46]. Further, Ball et. al.[47] modified the procedure of synthesis by addition of metal salt and the yield of TPP was increased from 4-5% to 10-11%. But the use of a sealed tube and length of time of 22- 48 hours for synthesis, made it inconvenient to synthesize TPP easily. This method was then modified by Adler[31], where a propionic acid was chosen as solvent and refluxing time was reduced to half an hour and the yield of the TPP was found around 20%. Thus, this method proved to be beneficial in all ways with respect to time for synthesis, yield of the product and nature of crystals followed by purity.

When metals are inserted in porphyrin hole by the replacement of two protons in TPP, the resulting compounds are called metalloporphyrins. When metals are divalent, four bonds are formed with four equivalent nitrogen atoms as shown in Fig. 2.2. For tri and tetravalent metals, five and six bonds are formed with central metals as shown in Fig. 2.3 and Fig. 2.4 respectively. The metalloporphyrins were synthesized by Rothemund and Menotti[48] by using TPP as precursor and different solvents with different duration of refluxing time. Further, Dorough et. al.[49] synthesized metalloporphyrins using glacial acetic acid as a solvent. Their synthesis involved porphyrins of divalent metal ions like Co^{+2}, Ni^{+2}, Cu^{+2}, Zn^{+2}, Ag^{+2} etc. Variety of metal porphyrins was also synthesized by Thomas and Martell[50] but it suffered from optimization of refluxing time in general. In all the above methods, it was seen that poor solubility of metal carrier and TPP in the same selected solvent for synthesis. When metal salt was soluble in a solvent, TPP exhibited poor solubility in the same solvent and vice versa. This fact was taken into account by Adler et. al.[32] and they investigated number of suitable solvents which showed maximum solubility of TPP and corresponding metal salts. The solvents used for synthesis were methanol, ethanol, propanol, butanol, phenol, tetrahydro furan, dimethyl sulfoxide and N, N' dimethyl formamide. Among these solvents dimethyl formamide showed higher solubility of TPP i.e. 1g /100mL with high dielectric constant. The refluxing reactions were completed within 10 minutes with the exception for $SnTPPCl_2$. For Sn(IV) and Mg(II) porphyrins, the synthesis took more than two and half hours. This method was equally applicable for the synthesis of trivalent and tetravalent metals Fe^{3+}, Cr^{3+},

Mn^{3+}, Sn^{4+}, alkali metal porphyrins like Ba^{2+}, Ca^{2+} meso-tetraphenyl porphyrin, proto, hemato, deuteron, meso, phyllo, rhodo and meso-tetra(p-methyl)phenyl porphyrins. This reaction medium has also proven very convenient for the kinetic study of these reactions. With regards to the synthesis of non-aqueous dimers, it was observed by Fleisher et. al.[33] that in alkaline medium monomers MnTPPCl and FeTPPCl undergo dimerization to form [O-$(MnTPP)_2$] and [O-$(FeTPP)_2$] respectively. These dimers were further isolated in the form of solids.

Water soluble porphyrins were synthesized to improve upon the limitations produced by non-aqueous porphyrins of TPP. Due to insolubility of TPP and its metalloporphyrins in water, the study of physicochemical properties and oxidation-reduction reactions was hampered[51,52]. Therefore, attempts were made to synthesize aqueous porphyrins by substituting ionized groups to the porphyrin molecule. Fleischer[53] synthesized meso-tetra (4-pyridyl)porphyrin and some metal complexes with nickel, copper and zinc. The efforts were further carried on by various research workers[54,55] where carboxylic, sulphonic and N-methylpyridyl groups were substituted to convert TPP into water-soluble porphyrins. This theme of synthesis made Fleischer[33] to report tetraammonium tetra(p-sulphonyl)porphyrin followed by $TPPS_4$, $FeTPPS_4Cl$ and [O-$(FeTPPS_4)_2$]. The synthesis of $TPPS_4$ by this method proved that it was a tetra sulphonated but tri sodium derivative and was a cumbersome method. Contemporarily, Pasternack et al reported synthesis which was devised by Menotti and further developed by Winkleman et. al.[56] of tri sulphonated derivative ($TPPS_3$), tetraphenyltetracarboxyporphyrin (TCPP)[57], and tetra(N-methyltetrapyridyl)porphyrin(TMPyP). It was also observed that $TPPS_3$ and TCPP

contain negatively charged groups on their periphery while TMPyP contains positive groups at these positions. It was also shown that the nature of charge of the peripheral groups had a very large effect on the acidity and basicity of the porphyrin and more particularly, of the pyrrole nitrogens. Further, it was concluded that cationic porphyrins (TMPyP and TPyP) were considerably less basic than the anionic porphyrins ($TPPS_3$ and TCPP). Similarly, for meso- substituted porphyrins, the anionic porphyrins aggregate in water while the cationic porphyrins do not[58]. The more simplified version of synthesis of tetrasodium meso-tetra (p-sulphophenyl)porphyrin ($TPPS_4$) was devised and reported by T. S. Srivastava and M. Tsutsui[34]. This was confirmed by UV-vis spectroscopy, infrared spectroscopy and ^{1}Hnmr spectroscopy. This method involves long duration for synthesis but confirms the product accurately. Similarly by virtue of the method, it involves water of crystallization i.e. a hydrated free-base porphyrin. Recently, the newly synthesized water soluble free base porphyrins are reported[59], where substitution of Br, OH, is observed. It is also observed that porphyrins are synthesized by substitution of Br and SO_3H or OCH_3 and SO_3H on the same phenyl ring. In addition to above mentioned methods of synthesis of metalloporphyrins[33,53] the attempts were done by other research workers. Cheung et. al.[60] synthesized $CuTPPS_4$ and $ZnTPPS_4$ to study the rates of incorporation of Zn^{2+}, demetallation of Zn^{2+} and displacement of Zn^{2+} in $ZnTPPS_4$ by Cu^{2+} ions. Further, Corsini et. al.[61] studied the reactivity of $TPPS_4$ with variety of metals in the periodic table. They had the conclusion that $TPPS_4$ reacts slowly with metal ions and prolonged heating is required for metalloporphyrin formation. The extension of this study made Krishnamurthy et. al.[62] to examine

monomer-dimer equilibrium of water soluble porphyrins as a function of the co-ordinated metal ion. They further found that $TPPS_4$, and its Cu^{2+}, Pd^{2+} and Ag^{2+} complexes undergo dimerization whereas $TPPS_4$ complexes of Zn^{2+}, V^{4+}, Cr^{3+}, Mn^{3+} and Co^{3+} remain monomeric in nature. Horrocks et. al.[63] reported water soluble complexes of lanthanides where $TPPS_4$ ligand formed complexes with Ho, Er, Tm, Yb and Lu respectively. The method of synthesis required an inert atmosphere of dry nitrogen and metal acetylacetonates of corresponding metals.

2.3 Purification of porphyrins

Metalloporphyrins after isolation from the reactions are purified by three possible methods viz. i) adsorption chromatography or column chromatography ii) crystallization, and iii) sublimation[64].

i) Adsorption chromatography or column chromatography

In most of the cases alumina or silica are used as stationary phase and mobile phases may be chloroform, dichloromethane or benzene. If the complex is strongly adsorbed, due to the presence of axial ligands, methanol or solvents of similar polarity have to be added to the eluents. Chromatography generally separates unreacted porphyrin acid, chlorin, metallochlorin etc. The distinction among different components is done on the basis of their UV-vis spectra. In case of difficult separations, silica plates (20 × 100 cm) with an adsorbent layer of 0.5 - 1.0 mm. thickness are very effective[65]. These plates can be loaded with approximately 50 - 200 mg, according to the problems encountered. They are especially useful in separating complexes of very different polarity. Further, dry

column chromatography method was recommended for superior separations of components in a given mixture[66] but it had the disadvantage of separation of isomers in pure state.

ii) Crystallization

It was frequently observed that many porphyrins were not stable in the presence of sunlight or diffused light. In this situation, there was every possibility of decomposition of porphyrins on the column itself. Therefore, in such cases a method of recrystallization was used.

iii) Sublimation

This is another reliable method for the purification of porphyrins. This was tried by Adler et. al.[31] where crude TPP was sublimed using purified nitrogen gas as the carrier. In this method, large, single-crystal needles of TPP of high purity were obtained. Alternatively, TPP was also purified by vacuum sublimation, which gave octahedral or rhombohedral crystals, rather than needles.

2.4 Structural features of porphyrins

The unique nature of chemistry in metalloporphyrins has developed growing interest among chemists. The progress in synthetic porphyrins has shown that the porphyrin moiety is tetradentate but also can act as bi-, tri-, or hexadentate ligand[67-70]. In addition, metal ion has been observed to possess 4-, 5-, 6-, or 8-coordination. These things are of interest because of their obvious relevance as biological models. Metalloporphyrins are studied for other reasons such as the search for new semiconductors, conductors[71], catalysts[72] and chemical shift reagent[73].

Porphyrins like other π-macrocycles have a central 'hole' or 'core' (Fig. 2.1 – 2.6) of fixed size which can be altered by the puckering of the porphyrin macrocycle. The range of the variation of the 'core' has been observed to lie between 2.098 Å and 1.929 Å. In certain complexes the metal ion is unable to fit into this 'hole' and therefore lies out of the porphinato nitrogen plane[74]. It was also observed that the ionic radius of a metal, which is a best–fit for the 'hole' in the moiety of the porphinato ligand was 0.64Å. This selection is based on the metal ion of ionic radius between 0.69 Å [Sn(IV)] and 0.60 Å [Ni(II)] may produce a coplanar MN_4- moiety in a metalloporphyrin and the smaller ions will produce considerable radial strain[75].

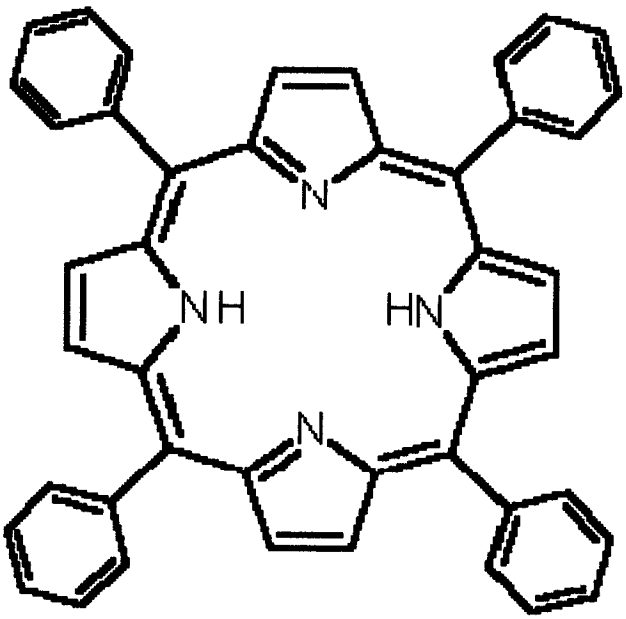

Fig. 2.1 Structure of free-base TPP

(I)

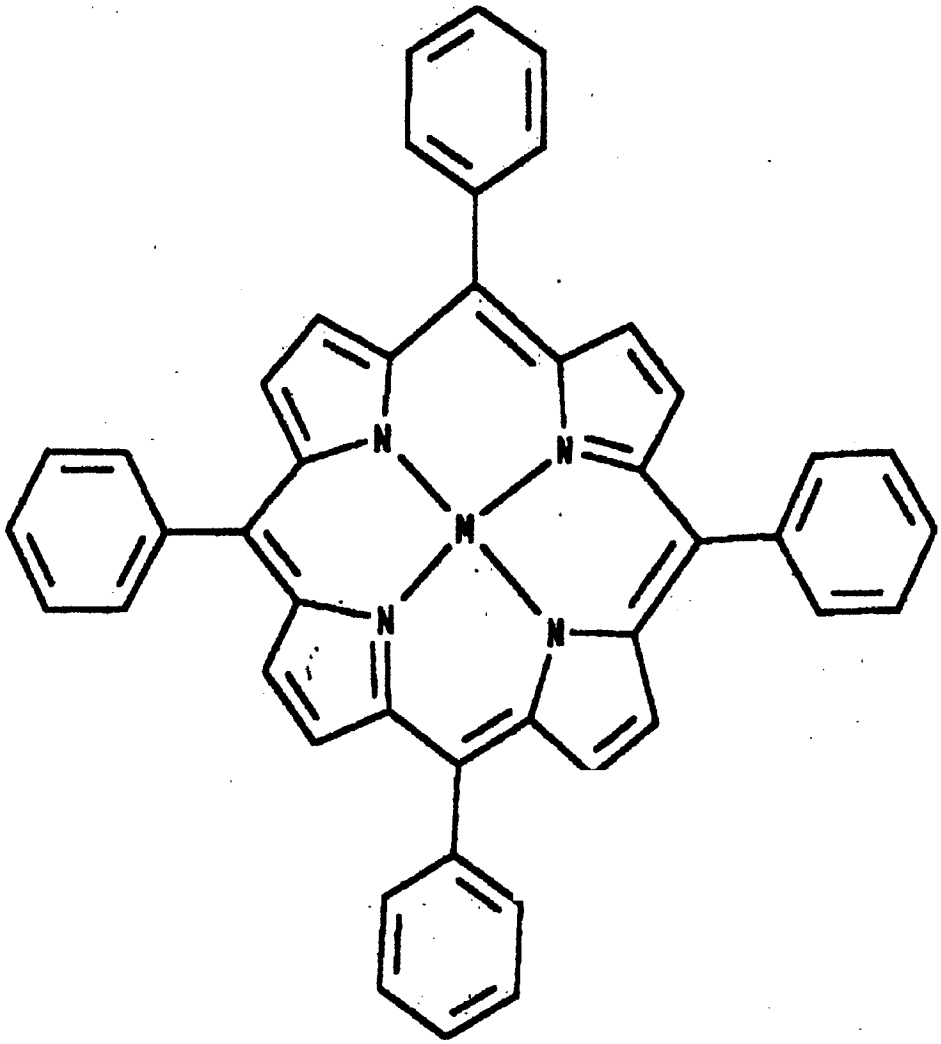

Fig. 2.2 Structure of MTPP, M = Co^{2+}, Ni^{2+}, Cu^{2+}, Zn^{2+}, and Ag^{2+}

(II)

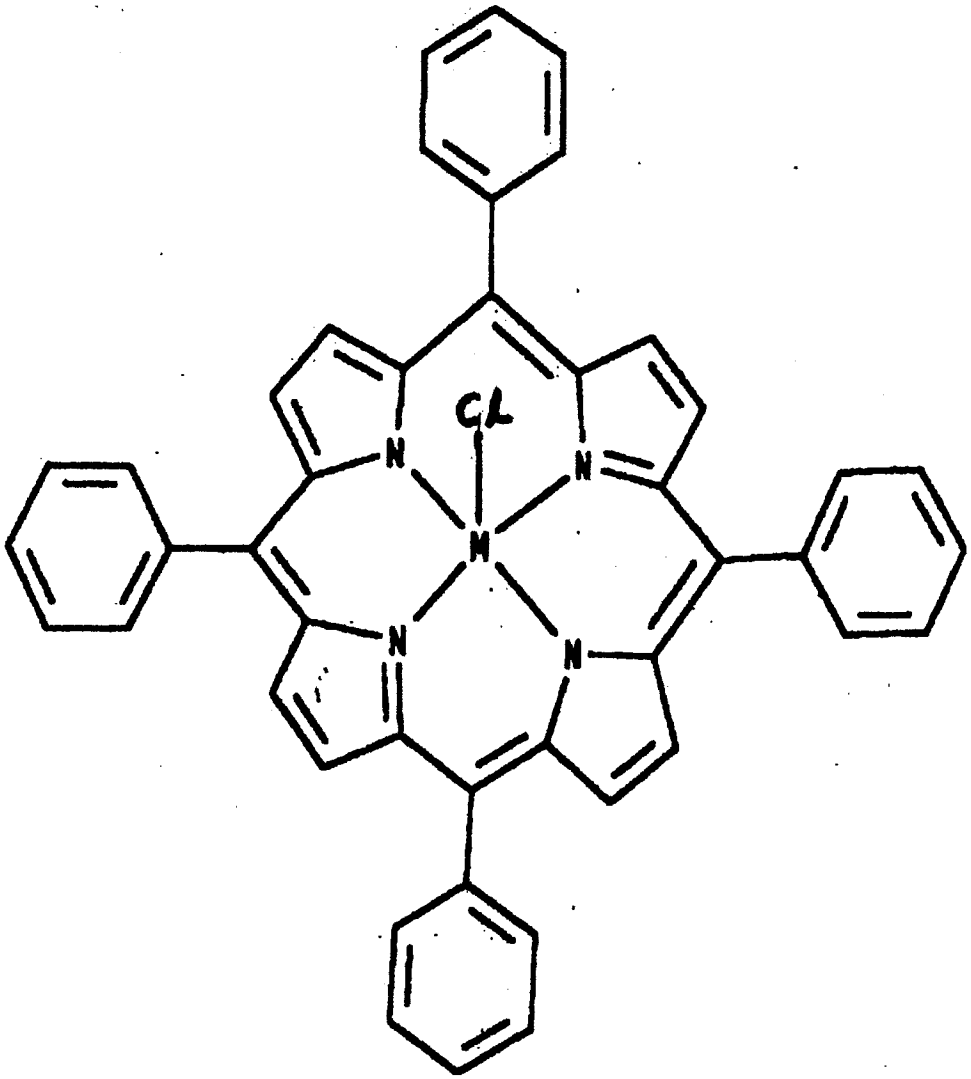

Fig. 2.3 Structure of MTPPCl, M = Mn^{3+} and Fe^{3+}

(III)

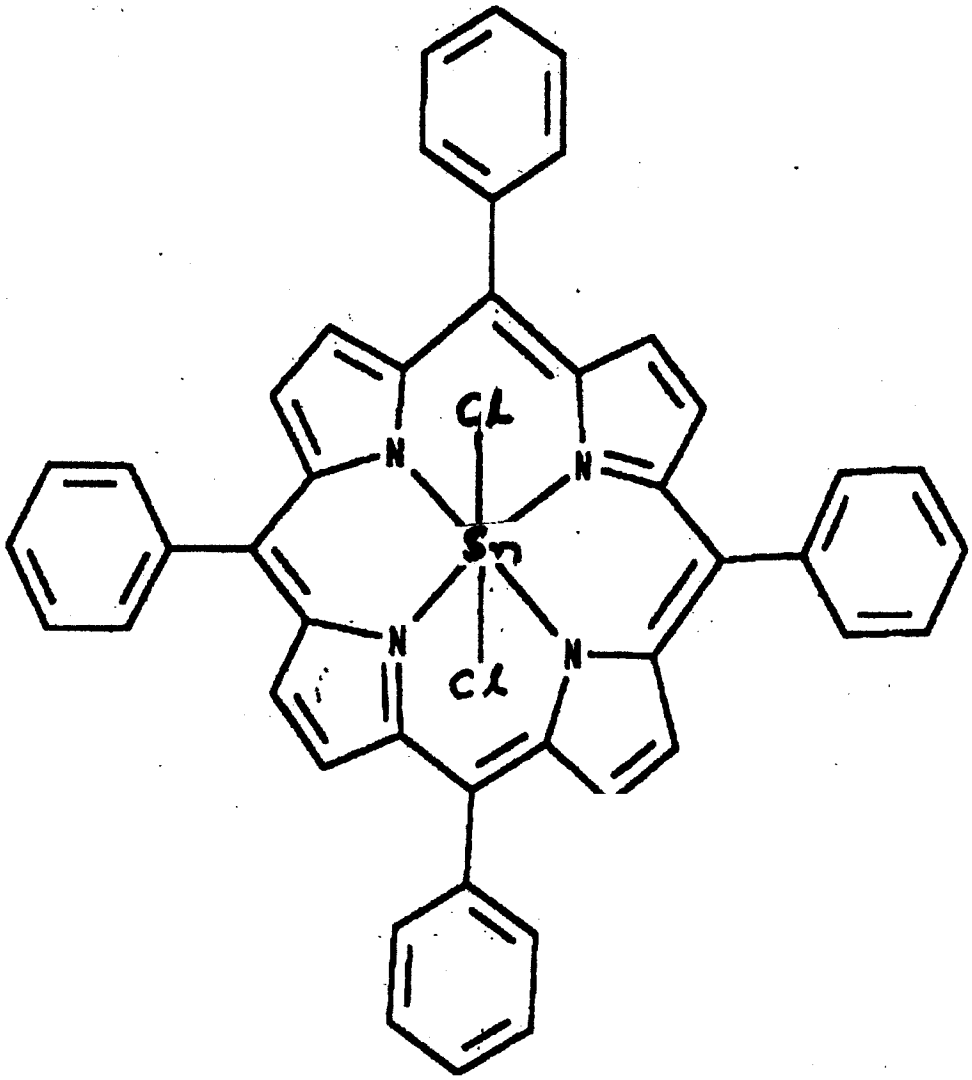

Fig. 2.4 Structure of $SnTPPCl_2$

(IV)

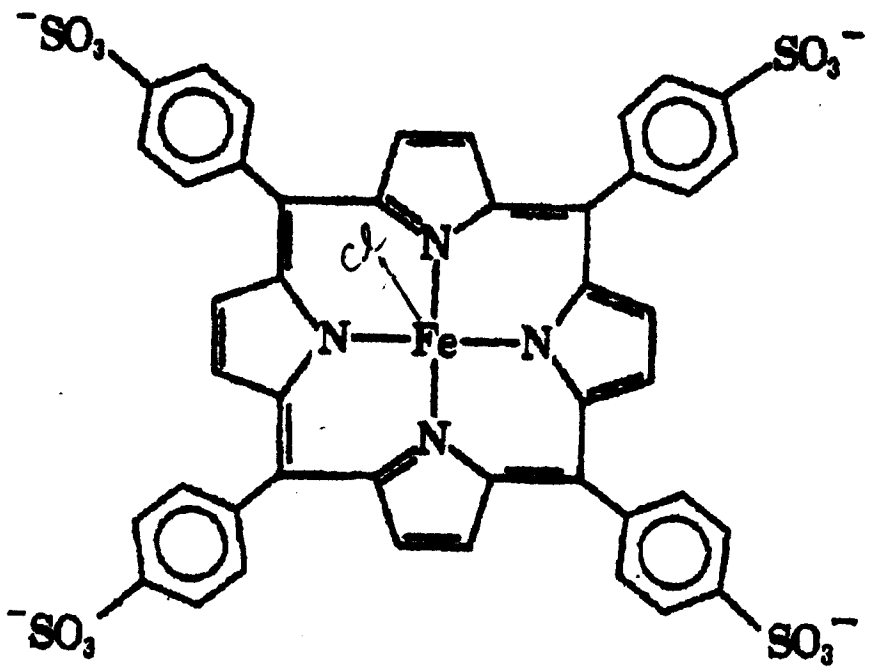

Fig. 2.5 Structure of free-base TPPS$_4$ and Fe-TPPS$_4$Cl

(V)

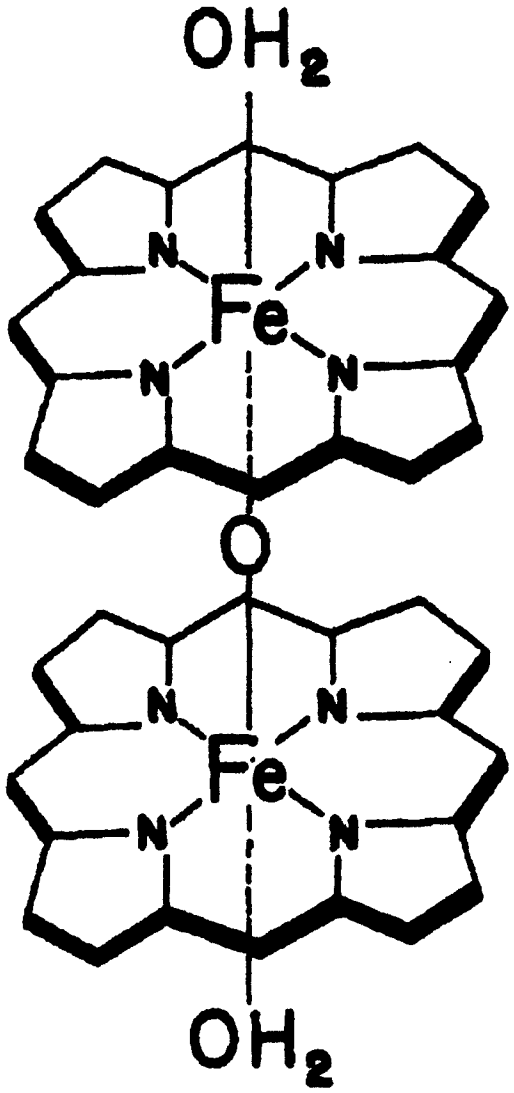

Fig.2.6 Structure of O-$(FeTPPS_4)_2$ dimer, the sulphonated phenyl groups are left out of clarity

(VI)

The basic unit of a free-base TPP [Fig. 2.1] is porphyrin ring which contains four pyrrole rings joined with four methine bridges and forms the conjugated system, which contains 18 delocalized π electrons (4n + 2, where n = 4). The pyrrole rings build up closed aromatic plane, playing the role of a nucleus of the compound. The four phenyl rings are perpendicular to the plane of porphyrin ring. The flat porphyrin ring can be deformed in the process of metalation, where a metal ion replaces the hydrogen atoms in imide groups of pyrrole. The porphyrin ring possesses rectangular geometry with D_{2h} symmetry. When acid is added to TPP it forms dication [$(H_4TPP)^{2+}$] and porphyrin possesses square geometry with four fold symmetry[76].

The process of metalation involves formation of P^{2-} moiety by replacement of two imide hydrogens and substitution of respective metal in the porphyrin core. When divalent metal ions like Co^{2+}, Ni^{2+}, Cu^{2+}, Zn^{2+} and Ag^{2+} are present (Fig. 2.2) then coordination number of metal is four with square planar geometry and D_{4h} symmetry. Thus in this case coordination sphere is completed by balancing the charge on the P^{2-} moiety by divalent metals. In this series of complexes, CoTPP, NiTPP and CuTPP are possessing ruffled cores whereas ZnTPP and AgTPP possess planar cores[77]. The complexes of this type are called four coordinate complexes.

For trivalent metals like Mn^{3+} and Fe^{3+}, central metal forms four bonds with four nitrogens and one bond with Cl to complete coordination sphere. This additional ligand Cl is called an axial ligand. Therefore, MnTPPCl and FeTPPCl

(Fig. 2.3) form five coordinate complexes with square pyramidal geometry. In these complexes, as per X-ray studies the metals are slightly shifted from the center of porphyrin core and are present out of plane of the porphyrin ring.

In case of $SnTPPCl_2$, in addition to tetradentate porphyrin ligand, two Cl ions are present one above and one below the plane of the porphyrin ring. This makes a complex six coordinate with octahedral geometry. Since, two axial ligands are identical; therefore, the complex possesses D_{4h} symmetry[78]. The metal Sn is present in the plane of porphyrin ring (Fig. 2.4).

In the context of water soluble porphyrins, sodium salt of sulphonic acid is substituted at the para- position (4-position) of four phenyl rings in TPP and is abbreviated as $TPPS_4$. Due to its well defined structure (Fig. 2.5) and properties, $TPPS_4$ is widely used in clinical experiments as a potential sensitizer for the photodynamic therapy[79,80,81]. The structural features of $TPPS_4$ and other corresponding metalloporphyrins with Co^{2+}, Ni^{2+}, Cu^{2+}, Zn^{2+}, Ag^{2+}, Mn^{3+}, Fe^{3+}, and Sn^{4+} are identical as mentioned for TPP and its metalloporphyrins.

Further, it was also investigated that dimers of MnTPPCl and FeTPPCl existed in basic medium and the structures have been determined by X-ray diffraction[82,83]. As discussed earlier the Fe^{3+} ions of two porphyrin rings are shifted slightly out of plane and they are bonded through a bridge of oxygen. Therefore, these compounds are named as μ-Oxo- bis[tetraphenylporphinatoiron(III)]. O-$(FeTPP)_2$ and O-$(MnTPP)_2$ μ-Oxo-bis[tetraphenylporphinatomanganese(III)]. These are five coordinate complexes[84] where each porphyrin ring is centrosymmetrically bonded to Fe^{3+}. Similarly, it was also found that $FeTPPS_4$ exist as monomer in

acidic solutions and undergoes dimerization in basic medium at pH greater than 9 to give a dimer, O-$(FeTPPS_4)_2$. This was a six coordinate complex, especially when it contained presence of water of hydration (Fig. 2.6). Further, Krishnamurthy et.al., reported that $TPPS_4$ and its complexes with Cu^{2+}, Pd^{2+}, and Ag^{2+} showed dimerization[62] whereas with Zn^{2+}, V^{4+}, Cr^{3+} Mn^{3+} and Co^{3+} were found in monomeric forms.

2.5 Properties of porphyrins

The porphyrins and their metal complexes are found to possess many interesting properties, which can be investigated by various analytical techniques. The characteristic properties of these molecules include spectroscopic, thermal stability, photoconduction, photoemission and surface activity.

2.5.1 UV-visible spectroscopy

The porphyrins exhibit high molar absorbance coefficients in the order of 10^4-10^6, which becomes their most specific property. This is the reason to make them to be identified by UV-visible spectroscopy[85-89]. On account of strong chromophore in porphyrins, in no way it allows the interference of absorbance bands due to metals. The free-base porphyrins and metalloporphyrins show characteristic spectra.

1) Q bands: There are two visible bands between 500 and 600 nm, which are separated by $\approx$ 1250 cm^{-1}. The lower energy band (sometimes called α) is the electronic origin Q (0,0) of lowest excited singlet state. The higher energy band

(sometimes called β) includes one mode of vibrational excitation[90] and is denoted Q (1,0).

2) B bands: An exceedingly intense band (sometimes called the Soret band) appears between 380 and 420 nm. It is the origin B (0,0) of the second excited singlet state. In this region one more band may be possible and is denoted by B (1,0).

3) N, L, M bands: To the blue of Soret band, metalloporphyrins generally show a weaker N band[91] at ≈ 325 nm and an M band at ≈ 215 nm. Between these bands often L band is present.

The spectra of metalloporphyrins can be classified as "regular" or "irregular depending on whether the metal inside the porphyrin ring has an open or closed valance electron shell[92]. The regular porphyrins show fluorescence e.g. TPP, $TPPS_4$, ZnTPP, $SnTPPCl_2$. The solid state samples are purple in colour and in solution form free-base porphyrins exhibit purple colour whereas metalloporphyrins show wine red colour. In normal type absorption spectra of regular porphyrins there are no or little interactions between the atomic orbitals of metal and π-molecular orbitals of porphyrin ring.

In case of "irregular" metalloporphyrins there are two types of spectra viz. hypso-, and hyper–type. The hypso-spectra show as usual in regular porphyrins but it is only blue shifted. Therefore, it is not recognized as a special case. The porphyrins of metal ions Co^{2+}, Ni^{2+}, Cu^{2+} and Ag^{2+} (i.e. d^6 - d^9 configurations) show hypso-type spectra.

The hyper- type spectra is a consequence of charge transfer and metal ligand interactions. There are two types in this category: p-type and d-type hyper spectra. The p-type hyper spectra are the consequence of charge transfer from the metal p-orbitals to the empty porphyrin π^*- orbitals. The metal ions like Sn^{2+}, Pb^{2+} and Sb^{3+} show this type of spectra. The d-type hyper spectra are seen due to the transfer of charge from filled porphyrin π-orbital to the empty d-orbitals of the transition metals. This process is called ring-to metal charge transfer. The examples of this type of spectra are porphyrins of Mn^{3+} and Fe^{3+} ions (d^1 - d^5 configurations). These types of porphyrins are brown or green coloured in solid state as well as in the solution form[93].

2.5.2 Infrared spectroscopy

The nature of the coordinate linkage in metal porphyrins was investigated by infrared spectroscopy. The weak N-H stretching vibrations above 3300 cm^{-1} for all ligands disappear in the chelates, since acidic hydrogens are replaced by respective metal ion. Replacement of these imino hydrogen atoms results in shifts of many absorption bands of the ligand to both higher and lower frequencies. The main absorption bands of the metal chelates of tetraphenyl porphyrin appear near 1600 cm^{-1} and at lower frequencies. The strong absorption band near 1000 cm^{-1} appears to be a vibration of the porphyrin ring or the pyrrole units, which is sensitive to the nature of metal ion and which is directly related to the strength of the metal-nitrogen bonds in the tetraphenyl porphyrin chelates[94,95,96]. It is also seen that the porphyrin ring and phenyl rings are not coplanar; therefore,

interactions of the substituents at meso- positions with metal-ligand bonds are inductive rather than resonance effect.

When metalloporphyrins are containing axial ligands, the metal-to-ligand vibrations are very characteristic but metal- to-nitrogen vibrations are difficult to recognize. Moreover, many axial ligands have their own characteristic inner vibrations that can be identified besides the porphyrin bands. For example, the metal-ligand moieties involved have the following typical bands: MO-H, 3580 – 3640 cm^{-1}; M = O, 820 – 1100 cm^{-1}; M-O-M, 630 – 900 cm^{-1}; M-O, 450 - 650; M-Cl, 260 - 360 cm^{-1}.

The axial ligands containing triply bonded atoms are, of course, very easily detected: N_3^- (2055 cm^{-1}), NCS^- (2042cm^{-1}), CN^- (2100 cm^{-1}), CO (1891 - 2100 cm^{-1}) etc.

2.5.3 Proton magnetic resonance spectrosopy (^{1}Hnmr)

In the early applications of NMR to porphyrins, ^{1}Hnmr was the most widely used as an analytical tool, and the new structural insights that are resulted were a major reason for the revival of interest in porphyrin chemistry. The first ^{1}Hnmr spectra of porphyrins were reported by Becker and Bradley [96] and by Ellis et. al.[97]. The early survey of a variety of porphyrin structures was carried out by Caughy and Koski[98]. Based on the extensive synthetic work, a series of researches were carried out by Abraham on a number of special aspects of porphyrin behaviour, especially the effects of substitution, the self aggregation in solution, isomerism of porphyrins, and interactions of nucleophiles with the central metal

atom of metalloporphyrins[99]. The effects of meso substitution on the ^{1}Hnmr of porphyrins differ significantly from the effects of β substitution. In addition to being qualitatively different, the changes in chemical shift from meso substituents are quantitatively much larger. The presence of methyl or phenyl group at a meso position, results in a general upfield shift for all outer peripheral protons and down-field shift for the inner N-H protons. This behaviour is consistent with a diminished ring current in the macrocycle[100]. The ^{1}Hnmr studies of porphyrins are classified into two classes, namely, diamagnetic and paramagnetic porphyrins. Free-base porphyrins and metalloporpyrins of. Ni^{2+}, Zn^{2+} and Sn^{4+} are found to be diamagnetic whereas porphyrins of Co^{2+}, Cu^{2+}, Ag^{2+}, Mn^{3+}, Fe^{3+} are paramagnetic in nature. It was also reported that the range of paramagnetic shifts is many orders of magnitude larger than the range of diamagnetic shifts for a given functional group.

2.5.4 Mass spectroscopy

The porphyrins and metalloporphyrins undergo fragmentations in the mass spectrometer which are easily rationalized in terms of normal organic mass spectrometry. In the absence of labile or certain functionalized side-chains, the base (100%) peak is usually molecular ion. The predictable intensity of the molecular ion is particularly useful for molecular weight determination. Mass spectra of porphyrins and their derivatives are best recorded at the lowest possible temperature[101] (usually approx. 200-250 °C). If higher temperatures are used, more opportunity for pyrolysis and fragmentation of the molecular ion is

possible. At very high temperatures (400-800 °C), thermal degradation of the nucleus into monopyrroles is known to occur [102,103]. The intensity of molecular ions in mass spectra of porphyrins has also been used [104,105] in the studies of deuteration (as a general example of electrophilic substitution) of porphyrins, metalloporphyrins and some reduced derivatives.

As is seen in usual mass spectrometry the physical appearance of the molecular ion enables one to ascertain the presence of halogens, metals etc. in compounds. This is useful in the identification of unknown matalloporphyrins because of the general tendency for metal ions not to be lost in fragementation process. Many metalloporphyrins sublime in high vacuum without decomposition[106]. Many others containing neutral axial ligands dissociate on heating. First the axial ligand L, and then, on further heating, the species M(P) or M(P)X appears in the mass spectrum. In these cases, it cannot be decided whether L is really present as an axial ligand or only a crystal solvate molecule. Occasionally, the solid or the vapour of a metalloporphyrin suffers thermolysis, hydrolysis, condensation, or both of the latter alterations. Therefore, it is recommended to rely on the mass spectra only in the straight forward situation. In spite of this fact, mass spectra, serve very well to identify the central metal because the $M(P)^+$ fragment ion is normally the one occurring with the highest intensity in the mass spectrum[106].

2.5.5 Fluorescence spectroscopy

It is generally accepted that the prominent electronic transition of porphyrins and their metal complexes are $\pi - \pi^*$ transitions associated with the porphyrin ring. Most of the luminescence and photochemistry observed from these compounds is associated with the π - π^* states of the porphyrin ring, even though, the lifetimes and reactivities of these states depend strongly on the metal ion incorporated[107]. In general most of the free base porphyrins, chlorins, and related compounds show strong fluorescence at room temperature and in rigid glasses they show fluorescence and phosphorescence. Metalloporphyrins luminescence falls into several categories, which is dependent upon the electronic structure of metal. For free-base TPP, fluorescence λmax and singlet energies are 660 nm and 45 kcal/mol. When metals are containing either empty or full d-shells and form complexes with tetraphenyl porphyrin or octaethyl porphyrin then they show fluorescence at room temperature[108,109] and both fluorescence and phosphorescence at liquid nitrogen temperature. The fluorescence yield tends to decrease with increasing atomic number of the metal as does the phosphorescence. The emission spectra are usually shifted to longer wavelengths as the square-planar metalloporphyrin accepts axial ligands in the fifth and sixth coordination positions [110].

The porphyrins besides fluorescence show three types of emissions.

i) Phosphorescence: Phosphorescent metalloporphyrins show weak fluorescence, that is, $\Phi f < 10^{-3}$, and in many cases no fluorescence at all is observed.

Phosphorescence yields are variable over the entire range from $1 > \Phi p > 10^{-4}$. Phosphorescence lifetimes are short, with $\tau_p < 3$ msec.

ii) Luminescence: Luminescent porphyrins contain paramagnetic metals. These emissions cannot be characterized as fluorescence or phosphorescence because the molecular states are not singlet and triplets. The emission yields are above 10^{-4}, and emission parameters often show strong temperature dependence.

iii) Radiationless emissions: Radiationless porphyrins show at most very weak emission, that is, total emission yields are under 10^{-4}. In many cases no emission at all has been documented [111].

2.5.6 X-ray diffraction studies

It was observed fact that within the accuracy of the experimental data, there exist small differences between naturally occurring porphyrins and the synthetic derivatives. For structural analysis, derivatives of symmetric porphyrins like TPP, OEP, TPyP (tetra pyridyl porphyrin) and Etio (Etioporphyrin) were used. When porphyrin acts as a tetradentate ligand, the symmetry and relative rigidity of the porphinato core are the properties of interest for a wide range of metal ions. The X-ray diffraction technique has been extensively used to determine the bond lengths and bond angles among the different atoms in a given structure. The parent compound TPP has four phenyl rings which are perpendicular to the plane of the porphyrin ring and establishes its non-coplanarity. It is also observed that depending upon the nature of the metal present in porphinato core the coordination number of metal changes and variety of structures are coming into

existence[112,113]. Thus the stereochemistry of the porphyrins is best studied by X-ray diffraction method. Therefore, it is quite rational to consider the stereochemistry as a function of d electron configuration in porphyrin chemistry[114].

i) The d^0 complexes include Mg, Ti, Hf and Zr derivatives. Magnesium porphyrins are of interest because of the importance of chlorophyll in photosynthesis. The large size of the Magnesium ion leads to five coordinate square-pyramidal geometry. In $H_2OMgTPP$[115] the magnesium ion is displaced 0.27 Å from the mean plane. Similarly, the large size of the Hf^{4+} and Zr^{4+} in $(OAC)_2HfOEP$ and $(OAC)_2ZrOEP$ the metal is displaced 1.0 Å from the plane of the nitrogen atoms.

ii) The d^1 complexes has onlyexample of vanadyldeoxophylloerythroetioporphyrin, which is an asymmetrically modified porphyrin[116] closely related to 'chlorophyll **a**'. The V^{4+} ion is displaced from the mean plane of four nitrogen atoms by 0.48 Å.

iii) The d^4 complexes are including the derivatives of Mn^{3+}, which are high spin derivatives with four unpaired electrons. Five coordinate Mn(III) structures include MnTPPCl. The reasons for the displacement of Mn(III) ion out of plane by 0.27 Å are not clear.

iv) The d^5 complexes include the stereochemistry of high spin Fe(III), which are the most thoroughly studied porphyrins. In FeTPPCl, a square-pyramidal complex, the Fe atom is displaced from the plane of four nitrogen atoms by 0.38 Å. The dimer of iron(III) i.e. [O-($FeTPP)_2$] where Fe atom is displaced[117] from the plane is by 0.50 Å

v) The d^6 complexes are containing Co(III), Fe(II), Ru(II), Os(II), Rh(III) in their respective porphyrins. In 2-MeImFeTPP complex, Fe is displaced out of plane by 0.42 Å whereas in ONFeTPP and (acetonyl)CoTPP, the respective Fe and Co are displaced by 0.21 Å and 0.11 Å from the porphyrinato plane.

vi) All cobalt porphyrins i.e. Co(II), are d^7 low spin complexes. The stereochemistry of cobalt porphyrins displays considerable diversity according to the oxidation state and the number of axial ligands. It was observed that in NMeImCoTPP[118] and DiMeImCoTPP[119] the Co(II) ion is displaced out of the porphyrinato plane by 0.14 Å and 0.18 Å.

vii) The d^8 metalloporphyrins have been studied intensively as Ni(II) derivatives. The square-planar coordination is especially stable for this electronic configuration and many low-spin four-coordinate complexes of Ni(II) have been characterized. The examples are NiTPP, NiOEP and NiEtio etc. these complexes are found to be planar or nearly planar with respect to four nitrogen atoms of porphyrin ring.

viii) The d^9 complexes prefer planar geometry. These complexes have little tendency to add axial ligands, and all characterized metalloporphyrins of this group are four coordinate. The examples of this type are, CuTPP, AgTPP etc. The crystals of CuTPP are isomorphous with the PdTPP derivative and accordingly have S_4 symmetry. The Cu-N bond distance is 1.981 Å. The porphinato core is slightly more ruffled than in PdTPP derivative with the methane carbon atoms displaced, + 0.42 Å and – 0.42 Å from the mean plane of the porphyrin nucleus. The crystals of meso-tetra-n-propylporphyrin (CuTPrP) have required C_i symmetry and the porphinato core is essentially planar. As a result, longer Cu-N bonds could be expected in this complex

compared to CuTPP. The crystal structure of AgTPP provides an example of a metalloporphyrin structure in which unequal M-N distances are observed.

ix) The d^{10} complexes of this group are closed shell ions of the main groups of periodic table. The size of the most metal ions of this group tends to be larger than the normal centre to nitrogen distance of the plane of porphyrin ring. The examples of this type are ZnTPP, PyZnTPyP, $H_2OZnTPP$, ClO_4ZnTPP, $SnTPPCl_2$ and $SnOEPCl_2$ etc. In PyZnTPyP, the Zn (II) ion is displaced 0.33 Å and in ZnTPP there is no displacement of Zn(II) ion from the plane of the porphyrin ring. In $SnTPPCl_2$ due to presence of two axial ligands the expanded porphinato core is seen and Sn(IV) is present at its centre. In $SnOEPCl_2$, the porphinato core expansion is not much as is seen in $SnTPPCl_2$ and Sn(IV) is at the centre.

2.5.7 Diffuse reflectance spectroscopy (DRS)

Diffuse reflectance spectroscopy (DRS) is a more convenient technique to characterize the materials under consideration than UV-Visible absorption spectroscopy, since it can be used in the solid state where an enhanced scattering of light is taken into account. The technique is non-destructive and is used to determine the energy gap (E_g) in semiconductors in optoelectronics[120-123]. A common way of determining band gap from absorption spectra is the percent reflectance (%R) is made function of wavelength and from the corresponding graph E_g is calculated. To arrive at more certain E_g values, the usual spectra are given Kubelka-Munk treatment, which involves intersection between the linear fit and the photon energy axis. This method of calculating E_g is also helpful when

there are erroneous results from usual UV-visible absorption peaks. The absorption peaks are obtained by plotting absorbance as a function of photon energy in electron volts (eV). A more common way of getting E_g is first derivative of absorption with photon energy and finding the maxima in the derivative spectra at the lower energy side[124]. The E_g is associated to the maximum in the spectrum, i.e. where the absorbance has a maximum increase with respect to photon energy. The first derivative method is convenient when the absorption peak dominates the spectrum as is observed in colloidal samples[125]. If the scattering effect is as high as the optical absorption process, it screens the absorption peak and makes calculation of E_g difficult. To avoid the difficulties in obtaining E_g from UV-Visible absorption spectroscopy in dispersed samples, diffuse reflectance spectroscopy (DRS) of dry powders can be performed. DRS values are calculated by plotting %R versus wavelength or Kubelka-Munk transformed reflectance versus photon energy. The latter method of plotting confirms the assignment of E_g with more certainty.

The theory which makes possible to use DRS was proposed by Kubelka and Munk. In the limiting case of infinitely thick sample, thickness and sample holder have no influence on the value of reflectance (R). In this case, the Kubelka-Munk equation at any wavelength becomes:

$$K/S = (1 - R_\infty)^2 / 2 R_\infty \equiv F(R_\infty) \quad \text{---------- (1)}$$

K and S are called K-M absorption and scattering coefficients respectively.

$F(R_\infty)$ is the so called remission or Kubelka-Munk function, where

$R_\infty = R_{sample} / R_{standard}$ [126]

In the parabolic band structure, the band gap E_g, and absorption coefficient α of a direct band gap semiconductor are related through well known equation[127].

$\alpha h\nu = C_1 (h\nu - E_g)^{1/2}$ ----------(2)

Where α is the linear absorption coefficient of the material, $h\nu$ is the photon energy and C_1 is proportionality constant. When the material scatters in perfectly diffuse manner (or when it is illuminated at 60° incidence), the K-M absorption coefficient K becomes equal to 2α. In this case, considering the K-M scattering coefficient S as constant with respect to wavelength, and using the remission function in Eq. (2), we obtain the expression:

$[F(R_\infty)h\nu]^2 = C_2 (h\nu - E_g)$ ----------(3)

Therefore, obtaining $F(R_\infty)$ from Eq. (1) and plotting the $[F(R_\infty)h\nu]^2$ against $h\nu$, the band gap E_g of a powder sample can be determined easily.

A simple diffuse reflectance UV-visible spectroscopic determination was used[128] for screening organic pigments like fringelites or porphyrins, in sediments and fossil specimen. In contrast to common inorganic pigments, like Fe_2O_3, these pigments exhibit well-structured characteristic absorption peaks which allow their recognition.

2.5.8 Electron spin resonance (ESR) studies:

The ESR technique enables one to detect and in many cases to characterize systems with one or more unpaired electrons. In the context of paramagnetic porphyrin system, one or more unpaired electrons may reside either on the π-ligand system or in the central metal atom, or in both. The underlying principle of

ESR depends upon the number as well as the location of the unpaired electrons in a system, thus making the technique very useful in porphyrin radical chemistry [129].

The magnetic moment μ of an unpaired electron is given by

$$\mu = g \beta S \qquad \text{----------} (1)$$

where 'g' is the ratio of the magnetic moment to the total angular momentum, 'S' is the spin angular momentum in units of $h / 2\pi$, and 'β' is the Bohr magneton. In the presence of an external magnetic field H, the component of S in the direction of H is quantized and can have two values $M_s = \pm 1/2$. Thus there are two energy levels $\pm(1/2)g\beta H$, and the frequency of electromagnetic radiation required to induce transitions between the two states is $\nu = (g\beta/h)H$.

The g-value is a dimensionless parameter which can be determined from the experimental ESR spectrum. It is determined solely by the spin and orbital angular momenta of the unpaired electron. In a spherically symmetric environment (S-state) the orbital angular momentum is zero, and the g has the free-spin value 2.0023. In solids, the g-value depends on the orientation of the magnetic field to the symmetry axes of the electric field about the ion, leading to anisotropy in the g-values. A major absorption takes place when the external magnetic field is perpendicular to the symmetry axis (say z), ($g_x = g_y \equiv g_\perp$) and minor absorption takes place if the applied magnetic field is parallel to the symmetric axis ($gz \equiv g_\parallel$). This situation is observed in most of the metalloporphyrins since the square-planar ligand field possesses an axial symmetry. When the environment is orthorhombic, one observes three different g-

values in the solid state. With solutions where the tumbling motions of molecules produce an average electric field, only a single g-value, i.e. $g_{avg} = 1/3\ (g_x + g_y + g_z)$ or $g_{avg} = 1/3(2g_{\perp} + g_{\parallel})$ is observed. The g-value is characteristic of the metal ion, its oxidation state and its molecular environment[130,131,132].

It is to be noted that if the electron spin and the nuclear spin are parallel prior to an ESR transition, they will be antiparallel after the transition and vice versa. A splitting of an ESR line due to interaction between the nuclear spin and the electron spin of the same atom is known as hyperfine splitting. The number of hyperfine splitted lines is given by the total number of orientations of the nuclear spin, i.e. (2I + 1). These lines are equally separated with a spacing of 'A' called as hyperfine splitting constant. If there are n equivalent nuclei of nuclear spin 'I', then the number of lines obtained[133] is (2nI +1). An important characteristic of Fe(III) porphyrins is that they do not give any ESR spectra at room temperature because the spin-lattice relaxation times are very short. Therefore, for a reasonably good ESR spectra are obtained at liquid nitrogen temperature and sharper and more intense lines are observed at liquid helium temperature.

Co(II) porphyrins are extensively studied by ESR because of their importance in oxygen adsorption. The three distinct types of ESR spectra of Co(II) are i) the adducts of Co(II) porphyrins with π-acceptors ii) the complexes of Co(II) porphyrins with Lewis bases (generally a five coordinate complex) iii) the molecular oxygen adducts of Co(II) porphyrins[134].

Copper porphyrins are most extensively studied and best understood class of metalloporphyrins. There are two reasons for this: i) they can be studied at room temperature and ii) it is simpler to interpret the electronic structure of d^9 system[135].

Silver porphyrins were not studied as extensively as copper porphyrins because of uncertainties in interpretations and experimental difficulties. The careful study of AgTPP in TPP single crystals[136] provided some reliable data.

2.5.9 Magnetic studies

The aim of magnetic susceptibility measurements of metalloporphyrins is to confirm or establish the oxidation state of the metal ion and to find if any peculiar magnetic interactions are present[137]. The experimental distinction between high-spin and low-spin complexes is based on the determination of their magnetic properties. Complexes are classified as diamagnetic if they tend to move out of a magnetic field and paramagnetic if they tend to move into a magnetic field. The extent of the paramagnetism of a complex is commonly reported in terms of the magnetic dipole moment it possesses. If higher the magnetic dipole moment of the complex, the greater the paramagnetism of the sample is observed[138]. For his purpose, μ_{eff} is compared with the 'spin only' value computed from the equation $\mu_{so} = \sqrt{N(N+2)}$, where N is the number of unpaired electrons. Many tabulations show the range of μ_{eff} values to be expected from a particular magnetically dilute

metal ion in a given environment. More information can also be obtained from susceptibility measurements at low temperatures and high field strengths, using single crystals. The susceptibility of solids or solutions can be measured on large scale by Gouy method when sample size is greater than 100 mg. The Faraday method, however, is more useful for porphyrin studies, where only a limited amount of solid material is available i.e. less than 5 mg. Balances for measurements from ambient temperatures to 77 °K can be inexpensively constructed[139,140]. Either method requires a standard of known susceptibility and $Hg[Co(SCN)_4]$[141] has been most widely used. Different groups of research workers[142] have shown that the temperature dependence of the susceptibility of this complex when measured by the Faraday method differs from that obtained by the Gouy method. Many workers determine metalloporphyrin susceptibilities in solution by Evans PMR method[143,144]. The shift of a proton resonance line of an inert reference substance due to a paramagnetic species given by $(\Delta H / H) = (2\pi/3)\Delta\kappa$, where $\Delta\kappa$ is the change in volume susceptibility. The same precision[145] in the measurement of the paramagnetic susceptibility can be obtained by a PMR study on 50 mg of material at 60 MHz where Gouy method requires 400 mg of the sample. Further, it is an observed fact that magnetic susceptibility measurements are routinely used by chemists to probe the stereochemistry and electronic state of metal ions in coordination compounds.

The magnetic susceptibilities of FeTPPCl and $[O\text{-}(FeTPP)_2]$ were determined by Faraday method[146] at 293 K, 194 K and 77 K respectively. The magnetic susceptibility of FeTPPCl follows the Curie-Weiss law. This indicates iron has a

spin of 5/2 and is in a high spin state. This has been observed for other Fe(III) porphyrins[147]. The dimer's magnetic properties definitely indicate an antiferromagnetic interaction between the two iron ions of the dimer. The magnetic susceptibility values were determined for MnTPPCl, [O-$(MnTPP)_2$] by Faraday method whereas for $FeTPPS_4$ and [O-$(FeTPPS_4)_2$], Evan's method was used. It was also seen that the water-soluble porphyrins of Fe(III) showed higher magnetic moment than carefully dried porphyrins. This has differentiated between the structural aspects of hydrous and anhydrous porphyrins[33].

2.6 Thermal studies

Edwards et. al.[148] determined the heats of sublimation for both porphyrins and phtahalocyanines. It was also revealed that these values of heats of sublimation were higher in magnitude for the above compounds and it certainly reflected upon the relatively strong interactive tendencies of these structures seen in so many of their other physical properties[149]. A series of porphyrin polymers containing different groups was synthesized and studied[150] using TG, DSC, and FTIR. The thermal behaviours including the possible conformation transition and phase transition of porphyrins were studied during the heating process at lower temperature. It was observed that porphyrins with spacer groups exhibited higher thermal stability than that without spacer group.

2.6.1 Photocatalytic studies

The heterogeneous catalysis is one of the powerful techniques which can be employed for the total oxidation of organic and inorganic water pollutants and various dyes used by different types of industries. The photoassisted catalytic decomposition employing semiconductors has been a promising method for the same purpose[151,152,153]. The main steps which can be envisaged in a photocatalytic processes are[154] :

i) Photogeneration of electron-hole pairs and their trapping by suitable reducible-oxidable species to avoid recombination;

ii) Chemical transformation of these species into suitable products and their separation (desorption) from the reacting media;

iii) Restoration of the initial conditions to photocatalysts

The photolytic process may occur with any type of solids but more favourably with semiconductors. The only condition is the formation of species containing chromophore groups and the use of suitable light irradiation. When semiconductors solids are used, the redox reaction mechanisms, specific for the semiconductors, may mix up with photolytic processes. Many different photocatalysts have been used in the field of photocatalysis. Among the various inorganic semiconductors TiO_2, ZnO ,CdS and SnO_2 are widely employed as photocatalysts for the degradation of variety of environmental contaminants due to their high photosensitivity and large bandgap, i. e. high driving force for

reduction and oxidation processes respectively[155,156,157]. Despite the positive aspects of these photocatalysts, there are some drawbacks associated with their use: i) the combination of charge carriers occurs within nano seconds and ii) the band edge absorption threshold does not allow the utilization of visible light[158]. To overcome these difficulties, many strategies have been proposed to improve the light absorption features and lengthen the carrier life time characteristics of the photocatalysts. It has been observed that the photocatalytic activity of a catalyst can be influenced by crystal structure, surface area, size distribution, porosity, bandgap and surface hydroxyl group density[159]. Further, it is also proposed that the rate of photo-oxidation of organic compounds on the surface of a catalyst is confined by the rate of electron transfer to molecular oxygen. It was also reported that a modification of the catalyst surface by incorporation of noble metals can increase the efficiency of photoassisted oxidation. Another approach to increase the efficiency of charge separation involves bringing the contact of one semiconductor particle with another semiconductor[160].

In semiconductors the highest occupied and lowest unoccupied bands are important. The highest occupied band is called valence band whereas lowest unoccupied band is called conduction band. The difference of energy between these bands is called bandgap energy 'E_g'. Semiconductors can be made more conductive by addition of electrons into conduction band or by removal of electrons from valance band. When an electron is removed from a valence band 'a positive hole' or simply a hole is created, which can be taken as a mobile entity. Thus electric current can be carried either by electrons in the conduction band or

holes in the valance band, or by both types of charge carriers. Mobile charge carriers can be generated by three different mechanisms:

i) Thermal excitation where a sufficiently small amount of thermal energy can promote electron from valence band to conduction band.

ii) The absorption of light radiations promotes electron from valence band to conduction band provided that $h\nu > E_g$ and

iii) By doping new energy levels are introduced into the bandgap. This brings about two types of semiconductors, n-type and p-type. For n-type doping, occupied donor levels are created very near to the conduction band edge and current is mainly carried by negative charge carriers. Similarly, in p-type doping empty acceptors levels are formed near the valence band, creating positive charge carriers. The current is carried by positive charge carriers.

The various inorganic semiconductors acting as photocatalysts are used of which TiO_2, ZnO and CdS are employed very widely. The bandgap energies for the corresponding semiconductors are 3.2 eV, 3.2 eV, and 2.4 eV respectively. In the context of photodegradation of several dyes different research workers have made attempts in different directions by varying experimental conditions.

Qumar M et. al.[161] carried out phothcatalytic degradation of Amido Black 10B and Chromotrope 2B in aqueous suspensions of TiO_2 under a variety of conditions such as reaction pH, catalyst concentration, substrate concentration and in presence of different electron acceptors such as H_2O_2, $KBrO_3$ and ammonium

per sulphate besides molecular oxygen. Shen-Peng et. al.[162] used Fenton-oxidation process for the degradation of Amido Black 10B. Under optimal conditions 99.2% degradation efficiency was observed in aqueous solution of dye after 60 minutes reaction. It was also seen that, chromophoric group was easier to destruct than the aromatic ring of Amido Black 10B. Degradation of 'Reactive Black 5' (RB 5) by Fenton/UV-C and ferrioxalate/H_2O_2/solar light was carried out by Lucas et. al.[163]. The experiment indicates that RB5 can be effectively decolorized to 98.1% by Fenton /UV-C and 93.2% by ferroxilate/H_2O_2/solar light after 30 minutes. Jian-Qiu Chen et. al.[164] used 'Pelagite', a photocatalyst for the first time to degrade Methyl Orange, where total degradation and decolourization was observed within 120 minutes. Rashed et. al.[165] carried out photocatalytic degradation of Methyl Orange in aqueous TiO_2 under different sources like tungsten halogen, fluorescent light and sunlight. It was observed that the rate of photo-oxidation of a dye depended upon initial dye concentration, irradiation time and irradiation intensity. It was concluded that dye undergo fast degradation with the natural sun light than other two sources. Methyl Orange was degraded in a neutral phosphate buffer solution by means of contact glow discharge eletrolysis (CGDE) by Gong Jianying and Cai Weimin[166]. Based on the analysis of ultraviolet (UV) spectra of the solution and the intermediate products from High Pressure Liquid Chromatography-Mass Spectrum (HPLC-MS), the reaction pathway was proposed. The attack of hydroxyl radicals was considered to be a key step to start the whole oxidation process. Sadik et. al.[167] carried out photodecolourization of Ponceau 4R dye by combination of TiO_2 and UV

irradiation at a pH of 6. The catalytic systems used were UV/TiO_2/$Na_2S_2O_8$ and UV/TiO_2/$NaIO_4$. It was also observed that the most effective catalytic system for the dye decolourization was UV/TiO_2/$NaIO_4$. It was concluded that degradation increases with the increase in dye concentration. Wu and Zhang[168] found that well-crystallized anatase thin films of TiO_2 induced complete degradation of Rhodamin B (RB) dye in water with an initial concentration of less than 0.02 mM after 4-5 hours of illumination under a high–pressure mercury lamp. The RB decayed directly to colourless end products of water and mineral acids. Li et. al.[169] carried out TiO_2 assisted photocatalytic degradation of Rhodamin B dye under visible light irradiation. The degradation intermediates were identified using infra red (IR) spectra, proton magnetic resonance (PMR) spectra, and gas chromatography-mass spectroscopy (GC-MS). The IR and PMR results showed that the large conjugated chromophore structure of RB was efficiently destroyed under visible light irradiation. Byrappa et. al.[170] carried out photocatalytic degradation of RB dye using hydrothermally prepared ZnO. In this regard, actual textile effluent containing RB as a major constituent along with other dyes and dyeing auxiliaries were treated using hydrothermally synthesized ZnO and the reduction in the chemical oxygen demand (COD) of the treated effluent revealed a complete destruction of the organic molecules along with colour removal. Jin-Ming Wu[171] showed photodegradation of RB in water assisted by titania nano-rod thin films subjected to various thermal treatments. It was found that photocatalytic activity of the titania nanorod film is found to increase with an increasing heating temperature up to 450 °C.

Heterogeneous photocatalysis was also effectively used by Sakthivel[159] for the determination of photocatalytic activity of α-Fe_2O_3, WO_3 and CdS deposited on ZnO for the photo-oxidation of dichloro acetic acid in aqueous solution illuminated under medium pressure mercury lamp. The experiment was conducted under following conditions.

i) under continuous purging with molecular oxygen **ii)** in the presence of naturally dissolved oxygen, and **iii)** in the absence oxygen. It was observed that in the presence of oxygen, there was a three fold enhancement in the rate of photocatalytic degradation of dichloro acetic acid. This was explained by an increased scavenging of the photogenerated electrons by O_2. Ollis[172] adopted water purification process by destruction of halogenated hydrocarbon contaminants with the help of TiO_2. This idea was further extended by Piscopo et. al.[173] for photocatalytic degradation of benzamide and para-hydroxy benzoic acid with TiO_2. Borgarello et. al.[174] showed the application of photocatalysis to some of the important environmental problems such as i) the photocleavage of hydrogen sulphide ii) the treatment of wastes, and iii) the photoreduction and recovery of metals on TiO_2. Serpone et. al.[175] used n-type semiconductors such as CdS and TiO_2 for the photocleavage of water, hydrogen sulphide and in the photo-oxidation of alcohols including carboxylate compounds.

2.6.2 Organic semiconductors

In the last 50 years, inorganic semiconductors have offered an interesting ground for investigation of the physics in solid state and also for development of the optoelectronic devices which have become basis of the information technology. So far optoelectronics has been dominated by inorganic materials (Ti, Ge, Si, Ga and As or other III/V or II/VI group compounds) with organics to carry out role of insulators. In the last 20 years, however, conjugated molecules and macromolecules in particular have been proposed as a novel class of semiconductors with technological potential for the treatment of information.

Organic semiconductors are carbon-based materials capable of transporting charged excitations and interacting with visible radiation. For this reason they can replace conventional inorganic semiconductors in optoelectronic devices such as light-emitting diodes (LED), photovoltaic cells and field-effect transistors (FET). Metal-organic compounds offer a wide variety of tools for these materials on account of substitution of carefully designed chemical groups. This also provides the opportunity for transduction of chemical or biochemical interactions into optoelectronic signals, and hence for the fabrication of chemo- and bio-sensors. The organic semiconductors possess very cheap manufacturing cost; cover large area and flexible substrates with an immense freedom for the observation of electronic and optical properties[176].

2.6.3 Porphyrins as photocatalysts

More recently porphyrins are used as model structures for explaining the general behaviour of the organic solid state itself and, more particularly, on their technological possibilities in various types of devices, electrodes, or solid catalysts for dealing with pollution problems or energy generating processes[36, 37, 38].

Hequet et. al.[177] showed the photocatalytic degradation of a pesticide 'atrazine' by porphyrin and phthalocyanine complexes. The study sought to assess an efficiency of the reaction in a mercury lamp reactor and under solar irradiation. These catalysts exhibit particular oxidation activities and the degradation rates have been found different between the semi-conductor and the metallic complexes. It was also observed that these complexes are able to cleave the triazinic ring more efficiently than the titanium dioxide. Mele et. al.[178] carried out photocatalytic degradation of 4-nitrophenol in aqueous suspensions by using polycrystalline TiO_2 impregnated with functionalized Cu(II)-porphyrin or Cu(II)-phthalocyanine. The results indicated that the presence of the sensitizers is beneficial for the photoactivity and suggest an important role of Cu(II). A comparison with similar samples impregnated with modified Cu(II)- and metal-free phthalocyanines showed that the presence of porphyrin is more beneficial both for the decomposition rate of 4-nitrophenol and for the disappearance of nonpurgeable organic carbon (NPOC). The extension of this study[179] was done for the degradation of 4-nitrophenol which contained TiO_2 based

photocatalysts impregnated with metallporphyrins. In this context, the photocatalytic polycrystalline TiO_2 systems were impregnated with sensitizers, i.e. copper, iron or manganese porphyrins and their photoactivity for 4-nitrophenol oxidation compared with that of bare TiO_2. A significant improvement of the photoreactivity was observed in the case of TiO_2 impregnated with copper porphyrin, while only a slight beneficial effect was observed in the case of iron porphyrin. The effect produced by the presence of manganese porphyrin appeared to be detrimental. Kalyanasundaram et. al.[180] carried out the experiment where efficient charge injection from the excited state of a zinc porphyrin to the conduction band of TiO_2 has been observed during the visible light irradiation of TiO_2 electrodes coated with a film of [tetrakis(4-carboxyphenyl)porphinatozinc(II)] (ZnTPPC). The mechanism of charge injection process has been studied in dye-adsorbed TiO_2 dispersions and colloids, using steady-state and time-resolved photolysis techniques. The process was found extremely sensitive to pH. Furuto et. al.[181] showed that oxygen sensing system using triplet-triplet reflectance of zinc porphyrin immobilized in polymer membrane studies by laser flash photolysis. The photosensitizers, zinc tetraphenylporphyrin (ZnTPP), zinc tetrakis(pentafluorophenyl)porphyrin (ZnTFPP), zinc etioporphyrin (ZnEtioP), zinc octaethylporphyrin (ZnOEP), zinc tetrabenzoporphyrin (ZnTBP) were suitable for oxygen sensing.

2.6.4 Mechanism

When energy of a photon matches with or exceeds the band gap energy E_g in a semiconductor then the electron from valence band is excited to conduction

band and hole is formed in the valence band. If this excited electron from conductance band comes to the ground state then it combines with hole producing heat. Therefore, recombination of hole and electron is prevented by introducing electron scavenger and subsequently photocatalytic activity of semiconductor is enhanced. In the process of dye degradation different groups of research workers have different mechanisms.

1) Rashed et. al.[165] carried out degradation of Methyl Orange on the surface of TiO_2 as below:

$TiO_2 + h\nu\ (UV) \rightarrow TiO_2\ (e_{CB}^- + h_{VB}^+)$

$TiO_2\ (h_{VB}^+) + H_2O \rightarrow TiO_2 + H^+ + OH^-$

$TiO_2\ (h_{VB}^+) + OH^- \rightarrow TiO_2 + OH^\cdot$

$TiO_2\ (e_{CB}^-) + O_2 \rightarrow TiO_2 + O_2^{\cdot-}$

$O_2^{\cdot-} + H^+ \rightarrow HO_2^\cdot$

$Dye + OH^\cdot \rightarrow$ degradation products

It was also seen that resulting $OH^\cdot$ radical, being a very strong oxidizing agent (standard redox potential +2.8V) can oxidize most of methyl orange dye to the mineral end-products.

2) Byrappa et. al.[170] showed photodegradation of aqueous solution of Rhodamine B on the surface of ZnO as shown by

$ZnO + h\nu \rightarrow ZnO^*$

$ZnO^* + H_2O \rightarrow ZnO^* + H^+ + OH^\cdot$

$OH^\cdot$ + dye molecule $\rightarrow$ intermediates $\rightarrow CO_2 \uparrow + H_2O$ + mineral acids

This proposed reaction mechanism was also supported by the fairly high positive values of the free energy of activation and enthalpy of activation which indicated that the transition state was highly solvated. While the small value of entropy of activation ΔS^* suggested that the intermediate complex was less ordered than the reactants, which supported higher degree of the dye molecule into simple products.

3) For photodegradation of Methyl Orange on ZnO, Daneshvar et. al.[182] proposed the following reaction mechanism.

The high oxidative potential of the hole (h^+_{VB}) in the catalyst permits the direct oxidation of the dye to reactive intermediates.

h^+_{VB} + dye $\rightarrow$ $dye^{\cdot+}$ $\rightarrow$ oxidation of the dye

Another reactive intermediate which is responsible for the degradation is hydroxyl radical ($OH^{\cdot}$). It is either formed by the decomposition of water or by reaction of the hole with OH^-. The hydroxyl radical is an extremely strong, non-selective oxidant (E° = +3.06 V) which leads to the partial or complete mineralization of several organic chemicals.

$h^+_{VB} + H_2O \rightarrow H^+ + OH^{\cdot}$

$h^+_{VB} + OH^- \rightarrow OH^{\cdot}$

$OH^{\cdot}$ + dye $\rightarrow$ degradation of the dye

4) The Fenton reaction system is based on the capture of a photon by a ferric hydroxyl with its conversion to a ferrous ion plus a hydroxyl radical[183]. This

reaction can be energized by photons from the ultra-violet into the violet and blue. The ferrous ion can be oxidized by molecular O_2 to restore the original ferric complex.

$Fe(OH)^{++}$ + photon $\rightarrow$ Fe^{++} + $OH^{\bullet}$

$Fe^{++} + H_2O_2 \rightarrow OH^{\bullet} + Fe(OH)^{++}$

Target molecule + $OH^{\bullet}$ $\rightarrow$ reaction products

Two $OH^{\bullet}$ radicals are generated for each H_2O_2 and for each photon absorbed, two H_2O_2 are needed to oxidize one carbon atom to CO_2

CHAPTER 3

Experimental Techniques

The tetraphenyl porphyrin (TPP), Tetrasodium meso-tetra(p-sulphophenyl) porphyrin ($TPPS_4$) and their corresponding metalloporphyrins with di, tri and tetravalent metals are found to be low band gap semiconductors. Further their photo catalytic activity was studied employing heterogeneous catalysis with solar radiations. The temperature range observed during the course of photolysis was 30 °C to 38 °C. Respective porphyrins were synthesized, purified, characterized using suitable methods and employed for photodegradation reactions.

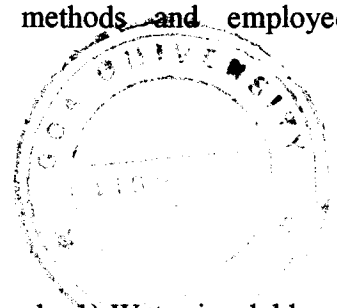

3.1 Synthesis of porphyrins

The two different series of porphyrins were synthesized 1) Water insoluble or non-aqueous porphyrins 2) Water soluble or aqueous porphyrins. The metals used for synthesis of metalloporphyrins of both the series were M = Co, Ni, Cu, Zn, Ag, Mn, Fe and Sn.

3.1.1 Water insoluble or non-aqueous porphyrins

In this context the tetraphenyl porphyrin (TPP) and its metalloporohyrins (MTPP) with above mentioned metals were synthesized. This involves following two steps :.

a) Synthesis of TPP and b) Synthesis of metalloporphyrins (MTPP).

a) Synthesis of TPP

The free base tetraphenyl porphyrin (TPP) was synthesized by suitable method [31]. Equimolar quantities of AR grade pyrrole and bezaldehyde were refluxed in propionic acid for half an hour. The reaction mixture was cooled and washed with hot methanol followed by hot water. The product was completely dehydrated and dried in a vacuum

desiccator for more than two hours. The purple shiny crystals of TPP were obtained with 17% yield. Purification of TPP was carried out using dry column chromatography. TPP was dissolved in AR grade $CHCl_3$ and silica gel (100-200 mesh) was added. The mixture was thoroughly stirred and the excess of $CHCl_3$ was evaporated on water bath. At this point, the silica becomes free flowing which is then loaded on the column of 45 cm ×3 cm diameter, already containing silica gel (100-200 mesh). The top of the column was covered with cotton and AR grade $CHCl_3$ was used as a mobile phase. At a time 1 g TPP was purified. The impurity of tetraphenyl chlorin (TPC) remains at the top and entire TPP gets eluted in the course of time. The recovered yield of purified TPP was found around 90%. The purity of TPP was checked on thin layer chromatography (TLC) using petroleum ether and chloroform (80%: 20%) and found to be pure.

b) Synthesis of metalloporphyrins (MTPP)

The above purified TPP was used to synthesize metalloporphyrins (MTPP) by suitable method [32]. The divalent metals used were Co, Ni, Cu, Zn and Ag. During the synthesis of metalloporphyrins of cobalt tetraphenyl porphyrin (CoTPP), Nickel tetraphenyl porphyrin (NiTPP), Copper tetraphenyl porphyrin (CuTPP), Zinc tetraphenyl porphyrin (ZnTPP) and silver tetraphenyl porphyrin (AgTPP) the salts of metals in more than double the amount of stoichiometry was used and refluxed with dimethyl formamide (DMF) at 153 °C. All reactions were refluxed for 10-15 minutes. Further, synthesis of metalloporphyrins containing trivalent metals Mn and Fe and tetravalent Sn was carried out by the above method.

The monomers tetraphenylporphinatomanganese(III)chloride (MnTPPCl) and tetraphenylporphinatoiron(III)chloride (FeTPPCl) were synthesized by above mentioned method and the refluxing time for the reactions was modified to more than one hour. The dimer of Mn i.e. μ-Oxo-bis[tetraphenylporphinatomanganese(III)] [O-$(MnTPP)_2$] was synthesized by dissolving purified MnTPPCl in pyridine and then 30% KOH was added. Then the reaction mixture was evaporated to dryness on a steam bath. The alkali was removed by washing the solid with water. This process was repeated for two times. The final dried product was recrystallized from benzene. The crystals were collected and dried in a vacuum desiccator. The dimer μ-Oxo-bis[tetraphenylporphinatoiron(III)] [O-$(FeTPP)_2$] was synthesized using suitable method [33] by dissolving purified FeTPPCl in $CHCl_3$ and adding 25% KOH and the solution was stirred for one hour. The chloroform layer was separated from water layer and further purified by column chromatography. The synthesis of tetraphenylporphinatotin(IV)chloride ($SnTPPCl_2$) was carried out by above method and the refluxing time was extended to three hours for complete insertion of metal. The completion of all the above metallation reactions was confirmed by withdrawing aliquots from time to time and checking spectrophotometrically. Further, the reaction mixture was allowed to cool and then cold water was added as much of the reaction mixture. This was further filtered and dried in a vacuum desiccator. The synthesized CoTPP, NiTPP, CuTPP, ZnTPP and AgTPP were purified by dry column chromatography. For the purification of divalent metal porphyrins the method was modified by introducing gradient elution which comprised of chloroform and petroleum ether (50% : 50%) followed by evaporation of the solvent mixture. NiTPP purification process was repeated twice with the same mobile phase. In CoTPP, CuTPP, ZnTPP and

AgTPP the recovery of pure compounds was more than 90% whereas in NiTPP it was less than 70%. The monomers and dimers of trivalent metals MnTPPCl, O-$(MnTPP)_2$, FeTPPCl, O-$(FeTPP)_2$ and the monomer of tetravalent Sn i.e. $SnTPPCl_2$ were purified by dry column chromatography as mentioned above. The mobile phase was modified to a gradient mixture of chloroform and methanol (50% : 50%). This type of mobile phase was used because axial ligands present in the structure of a molecule are strongly adsorbed on the column which requires sufficiently mobile gradient mixture for the movement of the desired fraction on the column. The purity of above metalloporphyrins was checked on TLC using petroleum ether and chloroform (80% : 20%) and found to be very satisfactory. At a time only 1 g of MTPP was purified.

3.1.2 Water soluble or aqueous porphyrins

The water soluble porphyrins were synthesized by substitution of sulphonic acid groups at the para position of the phenyl rings of TPP and then converted into its sodium salt. The new porphyrin thus obtained is called tetrasodium meso-Tetra (p-sulphophenyl)porphyrin ($TPPS_4$) which is subsequently used as a precursor for the synthesis of all water soluble metalloporphyrins.

a) Synthesis of $TPPS_4$

The synthesis of free-base $TPPS_4$ was carried out using standard methods [34] which was further modified to required experimental conditions. Finely ground pure TPP (0.003mole) and Con. H_2SO_4 (0.5 mole) were refluxed in a two neck flask for eight hours and the reaction mixture was kept aside for forty eight hours without any disturbance. Further, it was diluted with distilled water, heated and lime (CaO) was added until the

solution acquires permanent purple colour. The solution was filtered to remove $CaSO_4$, washed with hot water and the filtrate was concentrated to small volume (150-200 mL). Then concentrated solution of Na_2CO_3 was added and the pH of the solution was adjusted to 8-10. The precipitated $CaCO_3$ was removed by filtration and 90% C_2H_5OH was added periodically. The filtrate was concentrated on the steam bath and further dried in oven at 100 °C for two hours. At this stage, $TPPS_4$ crystals were collected and preserved in air tight capsule on account of its highly hygroscopic nature. Purification of $TPPS_4$ was accomplished by dry column chromatography using basic alumina as the stationary phase. The concentrated aqueous solution of $TPPS_4$ was added to alumina, stirred well and excess of water was removed on the steam bath until alumina becomes free-flowing. Further, it was loaded on the column of above mentioned dimension and covered with cotton plug. The mobile phase selected was a gradient solution[35] of water, methanol and acetone in the ratio 7 : 2 : 1. During the process of elution, only a purple fraction due to $TPPS_4$ was collected and other fractions were rejected.

b) Synthesis of metalloporphyrins ($MTPPS_4$)

The above purified $TPPS_4$ was used to synthesize aqueous soluble metalloporphyrins ($MTPPS_4$) by independently devised methods. The divalent metals used were Co, Ni, Cu, Zn and Ag. For the synthesis of $CoTPPS_4$, $NiTPPS_4$, $CuTPPS_4$, $ZnTPPS_4$ and $AgTPPS_4$ the stoichiometric amounts of $TPPS_4$ and respective metal salts dissolved in ethyl alcohol, were added together with minimum amount of water and the reaction mixture was refluxed on steam bath for half an hour. It was also observed that if metal salts added are more than the stoichiometric amount then the concentration of green coloured dication

$[H_4(TPPS_4)^{+2}]$ was correspondingly increasing. The reason for this may be the reaction between $TPPS_4$ and the acid evolved during the course of synthesis. The synthesis of trivalent metal porphyrin $FeTPPS_4Cl$ and its dimer $[O\text{-}(FeTPPS_4)_2]$ was carried out using method[33] whereas synthesis of $MnTPPS_4Cl$ was done by addition of slight excess of metal salt than stoichiometric requirement in the above procedure. The synthesis of tetravalent metal porphyrin $SnTPPS_4Cl_2$ was accomplished by addition of ten fold excess of metal salt to the aqueous solution of $TPPS_4$ and then above procedure was repeated.

The purification of all above mentioned metalloporphyrins was carried out using dry column chromatography as described above for purification of $TPPS_4$. During the course of elution, the colourless fraction, green coloured fraction and the fraction due to respective metalloporphyrin were collected. The colourless fraction is containing unreacted or excess of metal salt whereas green coloured fraction corresponds to dication $[H_4(TPPS_4)^{+2}]$. Both of these fractions were checked spectrophotometrically and rejected. The fraction due to corresponding metalloporphyrin was checked on the spectrophotometer and selected. In general the recovery of purified metalloporphyrins was found in the range of 80-85%. For divalent metal porphyrins when stoichiometric amounts of metal salts and $TPPS_4$ were used, the yield of the corresponding metalloporphyrins was more than 85% otherwise it was in the range of 50-60%. The tri and tetravalent metal porphyrins required metal salts in excess quantities than stoichiometric requirement. The purity of above metalloporphyrins was checked on TLC using a mixture of methanol, ammonia and petroleum ether in the ratio 5 : 40 : 55. The recovered compounds exhibited satisfactory purity.

3.2 Characterization

The above synthesized free-base porphyrins and metalloporphyrins from non-aqueous and aqueous series were characterized by UV-Visible spectroscopy, infrared spectroscopy (FTIR), proton magnetic resonance spectroscopy (^{1}Hnmr), elemental analysis, mass spectroscopy (MS), high resolution mass spectroscopy (HR-MS), fluorescence spectroscopy, X-ray diffraction technique (XRD), image analysis (IA), thermal studies (TG-DSC), magnetic measurements, electron spin resonance (ESR) and diffused reflectance spectroscopy (DRS)

3.2.1 UV-visible spectroscopy

The UV-visible absorption spectra were recorded for 10^{-4} M and 10^{-5} M concentrations for each porphyrin. The solvents used for non-aqueous and aqueous porphyrins were chloroform and distilled water respectively. The results were recorded using quartz cuvettes of 10 mm width and the wavelength range was selected from 300-800 nm on Shimadzu visible spectrophotometer (model uv/2450uv).

3.2.2 Infrared spectroscopy (FTIR)

The infrared spectra of all solid porphyrins were recorded in the range 4000-400 cm^{-1} on Shimadzu IR spectrometer (model prestige/ 21 FTIR). The respective porphyrin and dehydrated powdered KBr were mixed in the ratio 1 : 100, sufficiently ground to make the mixture homogenous and the results were recorded.

3.2.3 Proton magnetic resonance spectroscopy (^{1}Hnmr)

^{1}Hnmr spectra of non-aqueous porphyrins TPP, CoTPP, NiTPP, CuTPP, ZnTPP, AgTPP, MnTPPCl, FeTPPCl and $SnTPPCl_2$ were recorded in $CDCl_3$ whereas for aqueous- porphyrins $TPPS_4$, $CoTPPS_4$ and $MnTPPS_4Cl$ the solvent used was D_2O. The chemical shifts were recorded with respect to tetra methyl silane (Me_4Si) as a reference material. The NMR model used was Varian 300 MHz spectrometer.

3.2.4 Elemental analysis

The results of elemental analysis of non-aqueous and aqueous porphyrins were recorded on Prostar Varian C, H, N analyzer (model Flash 1112 series EA). TPP and CuTPP from non-aqueous porphyrins and $MnTPPS_4Cl$ from aqueous porphyrins were selected as representative samples.

3.2.5 Mass spectroscopy

The mass spectrum of $MnTPPS_4Cl$ was recorded as relative base peak intensity versus mass to charge (m/e) ratio. The fragmentation pattern of the compound gave the molecular ion peak from which molecular weight and molecular formula of the compound were calculated. The instrument used to record the results was IT mass spectrometer (model Varian 500-MS) with APCI source.

3.2.6 High-resolution mass spectroscopy (HR-MS)

High resolution mass spectrum for aqueous porphyrins $TPPS_4$ and $FeTPPS_4Cl$ were recorded as representative samples of the series. The relative intensity of the base peak versus m/z ratio gave mass spectrum, which gave molecular ion peak and thus molecular weight of a respective porphyrins were determined.

3.2.7 Fluorescence spectroscopy

The fluorescence intensities of non-aqueous and aqueous porphyrins were recorded as a function of wavelength in nm. The excitation wavelengths used for the non-aqueous and aqueous porphyrins were 420 nm and 300 nm respectively. The λ_{max} value for each porphyrin was determined for 10^{-4} M concentration. The results were recorded on single beam Shimadzu spectrofluorimeter (model RF-5301PC).

3.2.8 X-ray diffraction spectroscopy (XRD)

The X-ray diffractograms of TPP and ZnTPP were recorded a representative samples on ITAL X-ray diffractometer using Cu Kά radiation, filtered through Ni absorber, at a scanning rate of 0.1°/min. This was necessary to understand the nature and existing phases in the synthesized porphyrin materials.

3.2.9 Image analysis (IA)

The non-aqueous porphyrins TPP and $SnTPPCl_2$ and aqueous porphyrins $TPPS_4$ and $CoTPPS_4$ were subjected to image analysis for the knowledge of average size of the

particles. The areas of all particles of a given sample were converted into equivalent circular diameter (ECD) and measured in micrometer. The results were recorded on optical microscope from 'Leica' model MPS-30.

3.3 Magnetic susceptibility measurements

The magnetic susceptibility 'χ_g' of all porphyrins was measured in air at room temperature using Gouy method. The magnetic field employed was 8000 Gauss and the single pan analytical balance of DONA was used. Mercury tetra thiocyanatocobaltate(II) {$Hg[Co(SCN)_4]$} was used as a standard material. The sample tube was washed, dried and filled with respective material for each operation. In case of aqueous porphyrins since they are highly hygroscopic filling of the sample is done in air cooled atmosphere. The procedure adopted involved loading the filled sample tube in between two electromagnets of Gouy balance and the readings are recorded without and with magnetic field. The magnetic susceptibility 'χ_g' was calculated as given below.

In the first part of the calculation the tube constant (β) was evaluated and then magnetic susceptibility (χ_g) was obtained using following relation

$\chi_g = \beta \times \Delta W/W$ (χ_g =16.44×10-6 cgs units {Hg $(Co(SCN)_4$}

Where, β = tube constant

$\Delta W = \Delta W_1 + \Delta W_2$ (+ve for paramagnetic and –ve for diamagnetic)

$\Delta W_1 = W_4 - W_3$ and $\Delta W_2 = W_1 - W_2$

Where,

W_1= weight of the empty tube (without field)

W_2= weight of the empty tube (with field)

W_3= weight of the tube + standard (without field)

W_4=weight of the tube + standard (with field)

$W=W_3-W_1$=weight of the substance

The value of tube constant (β) is then substituted in the above relation to get χ_g .Further, molar susceptibility is calculated by relation

$\chi_m = \chi_g \times$ molecular weight

Where χ_m = molar susceptibility

χ_g = gram susceptibility

The magnetic moment μ effective (μ_{eff}) of the sample is calculated by using following equation.

$\mu_{eff} = 2.84 \sqrt{\chi_g \times T}$ B.M. where μ_{eff} is the magnetic moment and T is absolute temperature.

3.4 Electron spin resonance spectroscopy (ESR)

In the case of paramagnetic porphyrins, one or more unpaired electrons may reside either on the porphyrin ring or in the central metal system, or in both. The basic features of ESR spectra are strongly dependent on the number as well as the location of the unpaired electrons in a system. The ESR spectra of non-aqueous porphyrins CuTPP, AgTPP and MnTPPCl were recorded at room temperature at magnetic field 3000 Gauss. In case of CoTPP, FeTPPCl and O-$(FeTPP)_2$ there were no observable signals at room temperature therefore ESR signals of these compounds were recorded at liquid nitrogen temperature. From aqueous porphyrins, $CoTPPS_4$, $CuTPPS_4$, $AgTPPS_4$, $MnTPPS_4Cl$, $FeTPPS_4Cl$ and O-$(FeTPPS_4)_2$ were used to record ESR spectra. Further, ESR signals were used to calculate g-factor or Lande's splitting factor, number of unpaired electrons

and line width. Hyperfine splitting constant (A) was calculated in case of CoTPP, CuTPP, AgTPP, MnTPPCl and $MnTPPS_4$. The results were recorded on Varian E-112 X-band ESR spectrometer.

3.5 Diffuse reflectance spectroscopy (DRS)

Diffuse reflectance spectra of non-aqueous and aqueous porphyrins were recorded on Shimadzu visible spectrometer (model uv/2450) using wavelength range from 300 to 800 nm and $BaSO_4$ as a reference material. Reflectance data are usually expressed in terms of percent reflectance (%R) which is analogous to percent transmission in absorption spectroscopy. When wavelength in nm was made a function of %R then the spectrum is obtained which was used to calculate band gap energy for synthesized porphyrins.

3.6 Thermal studies

The thermal studies were carried out with reference to a) TG-DSC studies and b) TG-EGA-MS studies.

a) Thermogravimetry-Differential scanning calorimetry (TG-DSC)

These studies for aqueous and non-aqueous porphyrins were carried out in synthetic air and argon atmospheres using NETZSCH-Geratebau Gmbh Thermal Analyser (STA 409 PC) from room temperature to 800 °C. The rate of heating the sample was maintained to 10 °C /minute. TG furnishes information about percent weight loss of a sample and physical processes such as vaporization, sublimation and decomposition. DSC gives information about melting point, loss of ligand and different decomposition

temperatures at different stages. It is also used as a tool for characterization and to distinguish between monomers and dimers. The sample quantity required was 10-15 mg.

b) Thermogravimetry-evolved gas analysis-mass spectroscopy (TG-EGA-MS)

The TG-EGA-MS results were recorded on some selective porphyrins in argon atmosphere from room temperature to 900 °C. The non-aqueous porphyrins like CoTPP, FeTPPCl and $SnTPPCl_2$ and aqueous porphyrins like $TPPS_4$ and $CoTPPS_4$ were selected for the study. For detection of the gases from the sample, the mass spectrometer was calibrated to some desired gases as can be expected from the structure of the compound. During the course of experiment, as the TG process advances, the respective gases are evolved which were subsequently detected by mass spectrometer. The temperature of delivery tube which carries the respective gases to the mass spectrometer was maintained below 125 °C.

3.7 Photocatalytic studies

It was necessary to select the suitable dyes for photodegradation studies in aqueous medium and organic medium. The criterion of suitability for dye was determined based on its self degradation in solar radiations. When it was observed that 10^{-5} M solution of a dye degrades comparatively faster in sunlight without the presence of a photocatalyst, then such dyes were not selected for the studies. The list of water soluble dyes which were tested were 1) Amaranth 2) Amido Black 10B 3) Tartrazine 4) Carmosine 5) Ponceau S 6) Indigo Caramine 7) Xylenol Orange 8) Eriochrome Black T 9) Phenol Red 10) Methylene Blue 11) Rose Bengal 12) Mehyl Violet 13) Murexide 14) Alizarin

Red 15) Thymol Blue 16) Methyl Orange and 17) Bromocresol Green. Depending on our experimentation it was seen that following dyes were suitable for our undertaken studies.

1) Amido Black 10B 2) Methyl Orange and 3) Ponceau S.

Further the dyes soluble in different organic solvents were tested. The list of the tested dyes was 1) Fluorescein 2) Methyl Red 3) Thymolphthalein 4) Rhodamin B.

Among these dyes Rhodamin B was selected for our photodegradation study.

The focus of our study was photocatalytic degradation of the dyes. The synthesized porphyrins were used as photocatalysts. Therefore, photocatalysis was carried out in two different ways.

a) Photodegradation of aqueous solution of dye by non-aqueous porphyrins and

b) Photodegradation of non-aqueous solution of dye by aqueous porphyrins

a) Photodegradation of aqueous solution of dye by non-aqueous porphyrins

The dyes used under this category were 1) Amido Black 10 B 2) Methyl Orange and 3) Ponceau S.

The stock solution of 10^{-4} M concentration of each dye was prepared and then it was diluted to 10^{-5} M concentration for actual experiment. To develop the optimum conditions for photolysis the solutions of above dyes were tested with and without oxygen, varying amounts of photocatalysts and at different pH conditions. Based on these observations the ideal condition was developed. The 100 mL of concerned dye solution was taken and saturated with oxygen for five minutes. Further, depending upon the results of optimum amount of photocatalyst, it was seen that Amido Black 10B and

Ponceau S required 25 mg and Methyl Orange required 20 mg of the photocatalysts for degradation of the solution. Thus required amount of synthesized photocatalyst was added, the solution was stirred thoroughly and closed assembly of the reaction was kept in solar radiations during the period 11.30 am to 3.30 pm within a temperature range of 30 °C to 40 °C. The aliquots of the reaction mixture were withdrawn with the help of a syringe at the regular intervals of one hour and the course of photodegradation reaction was monitored using Shimadzu visible spectrophotometer (model uv/2450uv). The photolysis reactions for selected dyes were studied at pH 6, 7 and 10 respectively for comparative studies.

b) Photodegradation of non-aqueous solution of dye by aqueous porphyrins

This type of experiment required selection of a suitable organic solvent, its non-carcinogenic nature, solubility of a dye in the solvent, insolubility of a photocatalyst in solvent and easy availability at a cheaper rate. As per our observations, it is seen that acetone is satisfying all these conditions. Thus acetone was selected as a non-aqueous solvent for photocatalysis. To acquire acetone of high purity, AR grade acetone was refluxed with $KMnO_4$ for two hours until the colour of $KMnO_4$ persists and then it was distilled. The stock solution of 10^{-4} M concentration of Rhodamin B was prepared in actone and then it was diluted to 10^{-5} M concentration for actual experiment. For optimum conditions of experiment, the dye solution was tested with oxygen, without oxygen and varying amount of photocatalysts in solar radiations. Based on these observations, it was seen that the amount of photocatalyst required was 5 mg for 50 mL dye solution. Therefore, 50 mL of 10^{-5} M solution of Rhodamin B was taken in a conical

flask and 5 mg of above synthesized photocatalyst was added. The solution was stirred thoroughly and the closed reaction assembly was kept in sunlight. Since, the rate of degradation was much faster, therefore, the aliquots were withdrawn at every five minute or ten minute with the help of a syringe. The course of photodegradation was monitored using Shimadzu visible spectrophotometer (model uv/2450uv).

In addition to UV-visible spectroscopy the above degradation processes were studied with the help of

i) Liquid chromatography-Mass spectrometry (LC-MS), where mass fragmentation pattern of a particular dye was obtained. This was helpful in predicting probable reaction mechanism in the course of dye degradation process. The degraded dye solution at pH 7 was selected for the study.The results were recorded on IT mass spectrometer (model Varian 500-MS) with APCI source.

ii) High performance liquid chromatography (HPLC)

This was helpful to resolve the number of components after the photodegradation process was completed. The results were recorded on HPLC unit Perkin Elmer SERIES-200. The column used for this was C18 with dimensions 250 mm × 4.6 mm and particle size diameter 5 micrometer. The solvent system selected was methanol and water (80%:20%) with UV detector which functions at 254 nm. The degraded dye solutions of Amido Black 10B and Methyl Orange at pH 6 and 7 were used. The solution of Rhodamine B was also studied for the number of components after degradation reaction.

iii) The qualitative and quantative study of mineralization of dyes during the course of phodegradation was studied using ion-chromatography. The equipment required for this involves cation and anion exchangers with suitable stationary and mobile phases. The degraded solution of Amido Black 10B and Methyl Orange at pH 7 and Rhodamine B solution were used for study.

CHAPTER 4

Spectroscopic studies of porphyrins

The above synthesized free-base porphyrins and metalloporphyrins from non-aqueous and aqueous series were characterized by UV-Visible spectroscopy, infrared spectroscopy (FTIR), proton magnetic resonance spectroscopy (^{1}Hnmr), elemental analysis, high resolution mass spectroscopy (HR-MS), fluorescence spectroscopy and diffuse reflectance spectroscopy (DRS). The experimental results obtained were compared with standard results from the literature. In case where reference results were not available, then elemental analysis and high resolution mass spectroscopy results were used for the confirmation of the respective porphyrins.

4.1 UV-Visible spectroscopy

The non-aqueous porphyrins, TPP and its metalloporphyrins where M= Co^{2+}, Ni^{2+}, Cu^{2+}, Zn^{2+}, Ag^{2+}, Mn^{3+}, Fe^{3+} and Sn^{4+} were characterized by UV-visible absorption spectroscopy. The porphyrins spectra are due to π - π^* transitions. The electron transitions for soret band are from $a_{1u} \rightarrow e_g$ (allowed) and for Q-band[28] $a_{2u} \rightarrow e_g$ (forbidden). The concentrations used for soret band and Q-band are10^{-5} M and 10^{-4} M respectively. In TPP the bands obtained are 416 nm (soret), 515, 549, 590, and 647 nm (Q-bands) whereas in CoTPP, NiTPP, CuTPP, ZnTPP and AgTPP the number of bands are reduced to two and in $SnTPPCl_2$ three in the visible region. Thus successful insertion of metal in porphyrins is confirmed by disappearance of 647 nm band[184] and reduction in number of Q-bands as compared to TPP. A free base TPP is having two hydrogens attached to two nitrogens in the porphyrin ring which

is having a rectangular geometry with D_{2h} symmetry. When metallation takes place, the geometry of the porphyrin ring becomes square with D_{4h} symmetry [185]. Thus when free base TPP is metallated the geometry becomes more symmetric, as a result the number of absorption bands obtained is minimum. It is observed that TPP, ZnTPP and $SnTPPCl_2$ form closed shell porphyrins and they show normal spectra, where, there is no or minimum interaction between metal and porphyrin ring. Therefore, they are classified as regular porphyrins. The porphyrins such as CoTPP, NiTPP, CuTPP and AgTPP have small interactions between the porphyrin and corresponding metal. As a result the nature of the spectra remains the same with slight shift in absorption peaks. Fig.4.1 shows UV-visible spectra of TPP and CoTPP. The porphyrins like MnTPPCl, O-$(MnTPP)_2$, FeTPPCl and O-$(FeTPP)_2$ are called hyper porphyrins where there is a strong interaction between metal and porphyrin ring. Due to this reason, hyper porphyrins show extra absorption peaks. Fig. 4.2 shows UV-visible spectra of MnTPPCl and $SnTPPCl_2$ The values of absorption peaks of all non-aqueous porphyrins in Soret and visible region with molar absorptivities are shown in Table 4.1 and are in agreement with literature values [49,185,33].

In the context of aqueous-porphyrins, there is substitution of four SO_3Na groups at the -para position of each phenyl ring. This makes a free-base porphyrin ($TPPS_4$) and the corresponding metalloporphyrins ($MTPPS_4$) soluble in water. TPPS4, ZnTPPS4 and $SnTPPS_4Cl_2$ show normal spectra due to the fact that $TPPS_4$ is open shell porphyrin whereas Zn^{2+} and Sn^{4+} form closed shell porphyrins. In the case of $CoTPPS_4$, $NiTPPS_4$, $CuTPPS_4$ and $AgTPPS_4$ on account of small interactions between porphyrin ring and metal, slight shifting of absorption of peaks from normal spectra is observed. Similarly, $MnTPPS_4Cl$, $FeTPPS_4Cl$ and O-$(FeTPPS_4)_2$ show hyper spectra, due to greater

interactions between ring and respective metals. Fig. 4.3 and Fig. 4.4 show the different absorption peaks for water soluble porphyrins in soret as well as visible region. Table 4.2 and 4.3 show electronic absorption peaks with corresponding molar absorptivities of aqueous-porphyrins containing for di, tri and tetravalent metal ions. These values are in agreement with literature values [60, 33].

Further, it is seen from the Table 4.1 that absorption peaks of non-aqueous hyper porphyrins, monomer MnTPPCl shows 376 nm and 425 nm bands in soret region whereas these bands are absent in its dimer O-$(MnTPP)_2$. In the visible region, the band due to dimer O-$(MnTPP)_2$ i.e. 527 nm is blue shifted in comparison with MnTPPCl band i.e. 582nm. Similarly, dimer O-$(FeTPP)_2$ shows blue shift in soret as well as in visible region in comparison with monomer FeTPPCl. When the absortion peaks of MnTPPCl and FeTPPCl are compared, it is seen that latter shows blue shift and their dimers, O-$(MnTPP)_2$ and O-$(FeTPP)_2$ when compared in soret and visible region, it is observed that, latter shows slight blue shift in comparison with that of former. This substantiates the fact that increase in atomic number of a metal shows hypsochromic or blue shift in hyper porphyrins.

In the context of aqueous-porphyrins, regular porphyrins such as $TPPS_4$, $ZnTPPS_4$ and $SnTPPS_4$ or irregular porphyrins formed with Co^{2+}, Ni^{2+}, Cu^{2+} and Ag^{2+} do not lead to any concrete conclusion as shown in Table 4.2 and Table 4.3. The porphyrins like $MnTPPS_4Cl$, $FeTPPS_4Cl$ and O-$(FeTPPS_4)_2$ belong to hyper class. Among them there appears blue shift in the soret region with the increase in the atomic number. In $MnTPPS_4Cl$, λ_{max} = 466 nm is a characteristic wavelength for the metalloporphyrin.

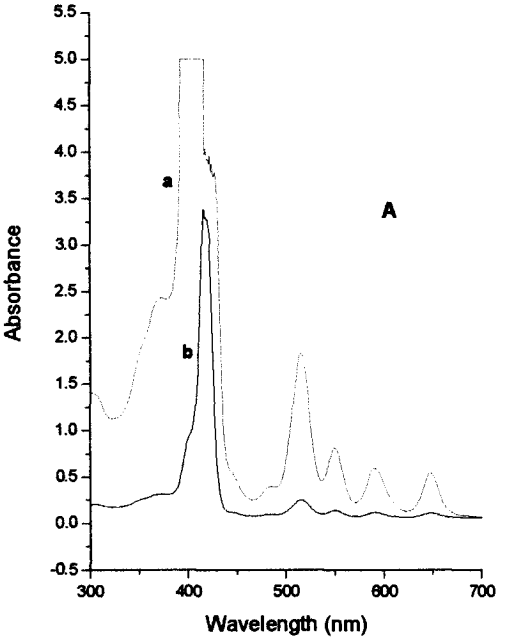

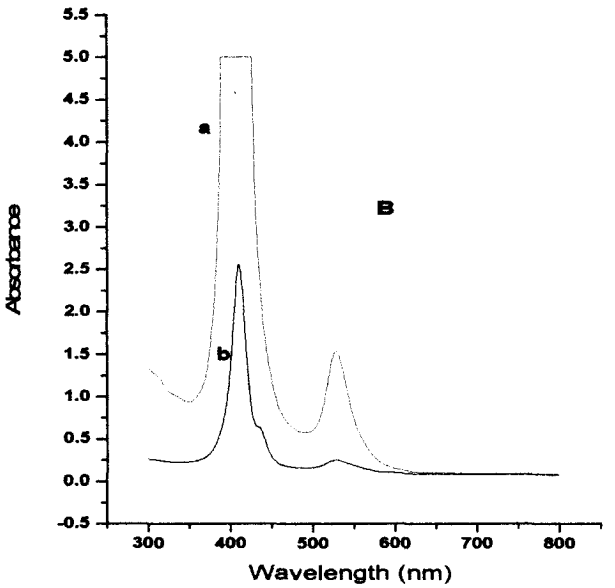

Fig. 4.1 UV-visible spectra of TPP (A) and CoTPP (B)

a) 10^{-4} M concentration b) 10^{-5} M concentration

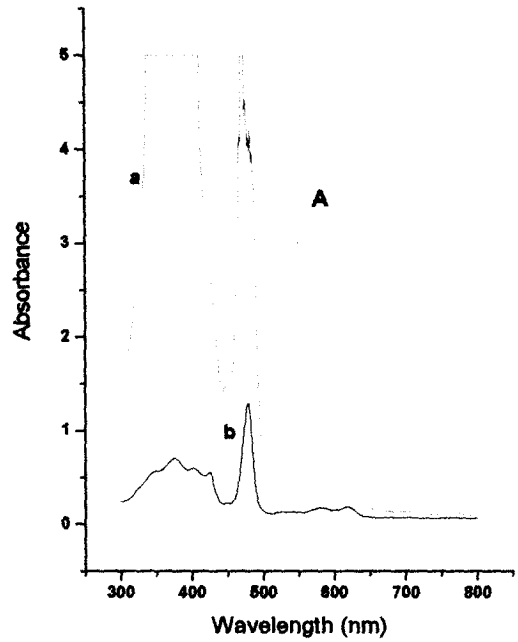

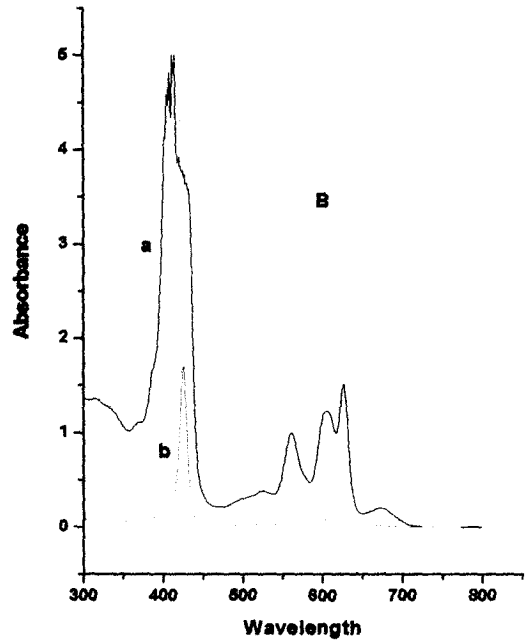

Fig. 4.2 UV-visible spectra of MnTPPCl (A) and $SnTPPCl_2$ (B)

a) 10^{-4} M concentration b) 10^{-5} M concentration

Table 4.1 The absorption peaks and molar absorptivities of non-aqueous porphyrins of divalent, trivalent and tetravalent metal ions

Sr. No.	Porphyrin	Absorption Bands				
		Soret band	←	Q-bands	→	
1	TPP	416 $\epsilon = 3.4 \times 10^5$	515 $\epsilon = 1.8 \times 10^4$	549 $\epsilon = 8.1 \times 10^3$	590 $\epsilon = 5.9 \times 10^3$	647 $\epsilon = 5.4 \times 10^3$
2	CoTPP	410 $\epsilon = 2.5 \times 10^5$	528 $\epsilon = 1.5 \times 10^4$			
3	NiTPP	416 $\epsilon = 3.1 \times 10^5$	528 $\epsilon = 1.9 \times 10^4$			
4	CuTPP	413 $\epsilon = 3.5 \times 10^5$ 423 $\epsilon = 4.5 \times 10^4$	539 $\epsilon = 2.1 \times 10^4$			
5	ZnTPP	418 $\epsilon = 6.3 \times 10^5$	547 $\epsilon = 2.4 \times 10^4$	584 $\epsilon = 4.3 \times 10^3$		
6	AgTPP	425 $\epsilon = 5.7 \times 10^5$	541 $\epsilon = 2.2 \times 10^4$			
7	MnTPPCl	376 $\epsilon = 7.0 \times 10^4$ 425 $\epsilon = 5.6 \times 10^4$	479 $\epsilon = 1.2 \times 10^5$	582 $\epsilon = 1.0 \times 10^4$	618 $\epsilon = 1.2 \times 10^4$	
8	O-$(MnTPP)_2$	-	479 $\epsilon = 7.0 \times 10^4$	527 $\epsilon = 4.1 \times 10^3$	580 $\epsilon = 6.1 \times 10^3$	616 $\epsilon = 6.1 \times 10^3$
9	FeTPPCl	416 $\epsilon = 1.2 \times 10^5$	509 $\epsilon = 9.3 \times 10^3$	572 $\epsilon = 4.5 \times 10^3$	- -	609 $\epsilon = 2.3 \times 10^3$
10	O-$(FeTPP)_2$	408 $\epsilon = 1.1 \times 10^5$	- -	- -	571 $\epsilon = 7.9 \times 10^3$	611 $\epsilon = 3.6 \times 10^3$
11	$SnTPPCl_2$	426 $\epsilon = 1.7 \times 10^5$	524 $\epsilon = 3.8 \times 10^3$	561 $\epsilon = 9.9 \times 10^3$	606 $\epsilon = 1.2 \times 10^4$	627 $\epsilon = 1.5 \times 10^4$

(ϵ in $cm^{-1} mol^{-1} L$)

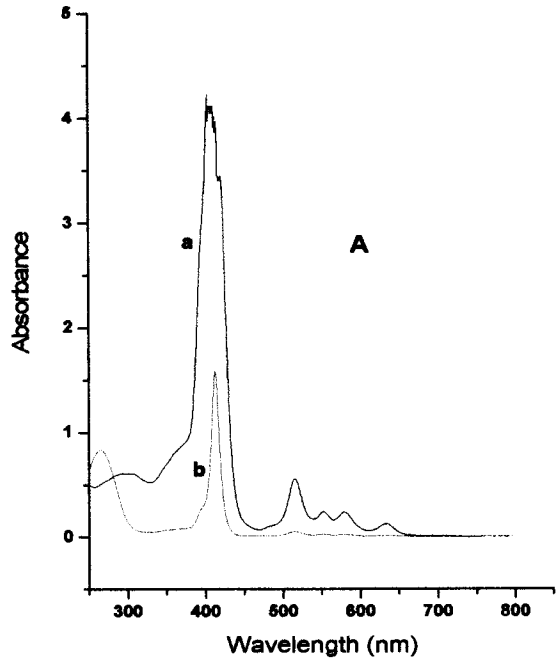

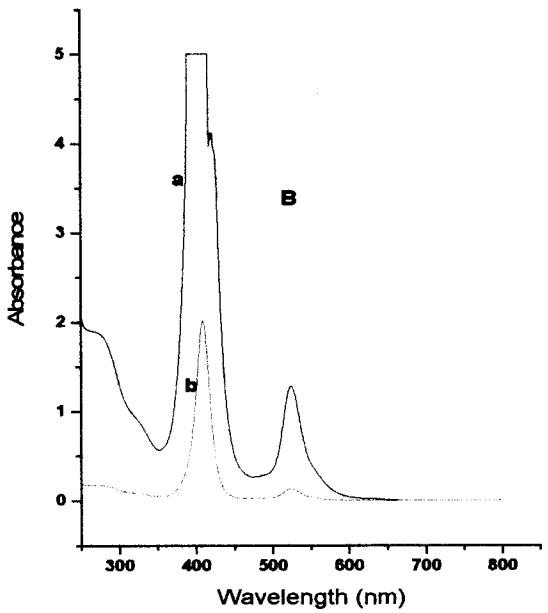

Fig. 4.3 UV-visible spectra of $TPPS_4$ (A) and $NiTPPS_4$ (B)

a) 10^{-4} M concentration b) 10^{-5} M concentration

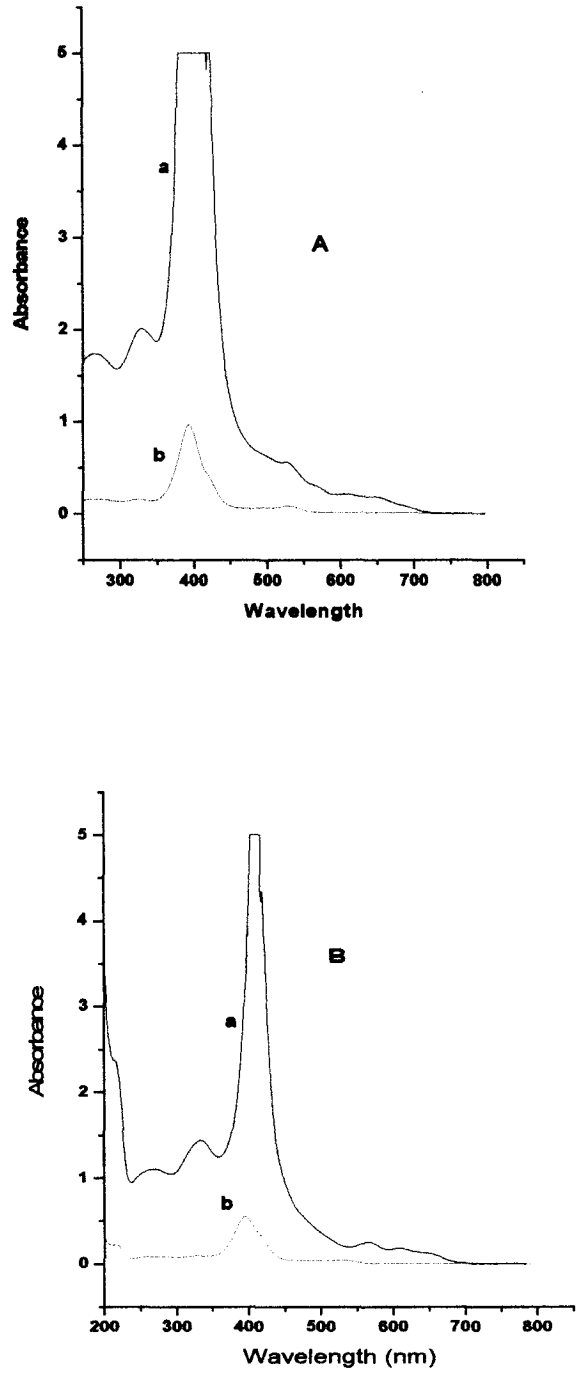

Fig. 4.4 UV-visible spectra of $FeTPPS_4$ (A) and O-$(FeTPPS_4)_2$ (B)

a) 10^{-4} M concentration b) 10^{-5} M concentration

Table 4.2 Absorption peaks and molar absorptivities of aqueous-porphyrins containing divalent metal ions

Sr. No.	Porphyrin	Absorption Bands				
		Soret	←	Q-bands	→	
1	$TPPS_4$	413 $\epsilon = 1.6\times10^5$	516 $\epsilon = 5.6\times10^3$	552 $\epsilon = 2.4\times10^3$	579 $\epsilon = 2.4\times10^3$	633 $\epsilon = 1.3\times10^3$
2	$CoTPPS_4$	425 $\epsilon = 9.4\times10^4$	540ϵ $\epsilon = 5.2\times10^3$			
3	$NiTPPS_4$	409 $\epsilon = 2.0\times10^5$	525 $\epsilon = 1.2\times10^4$			
4	$CuTPPS_4$	412 $\epsilon = 2.8\times10^5$	539 $\epsilon = 1.2\times10^4$			
5	$ZnTPPS_4$	421 $\epsilon = 2.9\times10^5$	556 $\epsilon = 1.2\times10^4$	595 $\epsilon = 5.0\times10^3$		
6	$AgTPPS_4$	422 $\epsilon = 2.7\times10^5$	540 $\epsilon = 1.1\times10^4$			

(ϵ in $cm^{-1}mol^{-1}L$)

Table 4.3 Absorption peaks and molar absorptivities of aqueous-porphyrins containing trivalent and tetravalent metal ions

Sr. No.	Porphyrins	Absorption Bands				
		Soret	←	Q-Bands	→	
7	$MnTPPS_4Cl$	413 $\epsilon = 2.5\times10^5$	516 $\epsilon = 1.1\times10^4$	553 $\epsilon = 5.6\times10^3$	579 $\epsilon = 5.2\times10^3$	633 $\epsilon = 2.3\times10^3$
8	$FeTPPS_4Cl$	394 $\epsilon = 9.6\times10^4$	526 $\epsilon = 5.6\times10^3$	-	608 $\epsilon = 2.1\times10^3$	644 $\epsilon = 1.8\times10^3$
9	O-(FeTPP)$_2$	395 $\epsilon = 5.5\times10^4$	-	567 $\epsilon = 2.5\times10^3$	609 $\epsilon = 1.9\times10^3$	-
10	$SnTPPS_4Cl_2$	418 $\epsilon = 1.0\times10^5$	515 $\epsilon = 6.2\times10^2$	553 $\epsilon = 4.2\times10^3$	593 $\epsilon = 2.0\times10^3$	-

(ϵ in $cm^{-1} mol^{-1} L$)

When non-aqueous porphyrins are compared with aqueous-porphyrins from Table 4.1, 4.2 and 4.3, some of the following salient features are observed.

i) The soret band and a characteristic free-base porphyrin band in visible region in $TPPS_4$ i.e. 413 nm and 633 nm are blue shifted in comparison with 416 nm and 647 nm as observed in TPP.

ii) The irregular porphyrins formed by divalent metal ions show blue shift in Soret region for $NiTPPS_4$, $CuTPPS_4$ and $AgTPPS_4$ in comparison with NiTPP, CuTPP and AgTPP respectively. The bathochromic or red shift is observed in soret region and in visible region for $CoTPPS_4$ and $ZnTPPS_4$ in comparison with CoTPP and ZnTPP respectively. The remaining porphyrins are exhibiting nearly equal absorption peaks in the visible region for aqueous- and non-aqueous porphyrins for the same metal ion.

iii) The sulphonated porphyrins i.e. $MnTPPS_4Cl$, $FeTPPS_4Cl$ and $O\text{-}(FeTPPS_4)_2$ showed hypsochromic shift in comparison with non-sulphonated MnTPPCl, FeTPPCl and $O\text{-}(FeTPP)_2$ in Soret as well as in visible region.

iv) Aqueous porphyrin i.e. $SnTPPS_4Cl_2$ showed blue shift in soret and visible region in comparison with non-aqueous $SnTPPCl_2$.

Therefore, in general, it can be concluded that sulphonated porphyrins absorb at shorter wavelength than non-sulphonated porphyrins with few exceptions as mentioned above.

4.2 Infrared spetrosopy

These porphyrins were further characterized by FTIR spectroscopy. A free base TPP shows medium N-H stretching vibrations at 3317 cm^{-1}. When a metal ion is inserted into a porphyrin ring the stretching vibrations due to N-H disappear on account of replacement of two acidic hydrogens by the metal ion. This also gives information about the presence or absence of TPP as an impurity in the corresponding metalloporphyrins (MTPP). Fig 4.5 and 4.6 show FTIR spectra of non-aqueous porphyrins of divalent, trivalent and tetravalent metal ions. The main intense absorption bands of the metal chelates of TPP appear near 1600 cm^{-1} due to C=C stretching of phenyl ring. At lower frequencies three sharp bands due to C–H rocking vibrations of the pyrrole ring are obtained at 960, 980 and 1000 cm^{-1} as shown in Table 4.4 and 4.5 respectively. The results were compared with literature values[50,33] and are found to be in good agreements. The strong absorption band near 1000 cm^{-1} appears due to vibration of the porphyrin ring or pyrrole units, which is sensitive to the nature of the metal ion. Further, it establishes the strength of the metal-nitrogen bonds in the TPP chelates. It is evident from the frequency values that the strength of the metal-nitrogen bond for porphyrins of divalent metal ions is in the following order ZnTPP < CoTPP = CuTPP < NiTPP = AgTPP. In case of trivalent and tetravalent metal ion porphyrins the sequence of stability is given as FeTPPCl < O-$(FeTPP)_2$ < MnTPPCl < O-$(MnTPP)_2$ < $SnTPPCl_2$. The strong band common to TPP and metal chelates near 800 cm^{-1} appears due to vibration of pyrrole ring. The FTIR spectroscopy is also useful to distinguish between monomers and dimers of Mn^{3+} and Fe^{3+} respectively.

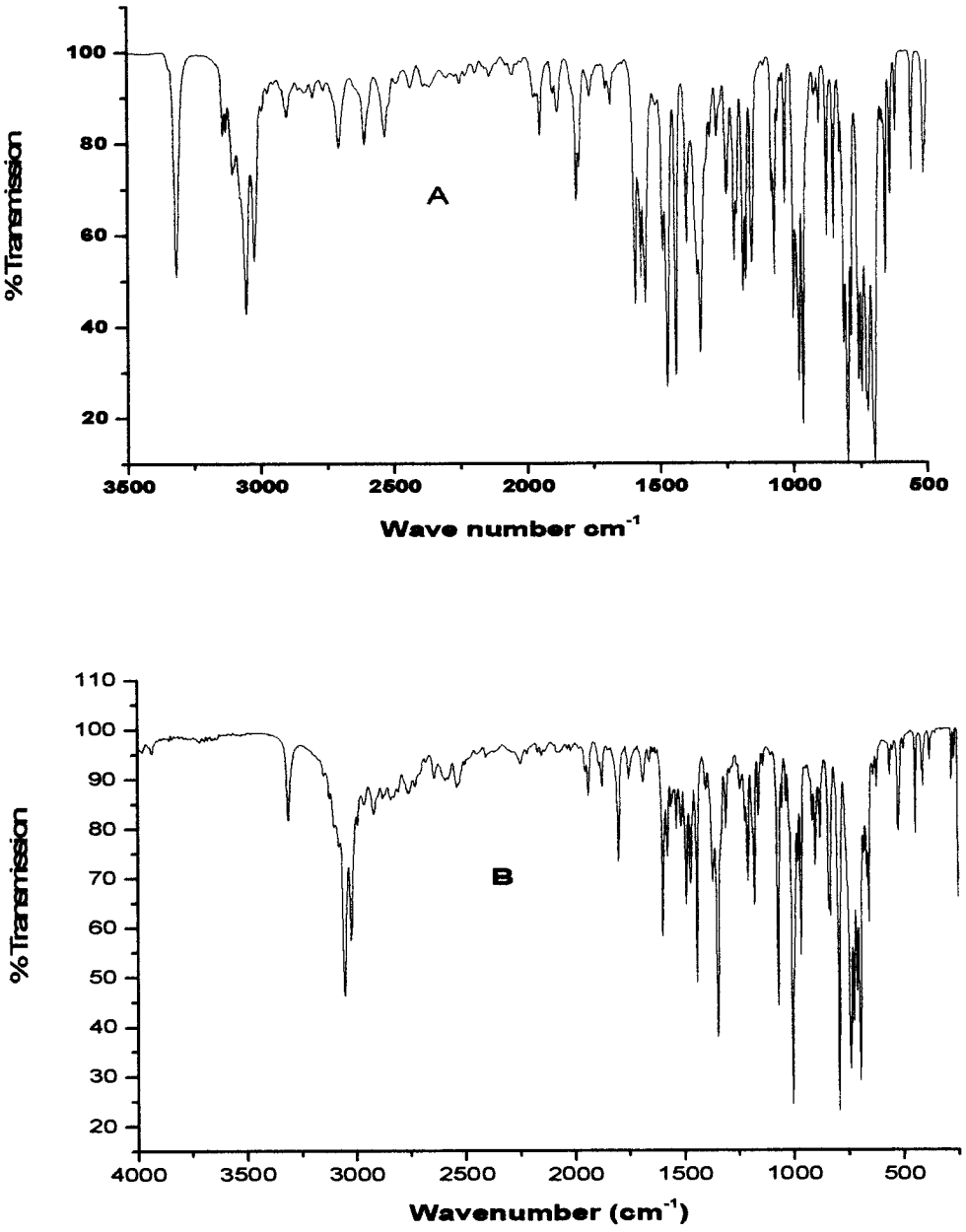

Fig. 4.5 Infrared spectra of TPP (A) and CuTPP (B)

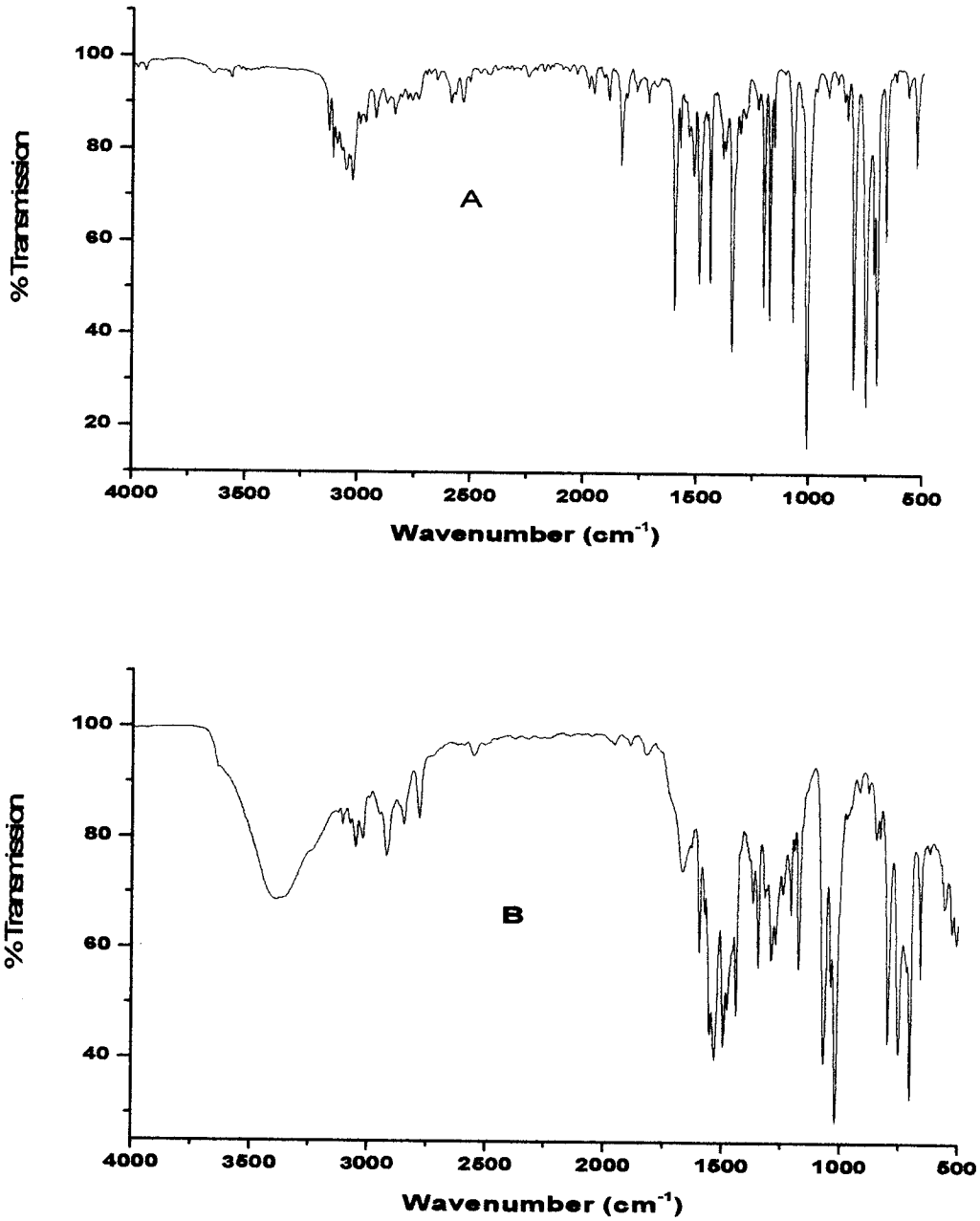

Fig. 4.6 Infrared spectra of MnTPPCl (A) and $SnTPPCl_2$ (B)

Table 4.4 Infrared frequencies and assignments for divalent metal ions

Sr.No.	Ligand	Metal ions					Assignment
	TPP	Co	Ni	Cu	Zn	Ag	
1	3317 (m)	—	—		—	—	N—H Stretching
2	3055 (m)	3053	3053	3051	3053	3053	C—H Stretching (Py)
3	3024 (m)	—	3024	3024	3024	3024	C—H Stretch (phenyl)
4	1595 (m)	1598 (m)	1599 (m)	1599 (m)	1595 (m)	1595 (m)	-C=C- (Phenyl)
5	1556 (m)	—	—	—	—	—	-C=C- (Py)
6	1443 (m)	1440 (m)	1441 (m)	1441 (m)	1441 (m)	1441 (m)	C—H bend (Py)
7	1350 (m)	1350 (m)	1352 (s)	1346 (m)	1341 (s)	1341 (s)	-C—N- Stretch
8	1001 (m)	1005 (s)	1007 (s)	1005 (s)	1003 (s)	1007 (s)	C—H Rock (Py)
9	798 (s)		793 (s)	793 (s)	—	792 (s)	Pyrrole ring

Table 4.5 Infrared frequencies and assignments

for porphyrins of trivalent and tetravalent metal ions

Sr.No	Ligand	Metal ions				Assignment
	TPP	Mn	Mn (di)	Fe (di)	Sn	
1	3317 (m)	-	-	-		N—H Stretch
2	3055 (m)	3055 (m)	3055(m)	3055 (m)	3053(w)	C—H Stretch (Py)
3	3024 (m)	3024 (w)	3024 (w)	3024 (w)	3024 (w)	C—H Stretch (Phenyl)
4	1595 (m)	1597 (m)	1597 (m)	1597 (m)	1595 (m)	-C=C- (Phenyl)
5	1556 (m)				1553 (s)	-C=C- (Py)
6	1443(m)	1438 (m)	1441 (m)	1441 (m)	1441 (m)	-C=C- (Py)
7	1350 (m)	1342 (m)	1341(m)	1339 (m)	1341 (m)	-C—N Stretch
8	1001 (m)	1007(s)	1011 (s)	1003 (s)	1022 (s)	C—H Rock (Py)
9	798 (s)	806 (s)	800 (m)		798 (m)	Pyrrole ring

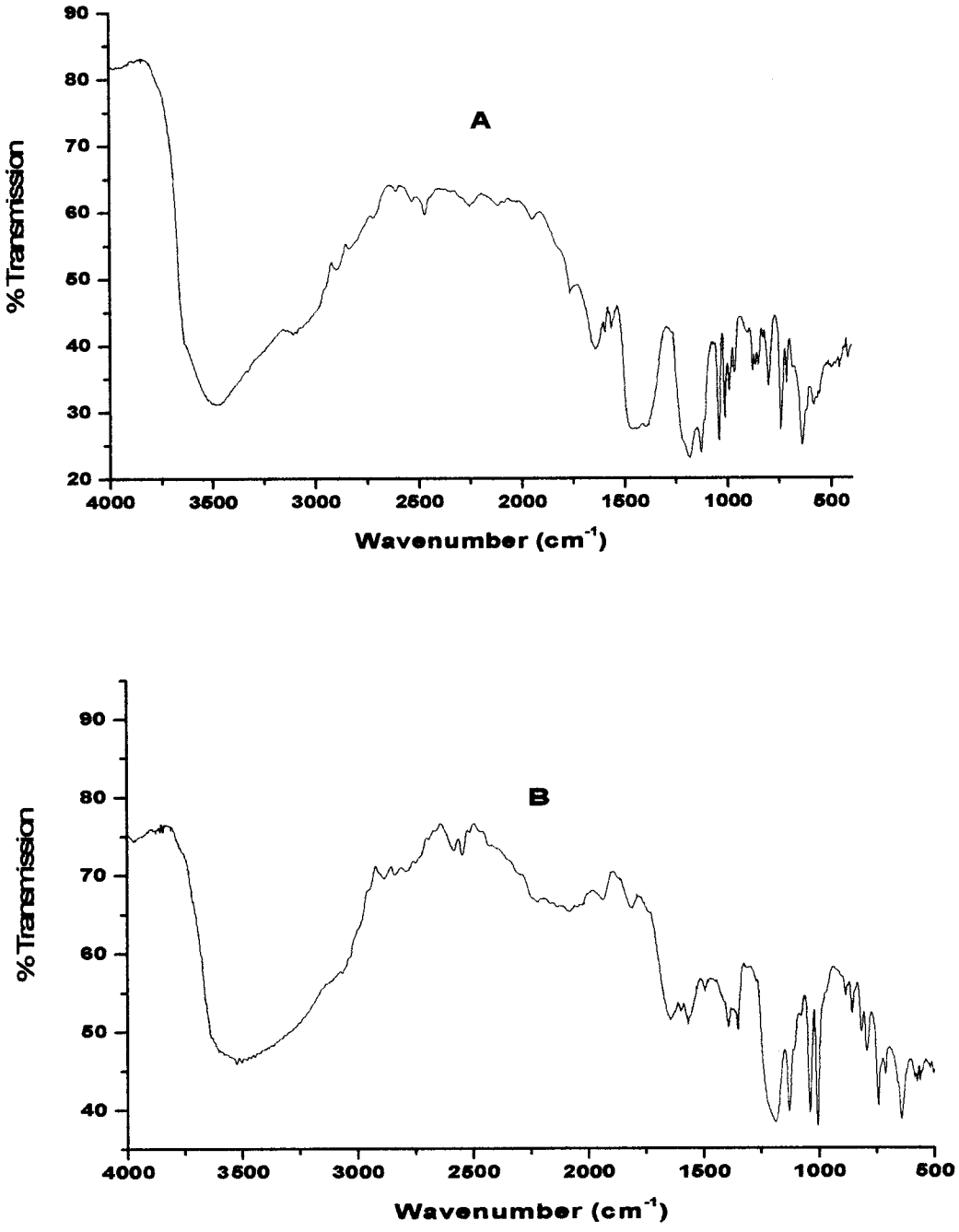

Fig. 4.7 Infrared spectra of $TPPS_4$ (A) and $NiTPPS_4$ (B)

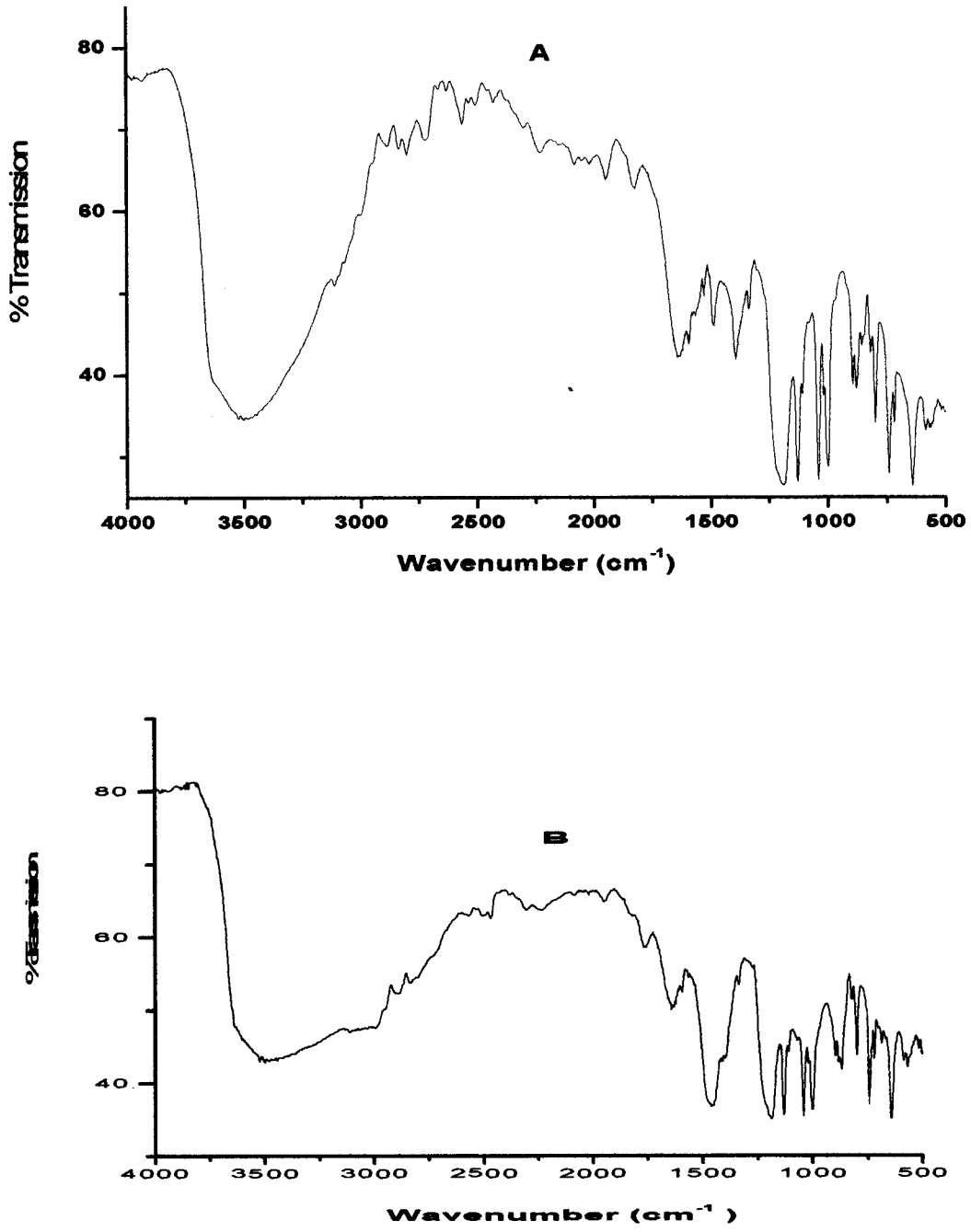

Fig. 4.8 Infrared spectra of $FeTPPS_4$ (A) and O-$(FeTPPS_4)_2$ (B)

Table 4.6 Infrared frequencies and assignments for porphyrins of divalent metal ions

Sr. No	Ligand	Metal ions					Assignment
	$TPPS_4$	Co	Ni	Cu	Zn	Ag	
1	3440-3590	3523	3523	3523	3508	3523	N—H Stretch & O—H Stretch
2	3113 (w)	3001 (w)	3064 (w)	3113 (w)	3120 (w)	3120 (w)	C—H Stretch(Py)
3	1593 (w)	1577 (w)	1573 (w)	1595 (w)	1577 (w)	1593 (w)	C= C (phenyl)
4	1560 (w)	1566 (s)	1560 (w)	1562 (w)	1566 (m)	1560 (w)	C= C (Py)
5	1420-1440 (s)	1420 (m)	1420 (vw)	1442(m)	-	-	C—H bend (Py) In plane
6	1184 (s)	1199 (m)	1188 (s)	1184 (s)	1193	1186	Sodium sulphonate
7	1128 (s)	1130 (m)	1128 (s)	1130 (s)	1128 (s)	1130 (s)	"
8	1041 (s)	1043 (m)	1039 (s)	1041 (s)	1041 (s)	1041 (s)	"
9	1012 (s)	1000-1010 (m)	1006 (s)	1010-999 (s)	999	1004	C—H Rock (Py)
10	800 (m)	797 (m)	795 (m)	800 (m)	797 (m)	795	Pyrrole ring

Table 4.7 Infrared frequencies and assignments for porphyrins of trivalent and tetravalent metal ions

Sr. No.	Ligand $TPPS_4$	Mn	Metal Fe	Fe(di)	Ions Sn	Assignments
1	3440-3590	3440-3530	3400-3650	3440-3590	3400-3545	N—H Stretch & O—H stretch
2	3113 (w)	3111 (w)	3111 (w)	3160 (w)	3132 (w)	C—H Stretch
3	1593 (w)	1595 (w)	1600 (w)	1595 (w)	1597 (w)	C=C (Phenyl)
4	1560 (w)	1562 (w)	1565 (w)	-	-	C=C (Py)
5	1420-1440(s)	1396 (m)	1392 (m)	1440-1470 (m)	1384 (s)	C—H bend (Py)
6	1184 (s)	1192 (s)	1175-1240 (s)	1188 (s)	1195 (s)	Sodium sulphonate
7	1128 (s)	1128 (s)	1130 (s)	1128 (s)	1130 (s)	"
	1041 (s)	1041 (s)	1041 (s)	1041 (m)	1041 (s)	"
8	1012 (s)	1012 (s)	1001,1012 (s) (w)	1001,1012 (s) (w)	1006,1012 (s) (w)	C—H Rock (Py)
9			850 (w)	881 (s)		
10	800 (m)	804 (m)	798 (m)	798 (m)	806 (m)	Pyrrole ring

In FeTPPCl and MnTPPCl the weak bands obtained are 833 and 834 cm^{-1} whereas in dimer O-$(MnTPP)_2$ and O-$(FeTPP)_2$ the bands are 879 and 877 cm^{-1} respectively. The bands obtained in dimers are attributed to Mn-O-Mn and Fe-O-Fe stretching [82].

In the context of aqueous-porphyrins, the additional bands are obtained due to sulphonation of porphyrins in addition to all bands present in non-aqueous porphyrins. These bands in $TPPS_4$ are 1041, 1128 and 1184 cm^{-1} which confirms substitution of SO_3Na group in each of the four phenyl rings at -para or 4- position. Since aqueous porphyrins are containing water of crystallization, -OH stretching frequency is seen as shown in Table 4.6 and 4.7 for base-free and other metalloporphyrins. The FTIR spectra of some of the porphyrins were confirmed by comparison with literature values [33, 34]. It is also observed from the tables that C-H rocking vibrations of the pyrrole ring are reduced with divalent metals and remained nearly same with trivalent metals as compared with the free-base $TPPS_4$. The vibration bands due to SO_3Na increase in magnitude after metalalion with divalent, trivalent and tetravalent metals with the exception of $CuTPPS_4$. The monomer $FeTPPS_4Cl$ and dimer O-$(FeTPPS_4)_2$ are differentiated from each other by 850 and 881 cm^{-1} bands due to Fe-O-Fe stretching in dimer.

When non-aqueous and aqueous-porphyrins are compared following features are revealed.

i) Disappearance of N-H stretching vibrations indicate metalation reaction and removal of imputity due to TPP or $TPPS_4$ in metalloporphyrins.

ii) The C-H rocking vibrations of pyrrole ring in non-aqueous porphyrins are depending upon the nature of the metal, which further explains the bond strength between metal and nitrogen of pyrrole ring. In aqueous-porphyrins, substitution of different metals in

porphrinato core does not produce any obseravable change, instead, it has shown decreasing values of C-H rocking vibrations as compared to $TPPS_4$.

iii) The O-H stretching in aqueous-porphyrins reveals that these porphyrins are hydrated whereas non-aqueous porphyrins do not show such stretching, which shows absence of water of hydration.

4.3. ^{1}Hnmr spectroscopy

These synthesized porphyrins contain meso-tetraphenylporphyrin (TPP), which is a parent compound. ^{1}Hnmr spectrum of TPP is characterized by two singlets arising from the β-pyrrole protons and N-H protons, respectively. The phenyl protons can be assigned to the two resonances with little fine structure; one results from the -ortho protons and the other from the -meta and -para protons[186,187]. The phenyl rings are generally considered to be restricted in their rotation and noncoplanar with the plane of the porphyrin ring.

Some of the representative metalloporphyrins are used for characterization of non-aqueous and aqueous porphyrins. The porphyrins can be classified as diamagnetic and paramagnetic metalloporphyrins. The salient features of ^{1}Hnmr spectra of compounds with unpaired spins are determined by hyperfine electron-nuclear interactions and by relaxation processes [188].

In above non-aqueous porphyrins, TPP, NiTPP, ZnTPP and $SnTPPCl_2$ are diamagnetic whereas CoTPP, CuTPP, AgTPP, MnTPPCl, O-$(MnTPP)_2$, FeTPPCl and O-$(FeTPP)_2$ are found paramagnetic in nature. Fig. 4.9 and Fig.4.10 show ^{1}Hnmr spectra of non-aqueous diamagnetic and paramagnetic porphyrins respectively. The chemical shifts of selected non-aqueous porphyrins are summarized in Table 4.8.

In the series of aqueous porphyrins, $TPPS_4$, $NiTPPS_4$, $ZnTPPS_4$ and $SnTPPS_4Cl_2$ are diamagnetic whereas $CoTPPS_4$, $CuTPPS_4$, $AgTPPS_4$, $MnTPPS_4Cl$, $FeTPPS_4Cl$, $O\text{-}(FeTPPS_4)_2$ are paramagnetic in nature. Fig.4.14 shows ^{1}Hnmr spectra of aqueous $TPPS_4$ and $MnTPPS_4Cl$ and Table 4.9 gives chemical shifts of some aqueous-porphyrins.

It is observed that in TPP β-pyrrole protons show the maximum low field signal whereas ortho-phenyl protons show comparatively shifting of the signal towards high field and meta- and para- phenyl protons are having overlapping resonance signal at still more higher field. This type of situation is also observed in NiTPP and ZnTPP respectively. When the proton nmr spectra of paramagnetic porphyrins like CoTPP is considered, it is seen that all types of proton signals are shifted to the maximum low field values with broadening of the resonance signals. In case of CuTPP, and AgTPP the signals due to pyrrole protons and ortho-phenyl protons are either absent or overlapping with meta- or para-phenyl protons. This was compared with literature values[187] and found to be in good agreement. In FeTPPCl and MnTPPCl, it is observed that due to presence of axial Cl proton nmr signals move toward the diamagnetic four-coordinated porhyrins [189,190].

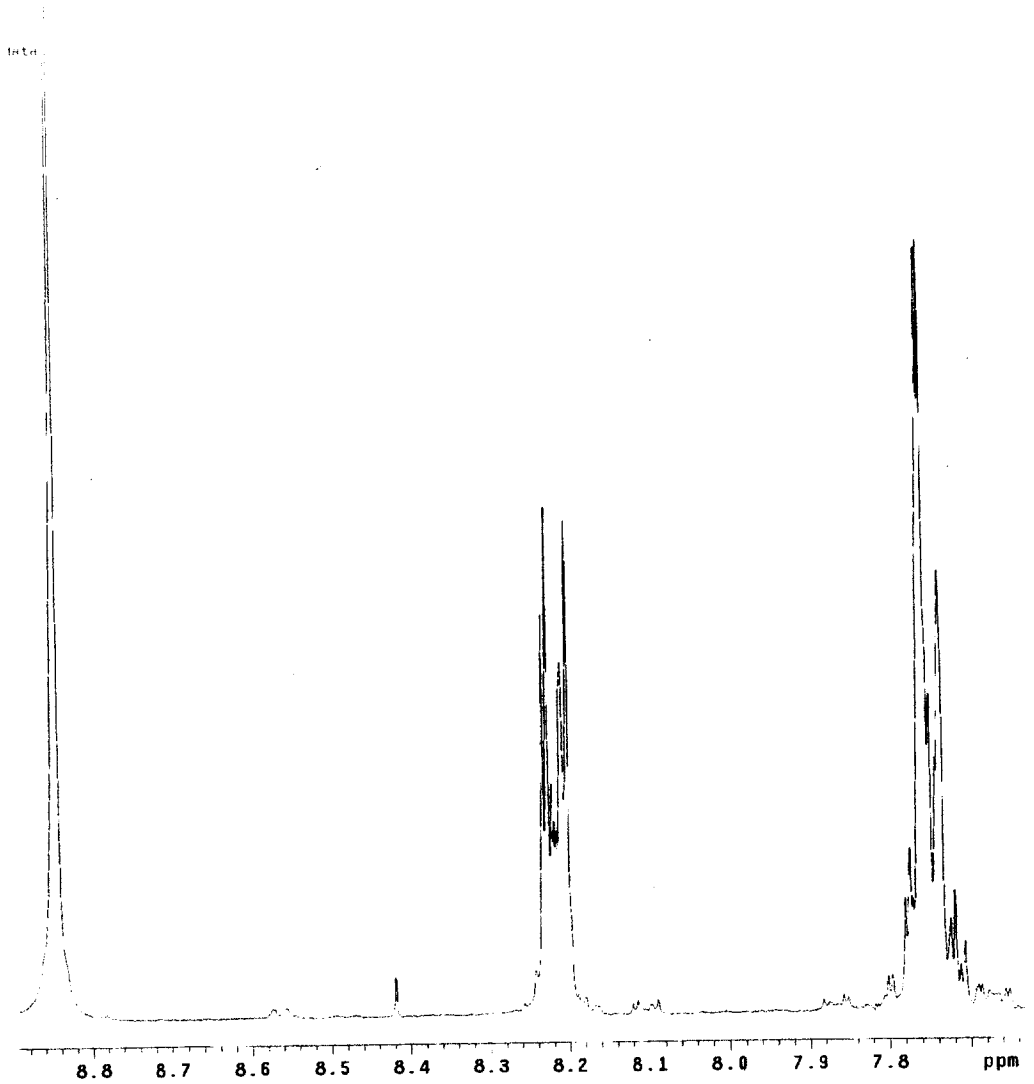

Fig.4.9 Proton NMR spectra of TPP

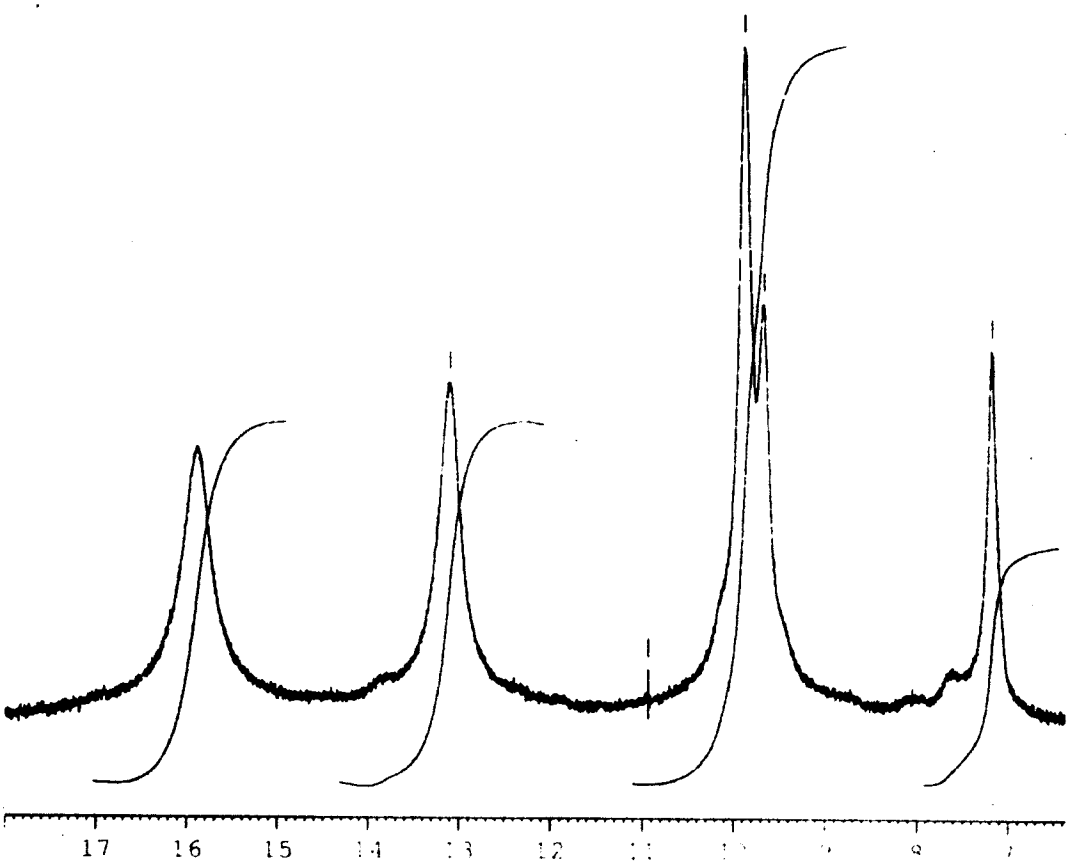

Fig 4.10 Proton NMR spectra of CoTPP

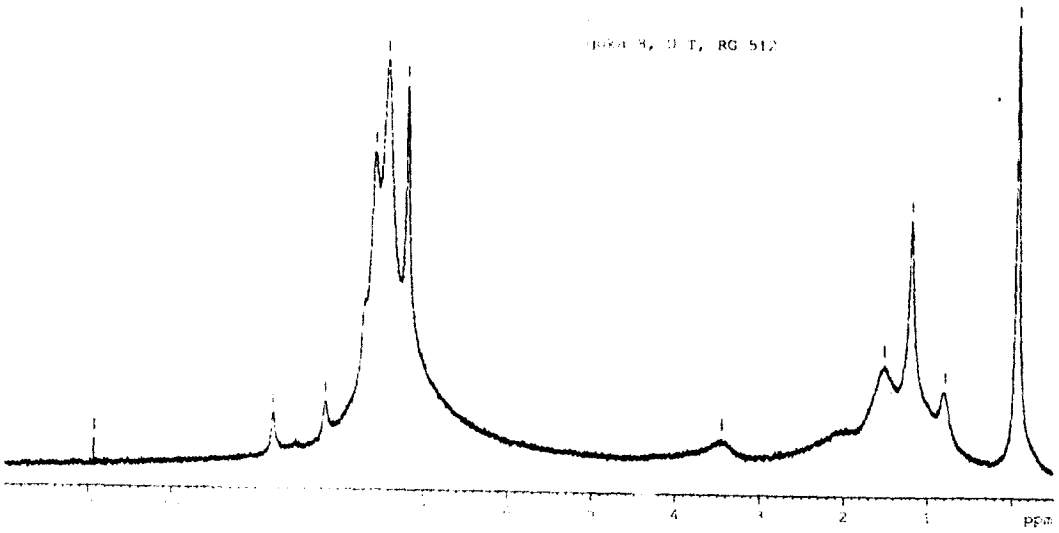

Fig.4.11 Proton NMR spectra of CuTPP

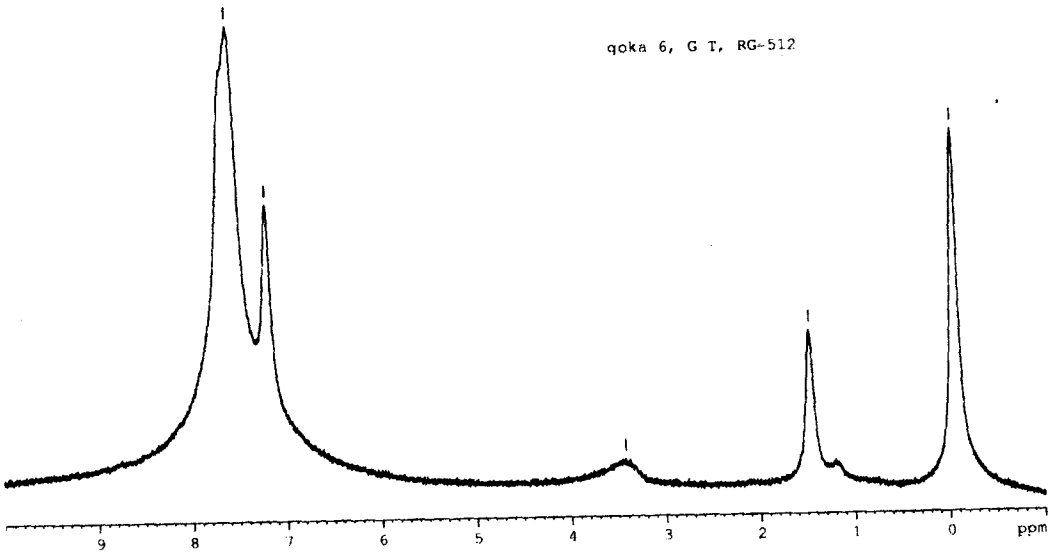

Fig 4.12 Proton NMR spectra of AgTPP

Table 4.8 Proton NMR chemical shifts (in δ ppm) for non-aqueous porpyrins

Sr.No	Porphyrin	o-Phenyl	m-phenyl	p-Phenyl	β-Pyrrole
1	TPP	8.22 (m)	7.74 (m)	X	8.84 (s)
2	CoTPP	13.0 (s)	9.88 (d)	9.67 (s)	15.9 (s)
3	NiTPP	8.0	7.7	7.7	8.7
4	CuTPP	X	7.58	7.2 (m)	8.78 (s)
5	ZnTPP	8.2 (m)	7.71	7.69 (d)	8.9 (s)
6	AgTPP	X	7.6	7.2	X
7	MnTPPCl	X	X	X	7.8—8.8
					(not resolved)
8	FeTPPCl	7.7	7.2	6.4	7.7

Note:

1) All spectra were obtained at 29°C and chemical shift values are mentioned in δ ppm w.r.t.$(CH_3)_4Si$

2) "X" entries indicate signals not detected due to large line width or overlap with other signals.

3) Solvent used is $CDCl_3$

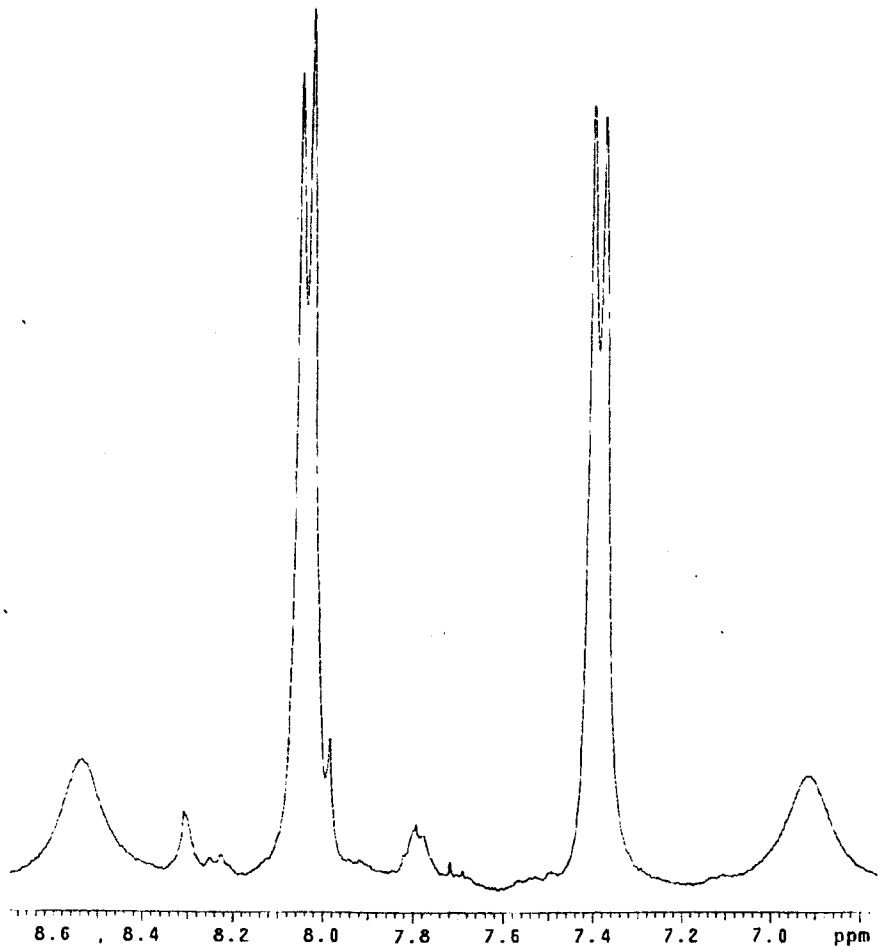

Fig. 4.13 Proton NMR spectra of $TPPS_4$

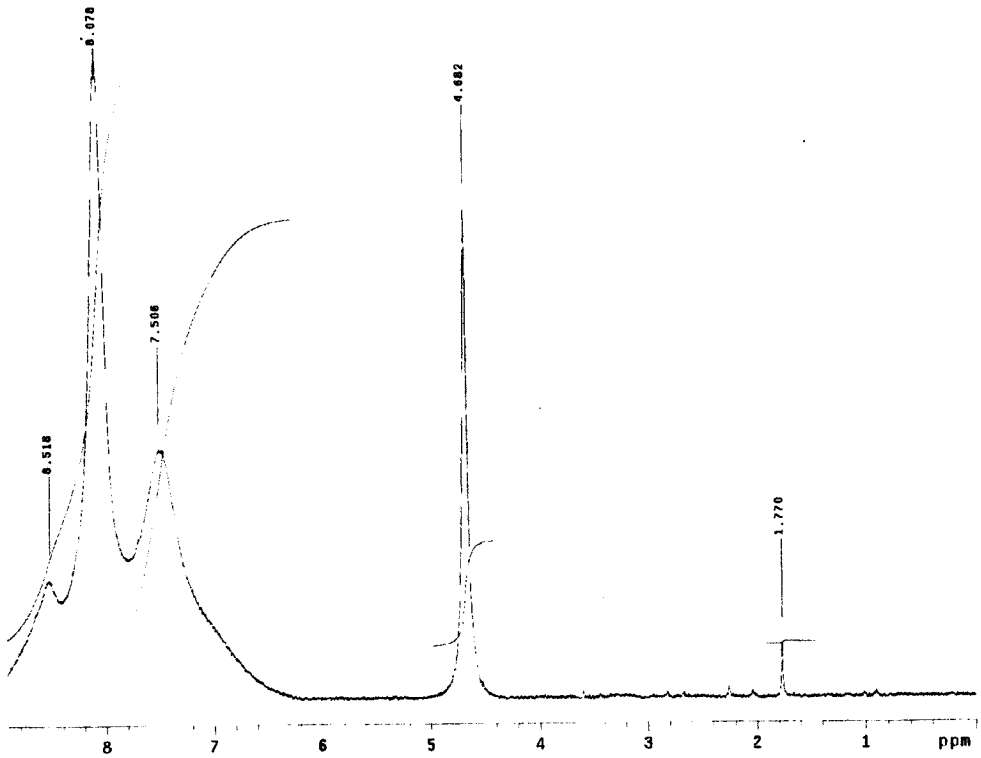

Fig. 4.14 Proton NMR spectra of $MnTPPS_4Cl$

Table 4.9 Proton NMR chemical shifts (in δ ppm) for aqueous porpyrins

Sr.No.	Porphyrin	0-Phenyl	m-Phenyl	β-Pyrrole
1	$TPPS_4$	8.53	7.38-7.4 (d)	8.05-8.03 (d)
2	$CoTPPS_4$	9.2	8.06	8.9
3	$MnTPPS_4Cl$	8.51	7.5	8.07

Note :

Here, o-phenyl protons are considered w.r.t. SO_3Na group. Threfore, these protons are deshielded and ultimately give more low field value than pyrrole protons.

In aqueous-porpyrins like $TPPS_4$, it is seen that ortho-phenyl protons are shifted to more down-field value as compared to pyrrole protons signal. The reason may be due to the presence of SO_3Na group at para position of the phenyl ring, ortho protons may be deshielded. Therefore, in aqueous-porphyrins o-phenyl protons have maximum down-field signal than β-protons. In $CoTPPS_4$, being paramagnetic in nature, the o-phenyl protons are still more shifted to down-field as compared to $TPPS_4$. In $MnTPPS_4Cl$, even though paramagnetic in nature, due to the presence of axial Cl ligand, the proton shifts are again seen at the position of diamagnetic porphyrins. Thus it is evident from above that; aqueous-porphyrins show more down-field proton shift than non-aqueous porphyrins on account of presence of SO_3Na group.

4.4 Elemental analysis

The elemental analysis being a characterization tool, it is included in this chapter to confirm the synthesized porphyrins, in addition to other spectroscopic methods. The selective non-aqueous porphyrins like TPP and CuTPP and aqueous-porphyrin like $MnTPPS_4Cl$ were subjected to elemental analysis with respect to C, H, and N analysis. The results of the same are summarized in Table 4.10

Table 4.10 Elemental analysis of non-aqueous and Aqueous-porphyrins

Sr.No.	Porphyrin	Amount	% C	% H	%N
1	TPP	Expected	85.95	4.92	9.10
		Found	84.01	4.90	8.96
2	CuTPP	Expected	78.13	4.26	8.28
		Found	76.52	4.33	8.16
3	$MnTPPS_4ClNa_4.12H_2O$	Expected	39.76	4.22	3.65
		Found	38.61	4.28	3.62

From the results in the above table, it can be concluded that there is sufficiently good agreement between expected results and experimental results, which reflects upon the routes of synthesis and methods of purification modified from time to time, are up to the expectation.

4.5 High resolution mass spectrometry (HR-MS)

The high resolution mass spectrum of $TPPS_4$ and $FeTPPS_4Cl$ were recorded as relative base peak intensity versus mass to charge (m/e) ratio. The fragmentation patterns of the compounds are shown in Fig.4.15 and 4.16 which gave the molecular ion peak from which molecular weight and molecular formulae of the aqueous-porphyrins were calculated.

In the mass spectrum of $TPPS_4$, the peak corresponding to m/z = 903.75 is a base peak and m/z =1047 is a molecular ion peak. This is the value obtained by the virtue of the operating system i.e sum of the molecular weight of $TPPS_4$ and Na, which shows 1047. When the atomic weight due to sodium is subtracted the value obtained is 1024.0075 as against expected 1023.02. Therefore, it is assigned as a molecular weight of TPPS4. In mass spectrometry the molecular weight of a substance is calculated without water molecules. Therefore, to know the exact chemical composition of a substance, FTIR and elemental analysis is supplemented to mass spectrometry. From the elemental analysis it is observed that the percentage of hydrogen matches with the 12 H_2O molecules. FTIR results have shown the presence of O-H stretching at the expected wave number (cm^{-1}). The TG-DSC results have shown loss of water molecules at the expected temperature range. Hence, $TPPS_4$ can be formulated as $TPPS_4.12\ H_2O$ and its molecular weight will be 1240.0075

The mass spectrum of $FeTPPS_4Cl$ shows (Fig 4.16) the molecular ion peak or parent peak at 1100.9292. The calculated weight of anhydrous $FeTPPS_4Cl$ is 1113.3 + 23 = 1136.3. But Cl being labile it is easily lost (peak 1137.9097), therefore, expected molecular ion peak is at 1136.3 – 35.5 = 1100.8. Thus there is good agreement between

experimental and calculated value. Based on these calculations, the porphyrin can be formulated as $FeTPPS_4Cl$ $.12H_2O$ with molecular weight of 1329. Using above results from the HR-mass spectroscopy, molecular formula and corresponding molecular weight of the aqueous-porphyrins were determined as shown in Table 4.11

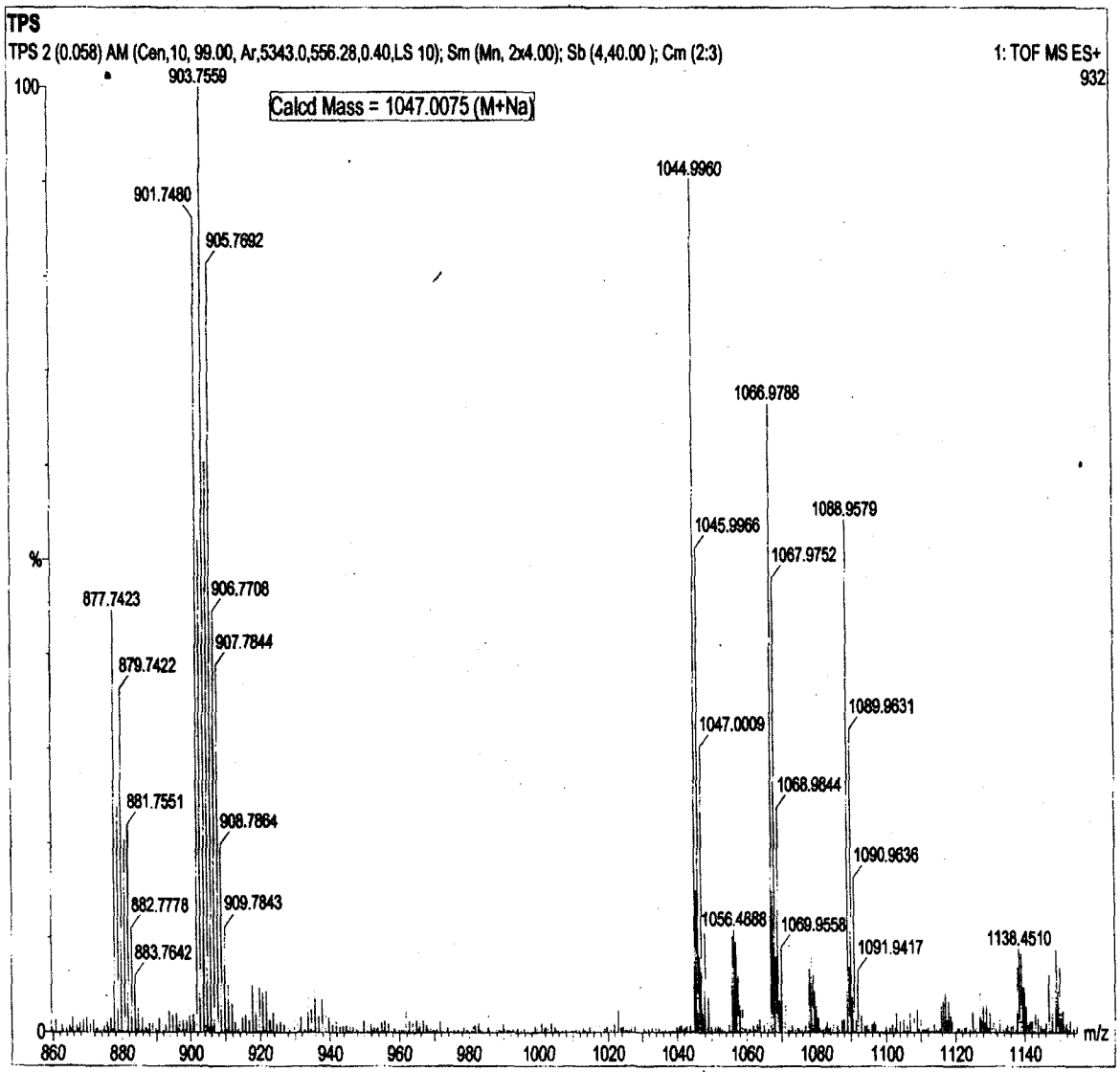

Fig 4.15 HR-MS spectra of $TPPS_4$

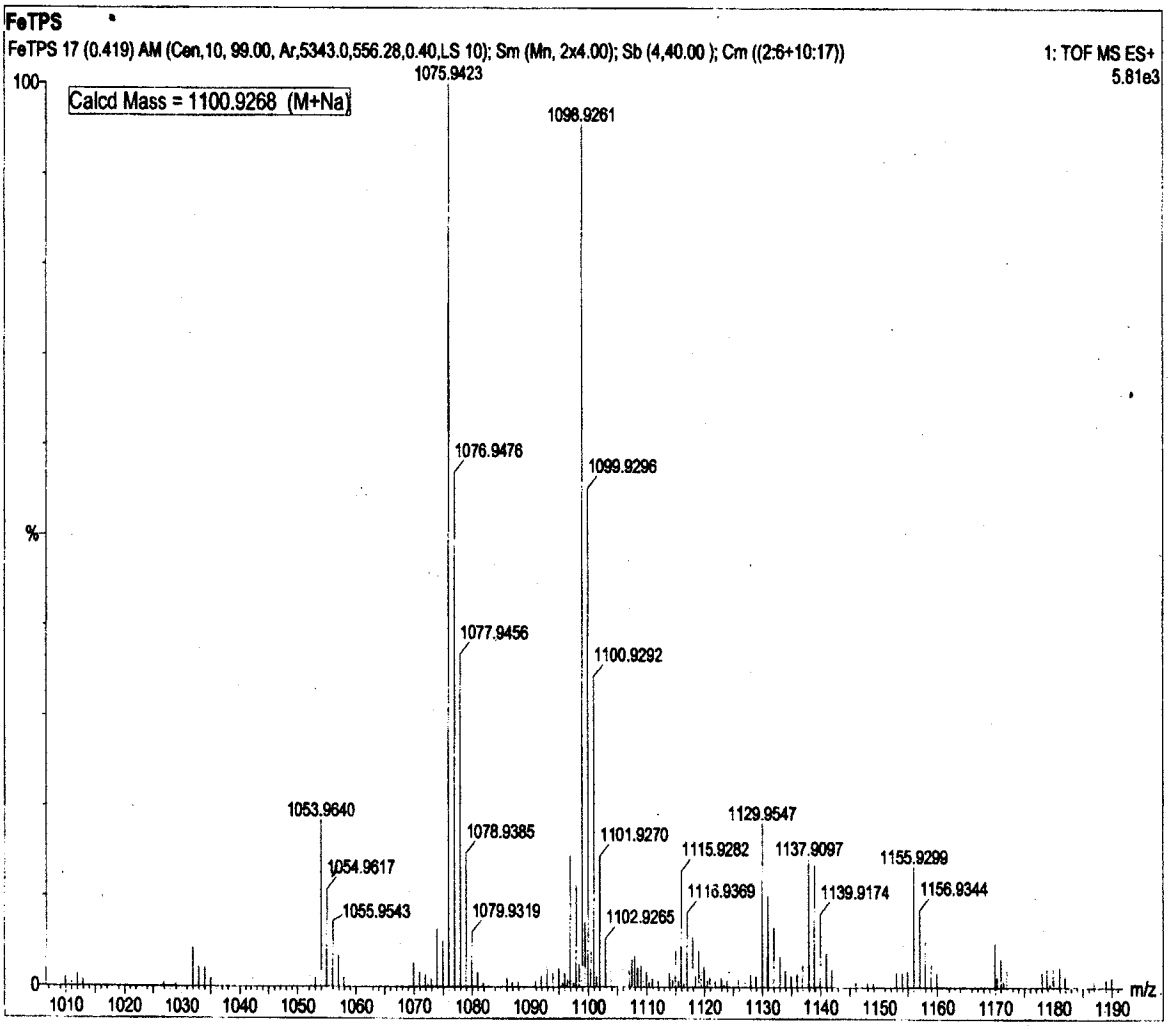

Fig.4.16 HR-MS spectra of $FeTPPS_4Cl$

Table 4.11 Molecular formulae and molecular weights of aqueous-porphyrins

Sr.No.	Molecular formula	Molecular weight
1	$TPPS_4.12H_2O$	1240
2	$CoTPPS_4.\ 12H_2O$	1297
3	$NiPPS_4.\ 12H_2O$	1296.6
4	$CuTPPS_4.12H_2O$	1301.5
5	$ZnTPPS_4.\ 12H_2O$	1303.4
6	$AgTPPS_4.\ 12H_2O$	1345.8
7	$MnTPPS_4Cl.\ 12H_2O$	1328.4
8	$FeTPPS_4Cl.\ 12H_2O$	1329
9	$O\text{-}(FeTPPS_4)_2.\ 24H_2O$	2603
10	$SnTPPS_4Cl_2.\ 12H_2O$	1427.7

Note: For convenience the $12H_2O$ molecules are not represented each time

4.8 Fluorescence spectroscopy

It is accepted that most of the luminescence and photochemistry observed from porphyrins is associated with the π - π^* states of the porphyrin ring, even though, the lifetimes and reactivity of these states depend strongly on the metal ion incorporated[107]. In general most of the free base porphyrins, chlorins, and related compounds show strong fluorescence at room temperature and in rigid glasses they show fluorescence and phosphorescence. Metalloporphyrins luminescence falls into several categories, which is dependent upon the electronic structure of the metal. For the free-base TPP, fluorescence λ_{max} and singlet energies are 660 nm and 45 kcal/mol. When metals are containing either empty or full d-shells, form complexes with tetraphenyl porphyrin or octaethyl porphyrin and then they show fluorescence at room temperature[108,109] as well as fluorescence and phosphorescence at liquid nitrogen temperature. The fluorescence yield tends to decrease with increasing atomic number of the metal as does the phosphorescence. The emission spectra are usually shifted to longer wavelengths as the square-planar metalloporphyrin accepts axial ligands in the fifth and sixth coordination positions [110].

The non-aqueous and aqueous porphyrins were first tested under UV lamp to check their fluorescence property and accordingly they were selected for quantitative determination of fluorescence intensity and corresponding wavelength i. e. λ_{max}.

In the series of non-aqueous porphyrins, TPP, ZnTPP, MnTPPCl, O-$(MnTPP)_2$ and $SnTPPCl_2$ are found to be fluorescent whereas CoTPP, NiTPP, CuTPP, AgTPP, FeTPPCl and O-$(FeTPP)_2$ are nearly non-fluorescent. In TPP emission intensity at λmax = 657 nm is 14.69 whereas in ZnTPP there are two well defined emission bands at 597 nm and 644 nm with emission intensity of 9.13 at λ_{max} as shown in Fig. 4.17. The values of λmax

obtained for TPP and ZnTPP are in good agreement with the literature values[192,193]. Further, it is seen that the MnTPPCl exhibits maximum fluorescence intensity in the series as shown in Fig. 4.18. Following sequence gives the intensities of non-aqueous porphyrins in the order MnTPPCl > O-$(MnTPP)_2$ > TPP > ZnTPP > $SnTPPCl_2$.

With reference to aqueous-porphyrins it is seen that $TPPS_4$, $ZnTPPS_4$, $AgTPPS_4$, $MnTPPS_4Cl$ and $SnTPPS_4Cl_2$ are fluorescent whereas $CoTPPS_4$, $NiTPPS_4$, $CuTPPS_4$, $FeTPPS_4Cl$ and O-$(FeTPPS_4)_2$ are nearly non-fluorescent. In this series, TPPS4 shows maximum emission intensity, $ZnTPPS_4$ and $AgTPPS_4$ show minimum and equal amount of intensities. Fig 4.19 shows fluorescence intensity for $TPPS_4$ and $ZnTPPS_4$ whereas Fig 4.20 shows the fluorescence for $MnTPPS_4Cl$ and $SnTPPS_4Cl_2$ respectively. The order of fluorescence intensity is given as $TPPS_4$ > $SnTPPS_4Cl_2$ > $MnTPPS_4Cl$ > $ZnTPPS_4$ = $AgTPPS_4$.

When non-aqueous and aqueous-porphyrins are compared it is observed that

1) The aqueous-porphyrins show hypsochromic or blue shift in emission wavelength as compared to non-aqueous porphyrins. The values can be compared as shown in Tables 4.12 and 4.13.

2) The aqueous-porphyrins show many fold higher fluorescence than non-aqueous porphyrins.

3) AgTPP is found to be non-fluorescent whereas after sulphonation i.e. $AgTPPS_4$ shows fluorescent property.

4) The excitation wavelength required for aqueous-porphyrins is 300 nm whereas for non-aqueous porphyrins it is 420 nm for 10^{-4} M concentration.

These observations may be explained on the basis of solvent effect as well as sulphonation of four phenyl rings at para position in aqueous porphyrins. It is also observed in the chapter 6 that the fluorescent porphyrins are more efficient photocatalysts than non-fluorescent porphyrins.

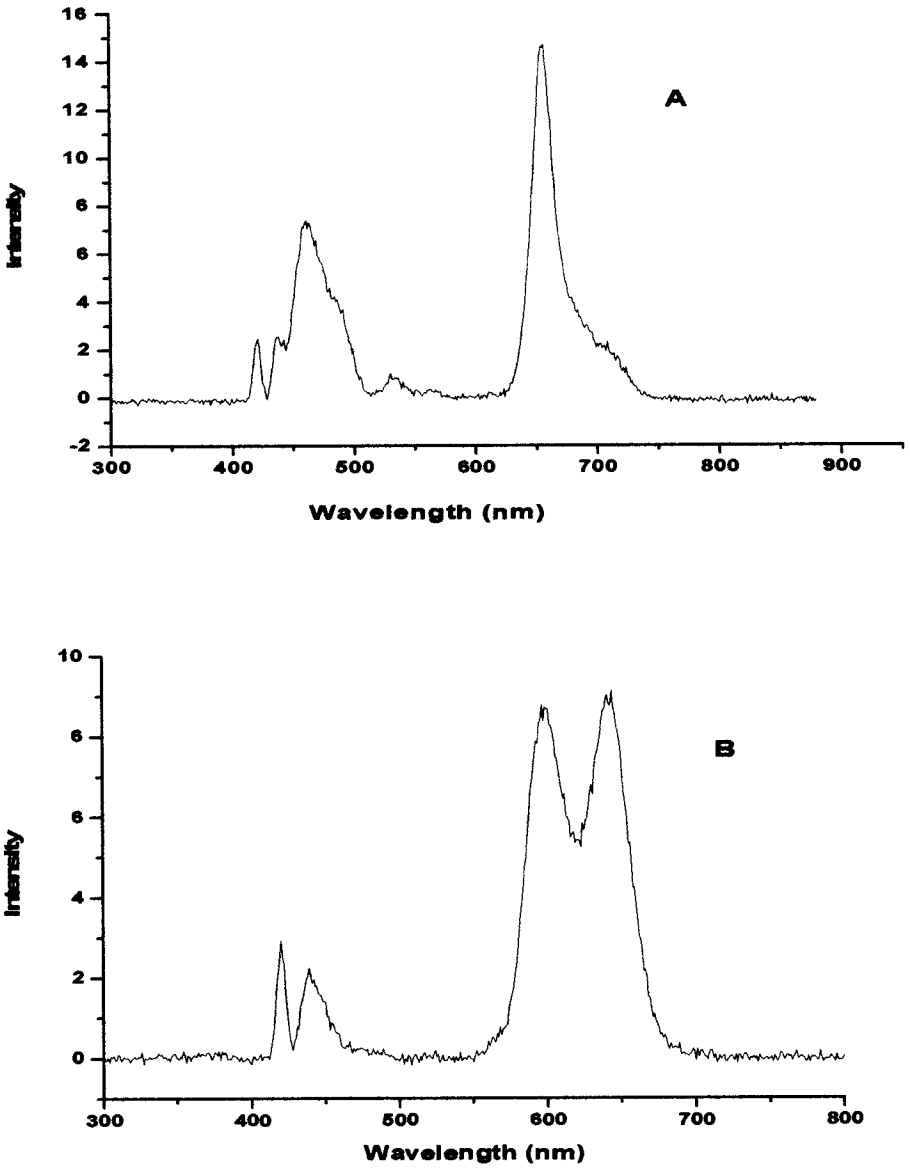

Fig 4.17 Fluorescence spectra of A)TPP B) ZnTPP

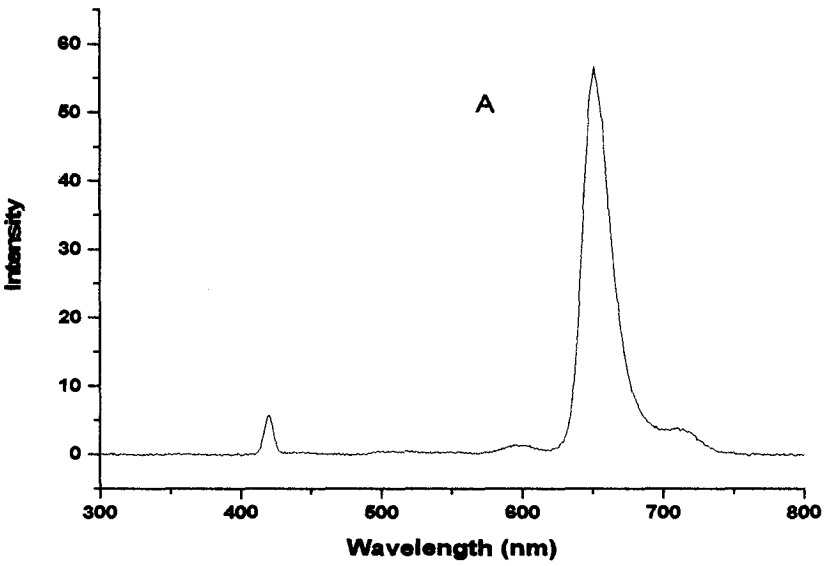

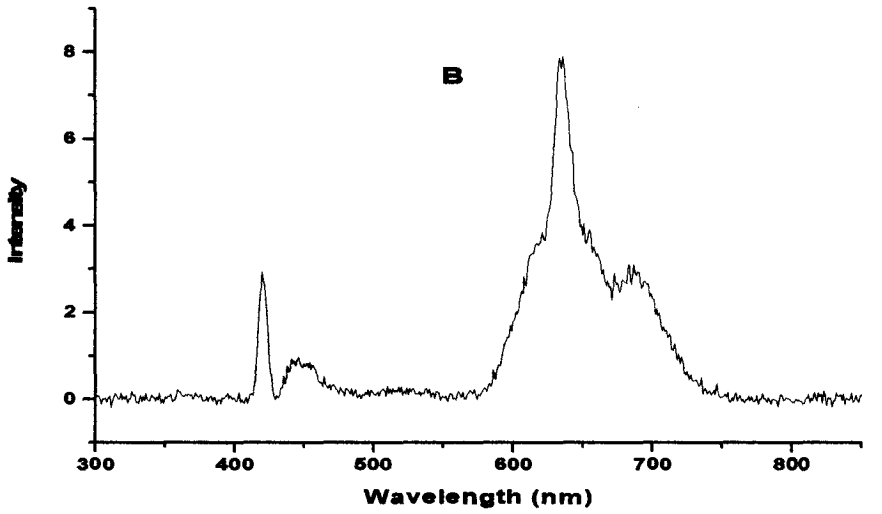

Fig. 4.18 Fluorescence spectra of A) MnTPPCl B) $SnTPPCl_2$

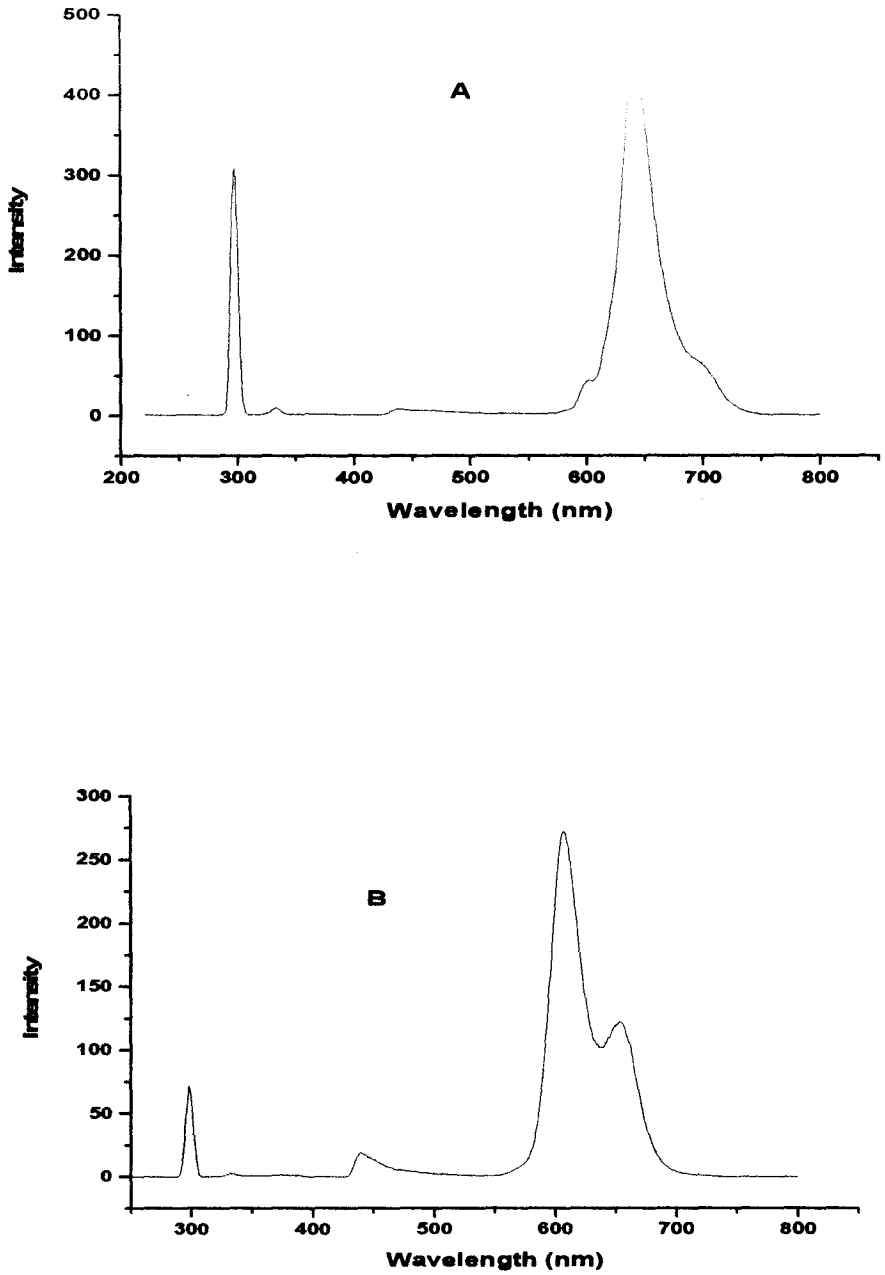

Fig. 4.19 Fluorescence spectra of A) $TPPS_4$ B) $ZnTPPS_4$

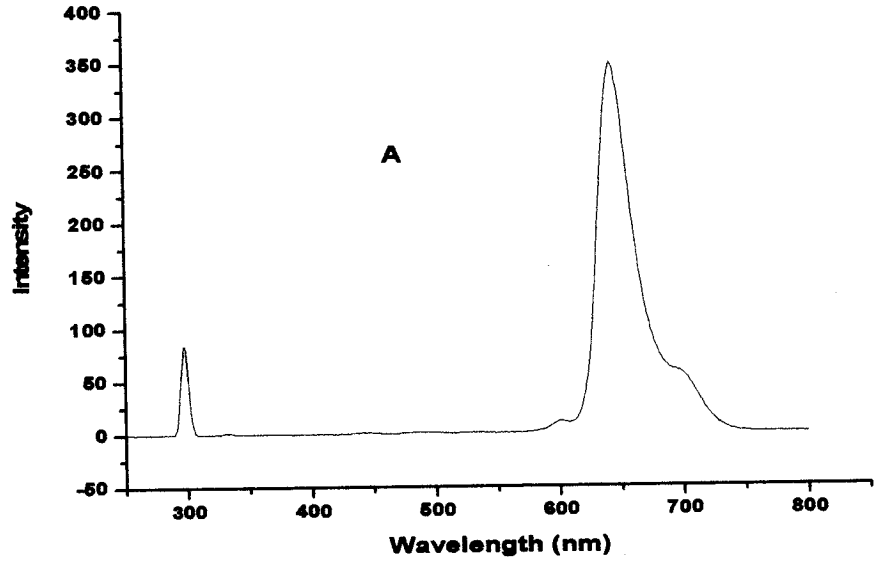

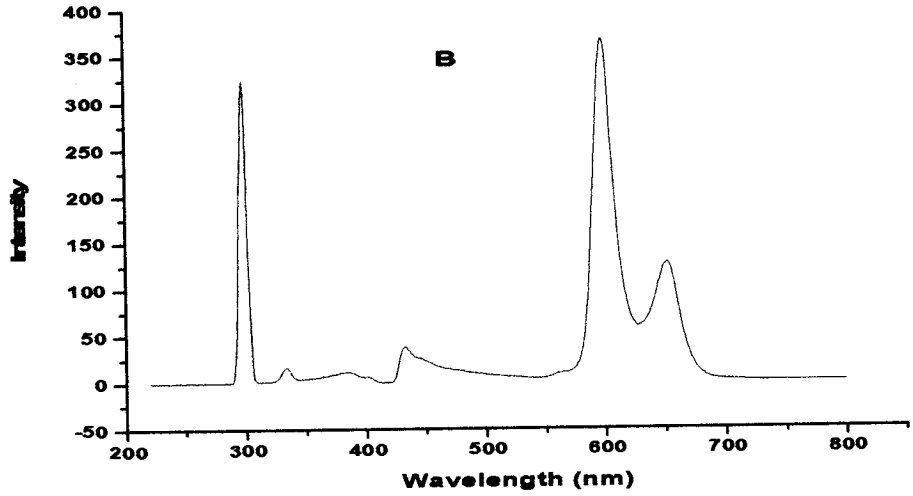

Fig.4.20 Fluorescence spectra of A) $MnTPPS_4Cl$ B) $SnTPPS_4Cl_2$

Table 4.12 Fluorescence data of non-aqueous porphyryrin

(Excitation wavelength = 420 nm)

Sr.No.	Porphyrin	λ_{max} (nm)	Fluorescence Intesity
1	TPP	657	14.69
2	CoTPP	421	2.837
3	NiTPP	421	2.911
4	CuTPP	420	2.578
5	ZnTPP	644	9.13
6	AgTPP	421	2.603
7	MnTPPCl	651	56.72
8	O-$(MnTPP)_2$	504	46.06
9	FeTPPCl	420	2.879
10	O-$(FeTPP)_2$	420	2.710
11	$SnTPPCl_2$	636	7.89

Table 4.13 Fluorescence data of aqueous-porphyrins

(Excitation wavelength = 300 nm)

Sr.No.	Porphyrin	λ_{max} in nm	Fluorescence Intensity
1	$TPPS_4$	642	448.06
2	$CoTPPS_4$	601	21.54
3	$NiTPPS_4$	643	14.58
4	$CuTPPS_4$	601	6.61
5	$ZnTPPS_4$	607	272.28
6	$AgTPPS_4$	607	272.28
7	$MnTPPS_4Cl$	643	349.28
8	$FeTPPS_4Cl$	600	6.03
9	$O\text{-}(FeTPPS_4)_2$	600	10.03
10	$SnTPPS_4Cl_2$	598	367.38

4.9 Diffuse reflectance spectroscopy (DRS)

Diffuse reflectance spectra of non-aqueous and aqueous porphyrins were recorded on using wavelength range from 300 to 800 nm and $BaSO_4$ as a reference material. Reflectance data are usually expressed in terms of percent reflectance (%R) which is analogous to percent transmission in absorption spectroscopy. The technique is non-destructive and is used to determine the energy gap (E_g) in semiconductors in optoelectronics[120-123]. A common way of determining band gap from absorption spectra is the percent reflectance (%R) is made function of wavelength and from the corresponding graph E_g is calculated.

In the series of non-aqueous porphyrins it is seen that the band-gap energy value of CoTPP is 1.92 eV whereas for CuTPP it is 1.61 eV. These are higher and lower values obtained for the selected series. The rest of the values are lying in between these two extreme values. The DRS curves for TPP, ZnTPP, MnTPPCl and $SnTPPCl_2$ are shown in Fig. 4.21 and 4.22 respectively. The band-gap (E_g) values for given porphyrins are calculated by using formula, band gap (eV) = 1239 / λ_{max} where, λmax is obtained from the respective DRS curves. Table 4.14 contains band-gap energy values for non-aqueous porphyrins in eV.

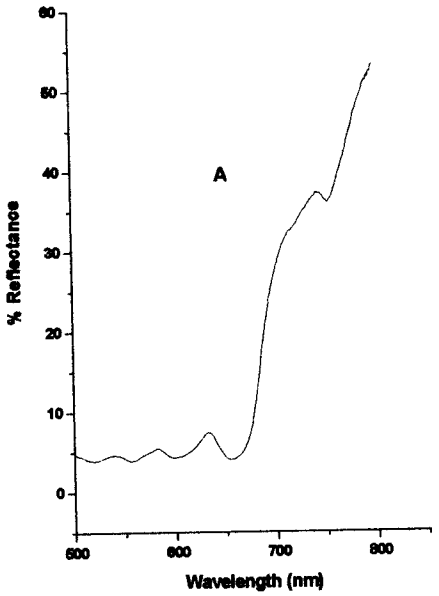

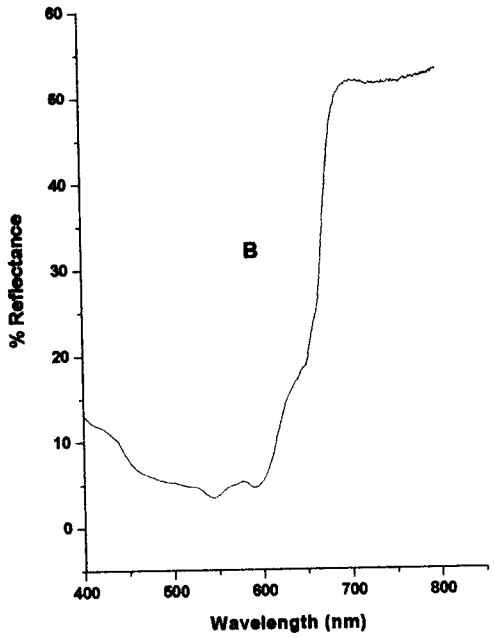

Fig. 4.21 DRS spectra of A) TPP B) ZnTPP

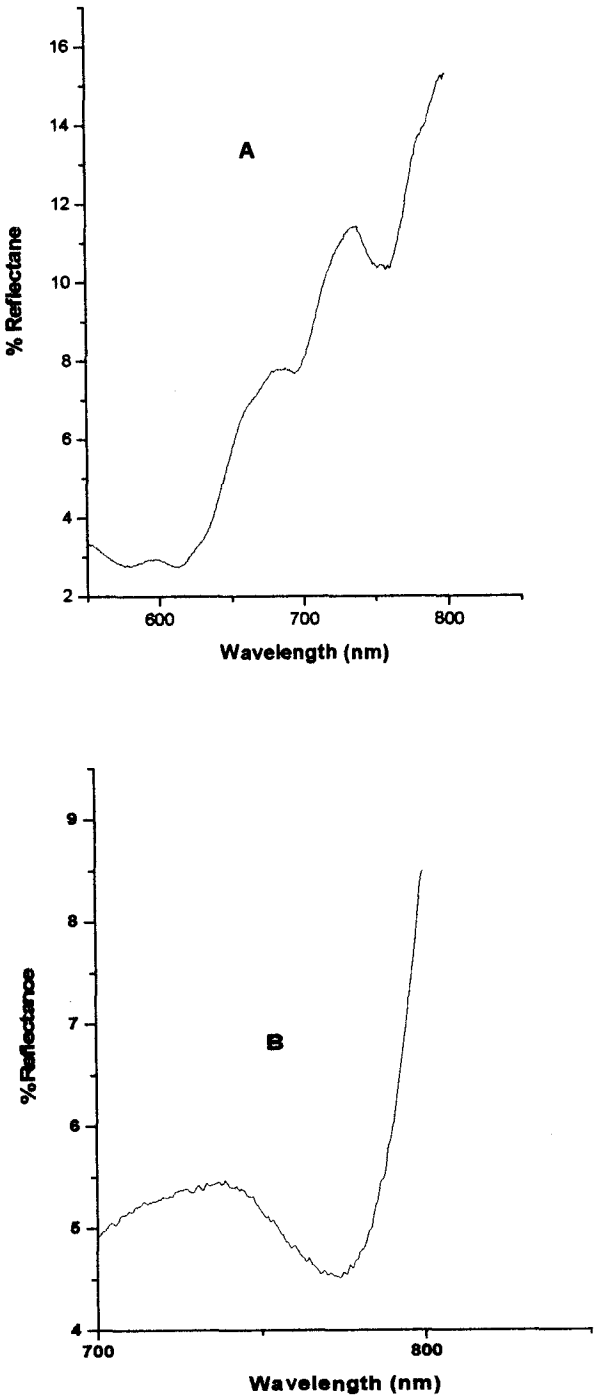

Fig. 4.22 DRS spectra of A) MnTPPCl B) $SnTPPCl_2$

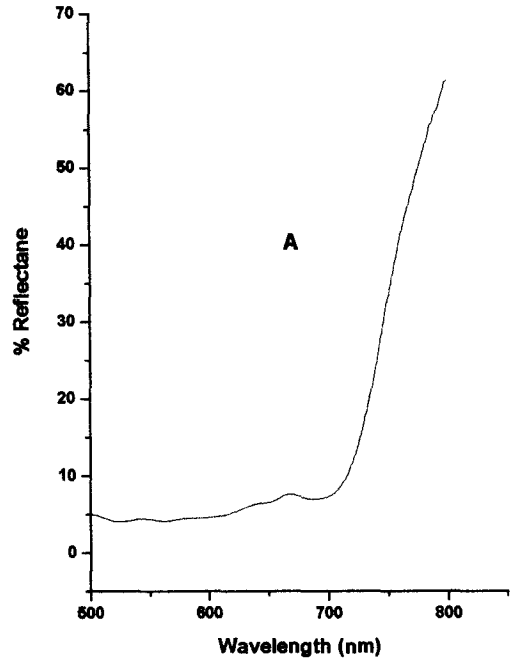

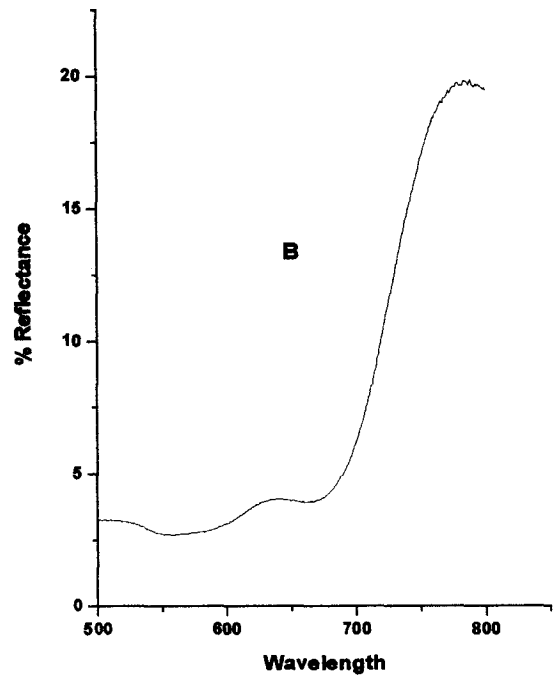

Fig.4.23 DRS spectra of A)$TPPS_4$ B) $AgTPPS_4$

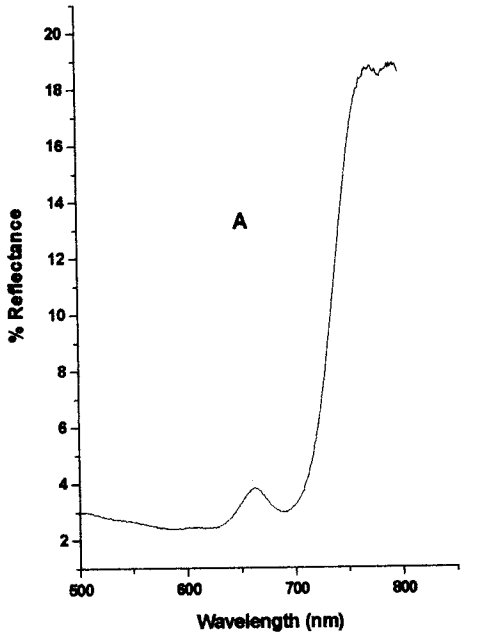

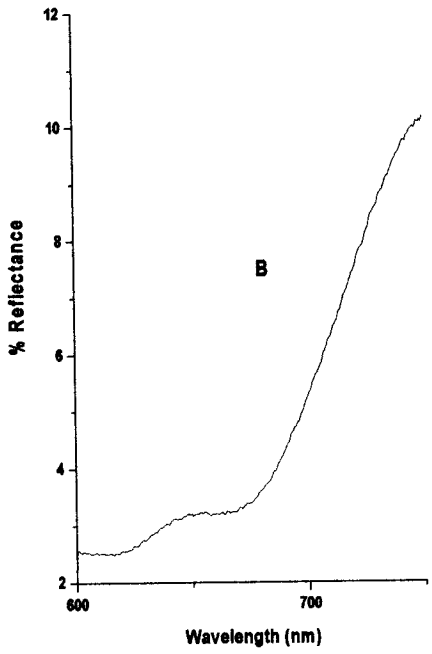

Fig.4.24 DRS spectra of A) $MnTPPS_4Cl$ B) O-$(FeTPPS_4)_2$

Table 4.14 Band gap energy values of non-aqueous porphyrins

Sr.No.	Porphyrin	Band gap (eV)
1	TPP	1.75
2	CoTPP	1.92
3	NiTPP	1.82
4	CuTPP	1.61
5	ZnTPP	1.86
6	AgTPP	1.75
7	MnTPPCl	1.70
8	O-$(MnTPP)_2$	1.69
9	FeTPPCl	1.71
10	$SnTPPCl_2$	1.68

Table 4.15 Band gap energy values for aqueous-porphyrins

Sr.No.	Porphyrin	Band Gap (eV)
1	$TPPS_4$	1.66
2	$CoTPPS_4$	1.76
3	$NiTPPS_4$	1.83
4	$CuTPPS_4$	1.79
5	$AgTPPS_4$	1.74
6	$MnTPPS_4Cl$	1.68
7	$FeTPPS_4Cl$	1.75
8	$O\text{-}(FeTPPS_4)_2$	1.73
9	$SnTPPS_4Cl_2$	1.75

In the series of aqueous-porphyrins, it is seen that $NiTPPS_4$ shows E_g = 1.83 eV and $TPPS_4$ shows E_g = 1.66 eV, which are maximum and minimum for the selected series. The other porphyrins show the E_g values in between these two extremes. The DRS curves of $TPPS_4$, $AgTPPS_4$, $MnTPPS_4Cl$ and dimer $O\text{-}(FeTPPS_4)_2$ are shown in Fig. 4.23 and 4.24 respectively. The values of all compounds were calculated using above mentioned formula and are summarized in Table 4.15

From the E_g values of non-aqueous and aqueous porphyrins, it is revealed that, these compounds are narrow-band intrinsic semiconductors where $E_g < 2$ eV. This makes them efficient photocatalysts in the process of degradation of different dyes in the course of photocatalysis.

CHAPTER 5

Magnetic, thermal and other studies

5.1 Magnetic studies

The magnetic susceptibility measurements of metalloporphyrins were carried out to confirm or establish the oxidation state of the metal ion and to find if any peculiar magnetic interactions are present[137]. The experimental distinction between high-spin and low-spin complexes can be done by measuring their magnetic properties. The diamagnetic complexs tend to move out of a magnetic field and paramagnetic complexes tend to move into a magnetic field. The extent of the paramagnetism of a complex is commonly reported in terms of the magnetic dipole moment it possesses. Further, magnetic susceptibility values are used to calculate magnetic moment (μ_{eff}) and subsequently for number of unpaired electrons. Thus it is possible to predict the d-electron configuration of a metal in complex. Table 5.1 and 5.2 show the magnetic susceptibilities of non-aqueous and aqueous porphyrins.

In the list of non-aqueous porphyrins it is observed that TPP, NiTPP, ZnTPP and $SnTPPCl_2$ are diamagnetic whereas CoTPP, CuTPP, AgTPP, MnTPPCl, O-$(MnTPP)_2$, FeTPPCl and O-$(FeTPP)_2$ are paramagnetic in nature. Further, it is also observed that, magnetic susceptibility values (χ_g) go on decreasing as the atomic number of a metal increases for divalent metals. In case of trivalent metalloporphyrins, same decreasing trend is seen with the increase in atomic number. The comparison between monomers and dimers i.e. MnTPPCl and O-$(MnTPP)_2$, or FeTPPCl and O-$(FeTPP)_2$ represents that dimers show decreased χ_g values than respective monomers. From this it may be

said that with the increasing atomic number of a metal, the concerned compound moves comparatively less into the magnetic field.

5.1 Magnetic measurements of non-aqueous porphyrins

Sr.No.	Porphyrin	Magnetic Susceptibility χ_g (cgs units)	μ_{eff} (B.M)	No. of unpaired electrons	Type of complex
1	TPP	Diamagnetic	—	—	—
2	CoTPP	2.25 × 10-6	1.924	01	Low spin
3	NiTPP	Diamagnetic	—	—	—
4	CuTPP	1.49 × 10-6	1.574	01	Low spin
5	ZnTPP	Diamagnetic	—	—	—
6	AgTPP	1.34 × 10-6	1.560	01	Low spin
7	MnTPPCl	1.30 × 10-5	4.74	04	High spin
8	O-$(MnTPP)_2$	9.8 × 10-6	4.1	03	High spin
9	FeTPPCl	1.18 × 10-5	4.52	02	Low spin
10	O-$(FeTPP)_2$	1.14 × 10-6	1.38	01	Low spin
11	$SnTPPCl_2$	Diamagnetic	—	—	—

5.2 Magnetic measurements of aqueous porphyrins

Sr.No.	Porphyrin	Magnetic Susceptibility χ_g (cgs units)	μ_{eff} (B.M.)	No. of unpaired electrons	Type of complex
1	$TPPS_4$	Diamagnetic	—	—	—
2	$CoTPPS_4$	8.39×10^{-7}	1.633	01	Low spin
3	$NiTPPS_4$	Diamagnetic	—	—	—
4	$CuTPPS_4$	6.78×10^{-7}	1.470	01	Low spin
5	$ZnTPPS_4$	Diamagnetic	—	—	—
6	$AgTPPS_4$	6.89×10^{-7}	1.501	01	Low spin
7	$MnTPPS_4Cl$	1.2×10^{-6}	1.822	01	Low spin
8	$FeTPPS_4Cl$	7.43×10^{-7}	1.556	01	Low spin
9	$O\text{-}(FeTPPS_4)_2$	8.19×10^{-7}	1.620	01	Low spin
10	$SnTPPS_4Cl$	Diamagnetic	—	—	—

From the Table 5.1, it is also observed that, the magnetic moment values (μ_{eff}) for CoTPP, O-$(MnTPP)_2$, FeTPPCl are higher than spin-only magnetic moments, which explains the orbital magnetic contribution is substantial in these porphyrins. The number of unpaired electrons were determined by using $\mu_{eff} = g / 2 \sqrt{n(n+2)}$ where, n is the number of unpaired electrons and g is spectroscopic splitting factor or g-factor. Further, using experimental value of g for each compound from ESR, the number of unpaired electrons is calculated. These calculations have shown that, only MnTPPCl and O-$(MnTPP)_2$ are high spin complexs whereas others are low-spin complexes. Based on these results, it is clear that, oxidation states of Co, Cu Ag, are +2 and for Mn and Fe oxidation states are +3.

In the series of aqueous porphyrins the results obtained are summarized in Table 5.2. The porphyrins such as $TPPS_4$, $NiTPPS_4$, $ZnTPPS_4$ and $SnTPPS_4Cl_2$ are found diamagnetic whereas $CoTPPS_4$, $CuTPPS_4$, $AgTPPS_4$, $MnTPPS_4Cl$, O-$(MnTPPS_4)_2$, $FeTPPS_4Cl$, O-$(FeTPPS_4)_2$ are found to be paramagnetic in nature. Among porphyrins of divalent metals, the magnetic susceptibility decreases in the following order i.e. $CoTPPS_4$ > $AgTPPS_4$ > $CuTPPS_4$. The porphyrins of trivalent metals show the order of χ_g as $MnTPPS_4Cl$ > O-$(FeTPPS_4)_2$ > $FeTPPS_4Cl$. From the values of μ_{eff} it is observed that only in $MnTPPS_4Cl$, in addition to spin-only value to some extent magnetic orbital contribution is present. All aqueous-porphyrins are low-spin complexes. Further, oxidation states of metals were calculated and found that Co, Ni, Cu and Ag are in +2 oxidation states whereas Fe is in +3 oxidation state.

When degree of paramagnetism of non-aqueous and aqueous porphyrins is compared, sulphonated porphyrins show slightly less magnetic moment than non-aqueous porphyrins for divalent metal porphyrins. In case of Mn and Fe porphyrins, degree of paramagnetism is considerably reduced in $MnTPPS_4Cl$ and $FeTPPS_4Cl$ as compared to MnTPPCl and FeTPPCl. Thus sulphonation of non-aqueous porphyrins exhibits observable effect on magnetic properties like magnetic moments.

5.2 Electron spin resonance (ESR)

The basic features of ESR spectra are strongly dependent on the number as well as the location of the unpaired electrons in a system. The information available from magnetic studies is used for the selection of the samples for ESR spectroscopy. Electron spin resonance (ESR) signal of CuTPP, AgTPP, MnTPPCl were recorded at room temperature whereas for CoTPP, FeTPPCl and O-$(FeTPP)_2$ spin-lattice times are short, therefore, their spectra were recorded at liquid nitrogen temperature. The respective 'g' factor, line width and hyperfine splitting constant (A) have shown in Table 5.3 The hyperfine splitting constant value (A) indicates an interaction between electron spin and nuclear spin of the same atom. The line width explains the life time of the excited state of the nuclear spin. ESR spectra of CuTPP and AgTPP as are shown in Fig. 5.1 and ESR spectra of CoTPS and $FeTPPS_4Cl$ are shown in Fig. 5.2 respectively.

ESR measurements of CuTPP the magnetic field set were at 3000 G (gauss) and scan range used was 2000 G at room temperature. When ESR spectrum of CuTPP is carefully observed, it is seen that, $g_{\|} = 2.184$ and $g_{\perp} = 2.066$. Further, $g_{average}$ is calculated as:

$g_{avg} = 1/3\ (g_{\|} + 2\ g_{\perp})$

$= 1/3\ (2.185 + 2 \times 2.066)$

$= 1/3\ (6.317)$

$$g_{avg} = 2.106$$

Similarly, hyperfine splitting constant can be given as $A_{||} = 2870 - 2670 = 200$ G, $A_{\perp}$ is not resolved. The ESR spectrum of AgTPP (Fig. 5.1) is also seen to be resolved into $g_{\perp}$ and $g_{||}$ which is to be averaged to 2.065 G . Further, hyperfine splitting constant $A_{||}$ is calculated. The above results are in good agreement with the literature values[191]. The ESR parameters for other non-aqueous porphyrins are summarized in Table 5.3. In case of CoTPP on account of lack of ESR signal at room temperature, the spectrum was recorded at liquid nitrogen temperature with $A_{||} = 130$ G. In FeTPPCl and O-$(FeTPP)_2$ hyperfine splitting is not seen therefore, 'A' was not calculated. The monomer of Mn^{3+}, i.e. MnTPPCl shows maximum hyperfine splitting at room temperature where constant is given by $A_{avg} =$ 100 G.

In the case of aqueous-porphyrins, ESR signals are recorded at room temperature. In Fig. 5.2 ESR spectra of $CoTPPS_4$ and $FeTPPS_4Cl$ are seen. Table 5.4 shows ESR parameters of aqueous-porphyrins of divalent and trivalent metal ions. It is also seen from the table that, only in case of $MnTPPS_4Cl$ (Fig. 5.3) hyperfine splitting is seen with $A_{||} = 25$ G.

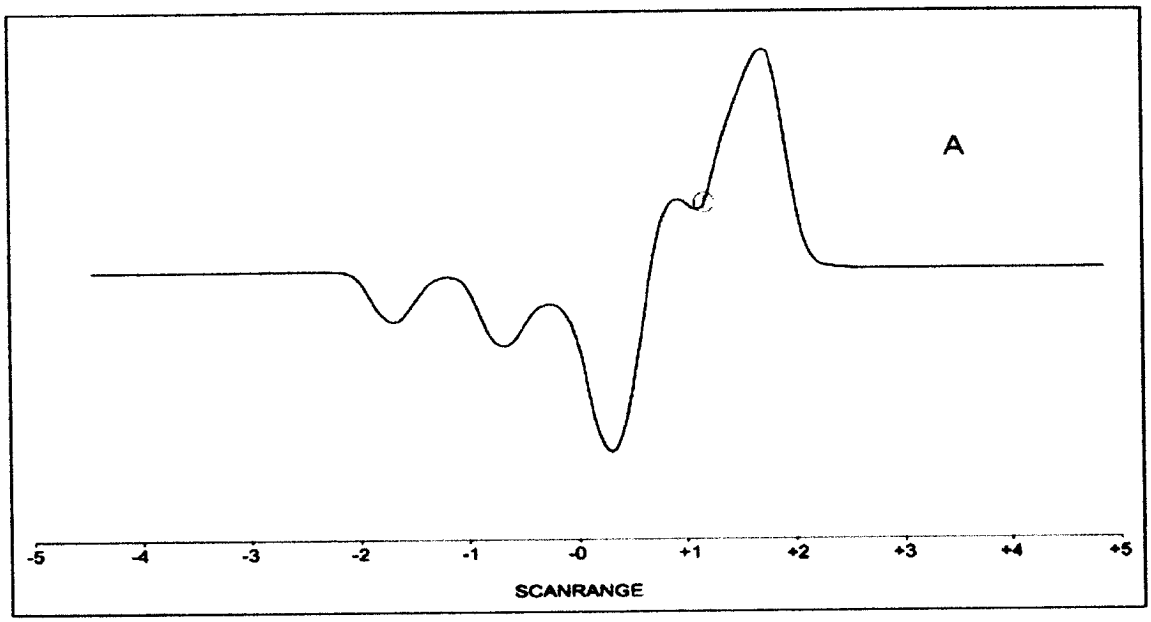

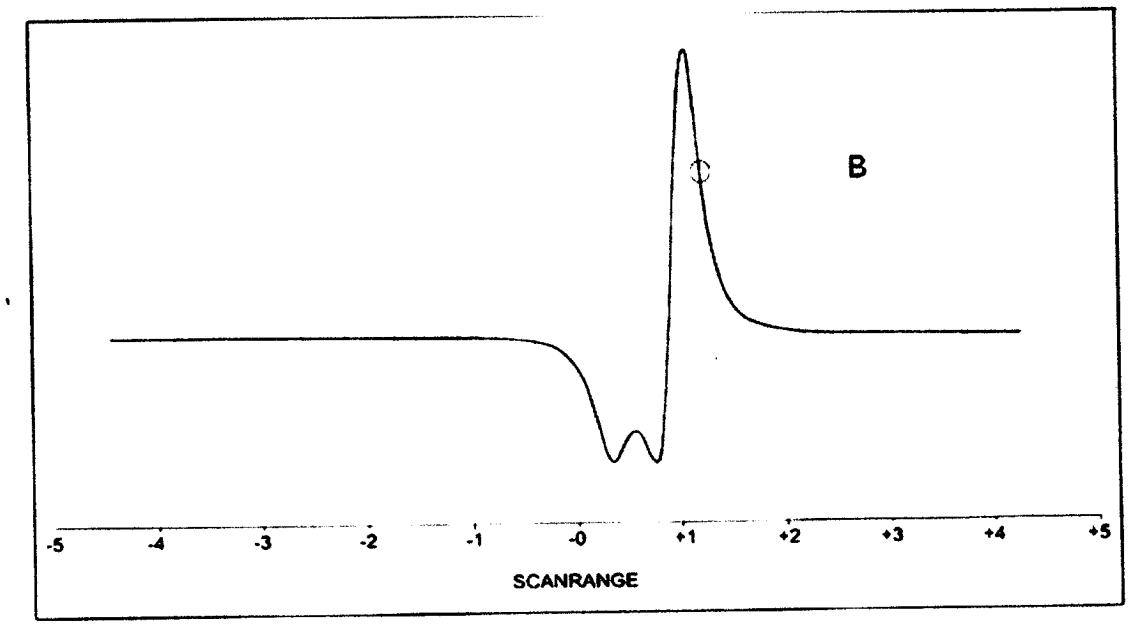

Fig 5.1 ESR spectra of A) CuTPP B) AgTPP

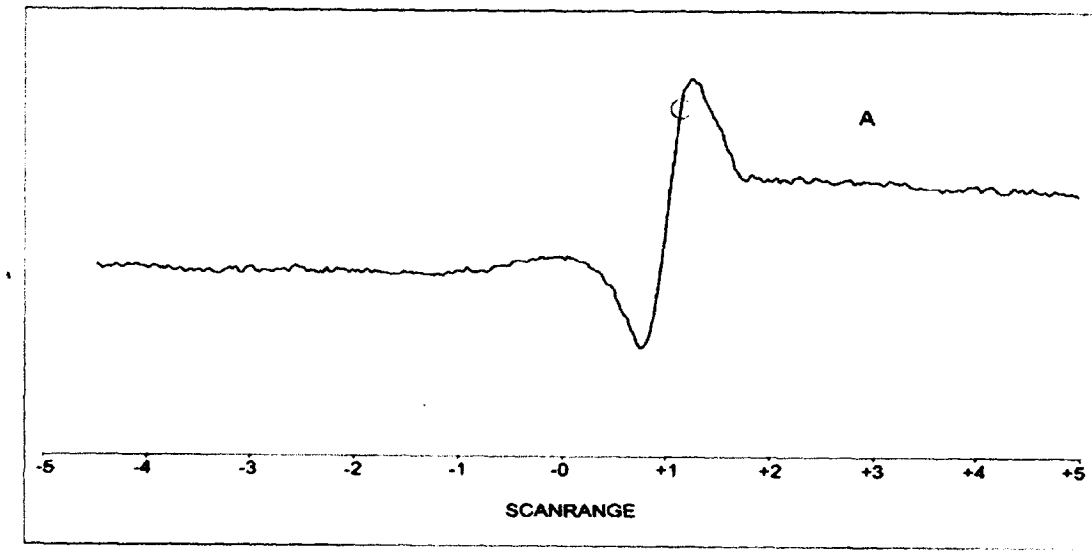

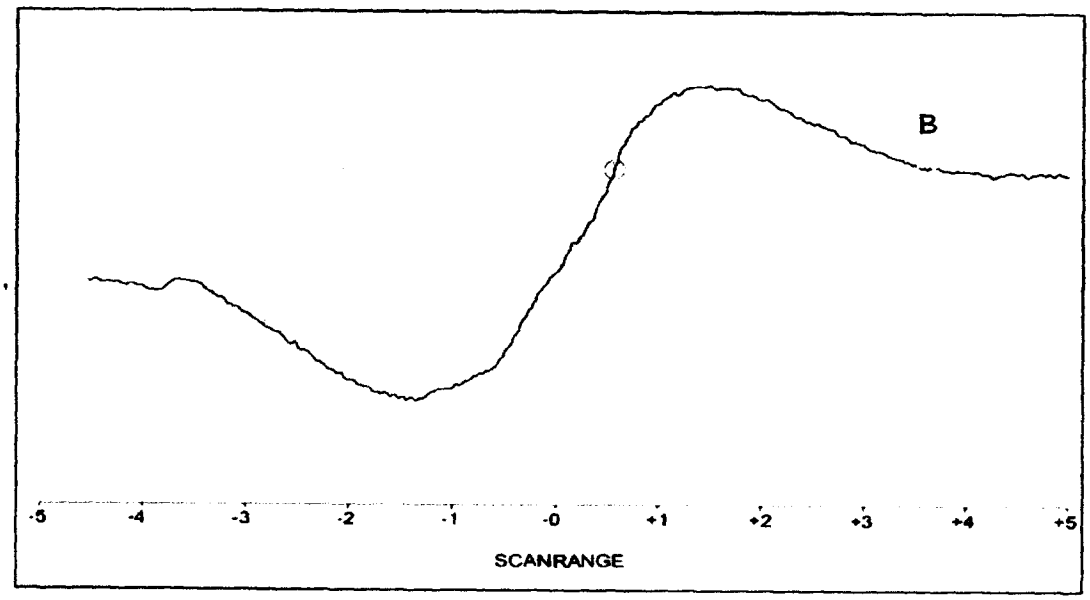

Fig. 5.2 ESR spectra of A) $CoTPPS_4$ B) $FeTPPS_4Cl$

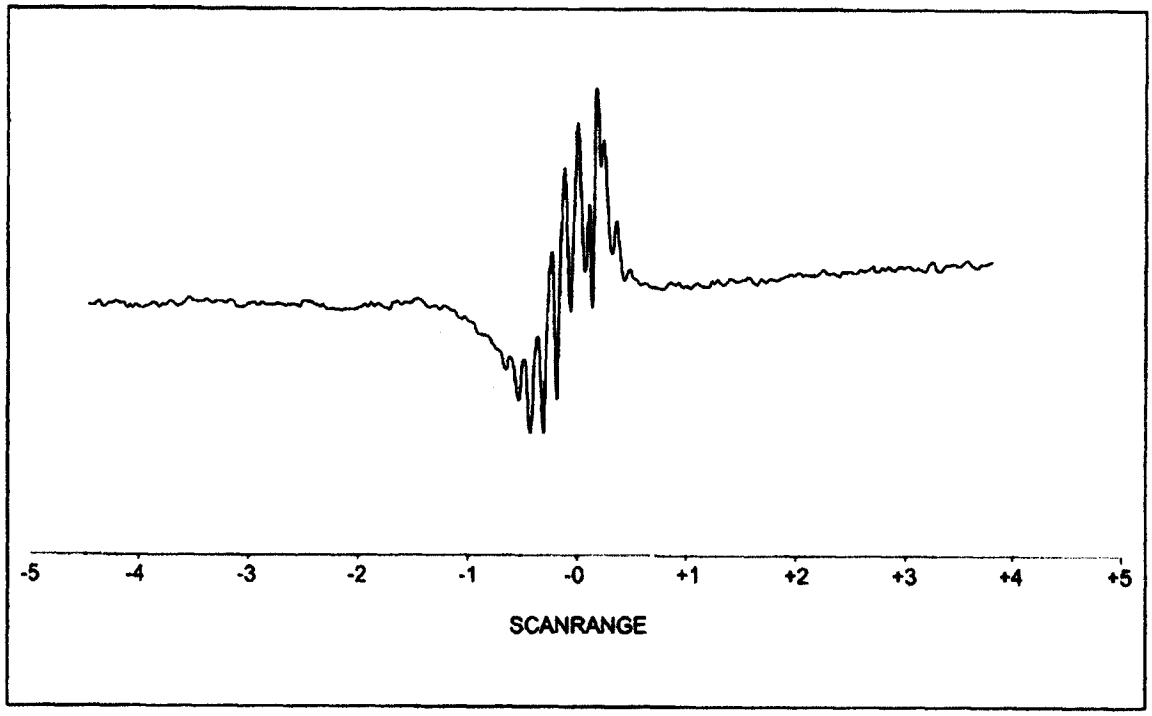

Fig. 5.3 ESR spectra of $MnTPPS_4Cl$

Table 5.3 ESR measurements of non-aqueous porphyrins

Sr.No.	Porphyrin	"g" factor	Linewidth in Gauss	Hyperfine Splitting constant "A" in Gauss
1	CoTPP	2.269	110	$A_{\|\|}$ =130
2	CuTPP	2.106	125	$A_{\|\|}$ =200
3	AgTPP	2.114	65	$A_{\|\|}$ =80
4	MnTPPCl	2.003	10	A_{avg} =100
5	FeTPPCl	4.024	200	—
6	O-$(FeTPP)_2$	2.0028	50	—

Table 5.4 ESR measurements of Aqueous-porphyrins

Sr.No.	Porphyrin	"g" factor	Line width in gauss	Hyperfine Splitting constant "A" in Gauss
1	$CoTPPS_4$	2.018	100	—
2	$CuTPPS_4$	2.073	100	—
3	$AgTPPS_4$	2.053	60	—
4	$MnTPPS_4Cl$	2.028	10	Aavg = 25
5	$FeTPPS_4Cl$	2.057	55	—
6	$O\text{-}(FeTPPS_4)_2$	2.121	100	—

5.3 X-ray powder diffraction

The main intention behind carrying out the X-ray analysis was to know the nature of synthesized porphyrins. The finely powdered forms of TPP and ZnTPP were subjected to XRD on ITAL X-ray diffractometer using Cu Kά radiation, filtered through Ni absorber, at a scanning rate of 0.1°/min. Fig. 5.5 and 5.6 show X-ray diffractograms of representative samples such as TPP and ZnTPP respectively. It is observed from the diffraction peaks that the compounds are polycrystalline in nature. It is also seen that these porphyrins are monophasic in nature which reflects upon their individual purity.

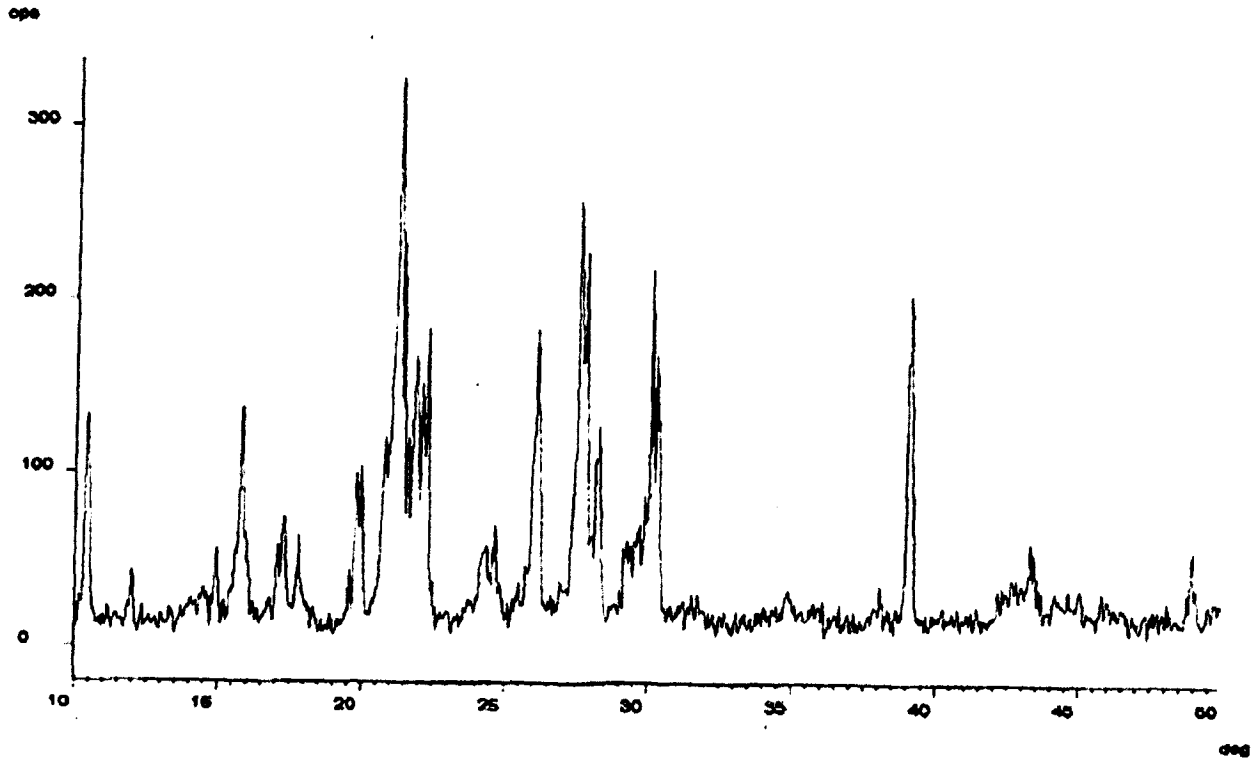

Fig 5.5 XRD pattern of TPP

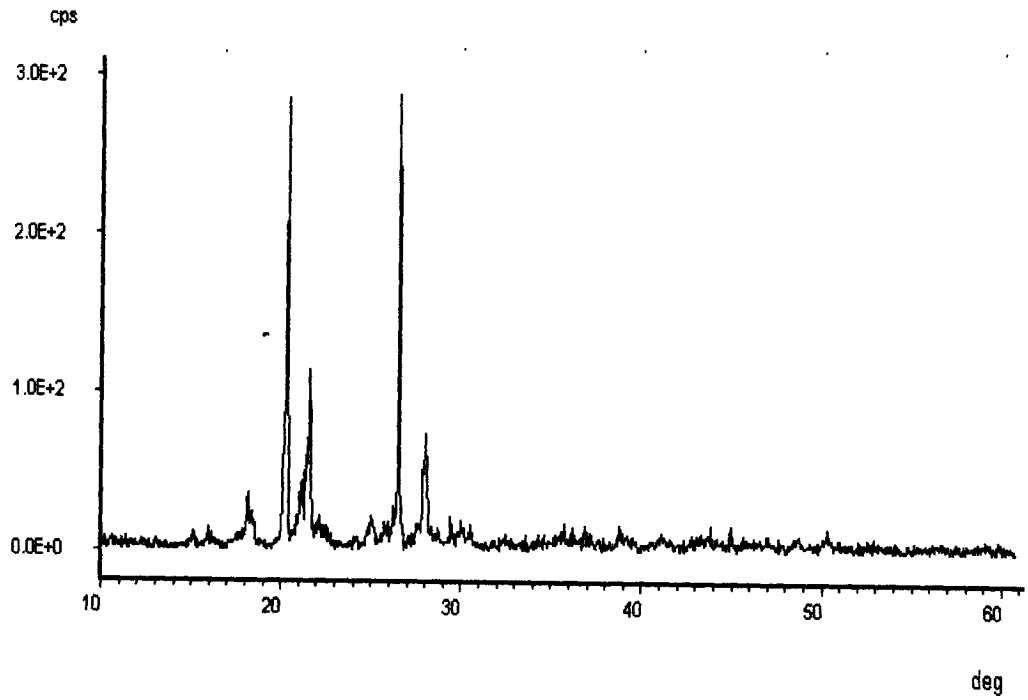

Fig. 5.6 XRD pattern of ZnTPP

5.4 Image analysis

Image analysis was carried out to know the size of the synthesized porphyrins. This was carried out with the help of optical microscope where any irregular area of a particle is converted into its equivalent circular diameter (ECD). The representative samples selected were TPP, $SnTPPCl_2$ from non-aqueous and $CoTPPS_4$ from aqueous porphyrins.

The image analysis micrograph obtained for TPP and $SnTPPCl_2$ is shown in Fig.5.7 and the Tables 5.5 and 5.6 show the size distribution of the particles in micrometers (μm). It is seen from the data given in the Tables that in TPP maximum particles are ranging between 5-10 μm followed by 10- 15 μm which is clearly seen from the histogram in Fig. 5.8.

Thus, it is seen that the particles having minimum, maximum and mean ECD are ranging from 4.79, 37.05 and 11.56 μm. In the case of $SnTPPCl_2$ similar situation is observed as seen from Table 5.6 and Fig. 5.9. In the context of $CoTPPS_4$, it is observed that, the minimum, maximum and mean ECD are 4.79, 53.80 and 10.96 μm this is shown in Table 5.7 and Fig. 5.10.

Therefore, it is observed that, irrespective of non-aqueous or aqueous porphyrins, the number of particles ranging between 5-10 μm is maximum with mean ECD around 11.0 to 12.0 μm.

A

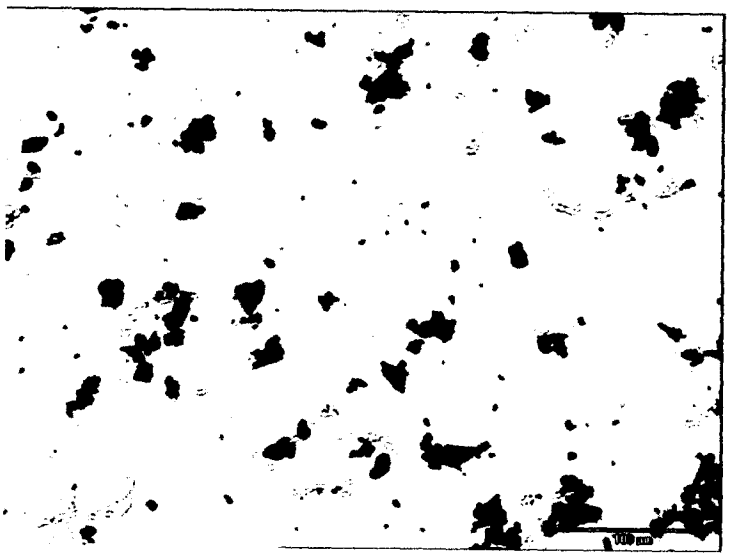

B

Fig. 5.7 Image analysis of A)TPP B) $SnTPPCl_2$

Table 5.5 Distribution of size of the particles in TPP

ID Class	From µm	To µm	No. of Particles	Statistical Function Base Unit	ECD µm
1	0.00	5.00	11	Minimum	4.79
2	5.00	10.00	124	Maximum	37.05
3	10.00	15.00	57	Mean	11.56
4	15.00	20.00	33	Standard Deviation	6.41
5	20.00	25.00	21		
6	25.00	30.00	8		
7	30.00	35.00	2		
8	35.00	40.00	1		
9	40.00	45.00	0		
10	45.00	50.00	0		
11	50.00	55.00	0		
12	55.00	60.00	0		

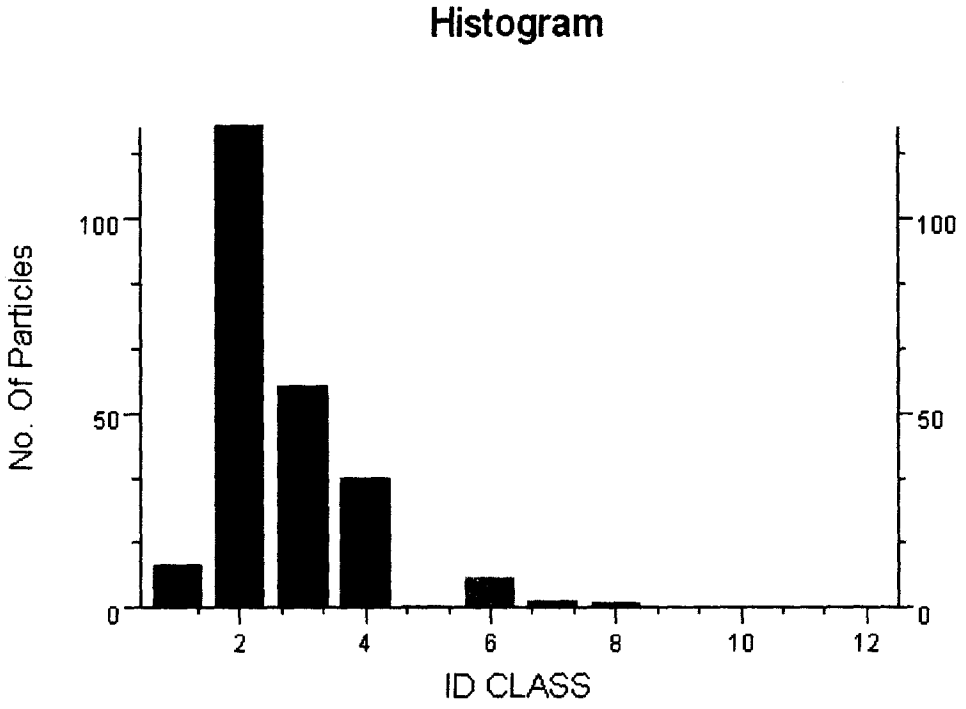

Fig. 5.8 Histogram for TPP

Table 5.6 Distribution of particle size in $SnTPPCl_2$

ID Class	From µm	To µm	No. of Particles	Statistical Function Base Unit	ECD µm
1	0.00	5.00	9	Minimum	4.79
2	5.00	10.00	143	Maximum	44.94
3	10.00	15.00	53	Mean	11.29
4	15.00	20.00	44	Standard Deviation	6.55
5	20.00	25.00	12		
6	25.00	30.00	4		
7	30.00	35.00	4		
8	35.00	40.00	2		
9	40.00	45.00	1		
10	45.00	50.00	0		
11	50.00	55.00	0		
12	55.00	60.00	0		

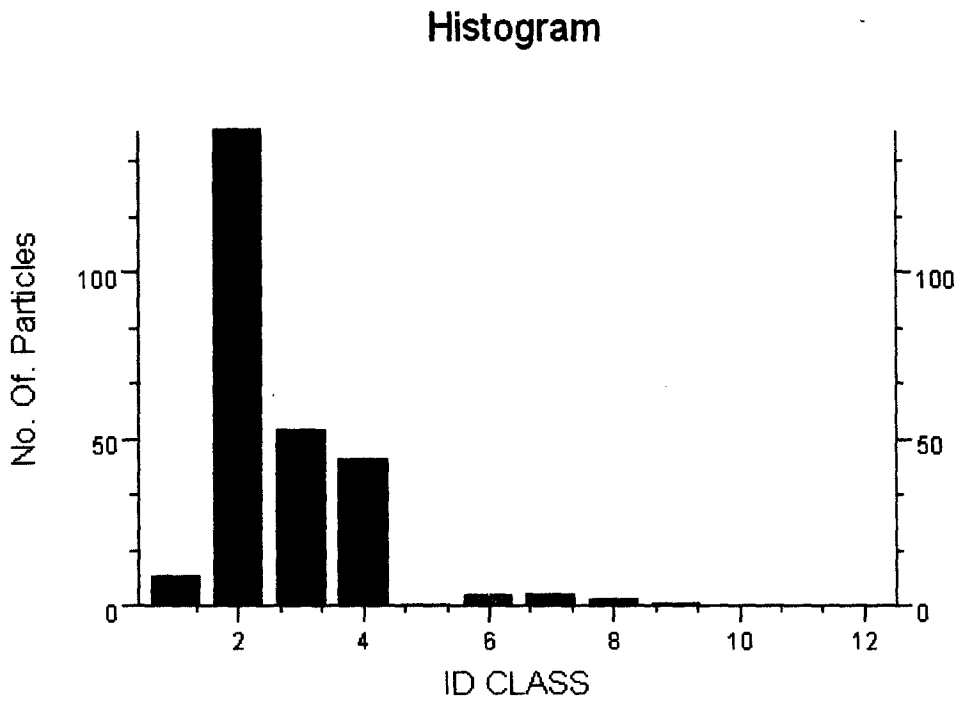

Fig. 5.9 Histogram for $SnTPPCl_2$

Table 5.7 Distribution of particle size in $CoTPPS_4$

ID Class	From µm	To µm	No. of Particles	Statistical Function Base Unit	ECD µm
1	0.00	5.00	13	Minimum	4.79
2	5.00	10.00	174	Maximum	53.80
3	10.00	15.00	69	Mean	10.96
4	15.00	20.00	49	Standard Deviation	6.40
5	20.00	25.00	15		
6	25.00	30.00	7		
7	30.00	35.00	2		
8	35.00	40.00	2		
9	40.00	45.00	0		
10	45.00	50.00	0		
11	50.00	55.00	1		
12	55.00	60.00	0		

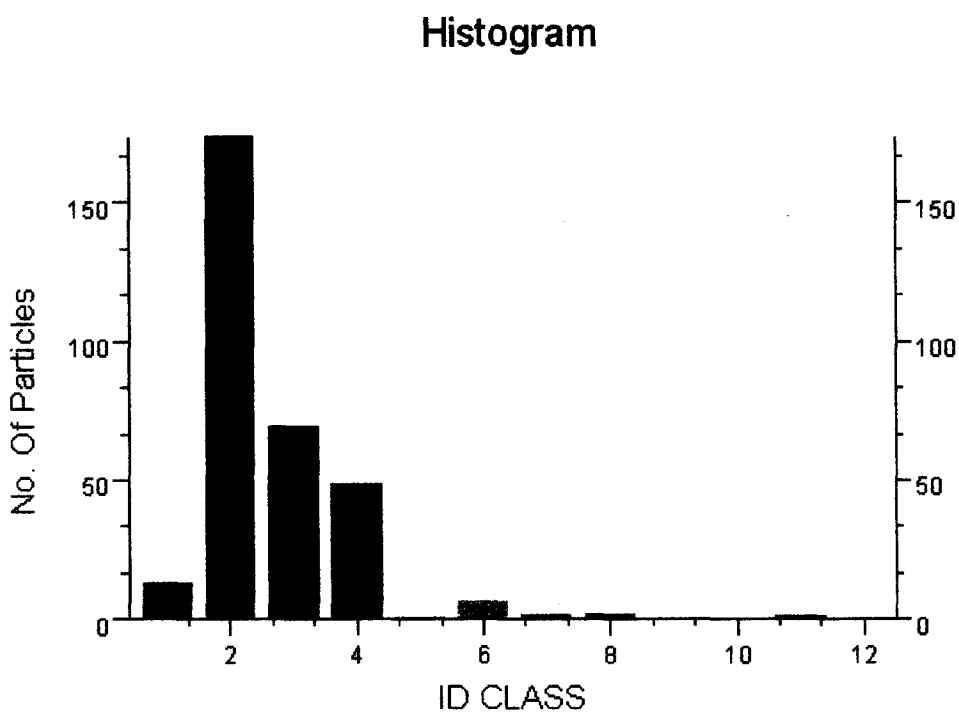

Fig. 5.10 Histogram for $CoTPPS_4$

5.5.1 TG-DSC studies

Thermal studies of all synthesized porphyrins were conducted in synthetic air. The combined display of thermogravimetry (TG) and differential scanning calorimetry (DSC) in the form of hermogram is used to explain the thermal properties like, % weight loss, decomposition temperature and loss of water of crystallization. It was also possible from TG-DSC curve to know whether the compound undergoes melting or not. Similarly, graphical representation made it clear that the different stages of decomposition and corresponding temperatures at which it occurs. Some of the representative samples selected from non-aqueous and aqueous porphyrins are TPP, ZnTPP, MnTPPCl, $SnTPPCl_2$, $TPPS_4$ and $FeTPPS_4Cl$, where temperature range used was from room temperature to 800 °C. It was also revealed that all base-free and metalloporphyrins are thermally stable up to around 400 °C. The details of the study for selective compounds are discussed below.

TPP starts decomposing after 400 °C as shown in Fig. 5.11. The TG curve shows loss in weight up to 20% in first stage, and remaining 80% in next stage. Thus it is seen that, TPP undergoes complete weight loss and no residue was left in the crucible. Further, from DSC it is clear that, TPP decomposes into four stages[194] i.e. 432 °C, 472 °C, 545 °C and 718 °C. This decomposition may be due to rupture of phenyl or pyrrole rings.

When metalloporphyrin like ZnTPP was subjected to thermal analysis, it has shown total weight loss of 90%. This explains that there is no complete decomposition and metal oxide is left in the crucible. The qualitative analysis of this metal oxide gave positive test for presence of metal. The TG-DSC curve of ZnTPP is shown in Fig. 5.12. From DSC curve, it is clear that there are four decomposition temperatures[194] for ZnTPP, viz.

480 °C, 535 °C, 647 °C and 680 °C respectively. MnTPPCl, as shown in Fig. 5.13, also showed weight loss of 90% which explains the presence of metal oxide. The DSC curve showed three stages of decomposition at 412 °C, 536 °C and 616 °C respectively. TG - DSC pattern of $SnTPPCl_2$ (Fig.5.14) shows 75% loss with two decomposition temperatures viz. 489 °C and 514 °C. There is one endothermic peak in the same graph which may be due to the loss of any moisture from the substance in the beginning. If we study the first decomposition temperature of each compound, the order obtained is MnTPPCl < TPP < ZnTPP < $SnTPPCl_2$. The reason for this may be explained on the basis of their molecular geometry.

In TPP, a free-base-porphyrin, the two N-H groups and two nitrogens are forming a core of the porphyrin ring with rectangular geometry and D_{2h} symmetry. This has shown the first decomposition temperature at 432 °C. When a divalent metal Zn is added to the porphyrin core, two hydrogens of N-H groups are removed by metal insertion and the geometry of the metalloporphyrin changes to square planar with D_{4h} symmetry. This change in the symmetry from D_{2h} to D_{4h} also increases the stability of the compound. Therefore, ZnTPP should be more stable than TPP, which can be seen from the first decomposition temperature of ZnTPP at 480 °C as compared to TPP decomposition temperature at 432 °C. When a ligand is added to four coordinated complex, it gives a complex of square pyramidal geometry with C_{4V} symmetry. Here, compared to square planar geometry, the stability of the structure decreases, due to shift of the metal from porphinato plane by fifth coordinating ligand. In MnTPPCl, the metal Mn, is shifted [114] from porphinato plane by 0.27 Å, therefore, its stability is expected lesser than

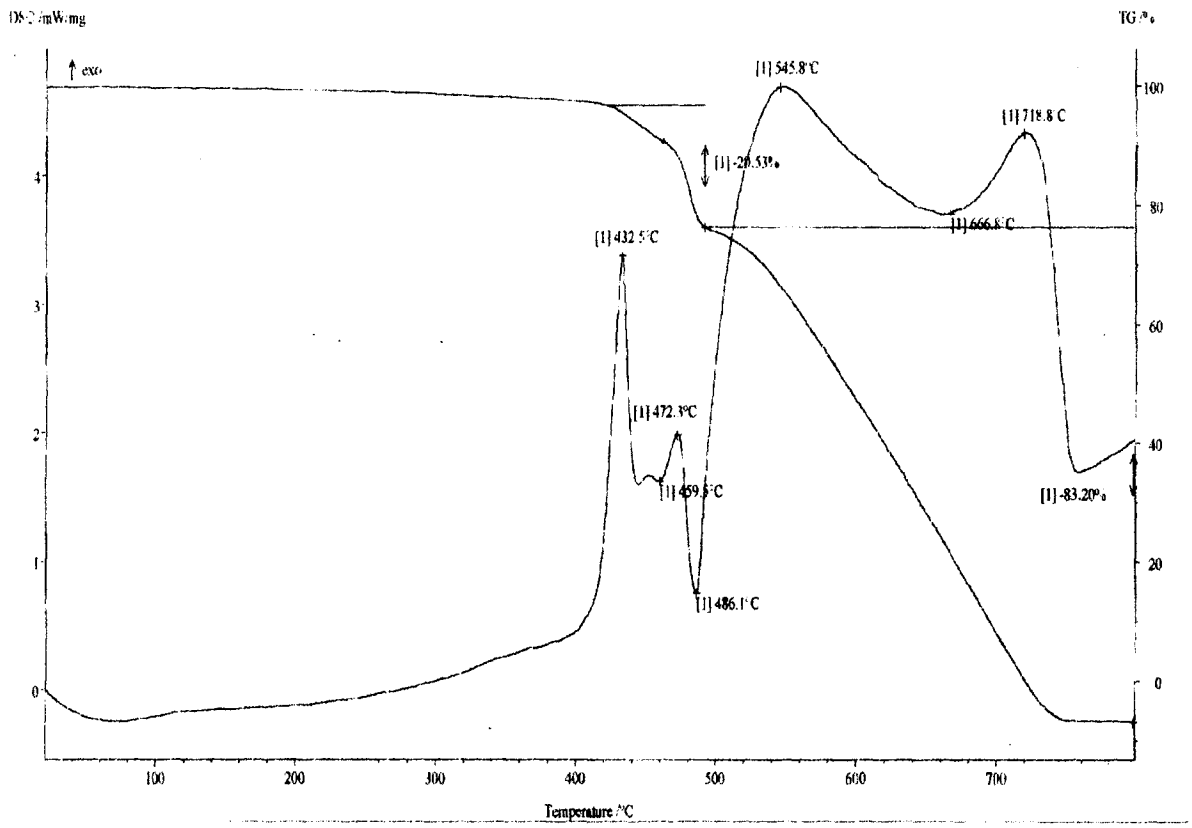

Fig. 5.11 TG-DSC thermogram of TPP

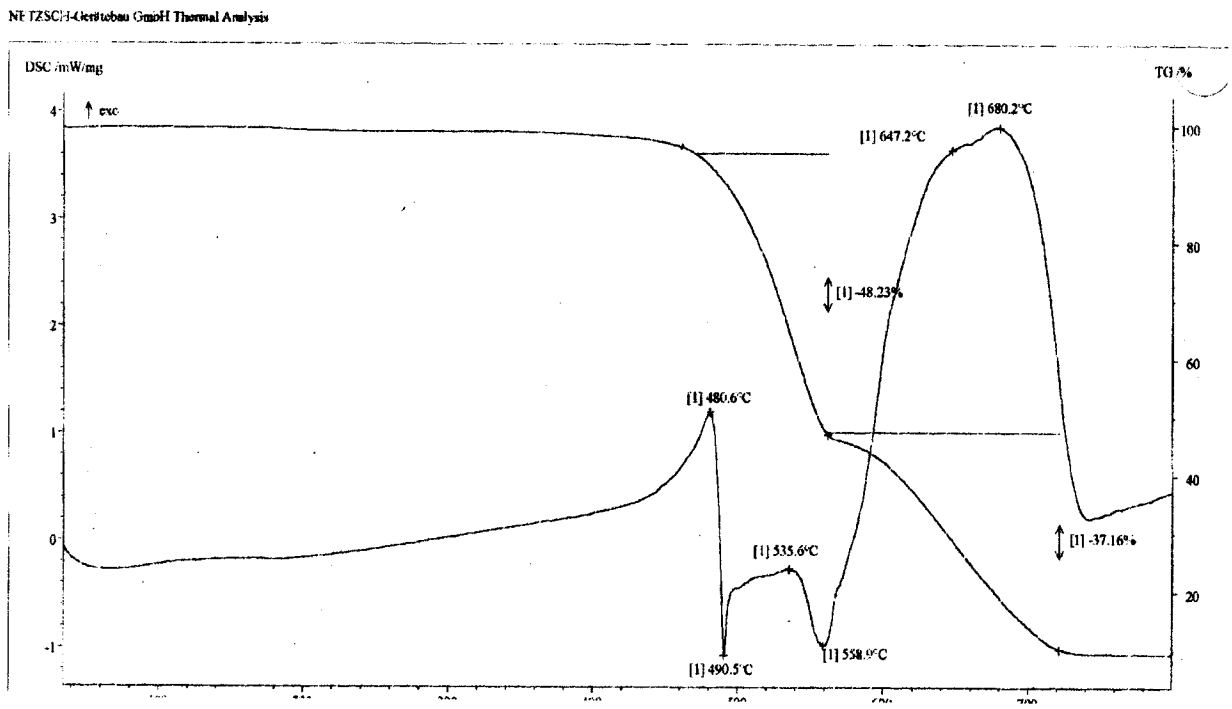

Fig. 5.12 TG-DSC thermogram of ZnTPP

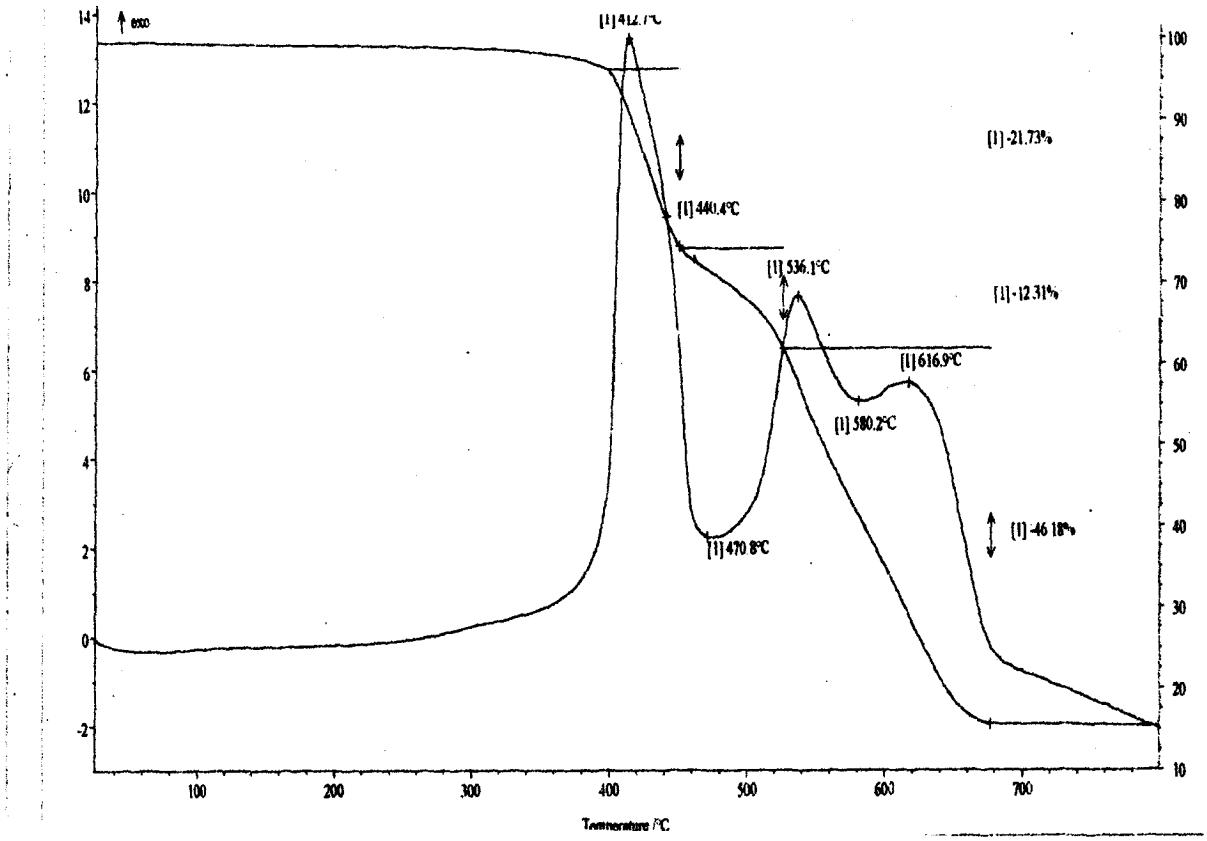

Fig. 5.13 TG-DSC thermogram of MnTPPCl

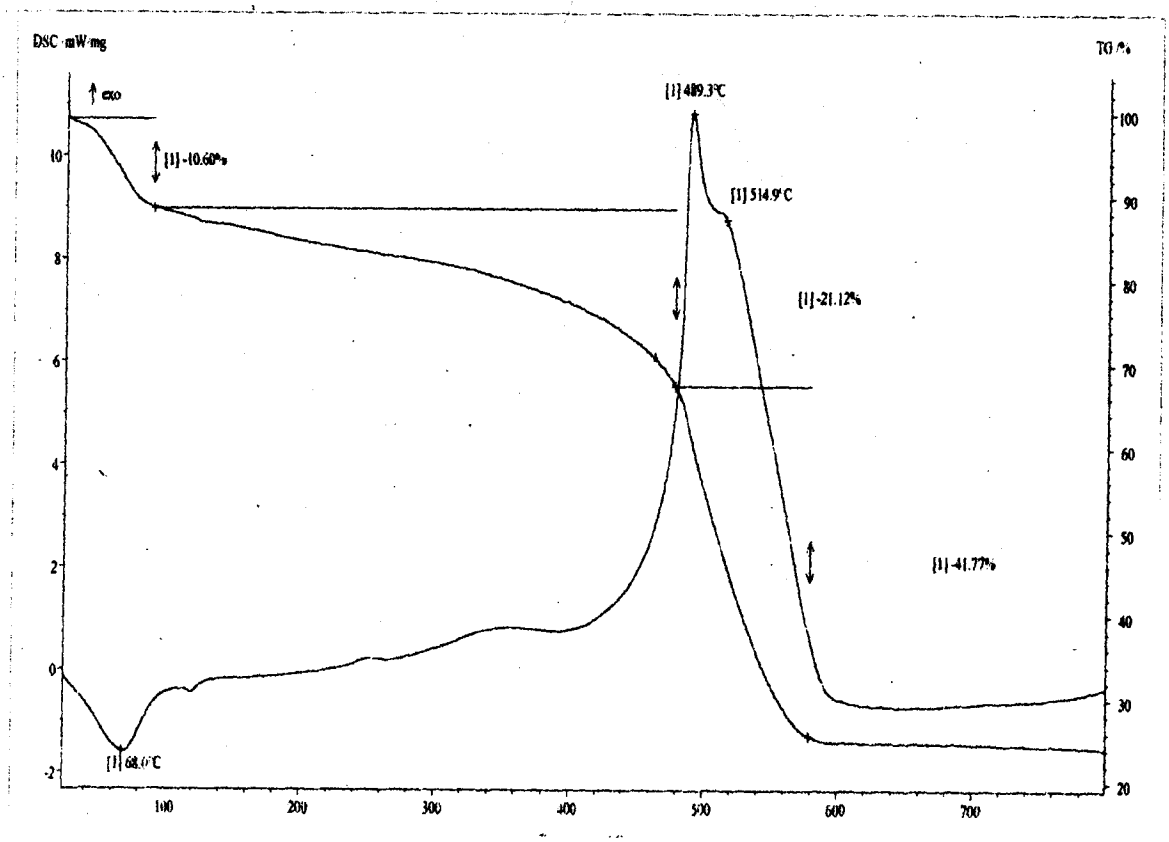

Fig. 5.14 TG-DSC thermogram of $SnTPPCl_2$

either TPP or ZnTPP. This can be confirmed by the first decomposition temperature of MnTPPCl at 412 °C as against TPP and ZnTPP respectively. When a six coordinated porphyrin such as $SnTPPCl_2$ is selected for study, it is evident that molecular geometry found is octahedral with D_{4h} symmetry. Here, two Cl ligands are stretching central Sn above and below the plane of four nitrogen atoms. Therefore, Sn is not shifted from porpinato plane[114]. Thus compared with square pyramidal MnTPPCl it should exhibit more stability but not as much as ZnTPP, which is a perfect square planar. This can be verified from the first decomposition temperature of $SnTPPl_2$ i.e. 489 °C as against 412° C of MnTPPCl and 480° C of ZnTPP.

All synthesized aqueous-porphyrins were subjected to thermal analysis in the environment of synthetic air. $TPPS_4$ and $FeTPPS_4$ were selected as representative samples. The TG-DSC curves are shown in Fig. 5.15 and 5.16 respectively. Since, aqueous-pophyrins are possessing water of crystallization, therefore they show one broad endotherm, where a water is lost at that temperature. This temperature differs from complex to complex and ranges between 70 – 90 °C and only in case of $SnTPPS_4Cl_2$ it shows 60 °C. From TG-DSC curve of $TPPS_4$ and $FeTPPS_4$ it is seen that, their first decomposition temperatures are 361 °C and 409 °C respectively. From Fig. 5.15, it is seen that $TPPS_4$ decomposes in three different stages at 361 °C, 467 °C and 605 °C respectively. Fig. 5.16 shows thermogram of $FeTPPS_4$, where the six different stages of decomposition are seen at 429 °C, 514 °C, 569 °C, 598 °C, 642 °C, and 732 °C respectively. This shows that, metalloporphyrins are comparatively more stable than free-base porphyrins.. This trend of stability is seen in almost all metalloporphyrins with the exception of $CoTPPS_4$. The qualitative analysis of the residue of $TPPS_4$ after thermal

analysis was carried out which has shown the presence of Na_2SO_4. Thus it is evident that. from 30 °C to 800 °C, SO_3^{2-} group from SO_3Na in the compound gets oxidized to SO_4^{2-}. On the basis of this observation, it can be concluded that in case of metalloporphyrins in addition to Na_2SO_4, respective metals are also found. It can be also seen that melting point of Na_2SO_4 is 884 °C whereas for other metal sulphates the decomposition temperatures range from 150 °C to 65 °C. Therefore, after thermal analysis the residue of corresponding metalloporphyrin should have the presence of Na_2SO_4 and metal oxide of the selected metal.

When the non-aqueous and aqueous-porphyrins are compared together following observations are seen.

i) Aqueous porphyrins are highly hygroscopic in nature whereas non aqueous porphyrins are non-hygroscopic in nature.

ii) Both types of porphyrins are thermally stable up to 400 °C. But in case of aqueous-porphyrins, due to loss of water of crystallization the TG curve shows loss in weight which is not seen in non-aqueous porphyrins.

iii) TPP shows complete weight loss whereas $TPPS_4$ shows 56% weight loss. This may be explained on account of oxidation of SO_3^{2-} group to SO_4^{2-} from SO_3Na in $TPPS_4$, and then remains in the cruible

iv) In non-aqueous metalloporphyrins the residue after thermal analysis contains the oxide of the metal whereas in aqueous metalloporphyrins the residue contains Na_2SO_4 and corresponding metal oxide.

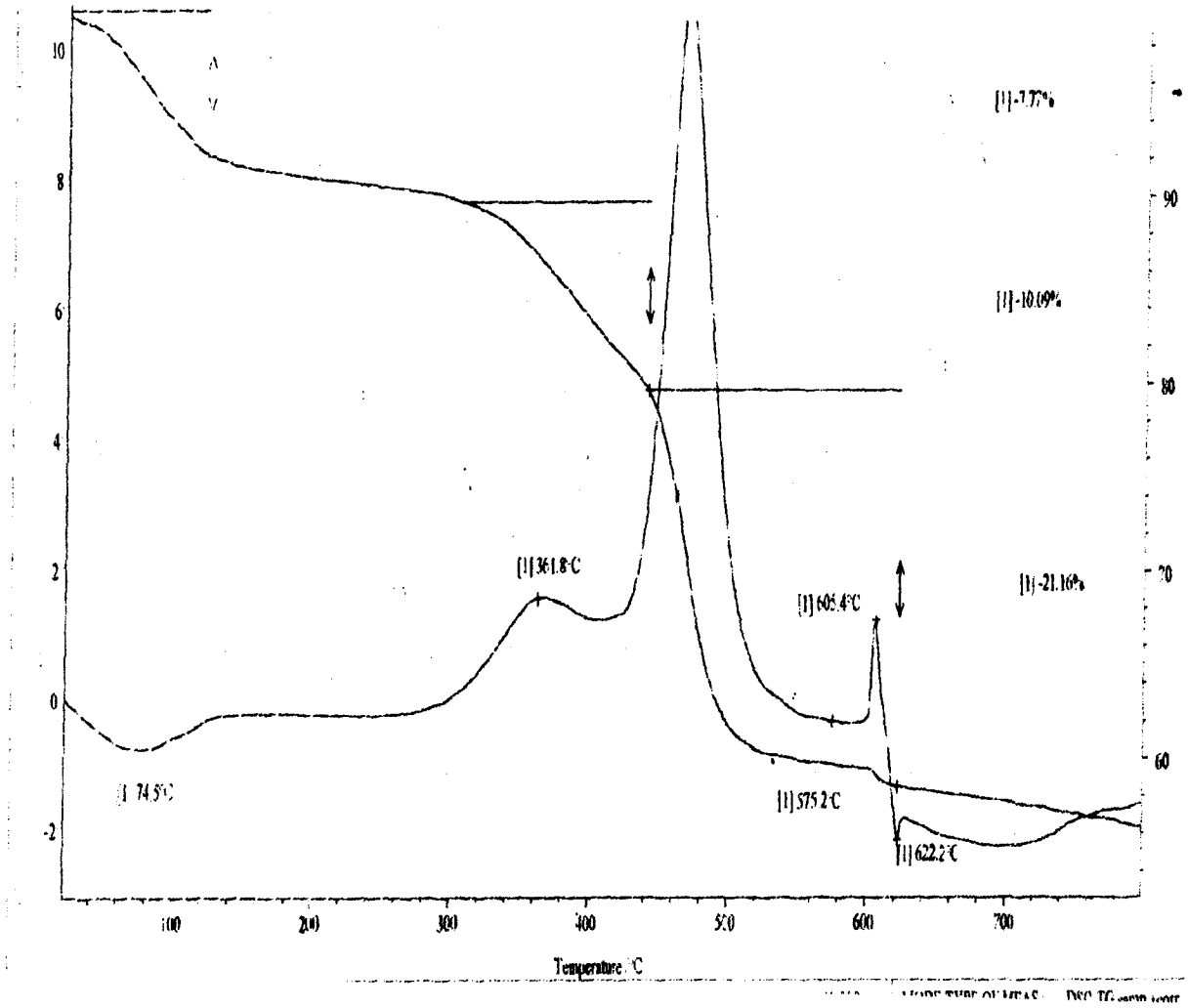

Fig. 5.15 TG-DSC thermogram of $TPPS_4$

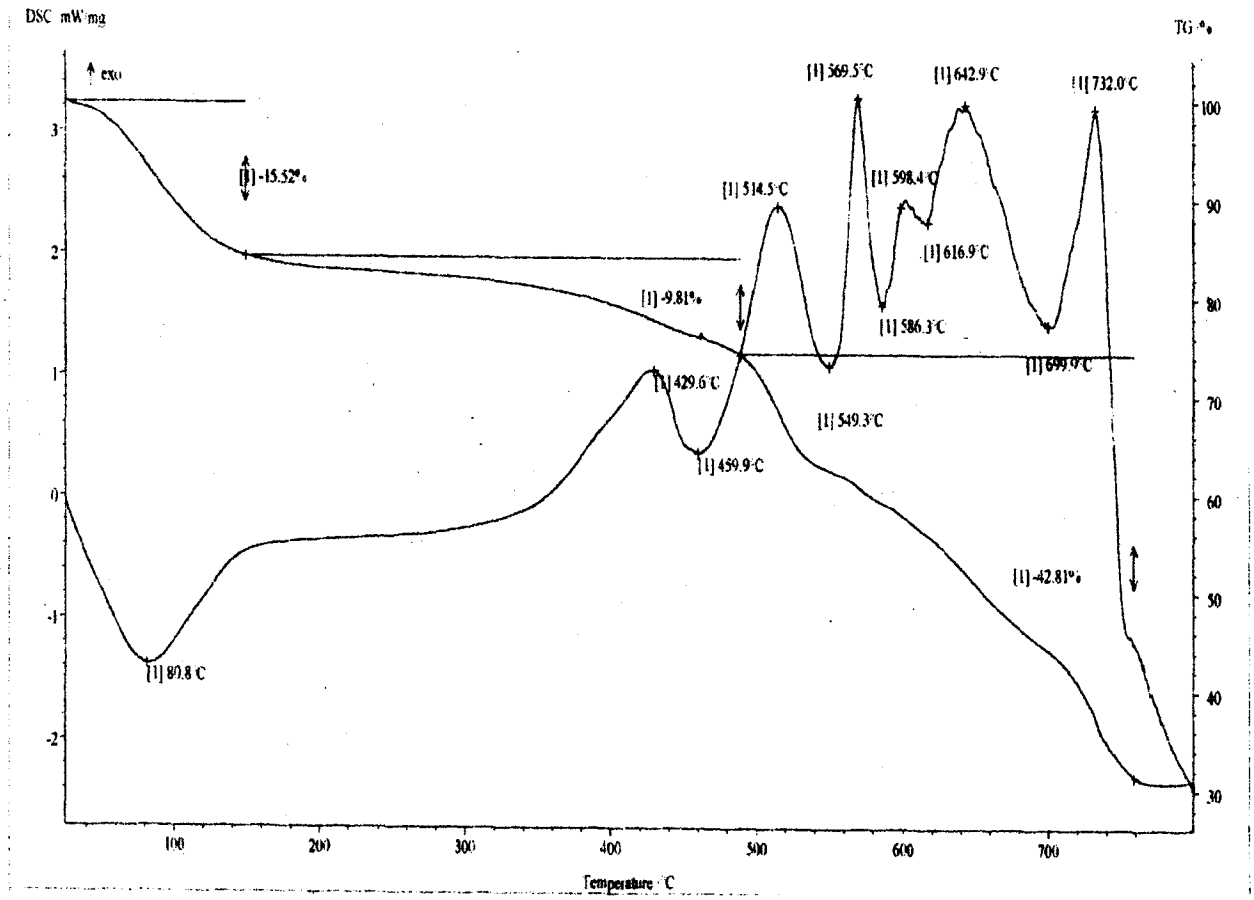

Fig. 5.16 TG-DSC thermogram of $FeTPPS_4$

5.5.2 TG-EGA-MS studies

The extension of TG-DSC study was done with the help of TG-EGA-MS study. Here, thermogravimetry and evolved gas analysis were carried out simultaneously. Thus loss in weight of a compound and subsequently the different gases and organic species evolved were recorded. First of all, depending upon the structure of the compound, some gases were expected. Then accordingly the mass spectrometer was calibrated for the same and then the respective species were recorded. It is also possible that the non-calibrated gas may escape during the event of evolution of gases. The temperature of delivery tube which carries the respective gases to the mass spectrometer was maintained below 125 °C. The compounds selected were CoTPP, FeTPPCl, and $SnTPPCl_2$ as non-aqueous porphyrins and $CoTPPS_4$ as aqueous-porphyrin. The temperature range used for TG analysis is from room temperature to 900 °C in an argon atmosphere.

The TG-EGA-MS diagram of CoTPP is shown in Fig. 5.17 from which following information is available. As it is seen that in argon atmosphere, the CoTPP loses its weight up to 50% . During this process, the expected gases or species were, H_2 (2), CH (13), CH_2 / N (14), NH_3 (17), C_2H_2 (26), C_2H_4 / N_2 (28), CH_2NH_2 (30) and C_6H_5 (77). Therefore, the mass spectrometer was calibrated for all above mentioned gases and species. Further, it seen from the Fig. 5.17, that the evolved gases / species were, H_2, CH_2 / N, and C_2H_4 / N_2 respectively. It is also seen that, H_2 evolves at 475 °C to 750 °C, CH_2 / N evolves at around 725 °C and C_2H_4 / N_2 evolves at around 725 °C respectively. From these thermal events it is attempted to know more about the opening and fragmentation of porphyrin and phenyl ring. It is seen from Fig. 5.17 that there are two peaks during evolution of hydrogen at 475 °C and 750 °C respectively. The first peak may be due to

rupture of bonds between carbon and pyrrole protons whereas second peak may be due to phenyl protons. The reason may be compared to phenyl ring, pyrrole ring is less aromatic and it being heterocyclic ring can be comparatively easily ruptured. This makes pyrrole proton to detach first followed by phenyl protons. Immediately after this, it is seen that at around 725 °C there is presence of CH / N and C_2H_4 / N_2 species which strengthens the opening of pyrrole and phenyl rings. Thus EGA-MS analysis is helpful in giving mechanism of rupture of the porphyrin macrocycle sequentially.

In case of FeTPPCl, the mass spectrometer was calibrated for H_2 (2), CH_2 / N (14), NH_3 (17), C_2H_2 (26), C_2H_4 / N_2 (28) and HCl (36) and the experiment was conducted in an argon atmosphere. From Fig. 5.18, it is seen that FeTPPCl shows nearly 40% weight loss when temperature is maintained from room temperature to 900 °C. The first weight loss occurs from more than 400 °C to 500 °C whereas second weight loss takes from 700° C to nearly 800 °C. The EGA-MS curves show presence[195] of H_2, CH_2 / N, C_2H_4 / N_2 and HCl. The meticulous observation of the Fig. 5.18 indicates evolution of HCl takes place at around 400 °C, H_2 from 500 °C to 725 °C, CH_2 / N at around 725 °C and C_2H_4 / N_2 at around 750 °C respectively. This explains that Cl being axial ligand to the central Fe gets detached first from the square pyramidal geometry and combines with hydrogen to give HCl. Further, the porphyrin ring opens up as mentioned for CoTPP.

When $SnTPPCl_2$ was subjected to TG-EGA-MS analysis the results are obtained as shown in Fig. 5.19. The TG curve shows weight loss nearly 70% in the first step whereas successive loss in weight is minor in second step. For EGA-MS analysis mass spectrometer was calibrated for H_2 (2), CH (13), CH_2 / N (14), NH_3 (17), C_2H_2 (26), C_2H_4 / N_2 (28), C_2H_6 (30) and Cl (35) respectively. From the Fig. 5.19 it is seen that at around

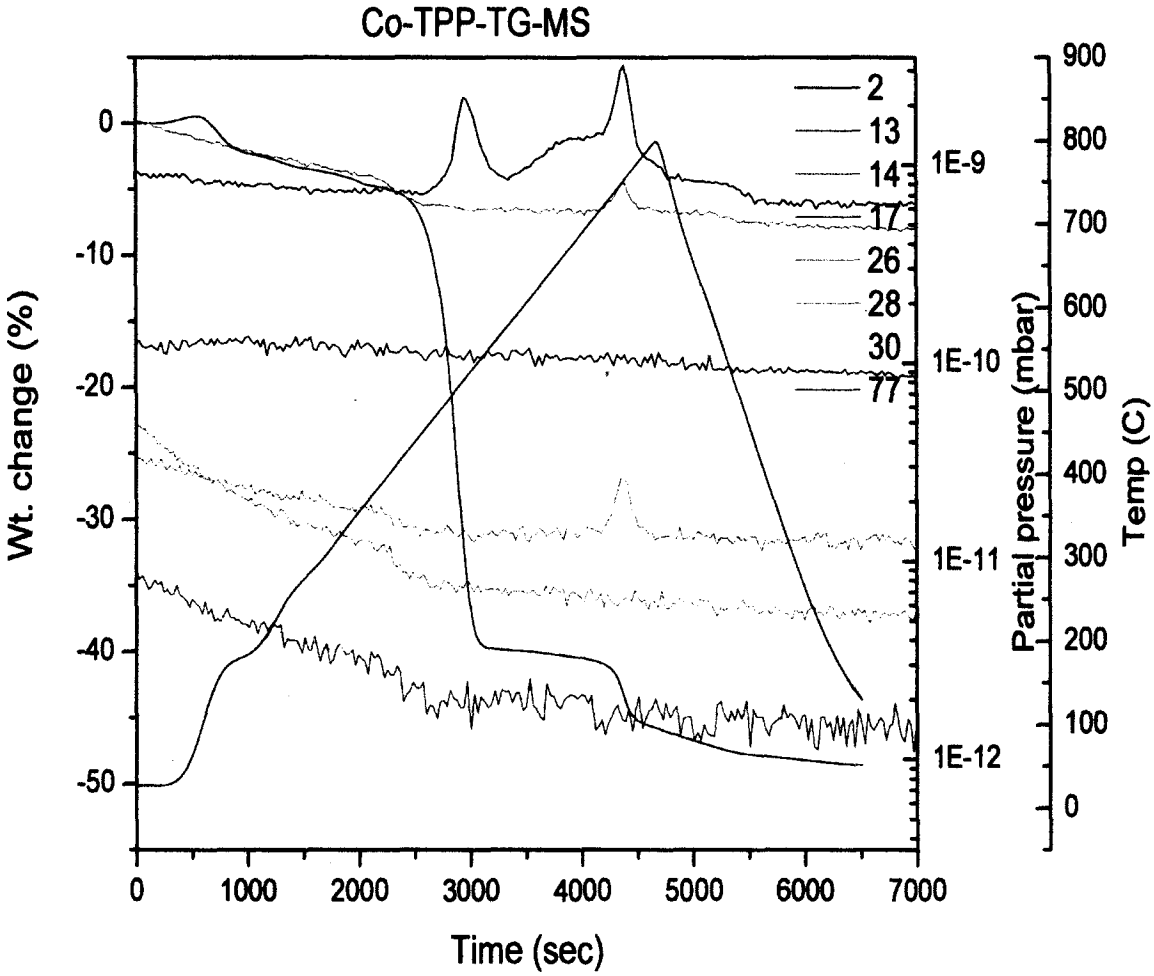

Fig. 5.17 TG-EGA-MS spectra of CoTPP

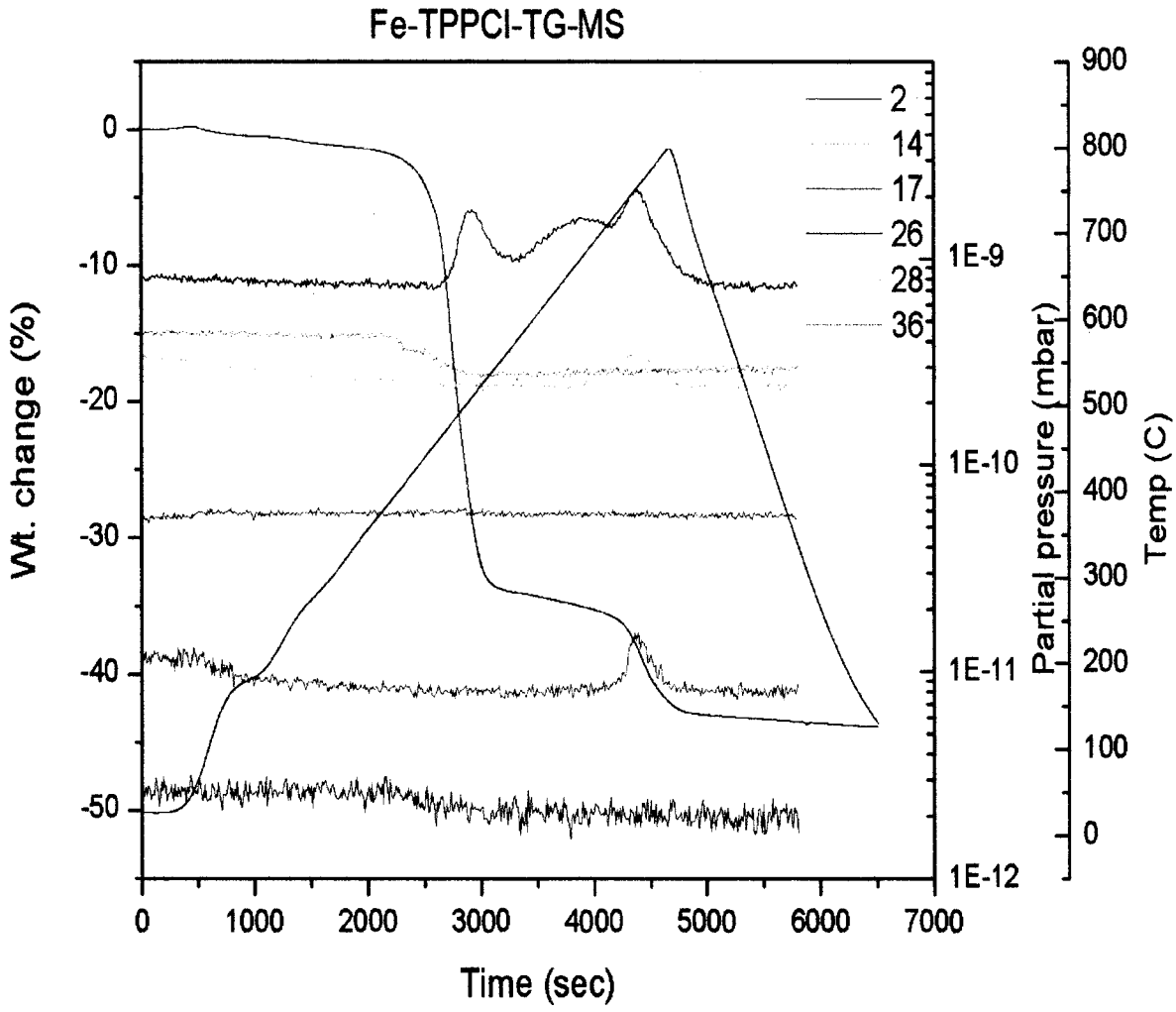

Fig. 5.18 TG-EGA-MS spectra of FeTPPCl

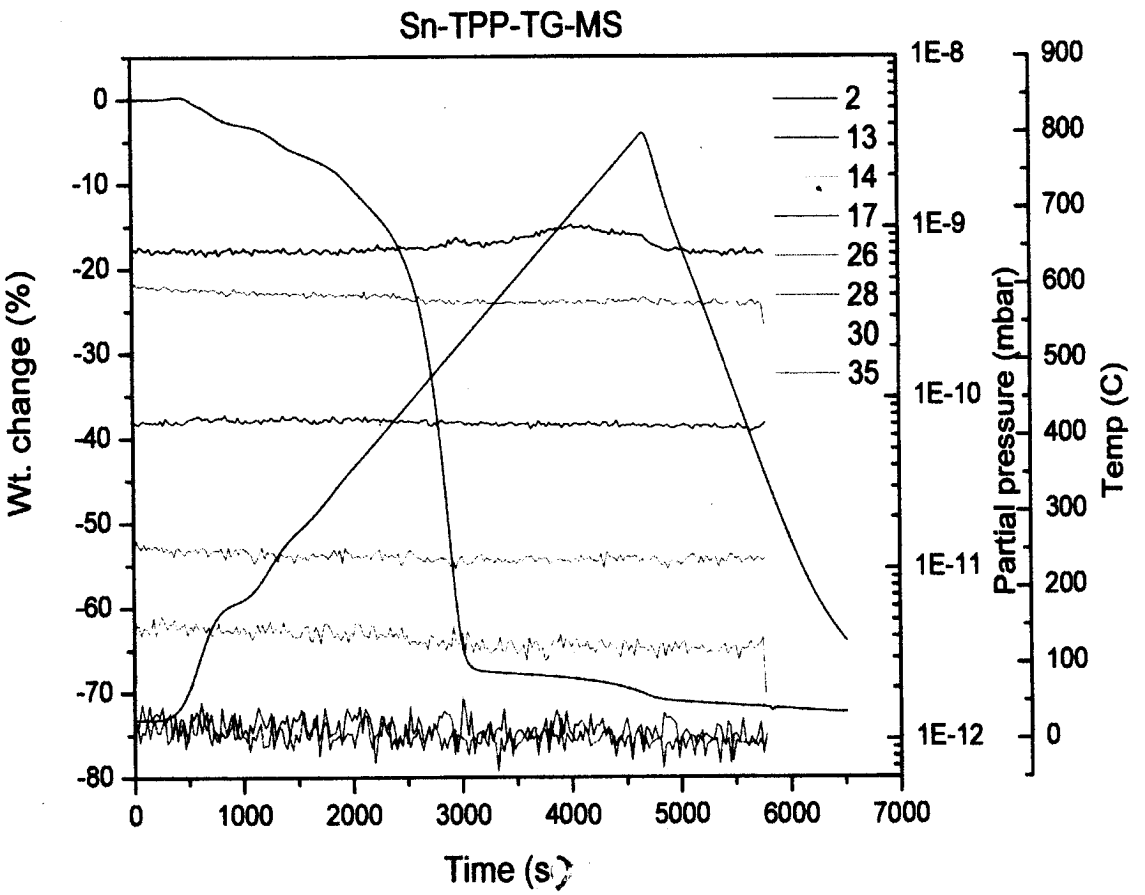

Fig. 5.19 TG-EGA-MS spectra of $SnTPPCl_2$

300 °C two Cl ions are detached from the central Sn , H_2 from 500 °C -750 °C, CH at around 550 °C, C_2H_4 / N_2 and C_2H_6 in the vicinity of 700 °C. Thus it is observed that when axial ligands are present in the structure, they are lost in the beginning followed by rest of the species as described above.

From the aqueous series the compound $CoTPPS_4$ was selected for TG-EGA-MS analysis as shown in Fig. 5.20. Taking into account the structure of the molecule the mass spectrometer was calibrated for H_2 (2), CH_2 / N (14), NH_3 (17), H_2O (18), C_2H_4 / N_2 (28), S^+ (32), HS (33) and H_2S (34) respectively. From the figure it is observed that the compound is showing nearly 40% weight loss when temperature was used from room temperature to 900 °C. The EGA-MS curve shows evolution of H_2 in between 500 °C – 725 °C, CH_2 / N and C_2H_4 / N_2 above 725 °C. The species S^+, HS and H_2S have shown presence of the multi modal peaks but resolution is not clear as it is for above species. There is always difficulty of condensation of species containing sulphur, hence from individual magnified view of each species the conclusion may be drawn. The sequence of detachment of different species and ring opening based on thermal events may be given water, NH_3, sulphur species, hydrogen, N / CH_2 and C_2H_4 / N_2 respectively.

Thus EGA-MS analysis when applied to non-aqueous and aqueous porphyrins, it is useful in giving information about the evolution of various gases and species at particular temperature. This throws light on the mechanism of the sequence of opening of pyrrole and phenyl rings in a porphyrin macrocycle.

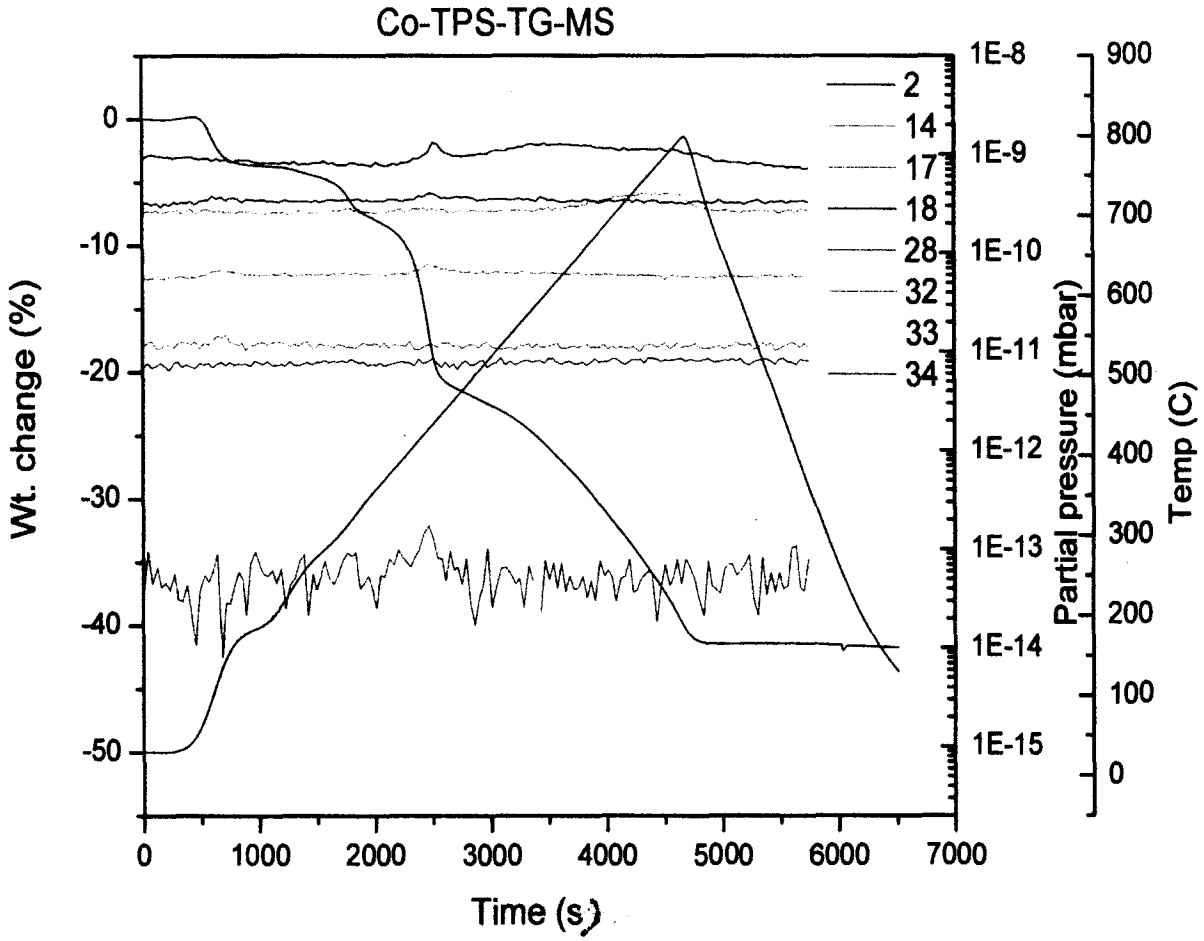

Fig. 5.20 TG-EGA-MS spectra of $CoTPPS_4$

CHAPTER 6

Photocatalytic studies

The photocatalysis denotes the acceleration of a reaction employing light and a catalyst. It refers to indicate that light and the catalyst are necessary entities to influence a reaction. The catalyst may accelerate the photoreaction by interacting with the substrate either in its ground state or in its excited state depending on the mechanism of the photoreaction. Therefore, the act by which an excited state is produced in an entity (molecule or photocatalyst) by the absorption of ultraviolet, visible or infrared radiation is called photoexcitation. Further, an electronically excited surface center (surface site) with a trapped photogenerated charge carrier, that interacts with atoms, molecules or ions at an interface with the formation of reaction products or intermediates is known as active state of a surface photocatalytic center[196]. The semiconductor based heterogeneous photocatalysis is an effective way of controlling environmental pollution or proposing the model reactions where photodegradation plays an important role. In photodegradation process, the photochemical transformation of a molecule into lower molecular weight fragments takes place either by oxidation or reduction processes. In photooxidation, where the light induced oxidation reactions take place and common processes involved are

i) The loss of one or more electrons from a chemical species as a result of photoexcitation of that species.

ii) The reaction of a substance with a reactive oxygen species (ROS : e.g. $OH^{\bullet}$, O_2^{-}, $HOO^{\bullet}$, H_2O_2, $^1O_2$) under the influence of light. When oxygen remains in the product this latter process is also called photooxygenation.

During photocatalysis when the photoreduction involves following processes are possible:

i) Addition of one or more electrons to a photoexcited species.

ii) The photochemical hydrogenation of a substance.

A semiconductor is a material whose electrical conductivity increases with increasing temperature owing to the thermal generation of free charge carriers. The band gap of an intrinsic semiconductor can be as high as about 2 eV. An intrinsic semiconductor is a material with negligible concentration of defects and impurities, and for which thermal excitation leads to band-to-band generation of both electrons and holes with identical concentrations of both types of carriers. The disappearances of free electrons and free holes due to the recombination of electrons from the conduction band to the valence band, is called recombination which is observed in solid photocatalyst.

6.1 Photodegradation studies

For the heterogeneous photocatalysis study, the dyes selected were Amido Black 10B, Methyl Orange, Poneau S and Rhodamin B respectively. Among these dyes Amido Black 10B, Methyl Orange and Ponceau S are azo dyes. Therefore, the chromophore N = N group is responsible for he colour of the respective dyes. These dyes were degraded by means of the synthesized non-aqueous porphyrins as photocatalysts in their aqueous solutions. The Rhodamin B (RB) has the same fundamental structure as the xanthene dyes, but phenolic groups of the xanthenes are replaced by amino groups. This dye was photodegraded in acetone medium with the help of aqueous-porphyrins. To know the process of degradation the aliquots were drawn from the reaction assembly with the regular interval of time and analysed on UV-visible spectrophotometer. It was observed that the rate of photodegradation

is dependent upon the factors such as amount of catalyst, effect of pH, concentration of dye solution, volume of dye solution, presence of O_2, absence of O_2, presence of promoter etc.

6.2 Photodegradation of Amido Black 10B

It is an important acid wool dye for black shades of moderate fastness. It contains two azo groups and has solubility 30 g / L at 20° C in water. It is an amino acid staining diazo dye used in biochemical research to stain for total protein on transferred membrane blots. It is also used in criminal investigations to detect blood present with latent fingerprints. It stains the proteins in blood a blue-black colour. Amido Black can be either methanol or water based as it readily dissolves in both the solvents.

6.2.1 Optimization of amount of photocatalyst

At the out set, it was necessary to optimise the amount of photocatalyst required to degrade the dye solution of selected conentration. Therefore, stock solution of 10^{-4} M of Amido Black 10B was prepared by dissolving AR grade reagent. Further, it was diluted to ten times to get 10^{-5} M solution which was used for the experiment. The dye solution was tested for self degradation under different experimental conditions. Then dye solution was irradiated in sunlight, without O_2, with O_2 and O_2 and promoter, sodium lauryl sulphate (SLS) for four hours from 11.30 a.m. to 3.30 p.m. without photocatalyst. It was seen that there were no observable changes due to variation of these factors. On the contrary, when TPP was added as a photocatalyst to the dye solution then it was observed that O_2 plays a very important role in the proess of dye degradation. Taking into account this point, the optimum quantity of photoatalyst was determined for the photoatalytic reaction. Thus 100 mL of amido black 10 B solution was taken and O_2 was bubbled into solution for five

minutes followed by addition of five drops of 0.1% of SLS solution. Then the requisite amount of photoatalyst was selected from 5 mg to 45mg. The Fig. 6.1 shows that at 25 mg the absorbance is minimum, therefore, it confirms the optimum amount of photatalyst. For this experiment, TPP being precursor, was chosen as a representative of the non-aqueous porphyrins as photocatalysts. It was also found that if the amount is exceeded 25 mg, the photodegradation activity decreases[197]. The reason for this is after a saturation point activity decreases because number of active sites on the photocatalysts as well as exposure to solar radiation per unit area decreases[16]. It is also reported that when a photocatalyst is loaded more than optimum amount then the rate of deactivation of activated molecules increases due to collision with ground state molecules of photocatalyst [159].

6.2.2 Photodegradation of Amido black 10B at different pH

As mentioned above, the effect of pH plays an imporant role in the process of degradaton of the dye solution. This was verified by employing all non-aqueous porphyrins in the process of photocatalysis.The porphyrins used are TPP, CoTPP, NiTPP, CuTPP, ZnTPP, AgTPP, MnTPPCl, O-$(MnTPP)_2$, FeTPPCl, O-$(FeTPP)_2$ and $SnTPPCl_2$.

1) Degradation of Amido Black 10B at pH 6

The solution of Amido Black 10B of 10^{-5} M concentration was taken and O2 was bubbled for five minutes and then 0.1 M solution of HNO_3 was added to adjust the pH of the solution at 6 using standardized pH meter. This solution was taken as a blank for subsequent photocatalytic reactions. Fig. 6.2 shows UV-visible spectrum of the dye where λmax observed is 619 nm. Further, to study the degradation process the reaction assembly was prepared as mentioned above for each photocatalyst. Then 25 mg of each

synthesized porphyrin was added to each reaction assembly and the reaction was carried out from 11.30 a.m. to 3.30 p.m. for outside temperature 30 °C to 38 °C respectively. The course of degradation reaction was monitored with the interval of one hour. Fig 6.3 and 6.4 show the detailed information regarding the course of reaction for porphyrins of divalent, tri and tetra valent metals.

From Fig. 6.3 it is seen that TPP and ZnTPP degrade the dye solution completely within two hours (i.e. 100%) whereas CuTPP, NiTPP, degrade to 53%, CoTPP to 48% and AgTPP degrade the dye solution to the extent of 39% within four hours. Thus the degrading efficiency of these photocatalysts decreases in the following sequence:

$$TPP = ZnTPP > CuTPP \approx NiTPP > CoTPP < AgTPP.$$

From Fig. 6.4 it is observed that , $SnTPPCl_2$ degrades the dye solution to 100% within two hours, O-$(MnTPP)_2$ dimer to 100% within 3.5 hours and MnTPPCl degrades nearly 98% within four hours. The remaining, O-$(FeTPP)_2$ dimer degrades to 43% and FeTPPCl to 32% within four hours. Thus the degrading efficiency for these compounds decreases in the following sequence:

$$SnTPPCl_2 > O\text{-}(MnTPP)_2 > MnTPPCl > O\text{-}(FeTPP)_2 > FeTPPCl$$

When both the series are combined irrespective of the charge on the metal, it is observed that TPP, ZnTPP , $SnTPPCl_2$, O-$(MnTPP)_2$ and MnTPPCl are the most efficient photoatalysts. CuTPP, NiTPP, CoTPP , O-$(FeTPP)_2$ and AgTPP are less efficient whereas FeTPPCl is the least efficient photoatalyst.

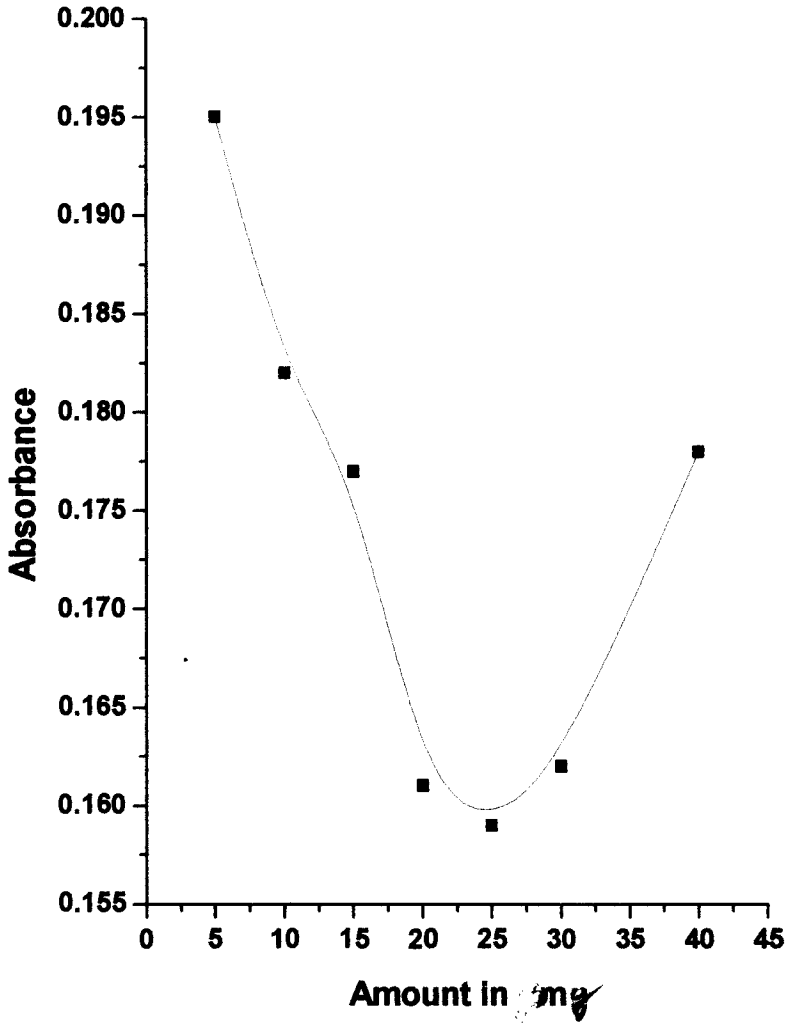

Fig. 6.1 Optimization of catalyst amount for degradation of Amido Black 10B

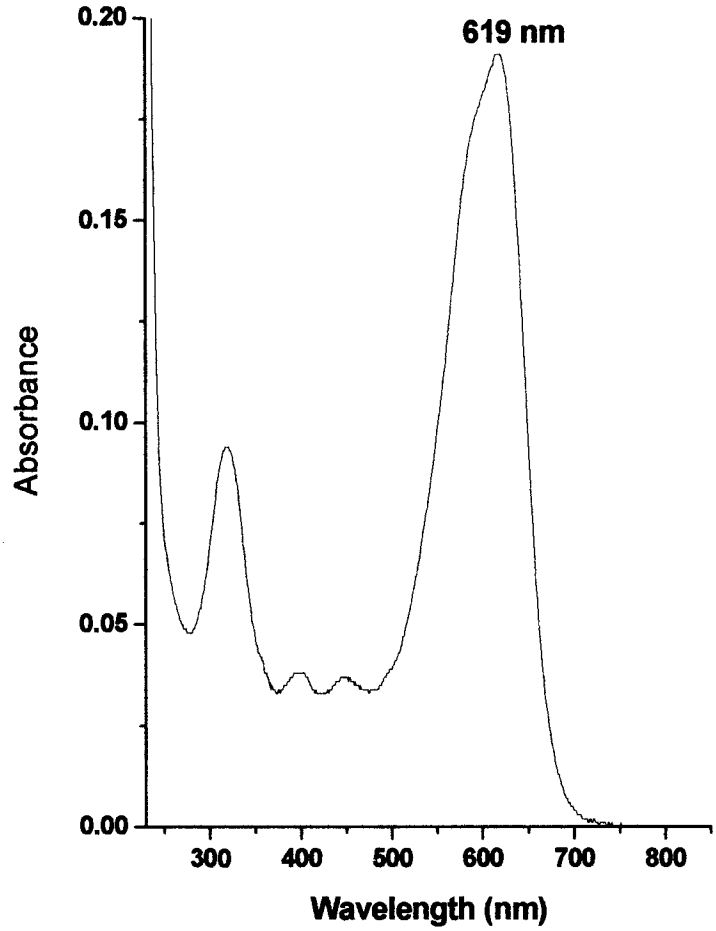

Fig. 6.2 UV- visible spectrum of Amido Black 10B

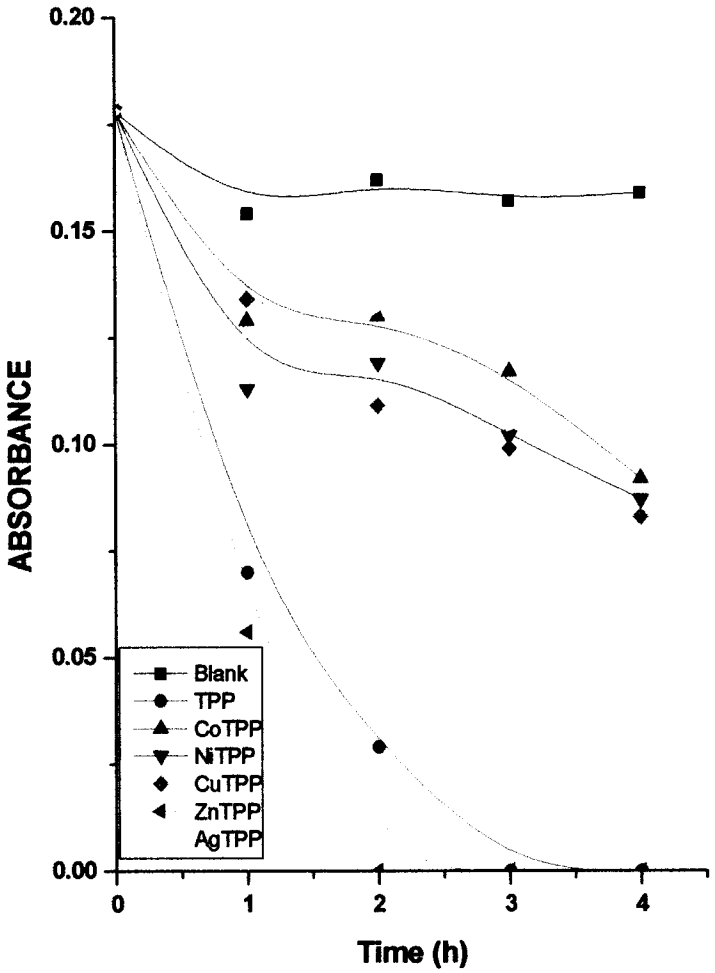

Fig. 6.3 Photodegradation of Amido Black 10B by TPP and metalloporphyrins containing divalent metals (pH= 6)

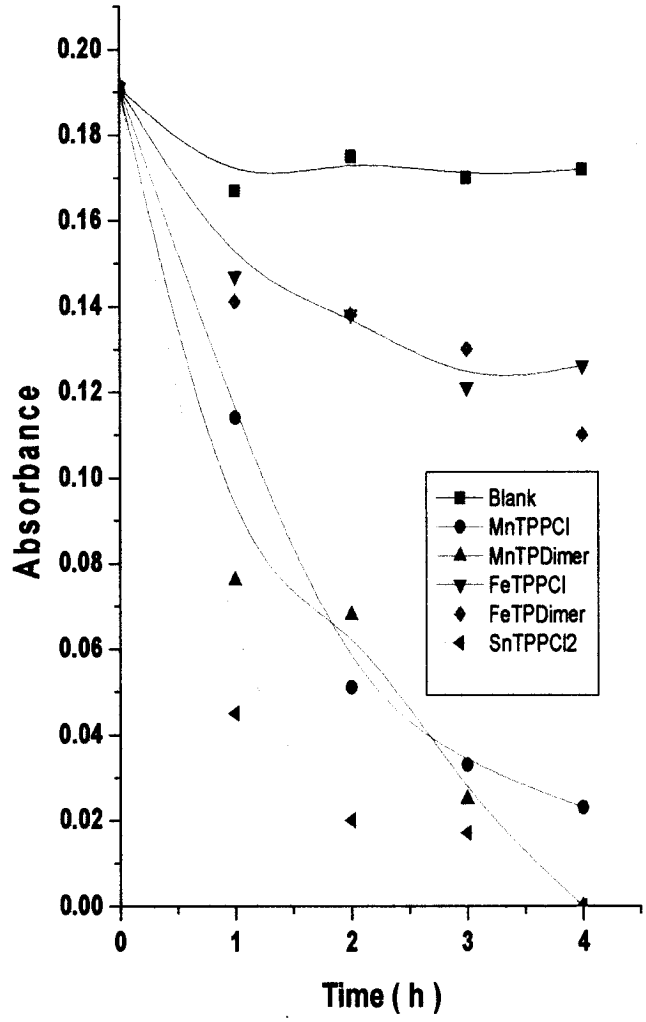

Fig. 6.4 Photodegradation of Amido Black 10B by metalloporphyrins containing trivalent and tetravalent metals (pH=6)

2) Degradation of Amido Black 10B at pH 7

The solution of Amido Black 10B of 10^{-5} M concentration was bubbled with O_2 for five minutes The pH 7 of the solution was confirmed with pH meter and then five drops of 0.1% of sodium lauryl sulphate (SLS) was added to the solution. Here,the role of SLS is to promote the photocatalytic reaction without being consumed in the reaction. When the reaction was carried out without SLS, it was seen that, the degree of degradation of a dye solution was considerably small. Further, the testing of dye solution with SLS showed no change in the λmax value i.e. 619 nm., therefore, chemical inertness of SLS with Amido Black 10B was confirmed. Then, the porphyrins of di, tri and tetravalent metals were added to reaction assembly as described above and the photocatalytic reaction was carried out from 11.30 a. m. to 3.30.p.m. The progress of the reactions is shown in Fig. 6.5 and 6.6 respectively.

As seen from Fig. 6.5, TPP has shown maximum degradation of the dye to the extent of 33%. Out of remaining photocatalysts, ZnTPP ,CuTPP CoTPP and NiTPP show the degradation to the extent of 17%, 13%, 9% and 4% within four hours resspectively. From this observation, it is seen that the photoatalytic activity decreases in the following order:

TPP > ZnTPP > CuTPP > CoTPP > NiTPP

Similarly, from Fig.6.6 it is observed that, $SnTPPCl_2$ shows maximum activity to 78%, followed by O-$(MnTPP)_2$ dimer, MnTPPCl, O-$(FeTPP)_2$ dimer, AgTPP and FeTPPCl to the extent of 54%, 37%, 8%, 8%, and 7% respectively. Therefore, it can be concluded that among all porphyrins used above, at pH 7, $SnTPPCl_2$ is the most effective photocatalyst. The other porphyrins such as O-$(MnTPP)_2$, TPP and MnTPPCl show moderate activity whereas O-$(FeTPP)_2$ and FeTPPCl show least photocatalytic activity.

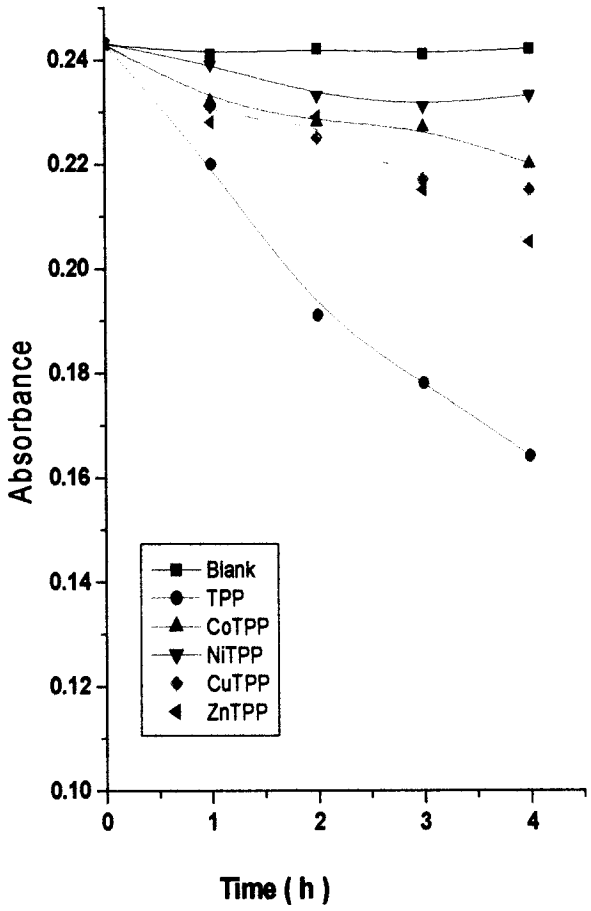

Fig. 6.5 Photodegradation of Amido Black 10B by TPP and metalloporphyrins containing divalent metals (pH= 7)

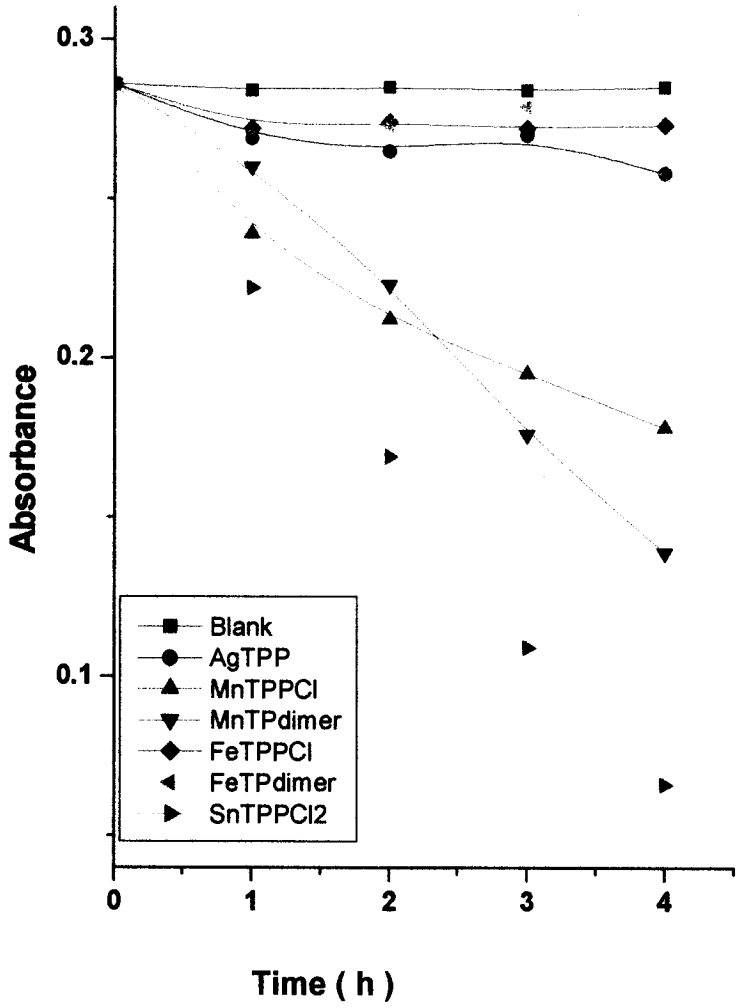

Fig. 6.6 Photodegradation of Amido Black 10B by metalloporphyrins containing di, tri and tetravalent metals (pH=7)

3) Degradation of Amido Black 10B at pH 10

As mentioned above the Amido Black 10B solution of 10^{-5} M concentration was bubbled with O_2 for five minutes and 0.1 M KOH is added dropwise to adjust the pH of the solution to 10. This was verified with the help of standardized pH meter. At this pH, it was observed that without SLS rate of degradation was comparataively slow. Therefore, five drops of 0.1% of SLS as a promotor was added to the solution. Then 25 mg of respective photocatalyst was added to the reaction assembly and the solution was stirred for two minutes for the thorough dispersion of catalyst in the solution. The reaction time was maintained from 11.30 a.m. to 3.30 p.m.

Fig. 6.7 shows photodegradation reaction for porphyrins of divalent metals at pH 10. It is observed that TPP and ZnTPP show the degradation of the dye to the extent of 83% and CuTPP show 73%. The remaining NiTPP, CoTPP, and AgTPP show degradation 30%, 29% and 27% in four hours respectively. This shades light on the photocatalytic efficiency of the catalyst in decreasing order of magnitude as

TPP = ZnTPP > CuTPP > NiTPP > CoTPP > AgTPP

Fig 6.8 shows degradation reaction of the dye with porphyrins of tri and tetravalent metals at pH 10. It is evident that $SnTPPCl_2$ and O-$(MnTPP)_2$ show degradation to 95% and 90% within one hour and nearly three hours whereas rest of the metalloporphyrins viz. MnTPPCl, O-$(FeTPP)_2$ and FeTPPCl show 38%, 32% and 29% degradation within four hours respectively. This fact reveals that $SnTPPCl_2$, O-$(MnTPP)_2$ dimer are effective photocatalysts and remaining are exhibiting comparatively low photocatalytic activity. Thus the effective catalysts for selected pH value of 10 are $SnTPPCl_2$, O-$(MnTPP)_2$ dimer, TPP, ZnTPP and

CuTPP respectively. Fig. 6.9, 6.10 and 6.11 show the degradation pattern for amido Black 10B at pH 6, 7,and 10 with TPP as a representative photocatalyst

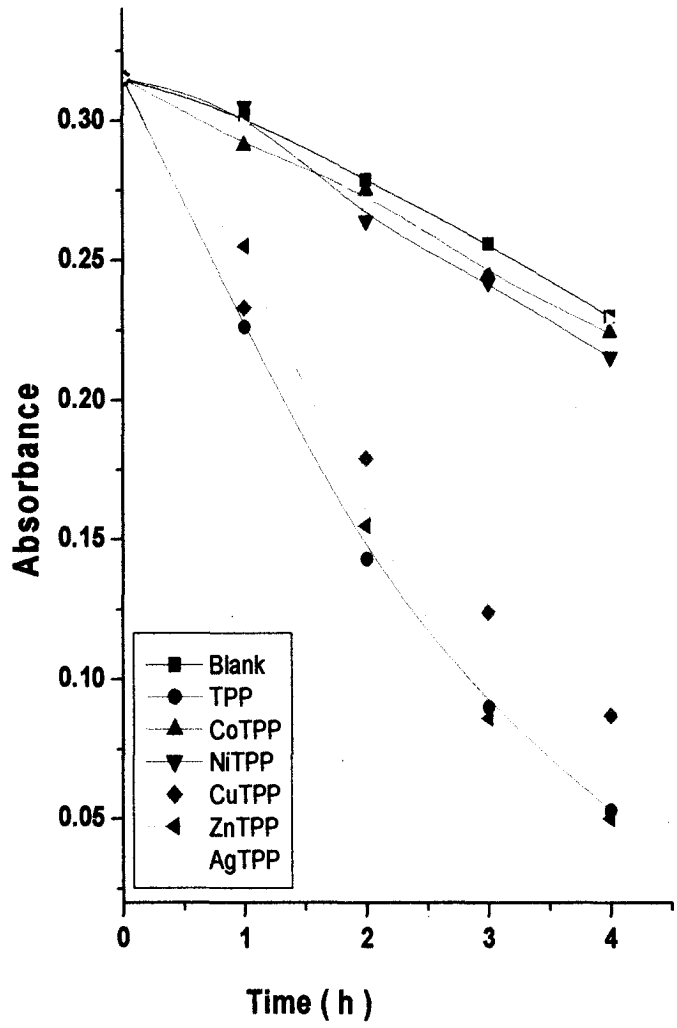

Fig. 6.7 Photo degradation of Amido Black 10B by TPP and metalloporphyrins containing divalent metals (pH= 10)

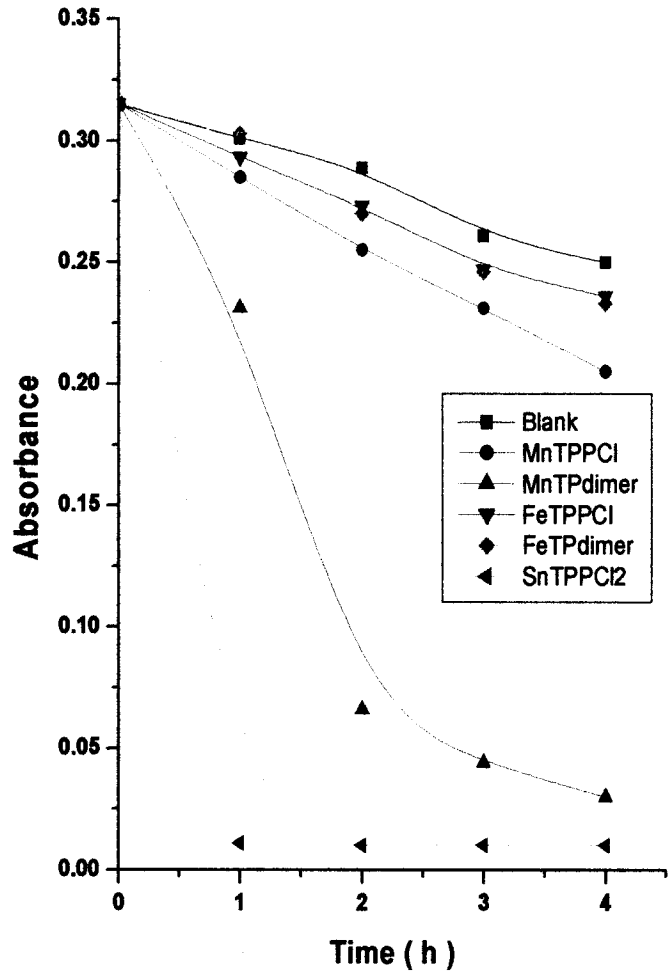

Fig. 6.8 Photodegradation of Amido Black 10B by metalloporphyrins containing di, tri and tetravalent metals (pH=10)

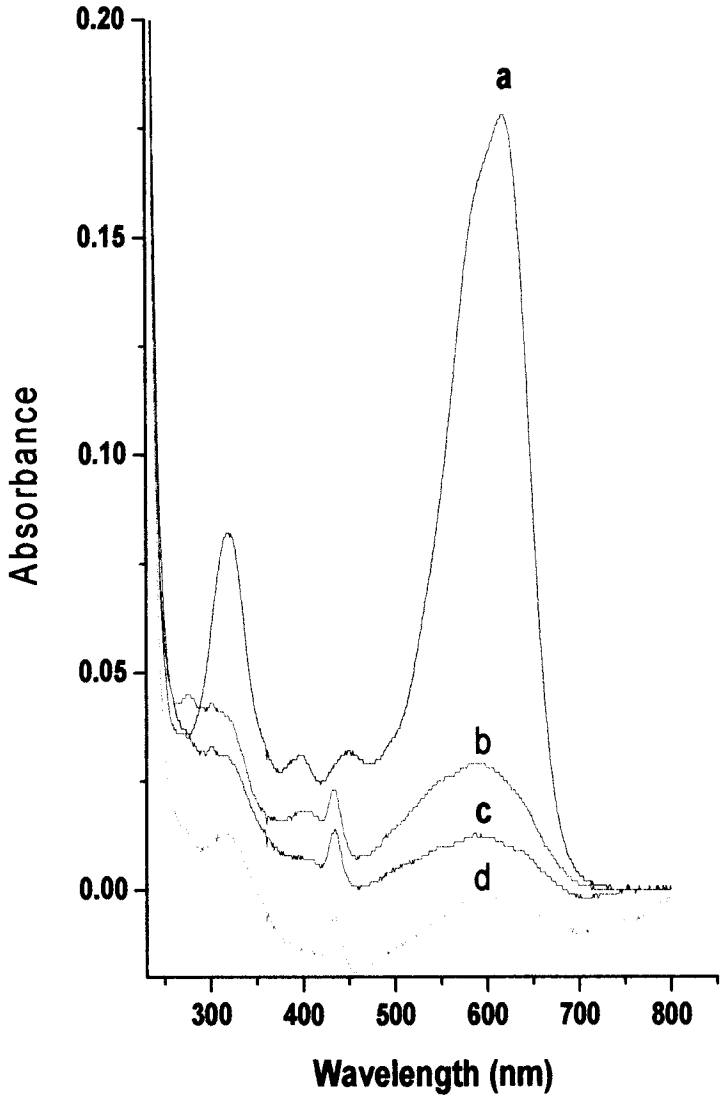

Fig. 6.9 Degradation of Amido Black 10B with TPP at pH= 6 for a) Blank b) 1 hour c) 2 hour and d) 3 hour

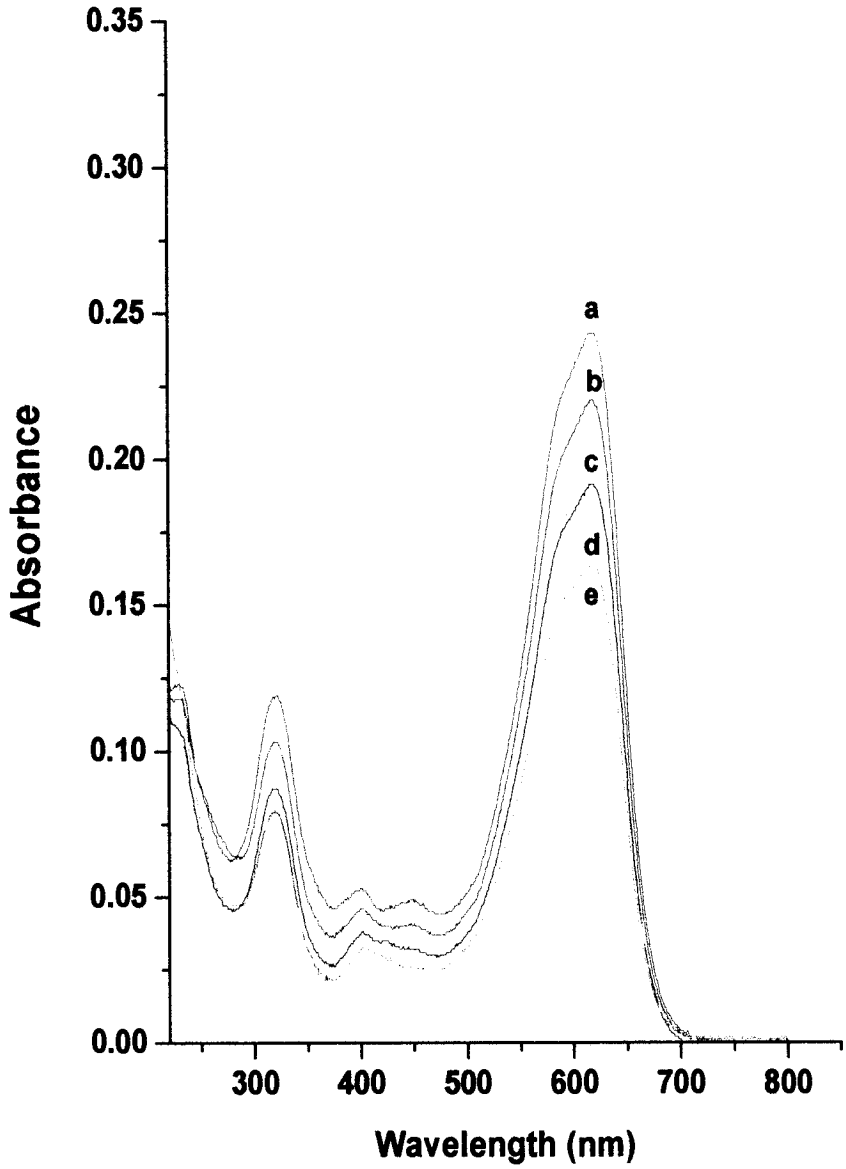

Fig. 6.10 Degradation of Amido Black 10B with TPP at pH= 7 for a) Blank b) 1 hour c) 2 hour d) 3 hour and e) 4 hour

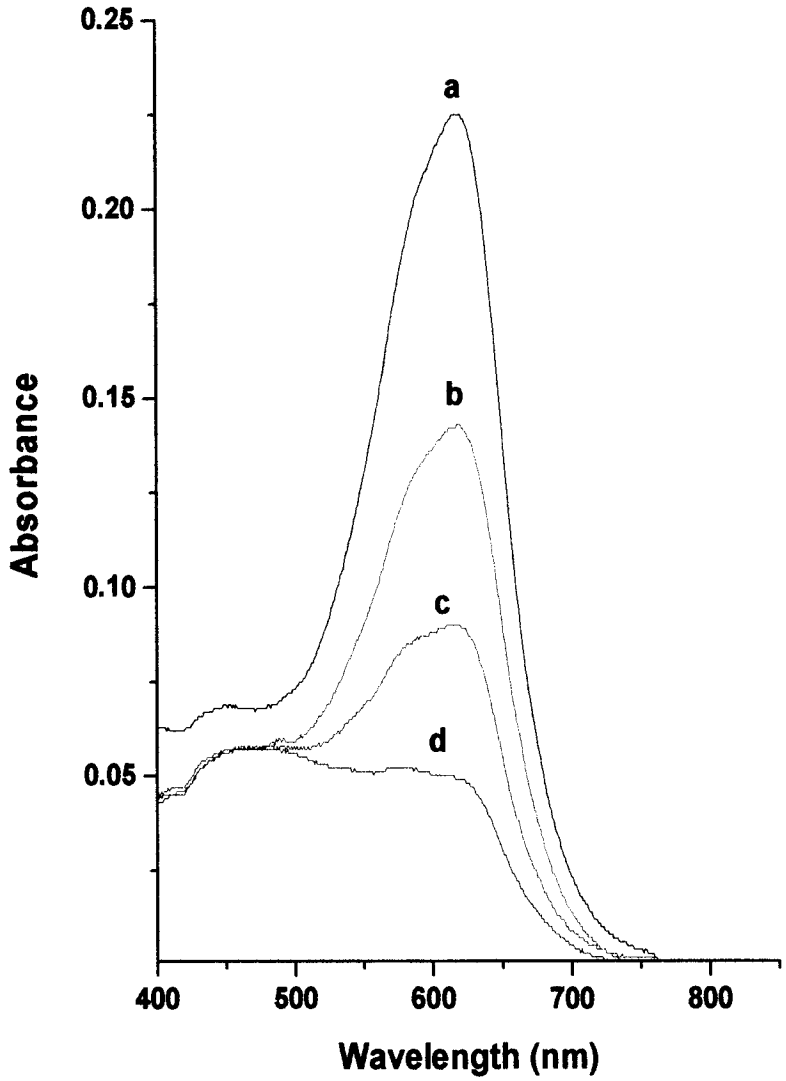

Fig. 6.11 Degradation of Amido Black 10B with TPP at pH=10 for a) Blank b) 1 hour c) 2 hour and d) 3 hour

From these graphs where absorbance is made a function of wavelength in nm at every hour the curve obtained gives information about the progress of the degradation reaction. It is observed that at pH 6 the rate of degradation of the dye is fastest, at pH 10 is moderate and at pH 7 the rate is slow and the extent of degradation is not complete as mentioned above. Similarly, Fig. 6.9, 6.10 and 6.11 also give information that as the process of degradation progresses the dye is degraded, which can be seen by decrease in the absorption. As the reaction advances for four hours every time the products are same, this observation is seen uniformly for the dye solution at pH 6, 7, and 10 respectively.

To know the reproducibility of the photocatalyst, TPP was selected and subjected for three times on three different days with freshly prepared Amido Black 10 B solution of 10^{-5} M concentration. Fig. 6.12 shows recycling of TPP for three times under exactly identical experimental conditions. It is observed that after first use the activity decreases to nearly 50% and then it remains approximately constant. It was also observed that after recycling of TPP there was no change in the chemical composition of the substance which is confirmed by UV-visible and FTIR spectroscopy. Thus it is seen that during photocatalysis chemical structure of a photocatalyst does not change, therefore, synthesized porphyrins can be safely reused for catalytic activity.

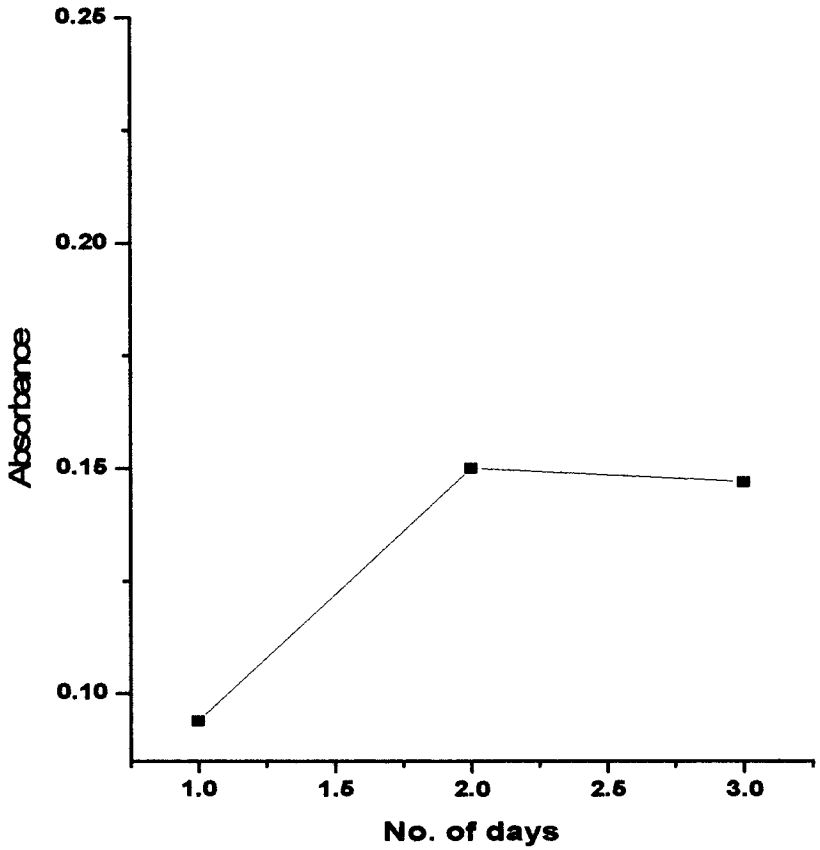

Fig. 6.12 Recycling of TPP for three times

6.3 Degradation product analysis of Amido Black 10B by HPLC

The degraded reaction mixture of Amido Black 10B at pH 6 and 7 was subjected to high performance liquid chromatography (HPLC) using C18 column with dimensions 250 mm × 4.6 mm and particle size 5 micrometer. The mobile phase selected was methanol and water (80% : 20%) at the rate of 1mL / minute with UV detector, which functions at 254 nm. Fig. 6.13 and 6.14 show the chromatograms obtained for degradation of dye and subsequent resolution of the components at different retention times. In Fig. 6.13, where an undegraded blank solution of dye of 10^{-5} M concentration was run through the column and a small peak at retention time 7.29 min. was obtained. Further, degraded solution of the same dye at pH 6 was run under same experimental conditions and is seen that three peaks at retention time of 3.32, 3.57 and 7.04 min. were resolved. This discloses that after degradation the dye has given three major components. Here, the components which are in minute concentrations are not considered. When the degraded solution of the same dye at pH 7 was run through the column (Fig.6.14), it is seen that again there are three major components which are resolved at 3.37, 3.61 and 7.17 min. Table 6.1 shows resolution of major components of the degraded dye solution at pH 6 and 7 respectively.

When retention times of the dye at pH 6 and 7 are compared, it is evident that they are matching very closely to each other. This shades light on the fact that irrespective of the pH of the solution, the same components are obtained after the degradation of a dye. The qualitative identification of the products was not done due to the complexity of the process.

A

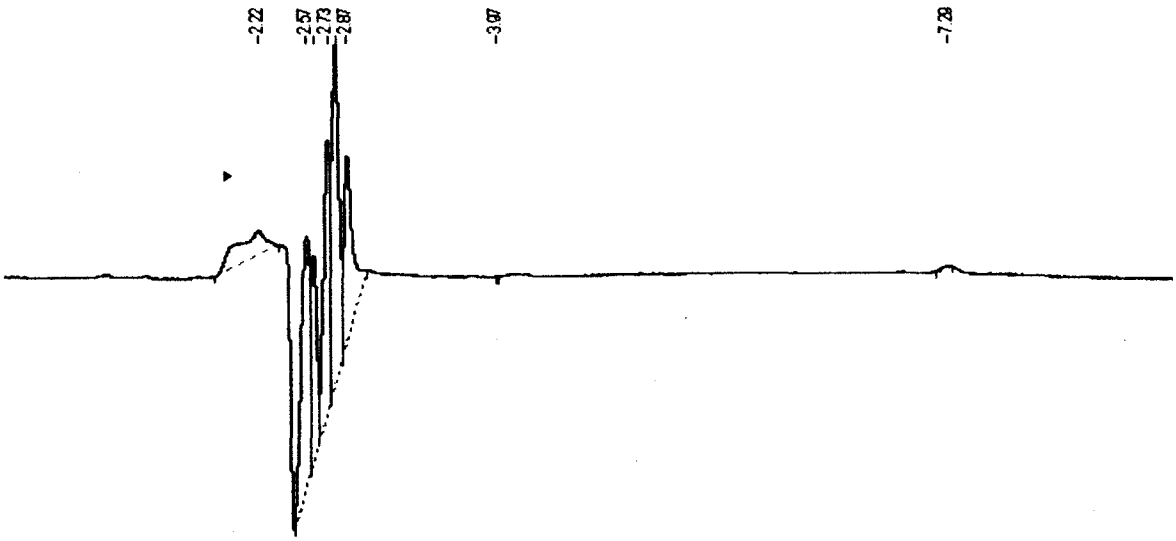

B

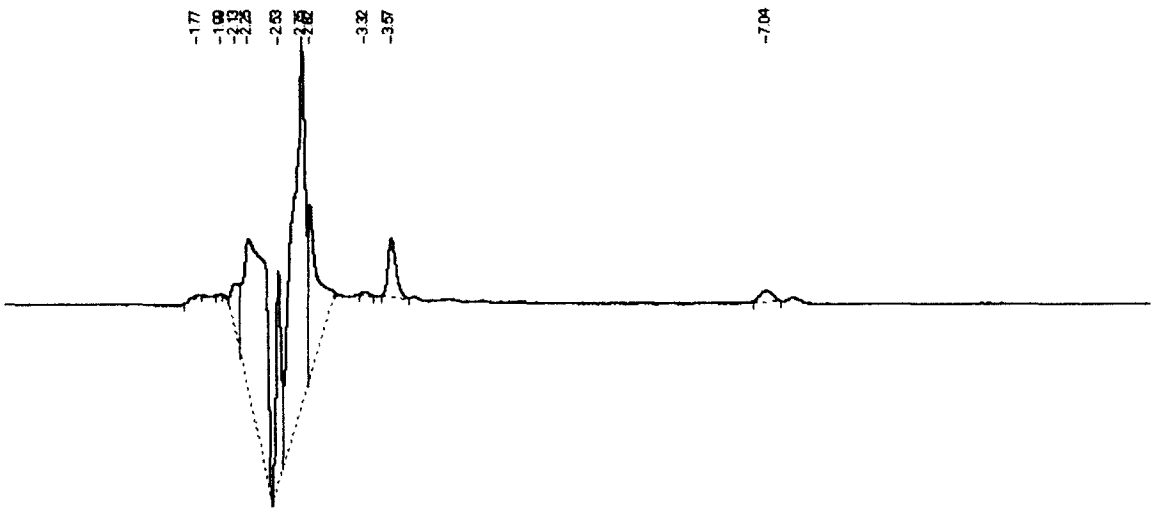

Fig. 6.13 HPLC chromatograms for Amido Black 10B

A) Before degradation B) After degradation at pH = 6

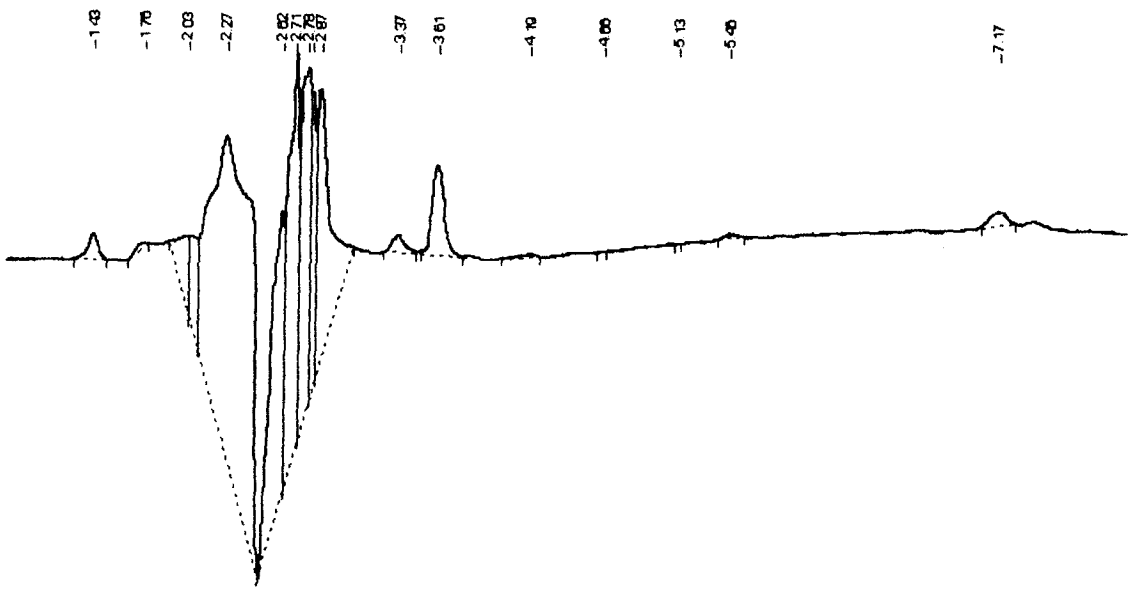

Fig. 6.14 HPLC chromatogram for degradation of Amido Black 10B at pH = 7

Table 6.1 HPLC results for degradation of Amido Black 10B at pH 6 and 7

Dye	pH	Retention time (R.T.)	Component
Amido Black 10B	**6**	**3.32**	**I**
	6	**3.57**	**II**
	6	**7.04**	**III**
Amido Black 10B	**7**	**3.37**	**I**
	7	**3.61**	**II**
	7	**7.17**	**III**

6.4 Degradation study of Amido Black 10B by Ion-chromatography

The degradation study was further extended to ion-chromatography to know the details of anions and cations present qualitatively and quantitatively. In ion-chromatography the signals in microvolt are recorded as function of retention time in minutes. The column for anion detection was calibrated for Cl- , SO_4^{2-}, NO_3^-, and NO_2^- depending upon the structure of dye. Here, Cl- being background impurity from undetected sources. Fig. 6.15 shows ion-chromatogram where background impurity Cl- is seen. Then the degraded dye solution of pH 7 was subjected to the column for detection and estimation of anions. Fig. 6.16 shows presence of NO_3^- and SO_4^{2-} ions. It is observed that NO_3^- is eluted first followed by SO_4^{2-} at different retention times. Further, depending upon the peak area of respective ion quantitative estimation of these ions in microgram (mcg) was carried out.

Similarly, the column for detection of cation was calibrated for Na^+ and NH_4^+ ions and then undegraded dye solution was run through the column. Fig.6.17 shows ion-chromatogram for undegraded Amido Black 10B solution where peak due to Na^+ ion is background impurity. Then degraded solution of dye solution at pH 7 was run through the column where Na^+ (excess amount) and NH_4^+ ions were detected as shown in Fig.6.18. Further, the quantitative estimation of these ions was done based on their respective peak areas. Table 6.2 shows amount of anions and cations in micrograms after degradation of the dye for four hours at pH 7.

This observation supports the fact that, mineralization of the dye takes place during the course of degradation. Thus it can be said that, in Amido Black 10B along with the rupture of the chromophoric groups, the auxochromic groups undergo mineralization.

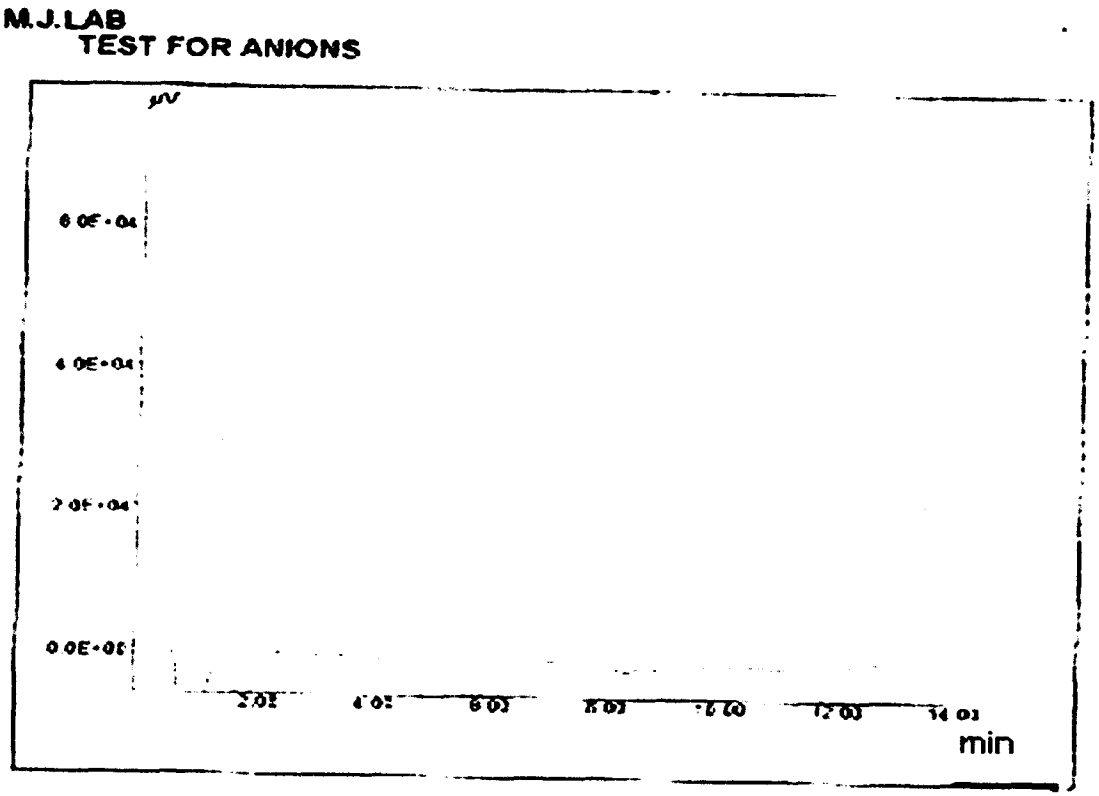

Fig. 6.15 Chromatogram for undegraded Amido Black 10B showing anions are absent

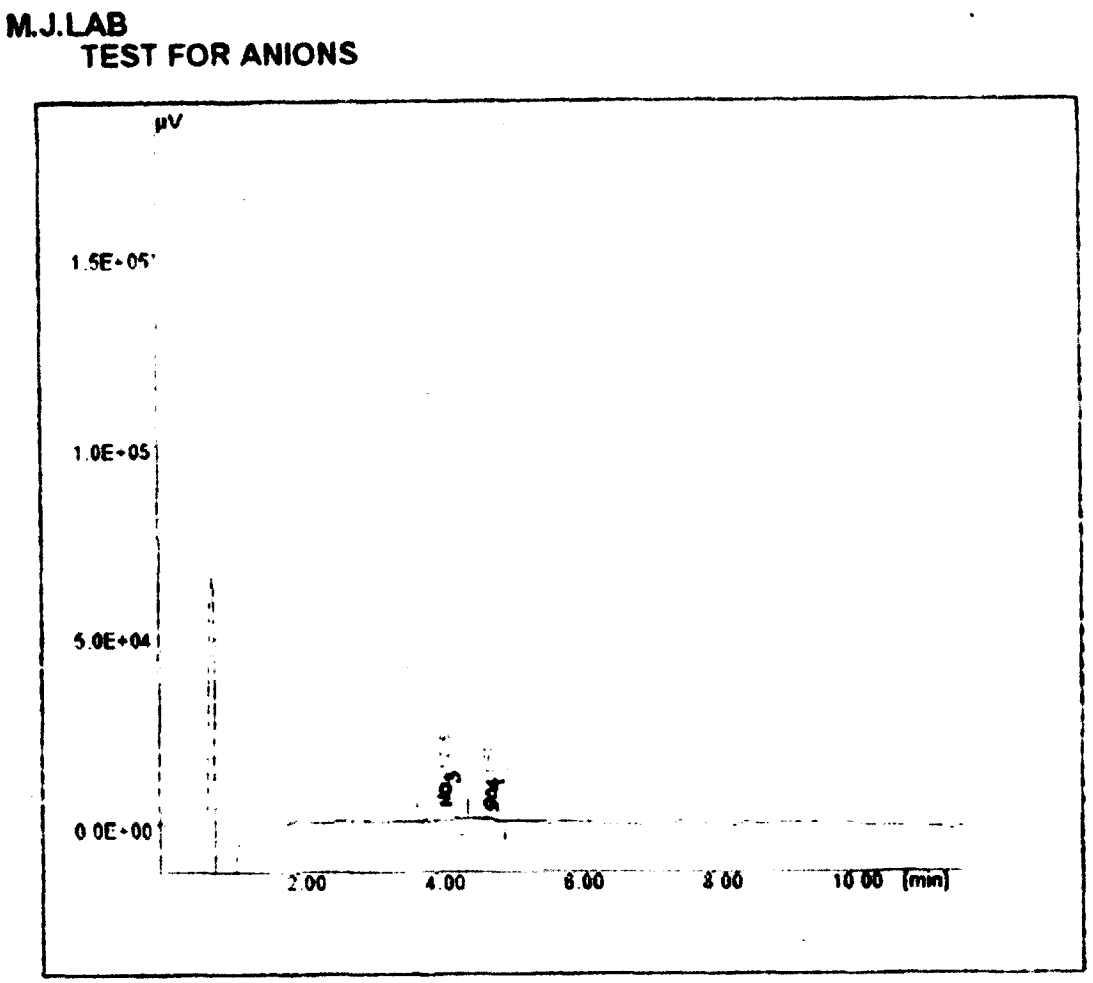

Fig. 6.16 Chromatogram for degraded Amido Black 10B showing NO_3^- and SO_4^{2-}

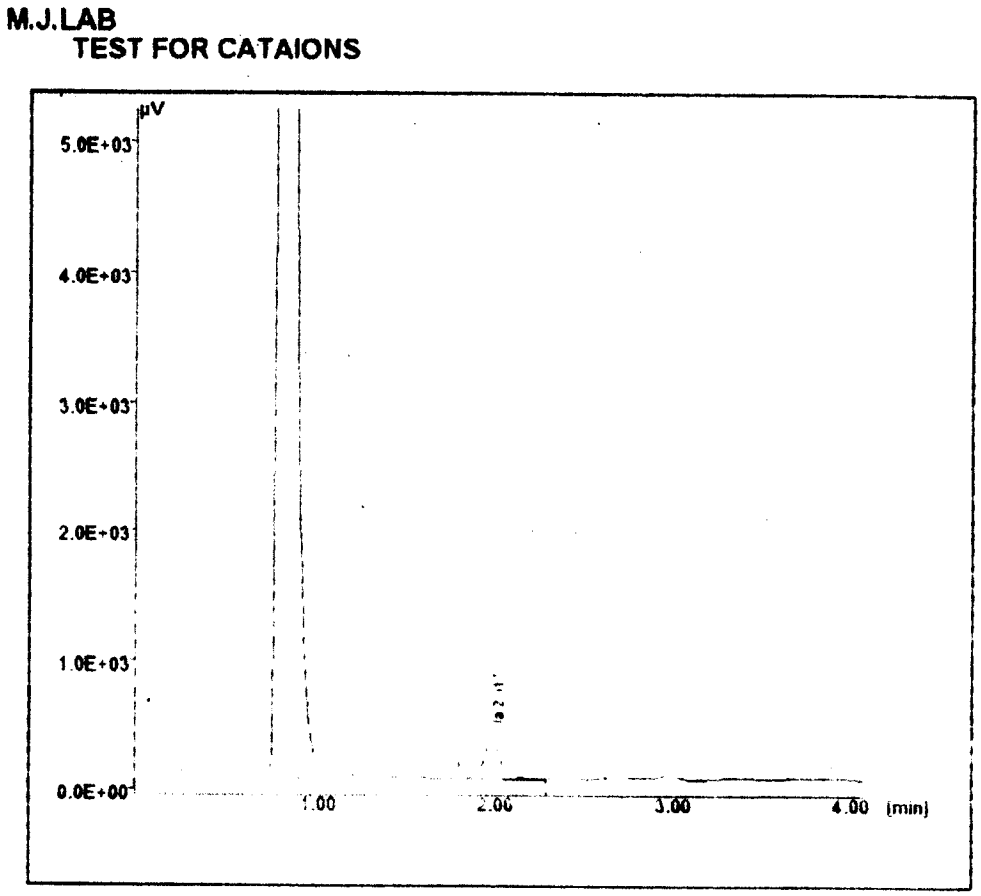

Fig. 6.17 Chromatogram for undegraded Amido Black 10B (with Na+ as background)

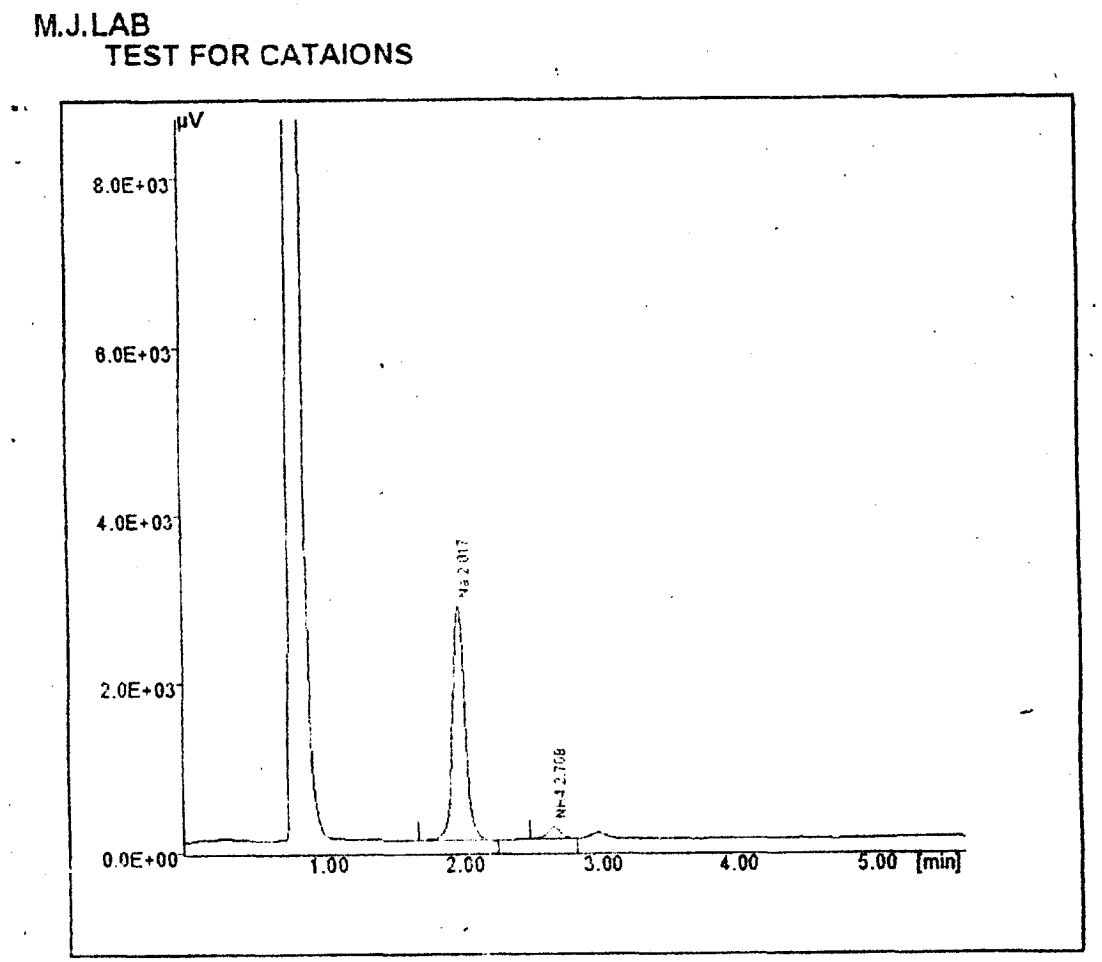

Fig. 6.18 Chromatogram for degraded Amido Black 10B showing Na^+ and NH_4^+ ions

Table 6.2 Ion-chromatography results for Amido Black 10B at pH 7

Sr.No.	Dye	Cation Concentration in μg/mL		Anion Concentration in μg /mL			
		Na^+	$NH4^+$	Cl^-	NO_3^-	SO_4^{2-}	NO_2^-
1	Amido Black 10B (blank)	—	—	—	—	—	—
2	Amido Black 10B (degraded)	9.88	0.59	—	2.11	0.50	—

6.5 General observations regarding photodegradation of Amido Black 10B

With regards to the process of phodegradation of the Amido Black 10B following observations can be generalized.

1) The most effective photocatalysts at pH 6, 7 and 10 are TPP, ZnTPP, MnTPPCl, O-$(MnTPP)_2$, $SnTPPCl_2$ and occasionally CuTPP.
2) From the degradation curves obtained by plotting absorbance versus wavelength, it is revealed that, when the dye undergoes degradation, the concentration goes on decreasing as the reaction advances with respect to time.
3) The HPLC results have shown that there are three major products which are common irrespective of pH of the dye solution. The three degradation products were distinguished on the basis of their different retention time.
4) Ion-chromatography results have shown that dye solution undergoes mineralization during the course of degradation as expected from the structural information of Amido Black 10B.

6.7 Phodegradation of Methyl Orange

Methyl orange is an intensely coloured compound used in dyeing and printing textiles. In chemical laboratories it is used in the titration of weak bases with strong acids. It changes from red (at pH 3.1) to orange yellow (at pH 4.4).

6.7.1 Optimization of amount of photocatalyst

In the beginning, it was necessary to optimise the amount of photocatalyst required to degrade the dye solution of selected concentration. Therefore, stock solution of 10^{-4} M of Methyl Orange was prepared by dissolving AR grade reagent. Further, it was diluted to ten times to get 10^{-5} M solution which was used for experiment. The dye solution was tested for self degradation under different experimental conditions. When this solution was irradiated at pH 5 it was seen that red colour of the dye starts degrading slowly. It becomes pale yellow within one hour and after second hour it starts degrading fast and becomes colourless at the end of 3rd hour. Then dye solution was irradiated without O_2, with O_2, and O_2 and promoter, sodium lauryl sulphate (SLS) for four hours from 11.30 a.m. to 3.30 p.m. It was seen that there were no observable changes due to variation of these factors. On the contrary, when TPP was added as a photocatalyst to dye solution then it was observed that O_2 plays a very important role in the process of dye degradation. Taking into account this point, the optimum quantity of photoatalyst was determined for the photocatalytic reaction. Thus 100 mL of Methyl Orange solution was taken and O_2 was bubbled for five minutes and the requisite amount of photocatalyst was selected from 5 mg to 25mg. The Fig. 6.19 shows that for 20 mg, the absorbance is minimum, therefore, it confirms the optimum amount of photcatalyst for 100 mL reaction solution. For this experiment, TPP being precursor, was chosen as a representative compound of the non-aqueous porphyrins as photocatalysts. It was also found

that if the amount is exceeded 20 mg the photodegradation activity decreases[197] as was found in the case of earlier dye Amido Black 10B.

6.7.2 Photodegradation of Methyl Orange at different pH

As is seen in the in the earlier section 6.2.2, the pH also plays important role in the process of degradation of Methyl Orange. To verify the details of the degradation process over porphyrins from non-aqueous series TPP, CoTPP, NiTPP, CuTPP, ZnTPP, AgTPP, MnTPPCl, O-$(MnTPP)_2$, FeTPPCl, O-$(FeTPP)_2$ and $SnTPPCl_2$ were employed.

1) Degradation of Methyl Orange at pH 6

The solution of Methyl Orange of 10^{-5} M concentration was bubbled with O_2 followed by requisite amount of HNO_3 to adjust the pH of the solution to 6 with standardized pH meter. Fig. 6.20 shows the UV-visible spectrum of the dye where λ_{max} value observed is 503 nm. Further, to study the degradation process the reaction assembly was prepared as mentioned earlier for each photocatalyst. Then 20 mg of each photocatalyst was added, the assembly was stirred thoroughly and kept in sun light from 11.30 a.m. to 3.30 p. m. from temperature range 30° C to 38° C respectively. Fig 6.21 and 6.22 show the efficiency of dye degradation with respect to each photocatalyst.

From Fig. 6.21 it is seen that, TPP and ZnTPP are effective catalyst and degrade Methyl Orange to 77% and 68% respectively. CuTPP shows only 30% degradation whereas remaining CoTPP, NiTPP and AgTPP show negligible photoactivity. In the Fig. 6.22 it is seen that $SnTPPCl_2$ exhibits 100% degradation within three hours, MnTPPCl degrades to 92% within only one hour and O-$(MnTPP)_2$ dimer 78% within four hours. The remaining porphyrins such as FeTPPCl, O-$(FeTPP)_2$ are very sluggish in photocatalytic reaction. Therefore, when

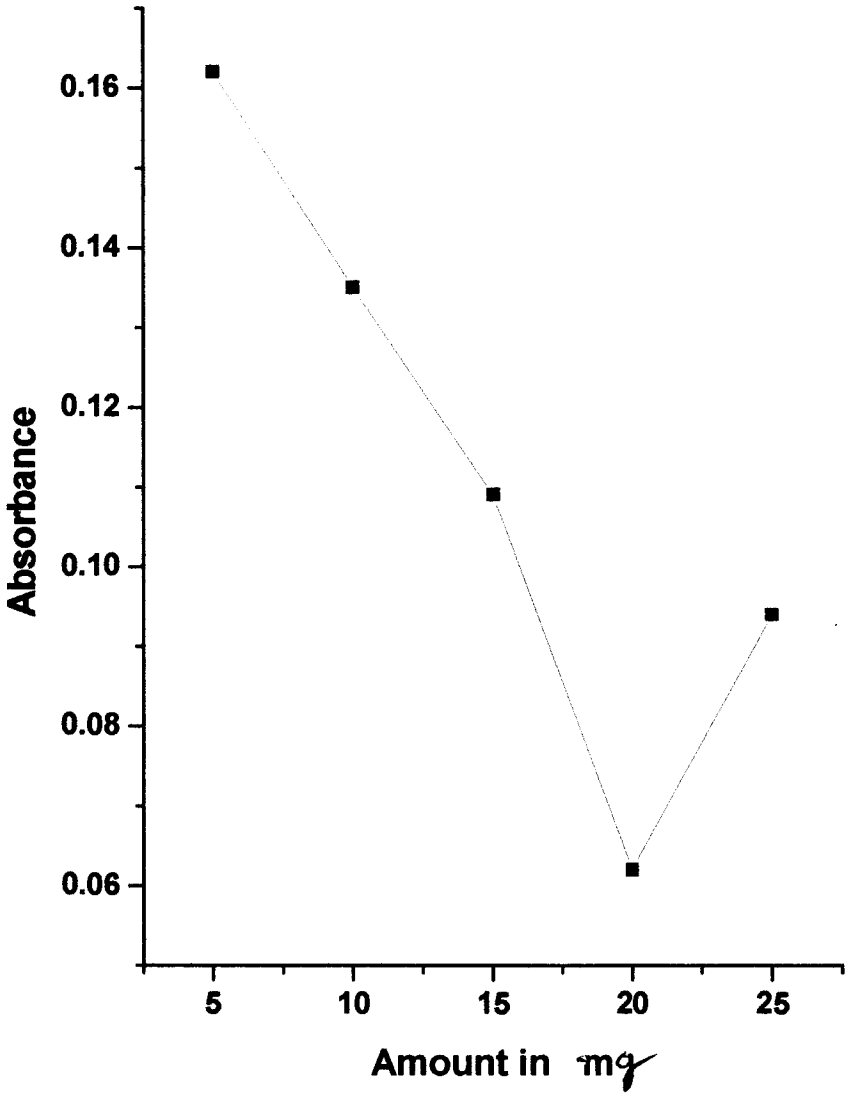

Fig. 6.19 Optimization of catalyst amount for degradation of Methyl Orange

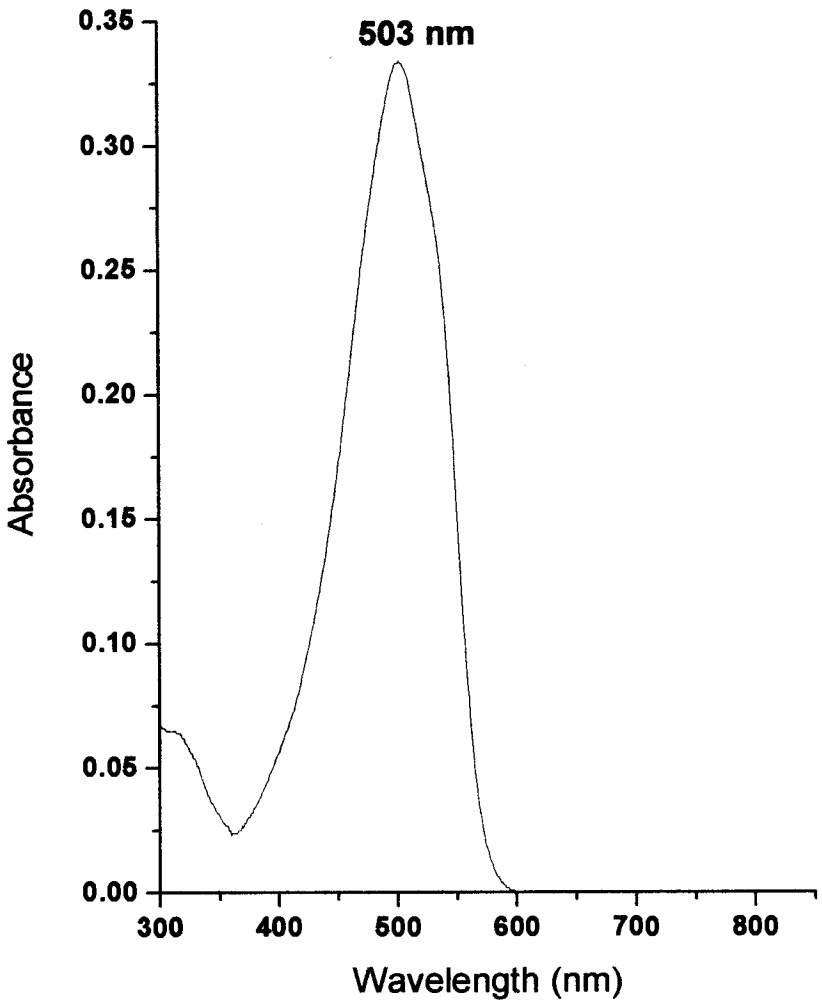

Fig. 6.20 UV-Visible spectrum of Methyl Orange at pH 6

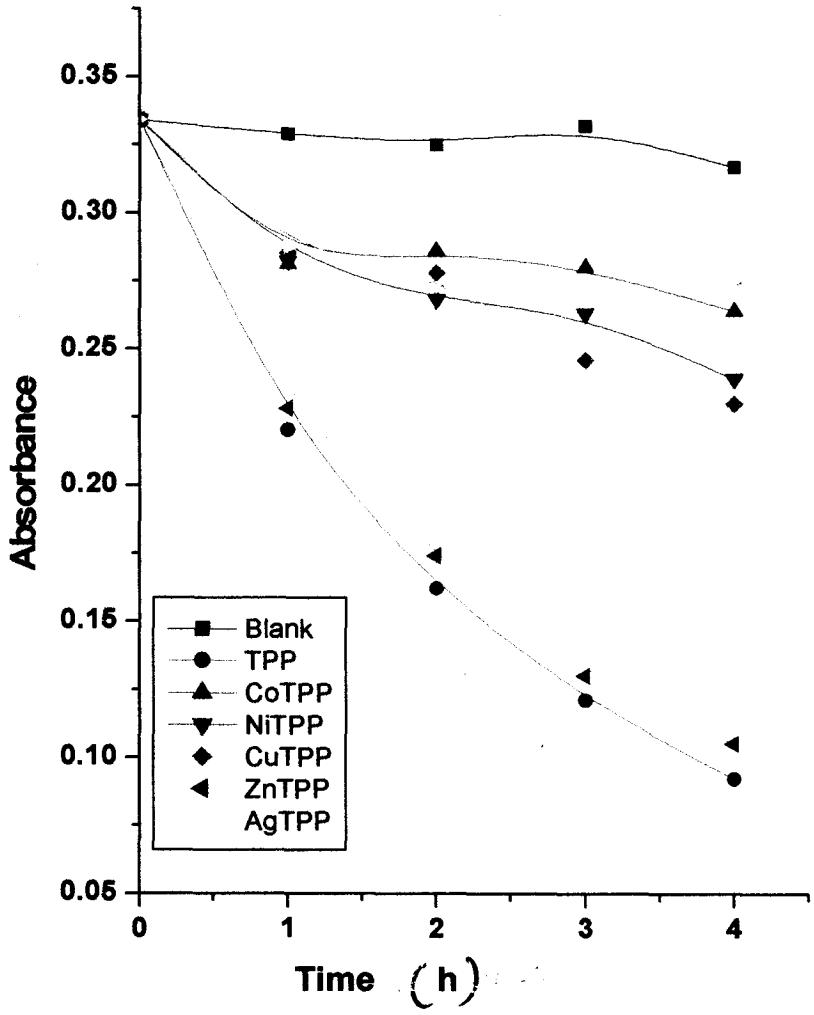

Fig. 6.21 Photodegradation of Methyl Orange by TPP and metalloporphyrins containing divalent metals (pH=6)

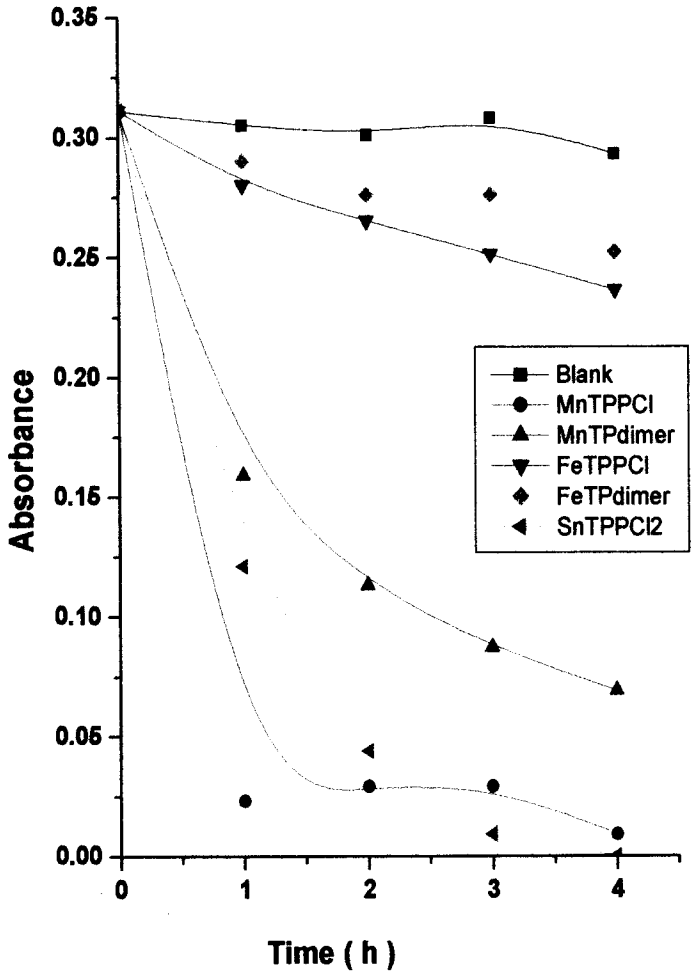

Fig. 6.22 Photodegradation of Methyl Orange by metalloporphyrins containing trivalent and tetravalent metals (pH=6)

Therefore, when the effective catalysts are arranged in a decreasing order of their efficiency following order is seen

$SnTPPCl_2 > MnTPPCl > O\text{-}(MnTPP)_2 > TPP > ZnTPP$

2) Degradation of Methyl Orange at pH 7

As it was verified that at pH 7 the catalytic activity was not so pronounced, therefore, to increase the activity five drops of 0.1% of SLS were added to the reaction assembly containing 10^{-5} M solution of Methyl Orange and O_2. Fig. 6.23 shows the degradation of the dye for some selected porphyrins viz. TPP, ZnTPP, O-$(MnTPP)_2$ and $SnTPPCl_2$. it was found that $SnTPPl_2$ shows maximum activity to the extent of 56%, and O-$(MnTPP)_2$ dimer shows only 36%. The rest of the two i.e. TPP and ZnTPP show very negligible activity.

3) Degradation of Methyl Orange at pH 10

The photocatalysis when carried out at pH 10, it was necessary to add five drops of 0.1% SLS to the dye solution of 10^{-5} M concentration. This has increased the activity of the catalyst to some extent as is seen from Fig. 6.24 and 6.25. The photoactivity of free-base porphyrin TPP is seen maximum whereas ZnTPP shows nearly 50% of activity compared to TPP. The rest of the metalloporphyrins CoTPP, NiTPP, CuTPP and AgTPP show considerably reduced activity at this pH. From Fig. 6.25 it is seen that $SnTPPCl_2$ degrades the dye nearly to 100% whereas O-$(MnTPP)_2$ dimer has low photoactivity. The remaining MnTPPCl, FeTPPCl and O-$(FeTPP)_2$ show very sluggish activities. Fig. 6.26 show the degradation pattern for TPP at pH 6 where absorbance was made the function of wavelength in nm. It is observed that as the time of reaction advances the concentration of the dye solution goes on decreasing and finally reaches to colourless state of solution or 100% degradation.

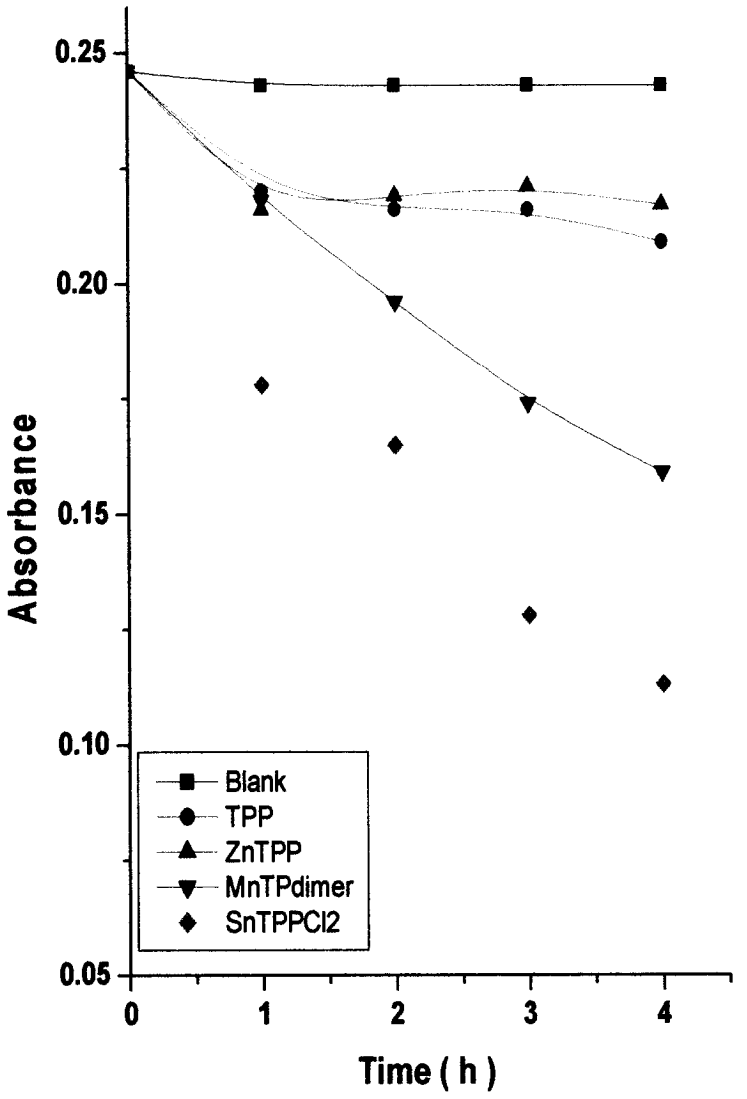

Fig. 6.23 Photodegradation of Methyl Orange by TPP and metalloporphyrins containing di, tri and tetravalent metals (pH=7)

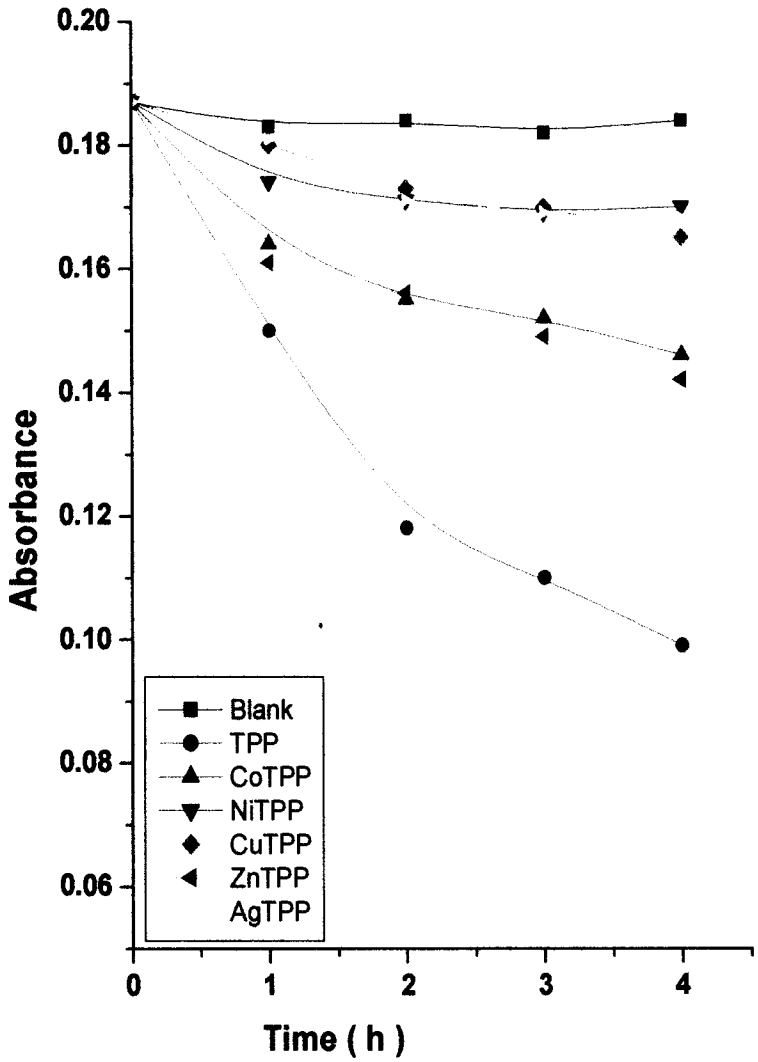

Fig. 6.24 Photodegradation of Methyl Orange by TPP and metalloporphyrins containing divalent metals (pH=10)

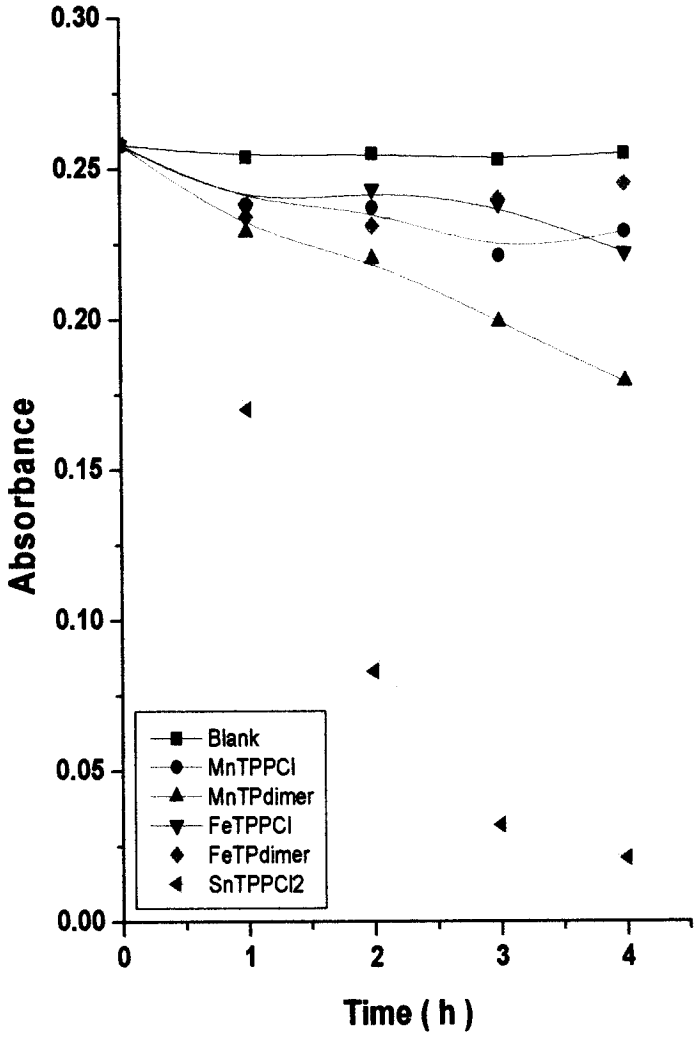

Fig. 6.25 Photodegradation of Methyl Orange by metalloporphyrins containing di, tri and tetravalent metals (pH=10)

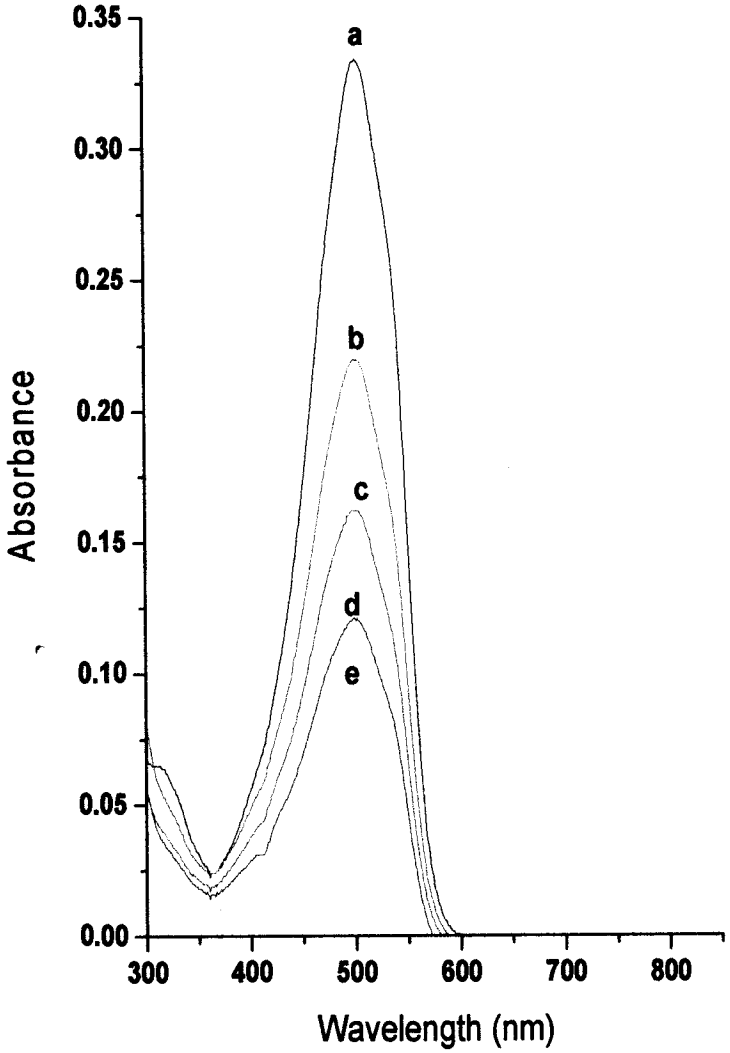

Fig. 6.26 Degradation pattern of Methyl Orange with TPP for a) Blank b) 1 hour c) 2 hour d) 3 hour e) 4 hour

Further, the recycling of the two representative samples viz. TPP and $SnTPPCl_2$ was carried out to check the reproducibility of the photodegradation reaction. Fig. 6.27 shows the plot of absorbance versus no. of days, where it is seen that for second and third use the activity goes on decreasing. When two catalysts are compared, it is also observed that $SnTPPCl_2$ retains its photoactivity more than free base TPP. Further, to check any structural changes of these catalysts, they were subjected to UV-Visible and FTIR spectroscopy and it was observed that these catalysts are remaining intact even after reuse for several number of times.

6.8 Degradation study of Methyl Orange by HPLC

The experiment set up for methyl orange is used as described for Amido Black 10B in section 6.3. In case of methyl orange there is a change in λ_{max} value depending upon the pH of the solution. At pH 6 it gives λ_{max} 502-503 nm whereas for pH 7 and above it shows λ_{max} 465 nm respectively. The chromatograms present in Fig.6.28 are shown for pH 6 where, the components present in the blank solution (a) and the components resolved in degraded solution (b) at the same pH are seen. There are two components resolved from degraded solution at the retention time 3.39 and 3.62 min respectively. In Fig. 6.29 the chromatograms for undegraded solution (a) and degraded solution (b) at pH 7 are seen. The three components which are separated at this pH have shown retention time 3.36, 3.60 and 7.30 min respectively. When the comparison of the resolved components at pH 6 and 7 is done, it is observed that the first two components are nearly same irrespective of the pH. But for pH 7 one more component at 7.30 min is resolved which is different from the component in the blank i.e. at 7.60 min. But its concentration seems to be very minute.

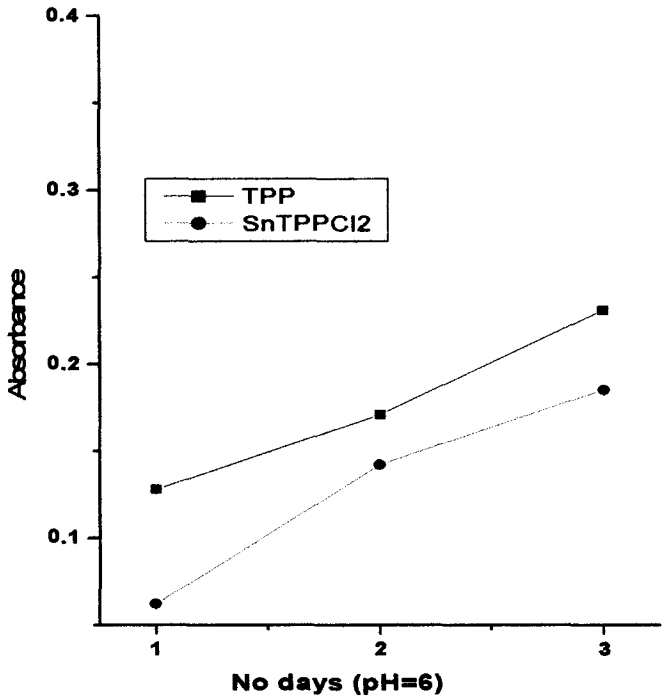

Fig. 6.27 Recycling of TPP and $SnTPPCl_2$ for three times

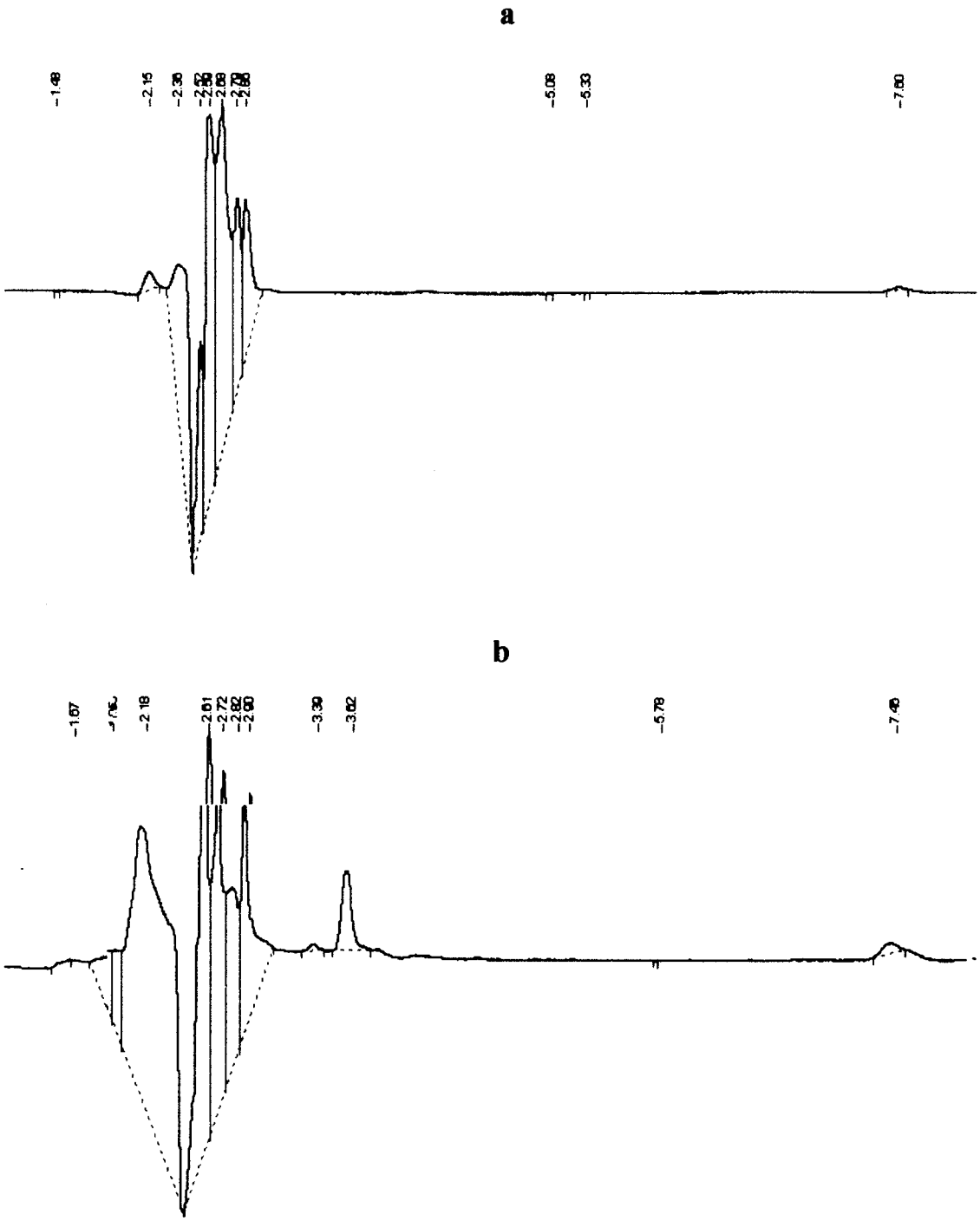

Fig. 6.28 HPLC chromatograms for Methyl Orange

a) Before degradation b) After degradation at pH=6

a

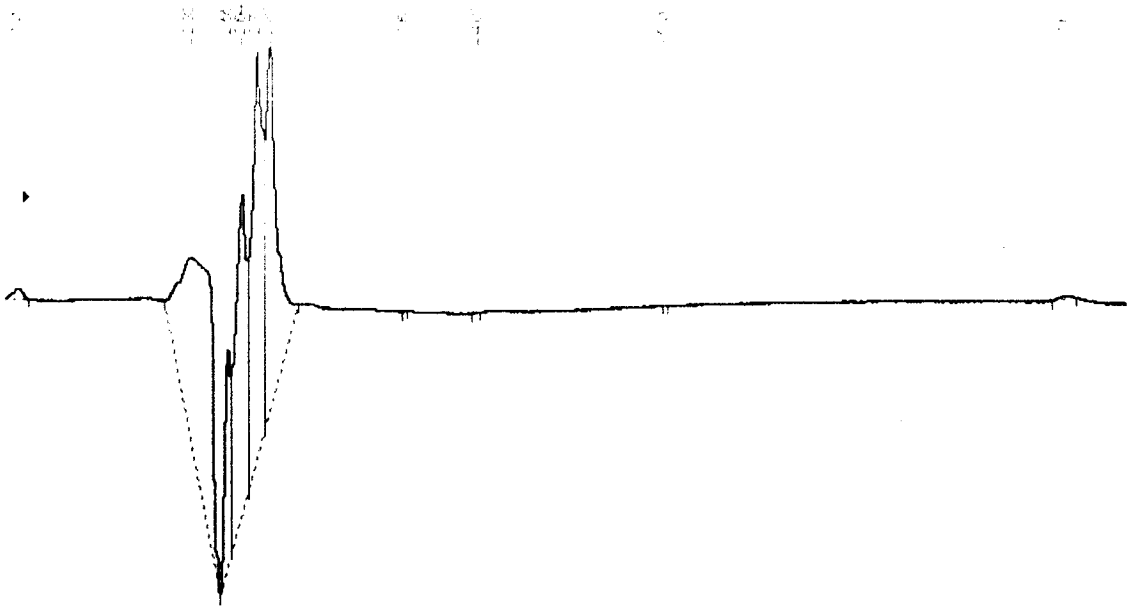

b

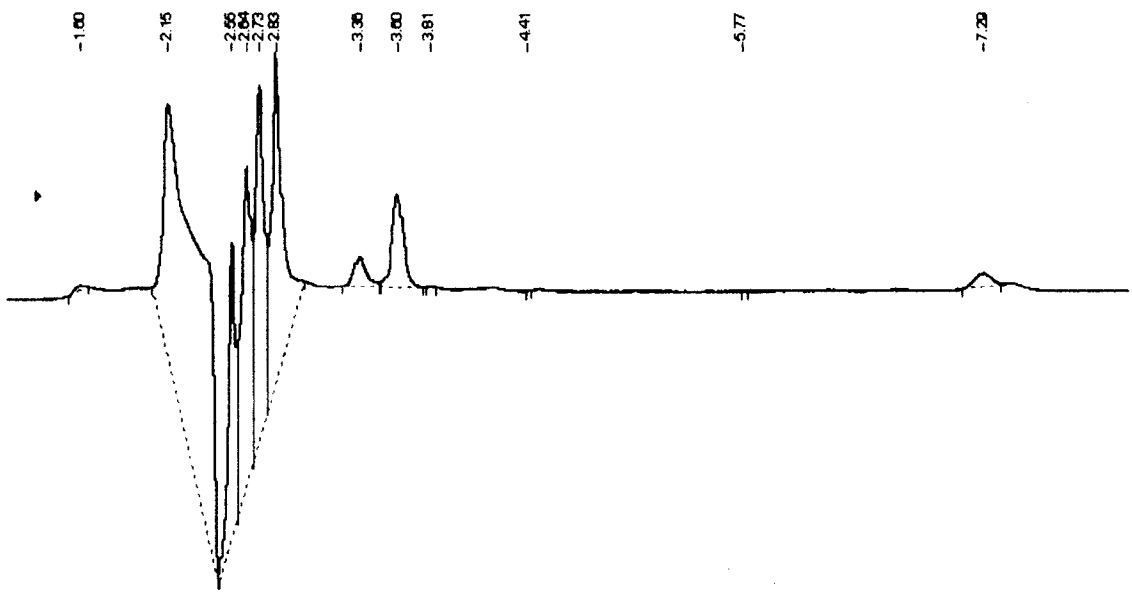

Fig. 6.29 HPLC chromatograms for Methyl Orange

a) Before degradation b) After degradation at pH=7

Table 6.3 HPLC results for degradation of Methyl Orange at pH 6 and 7

Dye	pH	Retention time	Component
Methyl Orange	**6**	**3.39**	**I**
	6	**3.62**	**II**
Methyl Orange	**7**	**3.36**	**I**
	7	**3.60**	**II**
	7	**7.3**	**III**

Table 6.13 shows HPLC results for the degradation of Methyl Orange at pH 6 and 7 respectively.

6.9 Degradation study of Methyl Orange by ion-chromatography

The ion-chromatography study is carried out in section 6.4, where the graph is obtained by plotting microvolt versus retention time in minute. Fig. 6.30 shows the chromatogram for blank solution of Methyl Orange at pH 7 where background concentration of Cl^- and NO_3^- are seen. Fig. 6.31 shows chromatogram where increased concentration of Cl^- and NO_3^- in microgram (μg) is seen because of same impurities is present inherently. Therefore, according to the structural features only concentration of NO_3^- may be taken into consideration. For the detection and estimation of cations the system was calibrated with respect to Na^+ and NH_4^+. Fig. 6.32 and 6.33 show presence of Na^+ and NH_4^+ in blank as well as degraded solution at pH 7. To evaluate the net increase in the amount of respective ions the subtraction of quantities in micro gram between degraded and undegraded dye solution is carried out. Table 6.4 shows net increase in the amount of NO_3^-, Na^+ and NH_4^+ respectively after photocatalytic reaction. This strengthens the fact that a process of degradation of dye takes place by destruction of chromophore followed by mineralization from auxochromic groups and other groups.

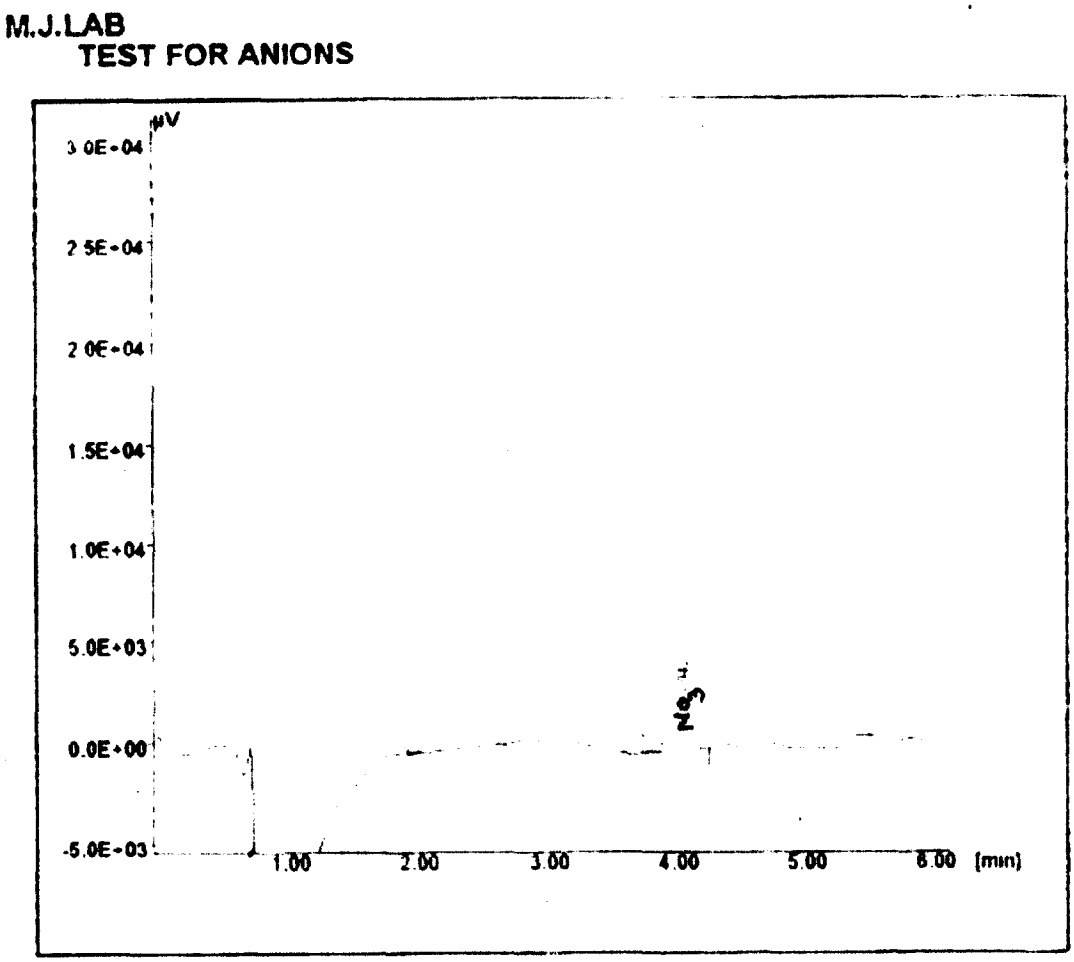

Fig. 6.30 Chromatogram for undegraded Methyl Orange (NO_3^- being background)

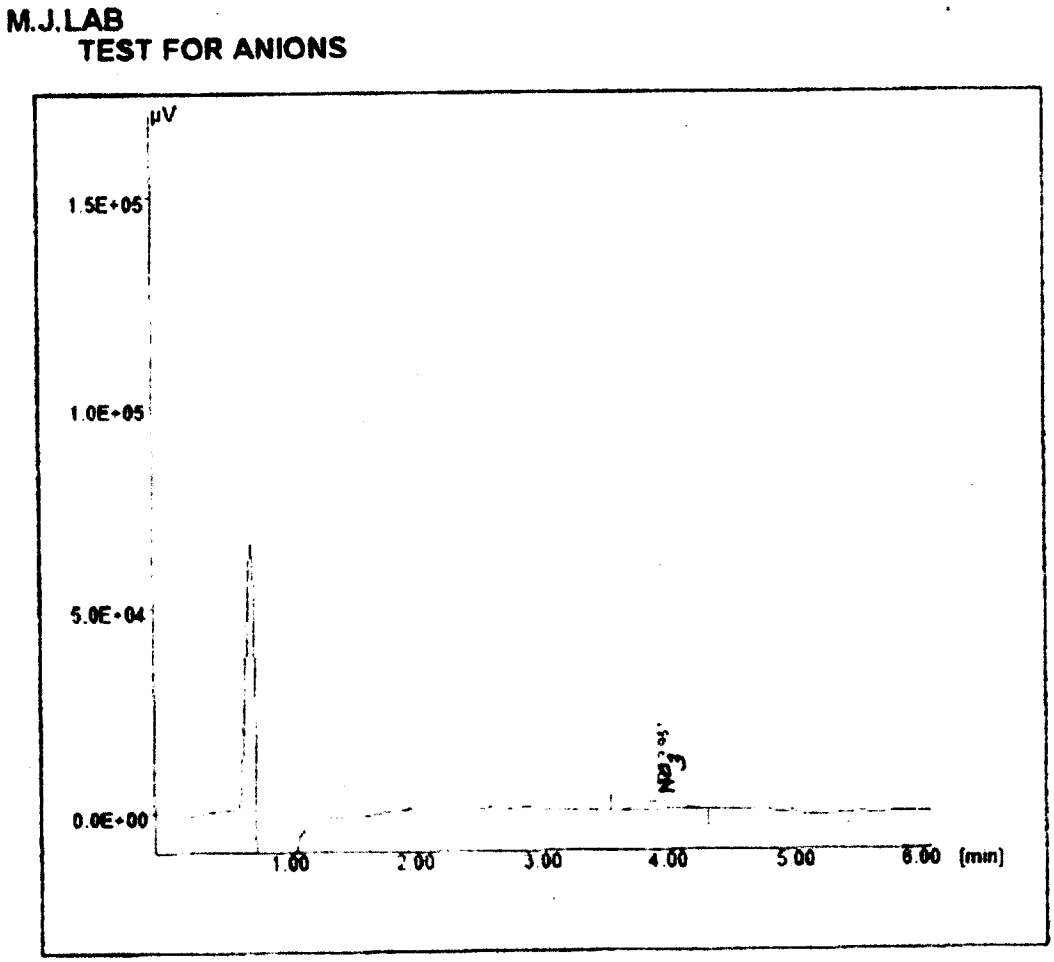

Fig. 6.31 Chromatogram for degraded Methyl Orange showing presence NO_3^-

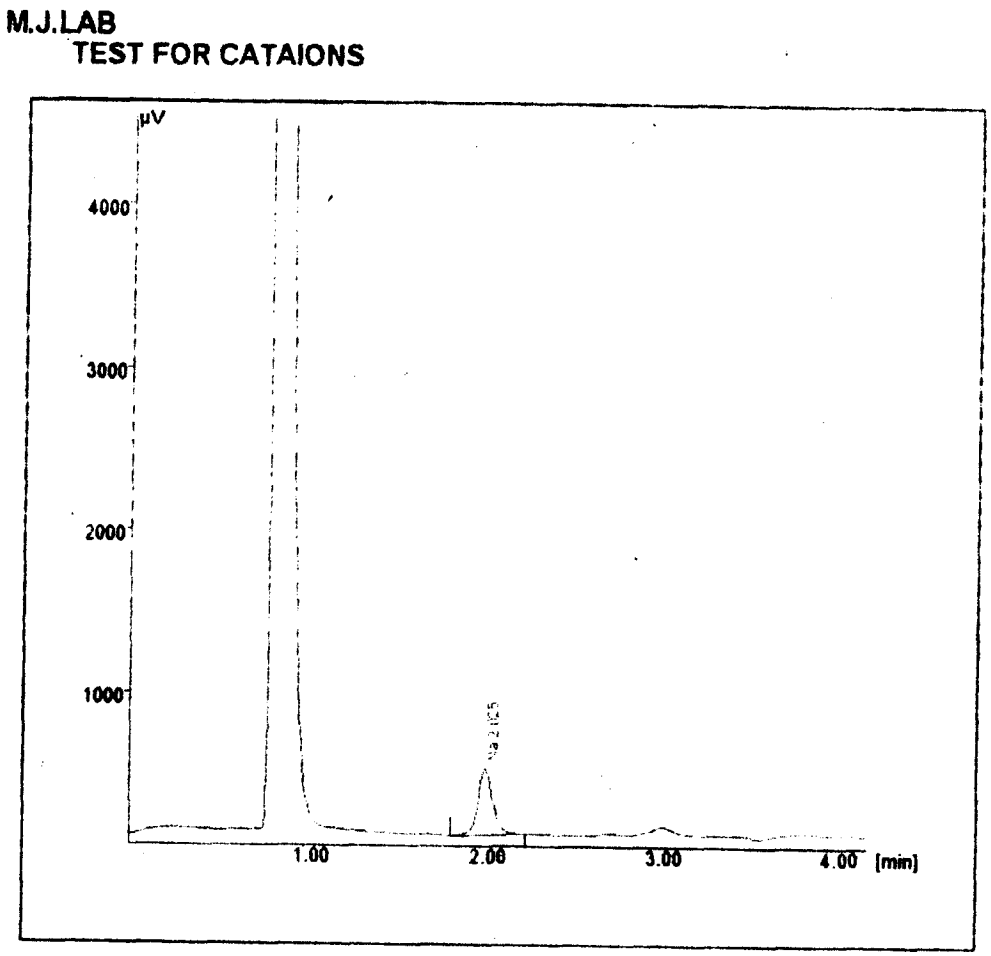

Fig. 6.32 Chromatogram for undegraded Methyl Orange (Na^+ being background)

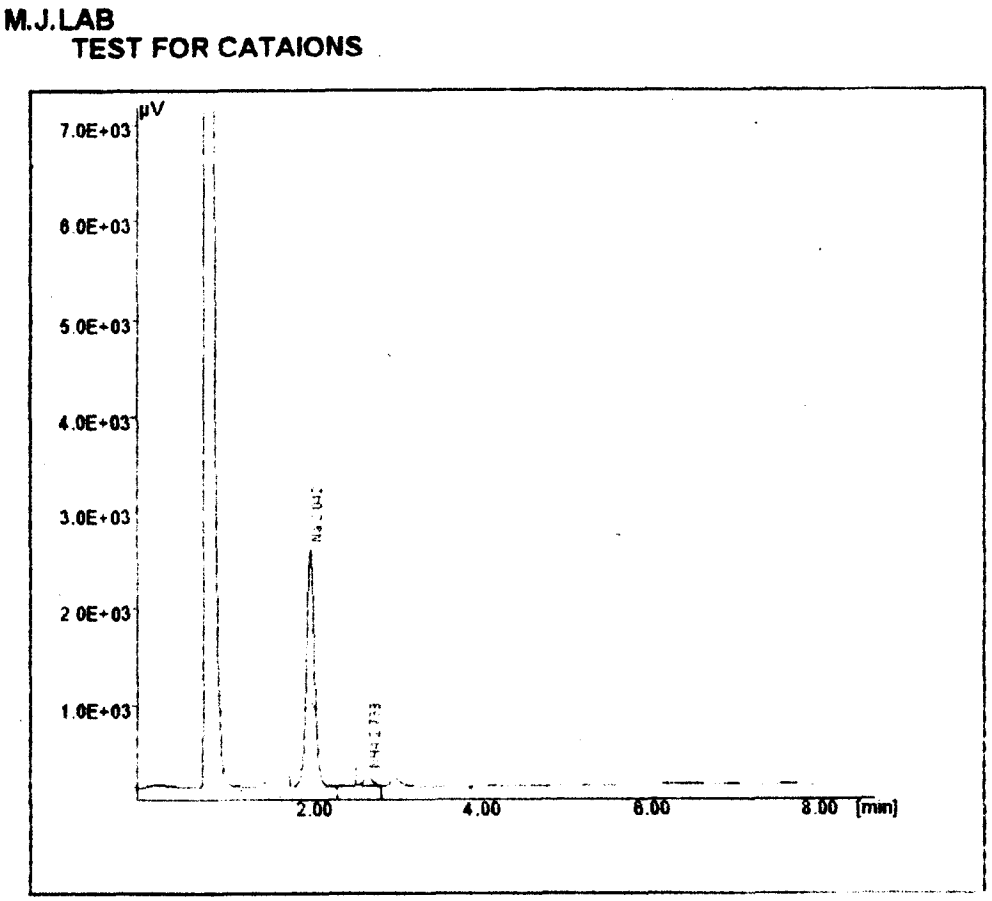

Fig. 6.33 Chromatogram for degraded Methyl Orange showing presence of Na^+ and NH_4^+

Table 6.4 Ion-chromatography results for Methyl Orange at pH 7

Dye	Concentration of ions in µg per mL		
	Na^+	NH_4^+	NO_3^-
Methyl Orange (blank)	-	-	-
Methyl Orange (degraded)	8.42	0.45	2.78

209

6.9 Photodegradation of Ponceau S

Ponceau S is a sodium salt of a diazo dye with four sulphonic acid groups and one OH group and is soluble in water at room temperature. It shows two absorption bands at 520 and 352 nm.

The dye is very stable towards solar radiations at pH 6, 7 and 10 but at pH 5 it shows self degradation within two and half hour. The concentration of the dye used for photocatalysis was 10^{-5} M as is explained in earlier sections 6.2.1 and 6.7.2 respectively for Amido Black 10B and Methyl Orange.

1) Photodegardation of Ponceau S at pH 6

In this case 50 mL of dye solution of 10^{-5} M is taken and bubbled with O_2 for five minutes and then requisite quantity of 0.1M HNO_3 is added to adjust the pH of the solution to 6. Then 25 mg of porphyrin is used as a photocatalyst for each of the reaction assembly to carry out photodegradation reaction with solar radiations during 11.30 a.m. to 3.30 p.m. from 30° C to 38° C respectively. As is seen from Fig. 6.34, ZnTPP is the most effective photocatalyst followed by TPP and NiTPP whereas CoTPP, CuTPP and AgTPP exhibit nearly least amount of photoactivity. Fig. 6.35 shows photocatalysis for metalloporphyrins of tri and tetravalent porphyrins. It is observed that $SnTPPCl_2$ shows pronounced activity whereas O-$(MnTPP)_2$ dimer and MnTPPCl exhibit moderate activity. FeTPPCl and O-$(FeTPP)_2$ dimer show the least amount of activity as seen in the preceding sections.

2) Photodegardation of Ponceau S at pH 7

From the primary observation it was seen that the dye is very stable towards solar radiations and especially at pH 7. Therefore, at pH 7, to increase the activity of catalysts 0.1% of SLS was added to each reaction assembly as promoter and some selected and effective porphyrins were used. Fig. 6.36 shows that the photoactivity of MnTPPCl is maximum followed by $SnTPPCl_2$ whereas remaining O-$(MnTPP)_2$, ZnTPP and TPP show moderate amount of activity. Under given experimental conditions it is seen that the dye solution is not completely degraded.

3) Photodegardation of Ponceau S at pH 10

The solution of Ponceau S of 10^{-5} M concentration was bubbled with O_2 and respective photocatalysts were added to the reaction assembly and the reaction was carried out in solar radiations. Fig. 6.37 shows photodegradation of dye solution on $SnTPPCl_2$, ZnTPP and O-$(MnTPP)_2$ dimer . It is observed that $SnTPPCl_2$ is the most effective porphyrin which degrades the dye solution nearly to completion. The rest of the two ZnTPP and O-$(MnTPP)_2$ dimer show very sluggish activity towards photocatalysis.

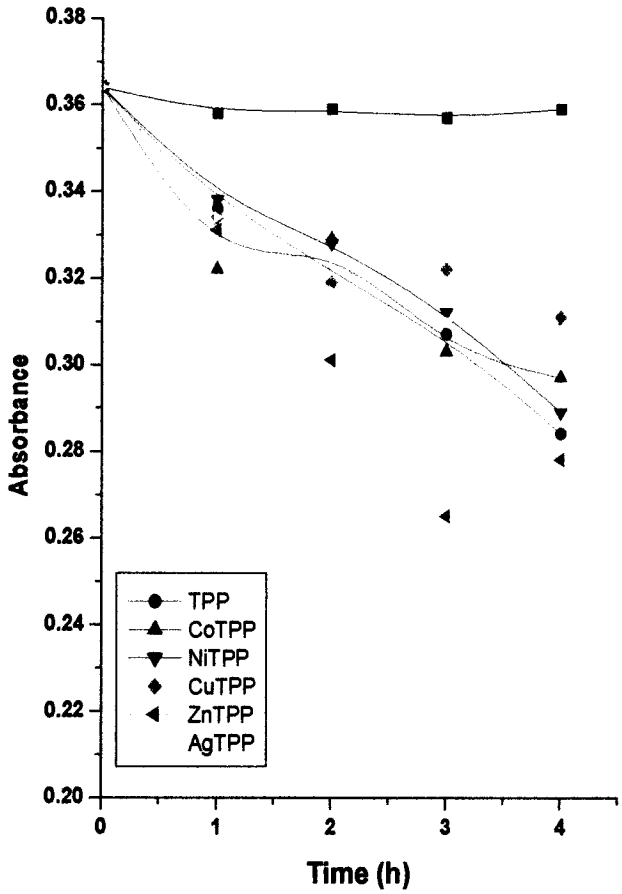

Fig. 6.34 Photo degradation of Ponceau S by TPP and metalloporphyrins containing divalent metals (pH= 6)

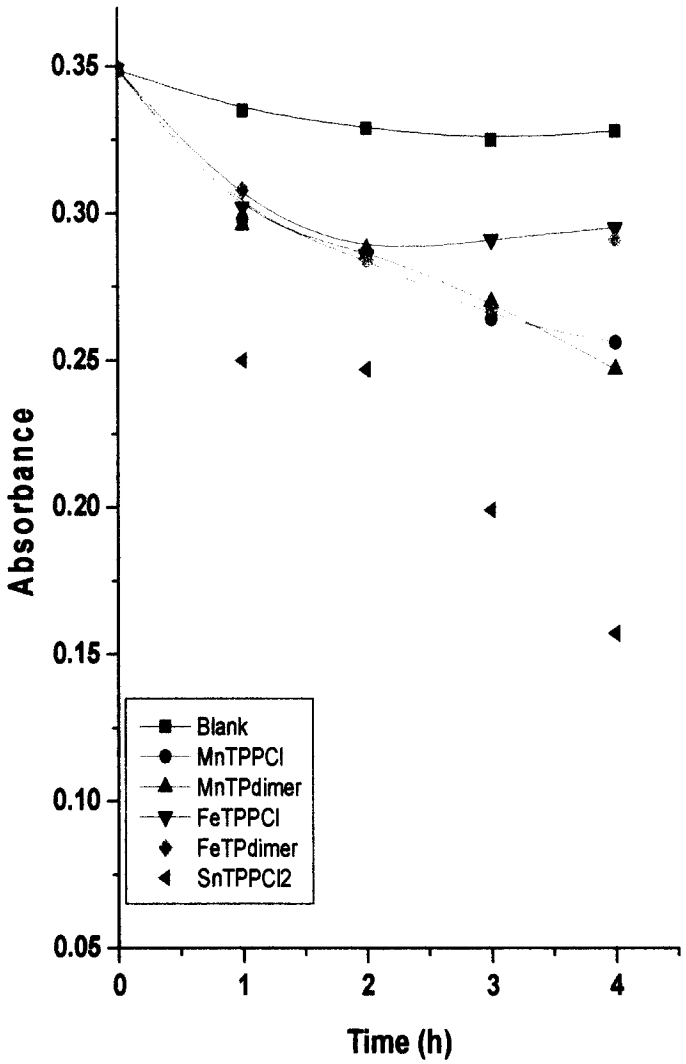

Fig. 6.35 Photo degradation of Ponceau S by metalloporphyrins containing trivalent and tetravalent metal ions (pH=6)

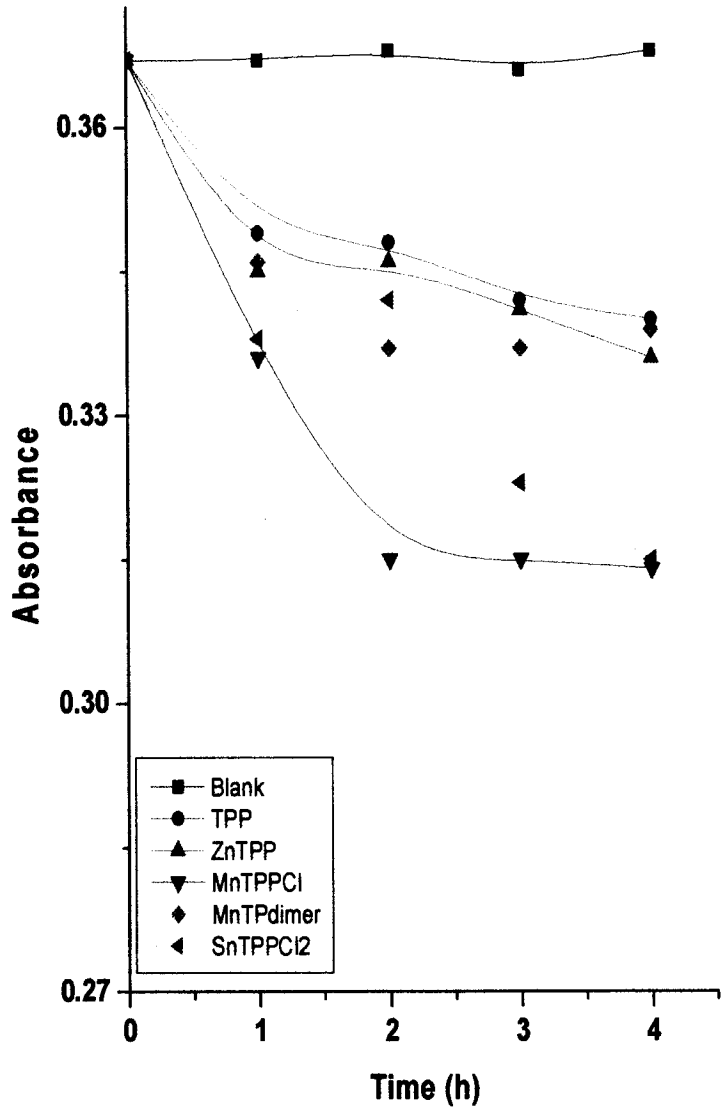

Fig. 6.36 Photo degradation of Ponceau S by TPP and porphyrins containing di, tri, and tetravalent metals (pH= 7)

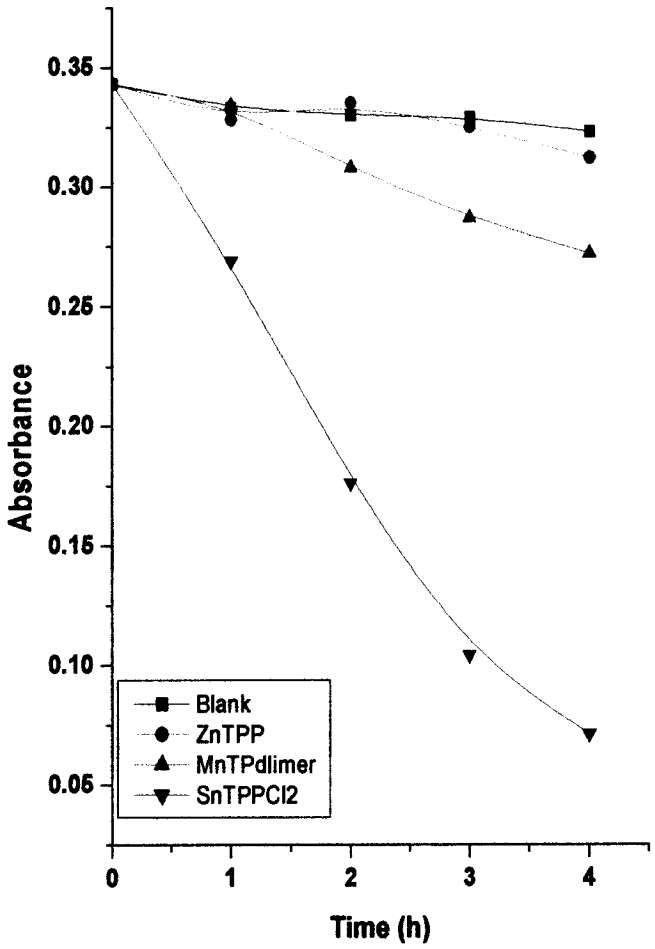

Fig. 6.37 Photo degradation of Ponceau S by metalloporphyrins containing di, tri and tetravalent metals (pH= 10)

6.10 General Mechanism for photocatalysis

In the preceding sections, the photodegradation of diazo dyes such as Amido Black 10 B , Ponceau S or monoazo dye like Methyl Orange was carried out on porphyrins as photocatalyst by means of heterogeneous photocatalysis in aqueous medium. The non-aqueous porphyrins required for this reaction were synthesized in the laboratory. Similarly, the reaction pH was selected at three discrete values as 6, 7 and 10 respectively. It was a noteworthy observation that for any of the dyes mentioned above, the photodegradation reaction was efficient at pH 6, good at pH 10 and comparatively slow at pH 7. With regards to the nature of the photocatalysts it is seen that in general, irrespective of the pH of the dye solution the porphyrins like TPP, ZnTPP, MnTPPCl, O-$(MnTPP)_2$ and $SnTPPCl_2$ are most effective. Similarly, CuTPP is occasionally photo-effective. The remaining porphyrins such as CoTPP, NiTPP, AgTPP, FeTPPCl and O-$(FeTPP)_2$ are seen less or in some cases not at all effective. The efficiency of the photocatalyst is measured on the basis of its capacity to degrade the dye solution as fast as possible with the destruction of chromophore and making it colourless as much as possible.

The efficiency of catalyst depends upon its long-lived excited state. Therefore, conversely it can be said that the effective photocatalyst like TPP, ZnTPP, MnTPPCl, O-$(MnTPP)_2$ and $SnTPPCl_2$ are possessing long-lived excited states. Now, it is also seen that all these porphyrins are fluorescent in nature. The fluorescent intensity is directly proportional to the solar radiations absorbed, therefore, it can be also said that these effective photocatalysts are comparatively strong absorber of solar radiations.

The process of degradation of dye on the surface of the photocatalyst may have different possible mechanisms. When dyes undergo photooxidation[159,165,170] then there are two possibilities which may be expected viz. i) direct oxidation of the dye due to hole and ii) oxidation of the dye due to formation of $OH^{\bullet}$ species[182]. When solar radiations are incident upon porphyrin molecules they get excited and electron transfer takes place from valance band to conduction band. Porphyrins maintain relatively long-lived excited states which make them ideal photosensitive materials. The oxygen present in the dye solution functions as an electron scavenger. This oxygen traps the electrons from conduction band and forms O_2^- species. This prevents recombination of positive holes in valance band and the electrons in conduction band. Further O_2^- is reacting with chemisorbed water on conduction band to produce $OH^{\bullet}$ and OH^- with the liberation of oxygen. Thus OH^- ions produced, then combine with positive hole to produce $OH^{\bullet}$ (free radical). Thus $OH^{\bullet}$ radical is responsible for degradation of dye leading to mineralization. The degradation reaction at pH 6 is quite faster. This may be explained on the basis of formation of $HO_2^{\bullet}$ species, detected by ESR[198] which is responsible for increased concentration of $OH^{\bullet}$ radical and thus comparatively faster degradation of dye. Excess of $OH^{\bullet}$ radicals recombine to produce H_2O_2 which further decomposes.

Different investigators have suggested many pathways for reaction mechanism. The photooxidation of the dye at the hole is common irrespective of the pH of the solution. Similarly, oxidation of the dye due to $OH^{\bullet}$ species, as per present study, is suggested by degradation at pH 6 by Scheme I and degradation at pH 7 and 10 by Scheme II respectively.

The high oxidative potential of the hole (h^+_{VB}) in the porphyrin permits the direct oxidation of the dye as shown below

h^+_{VB} + dye ⟶ $dye^{\bullet+}$ ⟶ oxidation of the dye

When solar radiations are incident upon porphyrin molecule 'P', it is excited and hole-electron pair is formed. The hydroxyl radical ($OH^{\bullet}$) which is formed in the course of reaction is an extremely strong oxidant ($E° = +2.80V$) which leads to mineralization as shown below

Scheme I for pH 6

$P \xrightarrow{hv} P^*$

$P^* \longrightarrow e^-_{CB} + h^+_{VB}$

$e^-_{CB} + h^+_{VB} \longrightarrow$ Recombination ⟶ heat

$e^-_{CB} + O_2 \longrightarrow O_2^-$ (superoxide anion)

$O_2^- + (H^+ + OH^-) \longrightarrow HO_2^{\cdot} + OH^-$

$HO_2^{\cdot} + OH^- + h^+_{VB} \longrightarrow OH^{\bullet}$

$OH^{\bullet}$ + Dye ⟶ Degradation products

Excess of OH^- recombine as

$OH^{\bullet} + OH^{\bullet} \longrightarrow H_2O_2$ (decomposition)

$H_2O_2 + e^- \longrightarrow OH^{\bullet} + OH^-$

Scheme II for pH 7 and 10

$P \xrightarrow{h\nu} P^*$

$P^* \longrightarrow e^-_{CB} + h^+_{VB}$

$e^-_{CB} + h^+_{VB} \longrightarrow$ Recombination $\longrightarrow$ heat

$e^-_{CB} + O_2 \longrightarrow O_2^-$ (superoxide anion)

$O_2^- + 2H_2O \longrightarrow 2\,OH^\bullet + 2\,OH^- + O_2$

$h^+_{VB} + OH^- \longrightarrow OH^\bullet$

$OH^\bullet +$ Dye $\longrightarrow$ Degradation products

Excess of OH^- radicals recombine to give

$OH^\bullet + OH^\bullet \longrightarrow H_2O_2$ (decomposition)

$H_2O_2 + e^- \longrightarrow OH^\bullet + OH^-$

6.11 Photodegradation of Rhodamine B (RB)

Rhodamine B is used as a dye laser gain medium and often used as a tracer dye within water to determine the rate and direction of flow and transport. It is used extensively in biotechnology applications such as fluorescence microscopy and flow cytometry. The dye is soluble in water, methanol and ethanol. It shows λ_{max} at 555 nm in visible region.

Rhodamine B was selected to test the photocatalytic activity of aqueous-porphyrins in organic medium. For the phodegradation of RB in organic medium, the following conditions were required to be satisfied.

i) The solvent should show no or minimum self degradation in solar radiations.

ii) The RB should have maximum solubility in the selected solvent.

iii) The synthesized aqueous-porphyrins should not be soluble in the chosen solvent.

iv) There should not be any chemical reaction between solvent and photocatalyst.

The above conditions were completely satisfied by acetone as a solvent , therefore, it was selected for the reaction medium.

The photodegradation of RB was carried out using the photocatalysts viz. $TPPS_4$, $CoTPPS_4$, $NiTPPS_4$, $CuTPPS_4$, $ZnTPPS_4$, $AgTPPS_4$, $MnTPPS_4Cl$, $FeTPPS_4$, O-$(FeTPPS_4)_2$, and $SnTPPS_4Cl_2$ respectively. The reaction was tried without O_2, since the rate constant of diffusion of O_2 in aetone is 3.8×10^{-10} $M^{-1}s^{-1}$ which is approximately seven times more than water (0.53×10^{-10} $M^{-1}s^{-1}$). Therefore, it is seen that photadegradation reaction with O_2 was immeasurably fast, which did not allow the the determination of course of degradation quantitatively. Thus for all photocatalytic reactions O_2 was not bubbled prior to the commencement of the photolysis. The AR grade acetone was refluxed with $KMnO_4$ for two hours till pink colour persists and then it

was distilled to get the solvent of desired purity. The 50 mL solution of Rhodamine (RB) of 10^{-5} M concentration was taken and 5 mg of porphyrin as a photocatalyst was added to the reaction assembly and then subjected to the solar radiations for photolysis.

6.11.1 Photodegradation of RB on porphyrins

The free-base $TPPS_4$ and other metalloporphyrins of divalent metals were used for the photocatalytic reaction as shown in Fig. 6.38 . It is seen from the figure that all porphyrins are degrading the RB solution to the extent of 100%. Further it is also observed that $CoTPPS_4$ is the most effective catalyst which degrades the solution within 5 min, followed by $AgTPPS_4$ in 10 min. Among rest of the catalysts $NiTPPS_4$ and $TPPS_4$ show degradation within 20 and 25 min whereas $CuTPPS_4$ and $ZnTPPS_4$ degrade the solution in 40 minute respectively. When inorganic photoatalyst e.g. SnO_2 was used for comparative study it is found that $CoTPPS_4$ and $AgTPPS_4$ were more effetive than SnO_2.

The photodegradation of RB by porphyrins of tri and tetra valent metals is shown in Fig. 6.39. It is observed that $O\text{-}(FeTPPS_4)_2$ degrades the dye within 25 min whereas $FeTPPS_4Cl$ in 35 min and $MnTPPS_4Cl$ and $SnTPPS_4Cl_2$ decolourize the dye within 40 minute. As a comparison SnO_2 was used which shows the degradation in 15 minute. Therefore, it can be said that porphyrins of divalent metals are more effective than porphyrins of trivalent metals. Similarly, an important striking fact is seen that in aqueous medium porphyrins of Co^{2+}, Ag^{2+} have shown minimum photoactivity but in organic medium like acetone they have shown pronounced ativity. In aqueous medium free-base porphyrin and porphyrins of Zn^{2+}, Mn^{2+} and Sn^{4+} have proved most effective but in acetone medium opposite effect is seen.

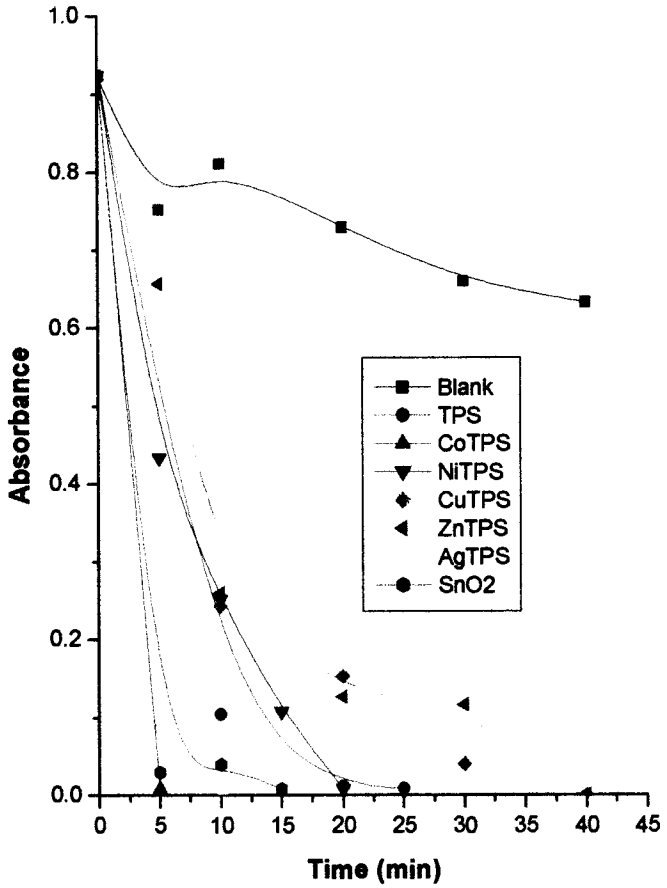

Fig. 6.38 Photodegradation of Rhodamine B by $TPPS_4$, metalloporphyrins and SnO_2

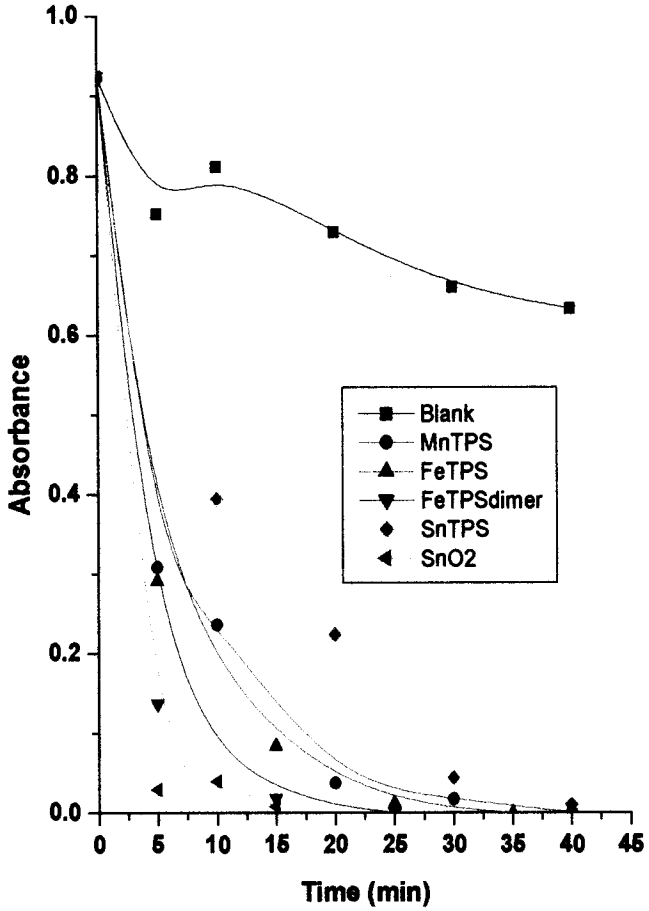

Fig. 6.39 Photodegradation of Rhodamine B by metalloporphyrins containing tri and tetravalent metals and SnO_2

Thus the observed fact may be attributed to the effect of medium of the photocatalytic reaction as well as the presence of sulphonic acid groups in aqueous porphyrins. When reproducibility of these catalysts is verified by recycling them for number of times, it is seen that even after using them many times their photoactivity remains good. Fig. 6.40 show recycling of $CoTPPS_4$ for six times. It is observed that, when the photocatalyst is recycled for three times the activity remains the same i.e. within five minutes degradation takes place but for further activity when recycled for three times it is seen that the degradation takes place within ten minutes. Thus for $CoTPPS_4$ photo activity dereases after third use and remains constant for subsequent uses.

In the context of $AgTPPS_4$ it is seen that , the first degradation takes place in ten minutes which is shown in Fig. 6.41. Further recycling decreases the activity of the catalyst and requires 40 min to degrade the RB solution. After one cycle there is no further decrease in the activity and remains constant for all subsequent cycles. The degradation pattern for RB is obtained when absorption is made a function of wavelength in nm. Fig. 6.42 shows degradation of RB by $TPPS_4$ (a) and by $AgTPPS_4$ (b). It is observed that TPPS4 degrades RB at the interval of 10, 20 and 25 min whereas $AgTPPS_4$ degrades RB at the interval of 5 and 10 min respectively.

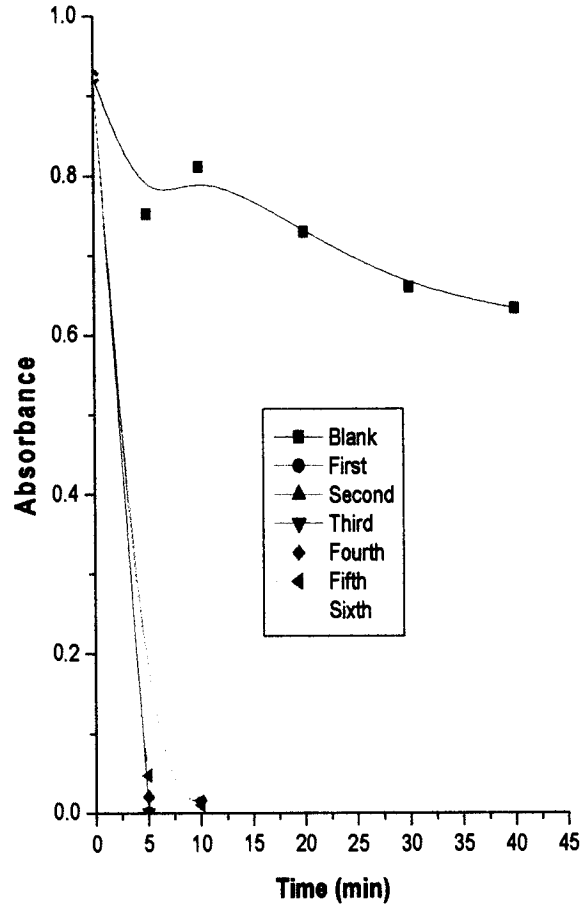

Fig. 6.40 Recycling $CoTPPS_4$ for six times

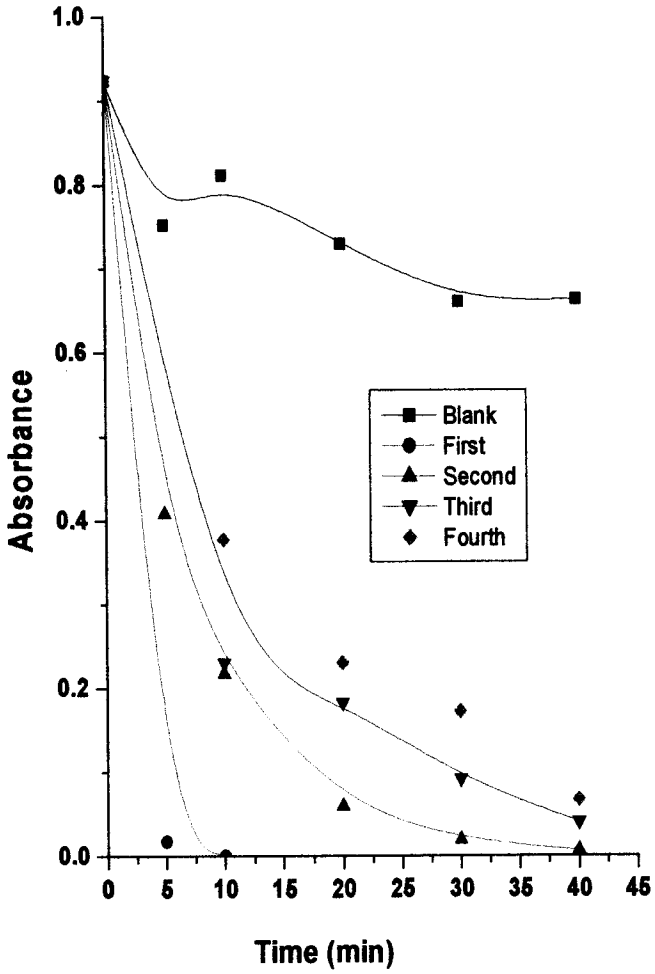

6.41 Recycling $AgTPPS_4$ for four times

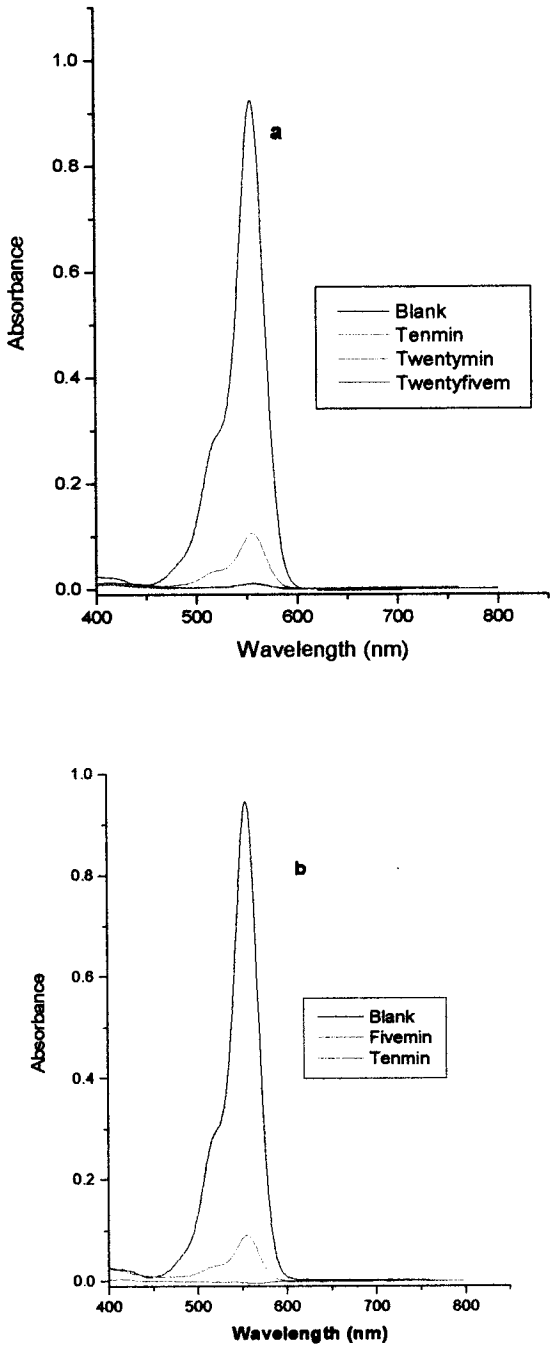

Fig. 6.42 Photodegradation of Rhodamine B by a) $TPPS_4$ and b) $AgTPPS_4$

6.12 Degradation study of Rhodamine B by HPLC and Mass spectrometry

The RB solution required the concentration 10^{-7} M to give the good resolution and measurable area under the peak. This made to dilute the experimental solution to 100 times and was subjected in the C18 column with mobile phase of methanol : water in the ratio 70 : 30 at the flow rate of 1 mL per minute. In the beginning, undegraded solution of RB was run through the column and the peak was resolved at the retention time of 3.23 min. Then the degraded solution of RB was run at the same flow rate and a peak was resolved at the retention time of 4.28 min. This is shown in Fig 6.43 which gives resolution of peaks before degradation (a) and after degradation (b) at the respective retention time. This indicates that two components before and after degradation are different from each other. Table 6.5 gives results for the RB before degradation and after degradation

To know more about the degradation product, the solution was subjected to mass spectrometry where number of counts was made a function of m/z ratio. The fragmentation pattern obtained is shown in Fig 6.44 where a molecular peak at 443 for RB is seen and after MS-MS, the peak is seen at 399, which is a base peak. Thus a loss of 44 from the molecular peak confirms loss of CO_2 from the structure of RB. Hence, it may be said that during degradation there is a loss of CO_2 followed by change in the symmetry of the molecule of RB. Thus, HPLC study followed by mass spectrometry, shades light on the mechanism of photodegradation of RB in acetone medium.

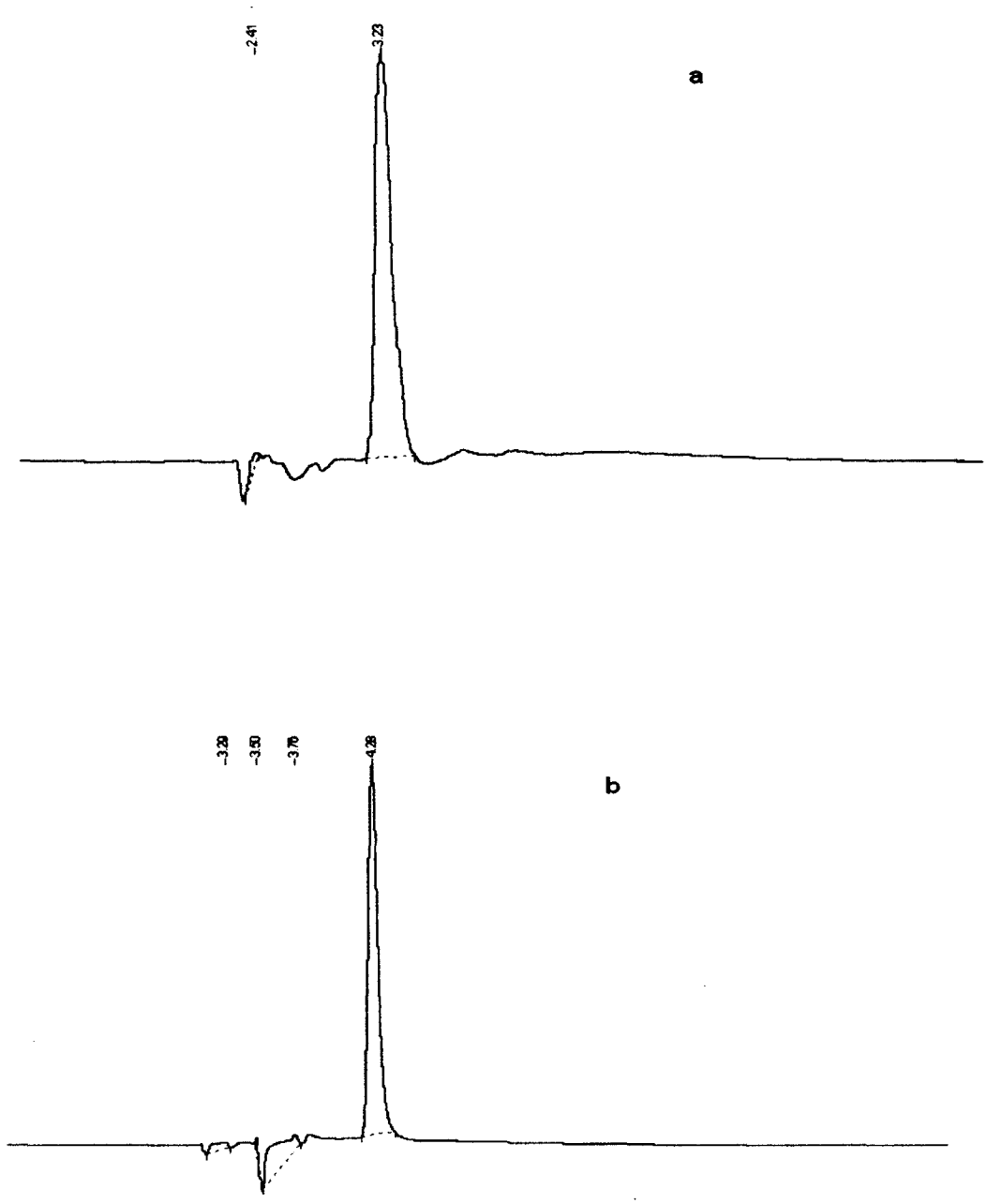

Fig. 6.43 HPLC chromatogram for Rhodamine B

a) Before degradation b) After degradation

Table 6.5 HPLC results for Rhodamine B

Sr.No.	Dye	Retention time (min)	Component
1	Rhodamine B (Blank)	3.23	I
2	Rhodamine B (degraded)	4.28	I

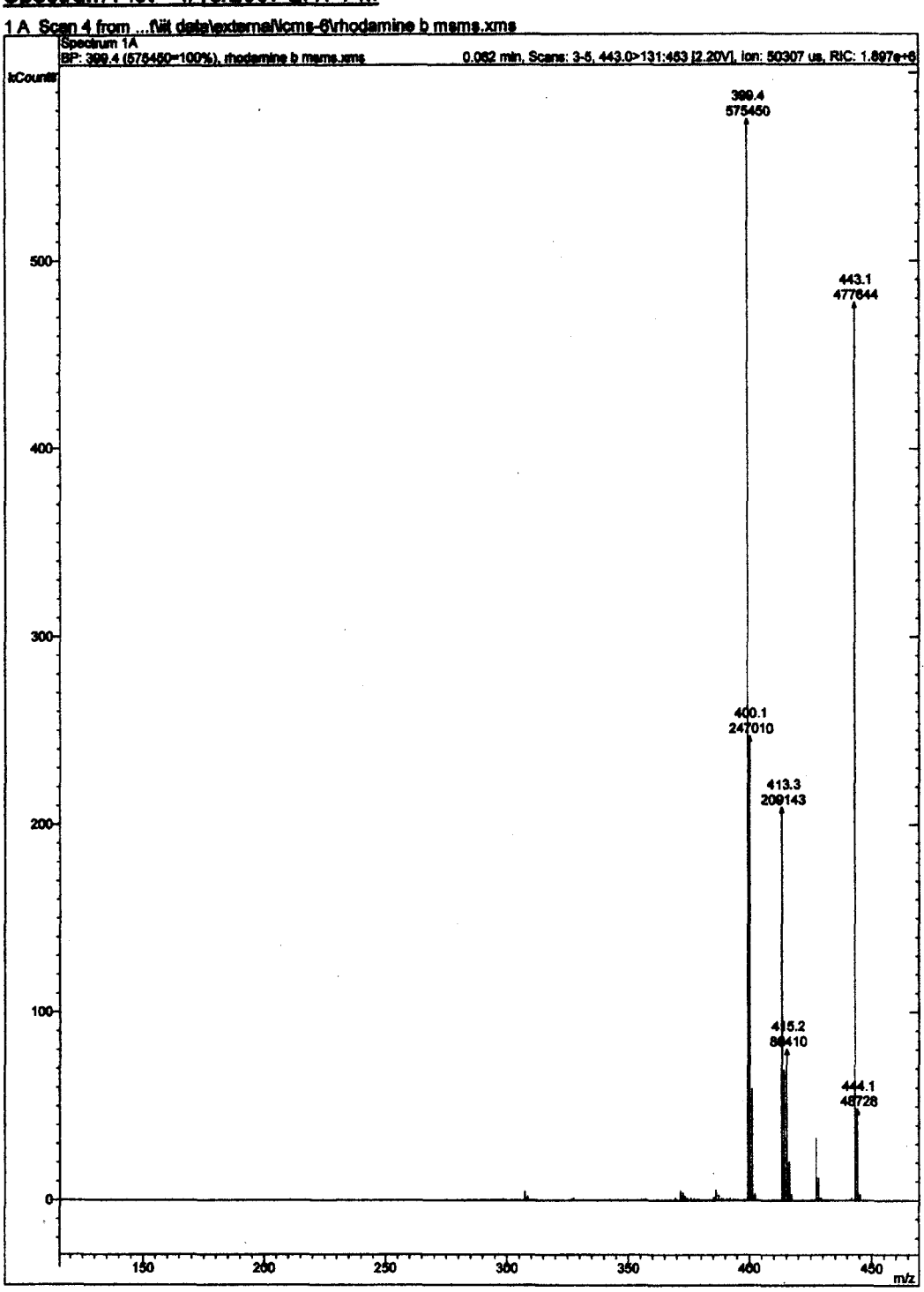

Fig. 6.44 MS-MS fragmentation pattern for degraded Rhodamine B

6.12 Degradation study of Rhodamine B by Ion-chromatography

After having the insight of mechanism of degradation of RB, there was need to know the mineralization of RB in organic medium. Therefore, blank and the degraded solution of RB were subjected to ion-chromatography. In this regard, as mentioned in earlier sections, the anion and cation columns were calibrated for respective ions. In Fig. 6.45 ion chromatogram for undegraded RB is seen where Cl^- and SO_4^{2-} are observed. Here, Cl^- presence is due to the ionization of RB in solution state whereas SO_4^{2-} is a background concentration of impurity in the system. Fig. 6.46 shows additional amount of Cl^- obtained after degradation and SO_4^{2-} is a background impurity. Thus while calculating net amount of Cl^-, subtraction of additional amount and amount due to ionization of molecule of RB is taken into account. Fig 6.47 shows ion chromatogram for cations where, Na^+ and NH_4^+ are seen as background impurity in the system. From Fig. 6.48 it is seen that cations are not found after the degradation of RB. Table 6.6 shows presence of Cl^- as a result of mineralization.

Therefore, it can be said that the process of degradation is accompanied by a process of mineralization.

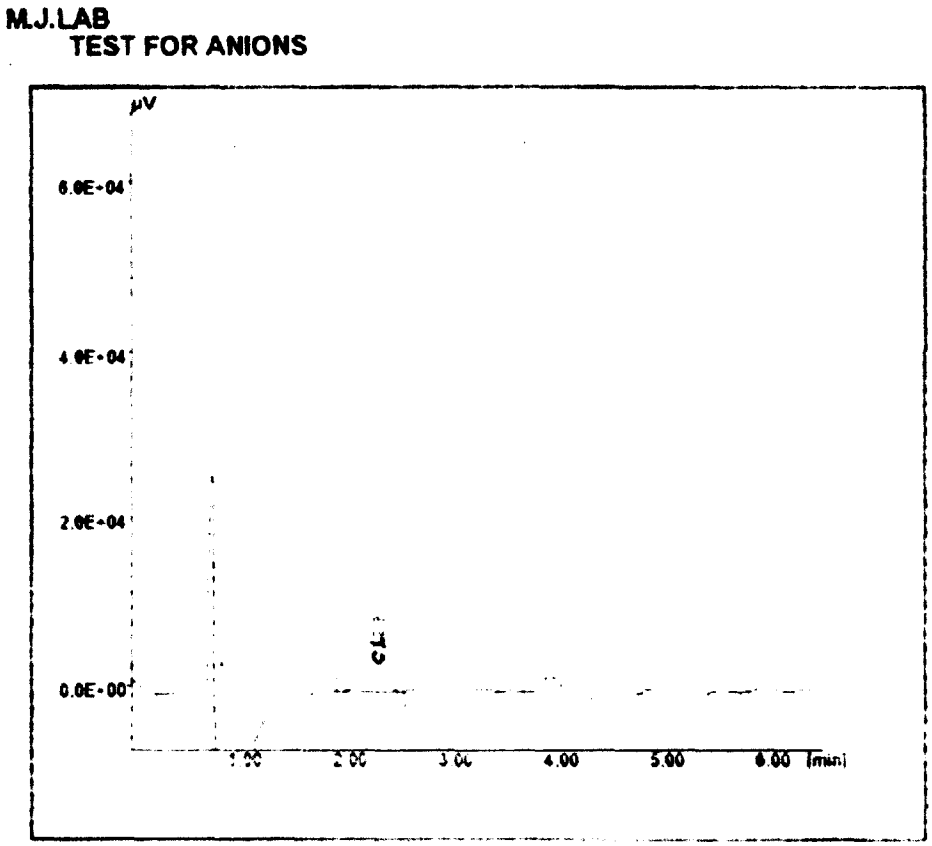

Fig. 6.45 Chromatogram for undegraded Rhodamine B

(Cl^-, being background)

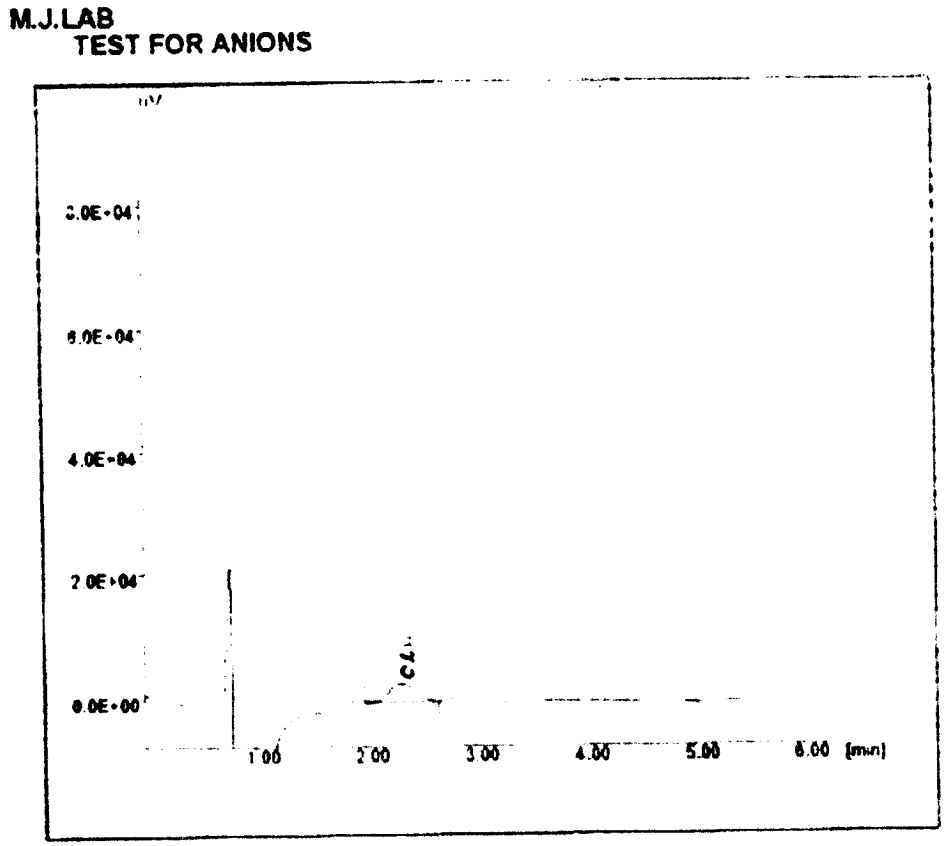

Fig. 6.46 Chromatogram for degraded Rhodamine B showing presence of Cl^-

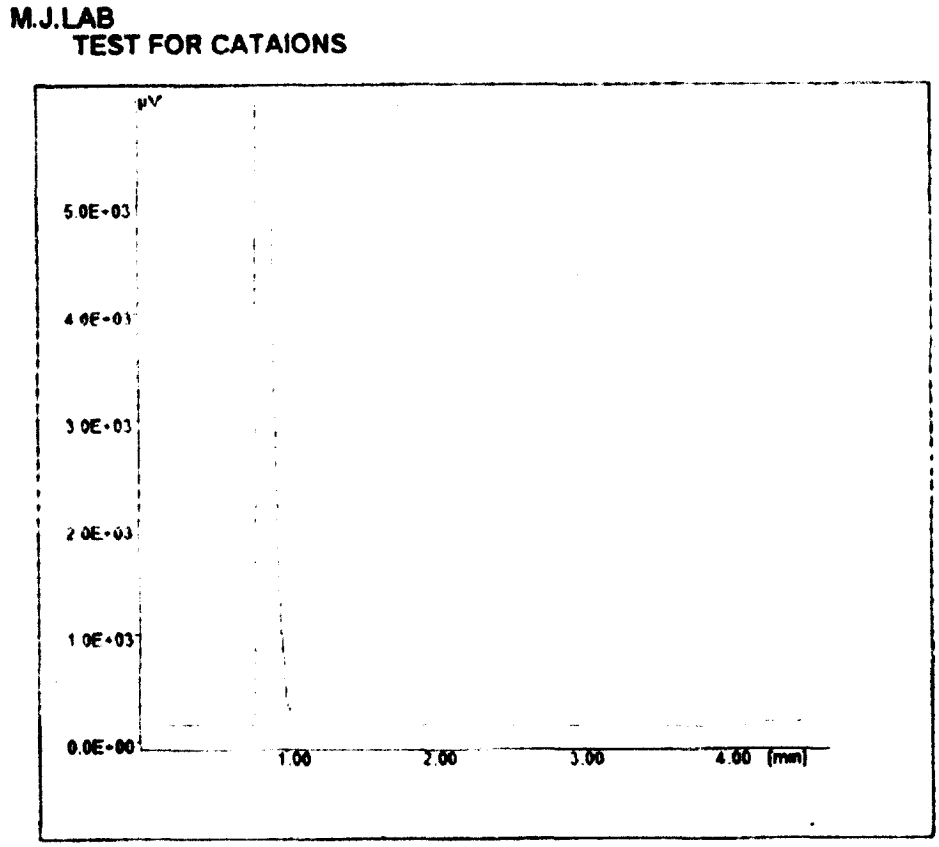

Fig. 6.47 Chromatogram for undegraded Rhodamine B

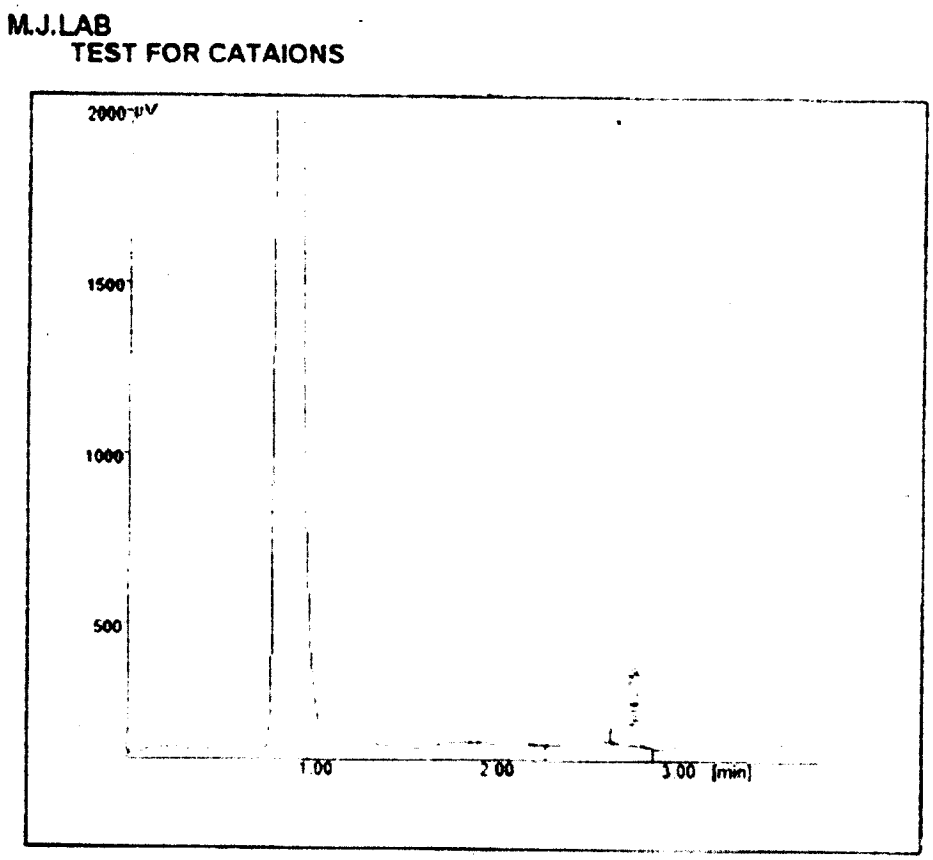

Fig. 6.48 Chromatogram for degraded Rhodamine B showing presence of NH_4^+

Table 6.6 Ion-chromatography results for Rhodamine B

Sr.No.	Dye	Concentration of NH_4^+ in μg per mL	Concentration of Cl^- in μg per mL
1	Rhodamine-B (blank)	—	—
2	Rhodamine-B (degraded)	0.15	0.55

CHAPTER 7

Conclusions

The environmental pollution has become a growing problem of serious concern in the advanced human society. The measure to check it by all possible means has become a necessary criterion for the peaceful survival of the society. The continuous and constant efforts are being carried out through out the globe to improve and investigate the new means and measures for the minimization of pollutants. Under such conditions, homogenous and heterogeneous catalysis play major roles in executing the theme of pollution-free world. With regards to the background of this scenario, an attempt to propose the heterogeneous photocatalysis through the model reactions induced by synthetic porphyrins as photocatalysts is made. In the present experimental work, the degradation of dyes by means of photoassisted semiconductor catalysts has been undertaken. The main theme behind this experimentation was the destruction of chromophores from azo dyes followed by mineralization of the auxochromic or other such groups. For this, the dyes selected were Amido Black 10 B, Ponceau S (diazo dyes), Methyl Orange (mono azo dye) and Rhodamine B (xanthene type dye). Among these dyes Amido Black 10B, Ponceau S and Methyl Orange were degraded in aqueous medium whereas Rhodamine B was degraded in organic medium (acetone). The photocatalysts selected for this work were synthetic porphyrins from non-aqueous and aqueous series. From non-aqueous series the porphyrins such as TPP, CoTPP, NiTPP, CuTPP, ZnTPP, AgTPP, MnTPPCl, O-$(MnTPP)_2$, FeTPPCl, O-$(FeTPP)_2$ and $SnTPPCl_2$ were used for the degradation of dyes in aqueous medium. The porphyrins from aqueous

series such as $TPPS_4$, $CoTPPS_4$, $NiTPPS_4$, $CuTPPS_4$, $ZnTPPS_4$, $AgTPPS_4$, $MnTPPS_4Cl$, $FeTPPS_4Cl$, O-$(FeTPPS_4)_2$ and $SnTPPS_4Cl_2$ were used to degrade the dye in organic medium. Further, the syntheses of non-aqueous and aqueous-porphyrin were carried out by established and self-modified methods. The most important task of the purification of these porphyrins was carried out using recommended methods as well as newly devised methods by us as per the requirements.

The synthesized porphyrins were then studied through various angles before they were used for photocatalysis. Further, depending upon the objective, they were classified and studied extensively by various methods as summarized below.

The synthesized porphyrins were characterized by different methods which include UV-visible spectroscopy, FTIR spectroscopy, ^{1}Hnmr spectroscopy, Fluorescence spectroscopy, Diffuse reflectance spectroscopy (DRS), Elemental analysis, and High-resolution mass spectrometry (HR-MS) respectively.

When porphyrins were characterized by UV-visible method, it was found that free-base porphyrins like TPP, $TPPS_4$ and porphyrins of Zn^{2+} and Sn^{4+} are forming a class of regular porphyrins. Further, irregular porphyrins are classified into two classes' viz. hypso porphyrins and hyper porphyrins. The porphyrins of Co^{2+}, Ni^{2+}, Cu^{2+} and Ag^{2+} are forming hypso porphyrins whereas porphyrins of Mn^{3+}, Fe^{3+} and their respective dimers are forming hyper porphyrins. The absorption bands in soret region and visible region, show characteristic property of a corresponding porphyrin and thus becomes a method of characterization. It was also observed that sulphonated porphyrins in general absorb at shorter wavelength than non-sulphonated porphyrins. Thus UV-visible spectroscopy has differentiated and confirmed porphyrins on the basis of their absorption bands.

FTIR spectroscopy is next important tool to characterize the porphyrins. The free base porphyrins such as TPP and $TPPS_4$ show N-H stretching at 3317 cm^{-1} and within 3340 – 3590 cm^{-1} respectively. When metals are substituted in the porphinato core, the N-H stretching disappears and confirms formation corresponding metalloporphyrin. Also it gives the information about presence of TPP or $TPPS_4$ as impurity in respective porphyrin. The important aspect of FTIR is that, at 1000 cm^{-1} there is a strong absorption which indicates the strength of the metal-nitrogen bond and has established the sequence of stability based on the experimentally obtained values. In case of aqueous-porphyrins FTIR confirms sulphonation of benzene ring on the basis of 1041, 1128 and 1184 cm^{-1} band. Further, O-H stretching vibrations in aqueous-porphyrins are confirming the hydrated nature of the compounds.

The proton NMR spectroscopy (^{1}Hnmr) has further confirmed the synthesized porphyrins depending upon the shift of their β- pyrrole protons and phenyl protons. In case of diamagnetic porphyrins it is seen that pyrrole protons show more low-field chemical shift than phenyl protons whereas in paramagnetic porphyrins magnitude of chemical shift of protons is higher and broadening of the resonance signals is seen. In aqueous porphyrins, ortho-phenyl protons are shifted to more down field than pyrrole protons. The reason for this behaviour was attributed to the presence of SO_3Na groups. Thus ^{1}Hnmr is useful for characterization of the compound, to make distinction between diamagnetic and paramagnetic porphyrins and to distinguish between aqueous and non-aqueous porphyrins.

The fluorescence spectroscopy is used to determine the fluorescent intensity of the porphyrins. It was found that free-base porphyrins such as TPP , $TPPS_4$ and porphyrins

containing Zn^{2+}, Mn^{3+} and Sn^{4+} are found to be fluorescent in nature. The λ_{max} obtained can serve as characteristic peak for emission intensity for a particular porphyrin. Further, a co-relationship between fluorescence intensity and photoactivity was established to prove the efficiency of a photocatalyst. The porphyrins of Co^{2+}, Ni^{2+}, Cu^{2+}, Ag^{2+}, and Fe^{3+} have proved non-fluorescent and sluggish towards photoactivity in aqueous medium.

The diffuse reflectance spectroscopy (DRS) was used to determine the band gap energy between the valence band and conduction band of the given semiconductor photocatalysts. The information obtained in this regard was the band gap energy (E_g) for aqueous or non-aqueous porphyrins is less than two, which indicate that synthesized porphyrins are narrow-band semiconductors. Perhaps, this would be making them as efficient photocatalysts.

The elemental analysis for TPP, CuTPP and $MnTPPS_4Cl$ were carried out as representative compounds from aqueous and non-aqueous porphyrins. From the comparison of expected and experimental results the molecular formulae of synthesized porphyrins were confirmed. In the context of aqueous porphyrins, from the percentage of hydrogen it was also possible to know the exact number of water molecules in a particular porphyrin. Thus elemental analysis has proved essential tool for the characterization.

The high-resolution mass spectrometry (HR-MS) was used to determine the exact molecular formula especially in case of aqueous-porphyrins. In this regard, $TPPS_4$ and $FeTPPS_4Cl$ were selected from aqueous-porhyrins. The results proved that the route of synthesis of porphyrins as well as methods of purification employed were satisfactory. This is even useful to know the exact number of SO_3Na groups in a given porphyrin

molecule. Thus, it also shades light on the complete sulphonation associated with the four phenyl rings of a particular porphyrin.

The porphyrins were subjected to magnetic susceptibility study, electron spin resonance (ESR), X-ray diffraction studies (XRD), Image analysis, TG-DSC, TG-EGA-MS analysis. The magnetic moment values of porphyrins were calculated using magnetic susceptibility measurements by Gouy balance at room temperature. Further, it was possible to know high spin and low spin complexes based on this knowledge. This information was also used to know the oxidation states of metals in metalloporphyrins which is based on the number of unpaired electrons. Thus it was established that Co, Cu, Ag, are possessing +2 oxidation state whereas Mn and Fe are possessing +3 oxidation state.

The ESR study was applied to paramagnetic porphyrins from non-aqueous and aqueous series. From ESR spectrum g-factor, line width and hyperfine splitting constant values were calculated. Further, using g-factor, number of unpaired electrons in a particular porphyrin was calculated. The porphyrins, where ESR signals were not available at room temperature in such cases signals were obtained at liquid nitrogen temperature.

The XRD study has shown that the synthesized porphyrins are polycrystalline and they are mono phasic in nature.

The TG-DSC studies have shown that on an average the porphyrins are thermally stable up to 400° C. It has given information that there is no melting point observed as far as synthesized porphyrins are concerned. It has given the insight of different stages of decomposition for aqueous and non-aqueous porphyrins. In case of aqueous-porphyrins,

it indicates the loss of water of crystallization and thus establishes the hygroscopic nature of the corresponding porphyrins. In the context of non-aqueous porphyrins, it shows the residue of corresponding metal oxide and for aqueous-porphyrins it shows presence of Na_2SO_4 in addition to metal oxide.

The TG-EGA-MS study has shown percent weight loss followed by evolution of different species and gases as the process of thermal analysis advances. This throws light on the sequence of out coming species within the observed temperature range and subsequent rupture of the porphyrin ring system.

The photocatalytic study with regards to the degradation of azo and xanthene type dyes were undertaken.

The Amido Black 10B, a diazo dye, is degraded by means of synthesized non-aqueous porphyrins as photocatalysts at pH 6, 7 and 10 in aqueous medium. It is observed that the photodegradation reaction is fast for pH 6, moderate for pH 10 and slow for pH 7 respectively.

The Methyl Orange, a mono azo dye, also shows the rate of photodegradation by semiconductor photocatalysts is fast for pH 6, moderate for pH 7 and slow for pH 7.

The similar observation is seen during the photodegradation of Ponceau S, a diazo dye. But compared with above two dyes, it seems to be more resistant towards photodegradation process. The extent of degradation is also not seen to reach to 100%. The reproducibility of catalysts was seen by recycling them for given number of cycles. The change in structure if any during recycling was verified by UV-visible and FTIR spectroscopy and it is observed that there are no structural changes taking place during

photolysis. The degradation products are studied with HPLC and mineralization study is done with ion-chromatography.

In this regard, it is assumed that the maximum activity at pH 6 was seen due to increased concentration of $OH^{\bullet}$ whereas at pH 10 the activity was moderate due to comparatively decreased concentration of $OH^{\bullet}$ due to excessive OH^{-} ions. At pH 7 the rate of production of $OH^{\bullet}$ is too low which hampers the process of degradation.

Rhodamine B comes under xanthene type dye which is degraded in acetone by means of aqueous-porphyrins. The rate of the degradation reaction is found very fast, which is ranging between 5 to 40 min. The reproducibility of the photocatalysts is verified by recycling them for number of times as per selection. The change in structural features if any due to recycling is examined with UV-visible and FTIR spectroscopy. It is observed that there is no alteration in the structures of the photocatalysts. The degradation products are further resolved by HPLC and mineralization study is carried out with ion-chromatography. The mechanism of degradation is studied by mass spectrometry and it is observed that the Rhodamine B undergoes degradation due to loss of CO_2 from the structure, followed by change in symmetry.

The photodegradation reactions involving semiconductor photocatalysts follow a route of photooxidation. This is an exercise to establish a model reaction for photodegradation of dyes in aqueous and organic media. The scope of the above reactions may be extended with the due considerations to the following points.

i) The porphyrins as extrinsic semiconductors of n-type or p-type may be devised for photocatalytic reactions and degradation reactions may be studied through different angles.

ii) The intrinsic or extrinsic porphyrins may be stirred continuously with dye solution for half an hour before photocatalytic reaction and the rate of photodegradation reaction may be studied.

iii) The reactions of photodegradation may be tried with the different types of sources and the results may be compared with the photolysis induced by solar radiations.

References

1) M. Sokmen, D. W.Allen, F.Akkas, N. Kartal, and F.Acar, Water Air and Soil Pollution., 132 (2001) 153.

2) T. Robinson, G. Mc Mullan, R. Marchant and P. Nigam, Bioresource Technol., 77 (2001) 247.

3) I. M. Banat, N. Poonam, and R. Marchant, Biores, Technol., 58 (1996) 217.

4) L. Ladakowicz , M. Solecka, and R. Zylla, J. Biotechnol., 89 (2001) 175.

5) D. Georgiou, P. Melidis, A. Aivasidis, and K. Gimouhopoulos, Dyes Pigments, 52 (2002) 69.

6) G. Mckay, J. F.Porter, G.R.Prasad, Water Air and Soil Pollution., 114 (1999) 423.

7) N. Kannan and M. Meenakshisundaram, Water Air and Soil Pollution., 138 (2002) 289.

8) Y. M. Slokar, and A. M. Le Marechal, Dyes Pigments, 37 (1998) 335.

9) J.Ge and J.Qu, Appl.Catal. B: Environmental, 47 (2004) 133.

10) W.Azmi, R.K.Sani and U.C.Banajee, Enzyme Microbial Technol., 22 (1998) 185.

11) V. Zope, M. Kulkarni and M. Chavan, J. Scientific and Industrial Research, 66 (2007) 414.

12) P.C. Vandevivere, R. Bianchi, and W. Verstraete, J. Chem. Technol. Biotechnol., 72 (1998) 289.

13) A. Marinas, G. Chantal, M.M. Jos, F.A. Amadeo, A. Ana, and H. Jean-Marie, Appl. Catal. B: Environ. 34 (2001) 241.

14) K.Tanaka and K.S.N. Reddy, Appl. Catal.B: Environ. 39 (2002) 305.

15) I. Konstantinou, and T.A. Albanis, Appl. Catal B: Environ. 40 (2004) 1.

16) P. Borker, and A.V.Salker, Materials Science and Engineering B, 133 (2006) 55.

17) W.A. Zeltner, X. Fu, and M.A. Anderson, Appl. Catal.B, 6 (1995) 209.

18) J.S.Youl, and P.S. Bin, Appl.catal. B, 25 (2000) 249.

19) N. Dutta-Gupta and T.J. Bardos, J. Heterocyclic chem., 3 (1996) 495.

20) L.R. Milgrom "The colours of life: an introduction to the chemistry of porphyrins and related compounds". Oxford University Press, UK, 1997.

21) P.J. Dandiker, F. Diederich, and J.P. Gisselbrecht, Angew. Chem. Int. Ed. Engl 23 / 24 (1995) 2725.

22) A.D.Adler, F.R. Longo, and W. Shergalis, J. Am. Chem. Soc., 86 (1964) 3145.

23) J. S. Lindsey, D.C. Mauzerall, and H. J. Linschitz, J. Am. Chem. Soc., 105 (1983) 6528.

24) M.R. Wasielewski, M.P. Niemczyk, W.A. Svec, and E.B. Pewitt, J.Am. Chem. Soc., 107 (1985) 5562.

25) A.V. Bogatskii, and Z. I. Zhilina, Russ. Chem. Rev., 51 (1982) 592.

26) G.Knor and A.Vogler, Inorg. Chem., 33 (1994) 314.

27) D.C. Rawlings, E.R. Davidson, and M. Gouterman, Int. J. Quantum Chem., 26 (1984) 251.

28) M. Gouterman "In The Porphyrins", D. Dolphin Ed: Academic press: New York, 1978, Vol III, Chapter I, pp. 59.

29) A. Vogler, A. Paukner, and H. Kunkely, Coord-Chem. Rev., 97 (1990) 285.

30) A.Vogler, and H. Nikol, Pure Appl. Chem., 64 (1992) 1311.

31) A. D. Adler, Longo F.R., and Finarelli J.D., J.Org. chem., 32 (1967) 476.

247

32) A.D. Adler, Longo F.R., Frank Kampas, and Jean Kim, J. Inorganic Nucl.Chem., 32 (1970) 2443.

33) E. B. Fleisher, J. M. Palmer, T. S. Srivastava, and A. Chatterjee, J. Am. Chem. Soc., 93 (1971) 3162.

34) T. S. Srivastava and M. Tsutsui, J. Org. Chem, 38 (1973) 2103.

35) W. DeW. Horrocks Jr, and E. G. Hove, J. Am. Chem. Soc., 100 (1978) 4386.

36) A. D. Adler, J. Polym. Sci., Part C, 29 (1970) 73.

37) A. D. Adler, Ann. N.Y. Acad. Sci., 244 (1975) 73.

38) G.A. Taylor and M. Tsutsui, J. Chem. Educ., 52 (1975) 715.

39) J. L.Hoard, G. H. Cohen, and M. D. Glick, J. Am. Chem. Soc., 89 (1967) 1992.

40) M. D. Glock, G. H. Cohen, and J. L. Hoard, J. Am. Chem. Soc., 89 (1967)1996.

41) R. Tinkovich, and A. Tulinsky, J. Am. Chem. Soc., 91 (1969) 4430.

42) E. B. Fleischer, Accounts Chem. Res., 3 (1970) 105.

43) T. R. Janson and J. J. Katz, in "The Porphyrins" (D. Dolphin Ed.) Vol 4, Chapter 1, Academic Press, New York, 1979, pp. 15.

44) S. S. Eaton and G. R. Eaton, J. Am. Chem. Soc., 97 (1975) 3660.

45) P. Rothemund, J. Am. Chem. Soc., 61 (1939) 2912.

46) P. Rothemund and A. R. Menotti, J. Am. Chem. Soc., 63 (1941) 267.

47) R. H. Ball, G. D. Dorough, and M. Calvin, J. Am. Chem. Soc., 68 (1946) 2278.

48) P. Rothemund and A. R. Menotti, J. Am. Chem. Soc., 70 (1948) 1808.

49) G. D. Dorough, J. R. Miller and F. M. Huennekens, J. Am. Chem. Soc., 73 (1951) 4315.

50) D. W. Thomas and Arthur E. Martell. J. Am. Chem. Soc., 81 (1959) 5111.

51) E. S. G. Barron, J. Biol.Chem., 121 (1937) 285.

52) J. F. Taylor, J. Biol. Chem., 135 (1940) 569.

53) E. B. Fleischer, J. Am. Chem. Soc., 1 (1962) 493.

54) T. P. Stein, and R. A. Plane, J. Am. Chem. Soc., 91 (1961) 607.

55) P. Hambright and E. B. Fleischer, Inorg. Chem., 9 (1970) 1757.

56) J. Winkelman, G. Slater, and J. Grossman, Can. Res., 27 (1969) 2060.

57) F. R. Longo, M. G. Finarelli, and J. B. Kim, J. Heterocycl. Chem., 6 (1969) 927.

58) R. F. Pasternack, P. R. Huber, P. Boyd, G. Engasser, L. Francesconi, E. Gibbs, P. Fasella, G. Cerio Venturo, and L. deC. Hinds, 94 (1972) 4511.

59) Z. Shi, and Fu. Ch, Talanta, 44 (1997) 593.

60) S. K. Cheung, F. L. Dixon, E. B. Fleischer, D. Y. Jeter, and M. Krishnamurthy, Bioinorganic Chem., 2 (1973) 281.

61) A. Corsini, R. DiFruscia, and O. Herrmann., Talanta, 32 (1985) 476.

62) M. Krishnamurthy, J. R. Sutter, and P. Hambright, J. C. S. Chem. Comm. 1178 (1974) 13.

63) W. Dew, Horrocks, Jr., and E. G. Hove, J. Am. Chem. Soc., 100 (1978) 4386.

64) J. W. Buchler, in "The Porphyrins " (D.Dolphin ed.) Vol I.,Chapter 10, Academic Press, New York, 1978, pp. 419.

65) J. W. Buchler, K. L. Lay, P. D. Smith, W. R. Scheidt, G. A. Rupprecht, and J. E. Kenny, J. Organomet. Chem., 110 (1976) 109.

66) B. Love and M. M. Goodman, Progr. Separ. Purif., 3 (1970) 73.

67) P. Hambright, Coord. Chem. Rev., 6 (1971) 247.

68) L. J. Boucher, Coord. Chem. Rev., 7 (1972) 289.

69) D. Ostfeld and M. Tsutsui, Acc. Chem. Res., 7 (1974) 52.

70) J. L. Hoard, Science, 174 (1971) 1295.

71) A. D. Adler, J. Polym. Sci., Part C, 29 (1970) 73.

72) E. B. Fleischer and M. Krishnamurthy, J. Am. Chem. Soc., 94 (1972) 1382.

73) A. R. Kane, J. F. Sullivan, D. H. Kenny, and M. E. Kenny,
Inorg. Chem., 9 (1970) 1445.

74) M. Tsutsui and G. A. Taylor, in " Porphyrins and Metalloporphyrins "
(K.M. Smith,ed.), Chapter 7, Elsevier, Amsterdam, 1975. pp. 280.

75) W. Buchler, in " Porphyrins and J. Metalloporphyrins "(K.M. Smith,ed.),
Chapter 5, Elsevier, Amsterdam, 1975. pp. 191.

76) J. L Hoard, in " Porphyrins and Metalloporphyrins "(K.M. Smith,ed.),
Chapter 8, Elsevier, Amsterdam, 1975. pp. 341

77) W. Robert Scheidt, in "The Porphyrins ". (D.Dolphin ed.) Vol III.,
Chapter 10, Academic Press, New York, 1978. pp. 497.

78) D. F. Shriver and P. W. Atkins, Inorganic Chemistry, Third Edition,
Chapter 4, Oxford University Press 1999, pp. 123.

79) C. M. L.West and J. V. Moore. Int. J. Radiat. Biol., 54 (1988) 612.

80) J. F. Evensen and J. Moan, Photochem. Photobiol., 46 (1987) 859.

81) K. Berg, J. C. Bommer, J. W. Winkelman, and J. Moan, Photochem. Photobiol.,
52 (1990) 775.

82) E. B. Fleischer, and T. S. Srivastava, J. Am. Chem. Soc., 91 (1969) 2403.

83) E. B. Fleischer, C. Miller, and L. Webb, J. Am. Chem., Soc. 86 (1964) 2342.

84) I. A. Cohen, J. Am. Chem. Soc., 91 (1969) 1980.

85) D. K. P. Ng, J. Jiang, Chem. Soc. Rev., 26 (1997) 433.

86) D. K. Lavallee, Z. Xu, and R. Pina, J. Org. Chem., 58 (1993) 6000.

87) R. F. Pasternack, E. J. Gibbs, A. Gaudemer, J. Am. Chem. Soc., 107 (1985) 8179.

88) K. Kano, H. Minamizono, and T. Kitae, J. Phys. Chem. A, 101(1997) 6118.

89) R. Purrello, A. Raudino, and L. Monsu Scolaro, J. Phys. Chem. B, 104 (2000) 10900.

90) J. R. Platt, in "Radiation Biology" (A. Hollaender, ed.), Vol. III, Chapter 2, McGraw-Hill, NewYork, 1956.

91) M. Gouterman, in "The Porphyrins ". (D.Dolphin Ed.) Vol III., Chapter 1, Academic Press, New York, 1978, pp. 12.

92) J. W. Buchler, in " Porphyrins and Metalloporphyrins " (K.M. Smith,ed.), Chapter 5, Elsevier, Amsterdam, 1975 pp.189.

93) A. Triebs, Ann. Chem., 728 (1969)115.

94) J. O. Alben, in "The Porphyrins " (D.Dolphin Ed.) Vol III., Chapter7, Academic Press, New York, 1978. pp. 323.

95) H. Burger, in "Porphyrins and Metalloporphyrins" (K.M. Smith,ed.), Chapter 11, Elsevier, Amsterdam, 1975 pp. 525.

96) E. D. Becker and R. B. Bradley, J. Chem. Phys., 31 (1959) 1413.

97) J. Ellis, A. H. Jackson, G. W. Kenner, and J. Lee, Tetrahedron Lett., 23 (1960).

98) W. S. Caughy and W. S. Koski, Biochemistry, 1 (1962) 923.

99) R. J. Abraham and P. F. Swinton, J. Chem. Soc. C, 903 (1969).

100) T. R. Janson and J. J. Katz, in "The Porphyrins " (D.Dolphin Ed.) Vol IV Chapter1, Academic Press, New York, 1978. pp. 25.

101) K. M. Smith, in "Porphyrins and Metalloporphyrins" (K.M. Smith,ed.), Chapter 9, Elsevier, Amsterdam1975 pp. 525.

102) R. L. Levy, H. Gesser, E. A. Halevi, and S. Saidman, J. Gas Chromatogr., 2 (1964) 254.

103) D. G.Whitten, K. E. Bentley, and D. Kuwada, J. Org. Chem., 31 (1966) 31.

104) R. Grigg, G. Shelton, A. Sweeney, and A. W. Johnson, J. Chem. Soc., Perkin Trans., 1 (1972) 1789.

105) G. W. Kenner, K. M. Smith, and M. J. Suttan, Tetrahedron Lett., 1303 (1973)

106) J. W. Buchler, in "The Porphyrins ". (D.Dolphin Ed.) Vol I, Chapter 10, Academic Press, New York, 1978. pp. 422.

107) F. R. Hopf and D. G. Whitten, in "Porphyrins and Metalloporphyrins" (K.M. Smith,ed.), Chapter16, Elsevier, Amsterdam 1975, pp. 667.

108) D. Eastwood and M. Gouterman, J. Mol. Spectrosc., 35 (1970) 359.

109) M. Gouterman, F. P. Schwarz, P. D. Smith, and D. Dolphin, J. Chem. Phys., 59 (1973) 676.

110) D. G. Whitten, I. G. Lopp, and P. D. Wildes, J. Am. Chem. Soc., 90 (1968) 7196.

111) M. G. Gouterman, in "The Porphyrins ". (D.Dolphin Ed.) Vol III, Chapter1, Academic Press, New York, 1978. pp. 48.

112) E. B. Fleischer, J. Am. Chem. Soc., 85 (1963) 1353.

113) E. B. Fleischer, C. K. Miller, and L. W. Webb, J. Am. Chem. Soc.,

86 (1964) 2342.

114) W. R. Scheidt, in "The Porphyrins" (D.Dolphin Ed.) Vol III, Chapter10, Academic Press, New York, 1978. pp. 470.

115) R. Timkovich and A. Tulinsky, J. Am. Chem. Soc., 91 (1969) 4430.

116) R. C. Pettersen, Acta Crystallogr. Sect. B 25, (1969) 2527.

117) A. B. Hoffman, D. M. Collins, V. W. Day, E. B. Fleischer, T. S. Srivastava, and J. L. Hood, J. Am. Chem. Soc., 94 (1972) 3620.

118) W. R. Scheidt, J. Am. Chem. Soc., 96 (1974) 90.

119) P. N. Dwyer, P. Madura, and W. R. Scheidt, J. Am. Chem. Soc., 96 (1974) 4815.

120) U. Ozgur et. al., J. Appl. Phys., 98 (2005) 041301.

121) D. M. Bagnall et al., Appl. Phys. Lett., 70 (1997) 2230.

122) T. Aoki, Y. Hatanaka, and D. C. Look, Appl. Phys. Lett., 76 (2000) 3257.

123) C. Boemare, T. Monteiro, M. J. Soares, J. G. Guilherme, and E. Alves, Physica B, 308-310 (2001) 985.

124) M. Becerril, H. Silva-Lopez, and O. Zeleya-Angel, Revista Mexicana De Fisica., 50 (2004) 588.

125) E. A. Meulenkamp, J. Phys. Chem. B, 102 (1998) 5566.

126) A. E. Morales, E. S. Mora, and U. Pal, Revista Mexicana De Fisica 53(5) (2007) 18.

127) R. A. Smith, Semiconductors, 2nd Ed. Cambridge University Press: Cambridge, 1978.

128) H. Falk, E. Mayr and A. E. Richter, Microchimica Acta., 117 (1994) 1.

129) J. Subramanian, in "Porphyrins and Metalloporphyrins"

(K.M. Smith,ed.), Chapter 13, Elsevier, Amsterdam1975, p. 555.

130) A. Abragam and B. Bleaney, in "Paramagnetic Resonance of Transition Metal Ions", Oxford University Press, (1970).

131) J. Wertz and J. R. Bolton, in "Electron Spin Resonance – Elementary Theory and Applications", Mcgraw Hill, New York (1972).

132) B. R. MGarvey in "Transition Metal Chemistry", Vol. 3, R. L. Carlin Ed. Marcel Dekker, New York (1966), pp. 89.

133) R. L. Dutta and A. Syamal in "Elements of Magnetochemistry", Second Ed., pp. 216

134) B. B. Wayland and Abd-Elmageed, J. Am. Chem. Soc., 96 (1974) 4809.

135) W. C. Lin, in "The Porphyrins" (D.Dolphin Ed.) Vol. IV, Chapter 7, Academic Press, New York, 1978, pp. 358.

136) A. MacGragh and W. S. Koski, J. Am. Chem. Soc., 85 (1963) 2375.

137) P. Hambright ,A. J. Bearden, and K. M. Smith, in "Porphyrins and Metalloporphyrins", (K.M. Smith, ed.), Chapter12, Elsevier, Amsterdam1975, 545.

138) D. F. Shriver and P. W. Atkins, in "Inorganic Chemistry; Third Ed., Chapter 7, Oxford University Press, pp. 231.

139) S. Sullivan, A. N. Thorpe, and P. Hambright, J. Chem. Educ., 48 (1971) 345.

140) L. F. Lindoy, V. Katvoic, and D. Busch, J. Chem. Educ., 49 (1972) 117.

141) B. N. Figgis and R. S. Nyholm, J. Chem. Soc., (1958) 4190.

142) G. A. Candela, and R. E. Munday, IRE Trans. Instrum., (1962) 106.

143) D. F. Evans, J. Chem. Soc., (1959) 2003.

144) K. Bartle, D. W. Jones, and S. Maricic, Croat. Chem. Acta., 40 (1968) 227.

145) K. Bartle, B. J. Dale, D. W. Jones, and S. Maricic, J. Magn. Reson., 12 (1973) 286.

146) E. B. Fleischer and T. S. Srivastava, J. Am. Chem. Soc., 91 (1969) 2403.

147) W. P. Hambright, A. N. Thorpe, and C. C. Alexander, J. Inorg. Nucl. Chem., 30 (1968) 3139.

148) L. Edwards, D. Dolphin, M. Gouterman, and A. D. Adler, J. Mol. Spectrosc., 38 (1971) 16.

149) V. Varadi, F. R. Longo and A. D. Adler, in "The Porphyrins" (D.Dolphin Ed.) Vol I, Chapter13, Academic Press, New York, 1978. pp. 586.

150) C. Guan, L. Li, D. Chen, Z. Gao and W. Sun, Thermochimica Acta, 413 (2003) 31.

151) D. F. Ollis, and C. S. Turchi, Environ. Prog., 9 (1990) 229.

152) M. R. Hoffmann, S. T. Martin, W. Choi, and D. W. Bahnemann, Chem. Rev., 95 (1995) 69.

153) A. Mills, and S. L. Hunte, J. Photochem. Photobiol., A: 108 (1997)1

154) V. Augugliaro, L. Palmisano, M. Schiavello, and A. Sclafani in "Homogeneous and Heterogeneous Photocatalysts" (E. Pelizzetti Ed.), pp. 567.

155) K. I. Okamoto, Y. Yamamoto, and M. Tanaka, Bull. Chem. Soc., Jpn., 58 (1985) 2015.

156) M. Ohnishi, M. Matsumura, H. Tsubomura, and M. Iwasaki, Ind. Eng., Chem. Res., 28 (1989) 719.

157) S. A. Sharma, P. Rao, R. P. Mathur, and S. C. Ametha, J. Photochem. Photobiol., A: 86 (1995) 197.

158) N. Serpone, D. Lawless, J. Disdier, and J. M. Herrmann, Langmuir, 10 (1994) 643.

159) S. Sakthivel, S. U. Geissen, D. W. Bahnemann, V. Murugesan, and A. Vogelpohl, J. Photochem. Photobiol., A: 148 (2002) 283.

160) N. Serpone, E. Borgarello, and M. Gratzel, J. Chem. Soc. Commun., (1983) 342.

161) M. Qumar, M. Saquib, and M. Muneer, Dyes and pigments, 19 (2003) 591.

162) S. Sheng-peng, G. Wang, and L. Qio, Dyes and pigments, 74 (2007) 647.

163) M. S. Lucas and J. A. Peres, Dyes and pigments, 74 (2007) 622.

164) J. Chen, D. Wang, M. Zhu and C.Gao, J. Hazardous Materials, 138 (2006) 182.

165) M. N. Rashed and A. A. El-Amin, Int. J. Phys. Sci.., 2 (2007) 73.

166) G. Jianying and C. Weimin, Plasma Sci. Technol., 9 (2007) 190.

167) W. Sadik, A. W. Nashed , M. Abdel-Ghaffar and M. Ei-Demerdash, J. Photochem. Photobiol., A: 189 (2007) 135.

168) J. Wu and T. Zhang, J. Photochem. Photobiol, A: 162 (2004) 171.

169) J. Li, W. Ma, P. Lei and J. Zhao, J. Environ. Sci., 19 (2007) 892.

170) K. Byrappa, A. K. Subramani, S. Ananda, K. M. Lokanatha Rai, R. Dinesh and M. Yoshimura, Bull. Mater. Sci., 29 (2006) 433.

171) J. Wu, Environ. Sci. Technol., 41 (5) (2007) 1723.

172) D. F. Ollis in "Homogenous and Heterogeneous Photocatalysis" (E. Pelizzetti Edn.) Series C: Mathematical and Physical Sciences, 174 (1986) 651.

173) A. Piscopo, D. Robert and J. V. Weber, Applied Catalysis B: Environmental, 35 (2001) 117.

174) E. Borgarello, N. Serpone, M. Barbeni, C. Minero, E. Pelizzetti and E. Pramauro in "Homogenous and Heterogeneous Photocatalysis" (E. Pelizzetti Edn.) Series C: Mathematical and Physical Sciences, 174 (1986) 673.

175) N. Serpone, and E. Pelizzetti, in "Homogenous and Heterogeneous Photocatalysis" "Homogenous and Heterogeneous Photocatalysis" (E. Pelizzetti Edn.) Series C: Mathematical and Physical Sciences, 174 (1986) 51.

176) F. Cacialli, in "Philosophical Transactions: Mathematical, Physical, and Engineering Sciences, 358 (2000) 173.

177) V. Hequet, P. Le Cloiree, C. Gonzalez and B. Meunier, Chemosphere, 41 (2000) 379.

178) G. Mele, R. Sole, G. Vasapollo, E. Garica-Lopez, L. Palmisano and M. Schiavello, J. Catalysis, 217 (2003) 334.

179) G. Mele, R. Sole, G. Vasapollo, E. Garica-Lopez, L. Palmisano, L. Jun, R. Slota and G. Dyrada, J. Research on Chemical Intermediates, 33 (2007) 433.

180) K. Kalyansundaram, N. Vlachopoulos, V. Krishnan, A. Monnier and M.Gratul, J. Phys. Chem., 91 (1987) 2342.

181) T. Furoto, S. Lee, Y. Amao, K. Asai and I. Okura, J. Photochem. Photobio., A: 132 (2000) 81-86.

182) N. Daneshvar, D. Salari, A. R. Khataee, J. Photochem. Photobiol., A: 157 (2003) 111.

183) I. Spiewak, R. Benmair, R. Messalem, and O. Radchenko, Proc. Indian Acad. Sci., (Chem. Sci.), 110 (1998) 229.

184) W. Buchler, in " Porphyrins and Metalloporphyrins " (K.M. Smith,ed.), Chapter 5, Elsevier, Amsterdam, 1975, pp. 187.

185) D. F. Marsh and Larry M. Mink. J. Chem. Educ., 73 (1996) 1118.

186) T. R. Janson and J. J. Katz in "The Porphyrins" (D. Dolphin ed) Vol. 4,

Chapter 1, Academic Press, New York, 1979, pp. 15.

187) T. R. Janson and J. J. Katz in "The Porphyrins" (D. Dolphin ed) Vol. 4, Chapter 1, Academic Press, New York, 1979, pp. 35.

188) H. Scheer and J. J. Katz in " Porphyrins and Metalloporphyrins " (K.M. Smith,ed.), Chapter 10, Elsevier, Amsterdam, 1975. pp. 473.

189) G. M. Godziela and H. M. Goff, J. Am. Chem. Soc., 108 (1989) 2237.

190) A. Shirazi and H. M. Goff, Inorg. Chem., 21 (1982) 3420.

191) W. C. Lin in "The Porphyrins" (D.Dolphin Ed.) Vol IV, Chapter 7, Academic Press, New York, 1978, pp. 360.

192) I. T. I Gupta and M. Ravikanth, J. Chem. Sci., 117 (2005) 161.

193) D. J. Quimby and F. R. Longo, J. Am. Chem. Soc., 97 (1975} 5111.

194) S.D.Gokakakar and A. V. Salker, Thermans, (2006), pp. 294.

195) S.D.Gokakakar and A. V. Salker, Thermans, (2008), pp. 224.

196) V.P. Parman, A. V. Emeline, and N. Serpone, Int. J. Photoenergy, 4 (2002) 103.

197) O. E. Kartal, M. Erol and H. Oguz, Chem. Eng. Technol., 24 (2001) 645.

198) A. Bard, Science, 207 (1980) 138.

Appendix – I

Publications

1. Thermal studies of some metalloporphyrins.

S. D. Gokakakar and A. V. Salker

Thermans (2006) pp. 294-295.

2. Thermal studies of free-base and metalloporphyrins.

S. D. Gokakakar and A. V. Salker

Thermans (2008) pp. 224-225.

3. Synthesis, characterization and photocatalytic degradation of Amido Black 10B over Co, Ni, and Zn metalloporphyrins.

S. D. Gokakakar and A. V. Salker

Material Chemistry and Physics, (2008), communicated.

4. Solar assisted photocatalytic degradation of Methyl Orange over synthesized copper, silver, and tin metalloporphyrins.

S. D. Gokakakar and A. V. Salker

J. Molecular Catal., (2008), communicated.

5. Thermal behaviour of Co, Fe and Sn metalloporphyrins

S. D. Gokakakar and A. V. Salker

J. Thermal analysis and calorimetry, (2008), communicated.